DEVELOPING CHEMICAL BIOLOGICAL TOOLS TO PROBE PHOSPHORYLATION IN *P. FALCIPARUM*

THESIS SUBMITTED FOR THE DEGREE OF

DOCTOR OF PHILOSOPHY

AT THE UNIVERSITY OF LEICESTER

By

Kathryn Maria Pugh, MChem (Leicester)

Department of Chemistry

University of Leicester

May 2014

Abstract

Developing chemical biological tools to probe phosphorylation in *P. falciparum*

Kathryn Maria Pugh

In 2010 there were an estimated 219 million cases of malaria worldwide, accounting for approximately 0.66 million deaths. With growing resistance to current antimalarial agents a challenge is placed on the scientific community to provide efficacious and cost effective methods for the diagnosis and treatment of malaria. As protein phosphorylation regulates most aspects of cell life, understanding the function of protein kinases in malaria parasites has the potential to uncover novel drug targets. To this end, this work focused on the study of three essential *Plasmodium falciparum* kinases using two different chemical genetic approaches: γ-modified ATP analogues for the investigation of *Pf*CK2; and covalent complementarity for the study of *Pf*CLK1 and *Pf*CLK3. The work presented here highlights the instability of the P-N bond of ATP phosphoramidates during the acidic conditions required for analysis by MALDI-TOF MS and seeks to overcome this through the development of alternative linkers to the γ-phosphate of ATP. Apparent IC_{50} values recorded provide evidence of *Pf*CK2α tolerating modification of the γ-phosphoryl group of ATP; however, no evidence was found to support GTP serving as an alternative co-substrate of *Pf*CK2α. The gatekeeper mutant kinases *Pf*CLK1F630C and *Pf*CLK3F444C were successfully produced. It was found that this mutation rendered *Pf*CLK3 inactive and was detrimental to the activity of *Pf*CLK1. Under the conditions used *Pf*CLK1F630C was not inhibited by a panel of 23 electrophilic inhibitors.

Acknowledgements

First of all I would like to thank my supervisors Prof Paul Cullis, Dr Glenn Burley and Prof Andrew Tobin for providing me with this opportunity as well as for their encouragement and advice throughout my PhD. I would like to thank Gerry Griffith for his help with NMR and Mick Lee for running numerous LCMS samples as well as saving my bacon by fixing equipment on more than one occasion.

I am very grateful to the members of the Tobin lab for giving up their time to help me in the lab, particularly Adrian when I first started and Mahmood with the CLK work. The members of the Organic Lab, past and present, have pooled ideas, and kept my spirits up when experiments and thesis writing were not going smoothly – thank you! My Protein Panic Person and Biological Support Network have been key to my PhD survival and I am sure we will exchange many more emails and phone calls of mutual panic and advice. A special thank you to Michele for sharing data, advice and laughs throughout our PhD journey together.

I would like to thank my housemates over the past few years – they have helped to keep me sane, cooked wonderful food, become hooked on TV series and coped with my PhD stress. Last, but by no means least, I would like to thank my friends and family for putting up with being neglected, especially during the final six months of my PhD!

Abbreviations

ACT	Artemisinin combination therapy
AMPPNP	Adenosine 5’-(β,γ-imido)triphosphate
aPK	Atypical protein kinase
ATP	Adenosine triphosphate
ATPγS	Adenosine 5’-[γ-thio]triphosphate
BOC	Tertiarybutyl oxycarbonyl
cAMP	Cyclic Adenosine monophosphate
CDPK	Calcium-Dependent Protein Kinase
cGMP	Cyclic guanosine monophosphate
CK1	Caesin kinase I
CK2	Caesin Kinase II
CLK	Cyclin-dependent kinase-like kinase
Cpm	Counts per minute
CRT	Chloroquine resistance transporter
CV	Cyclic voltammetry
Cyt	Cytochrome
DCC	N,N’-Dicyclohexylcarbodiimide
DDT	Dichlorodiphenyltrichloroethane
DHOD	Dihydroorotate dehydrogenase
DNA	Deoxyribonucleic acid
DTT	Dithiolthreitol
dTTP	Thymidine triphosphate

EDC	N,N’- N-(3-Dimethylaminopropyl)-N’-ethylcarbodiimide hydrochloride
ePK	Eukaryotic protein kinase
GSKs	Glycogen synthase kinases
GST	Glutathione S-transferase
GTP	Guanosine triphosphate
GTPPNP	Guanosine 5’-(β,γ-imido)triphosphate
GTPγS	Guanosine 5’-[γ-thio]triphosphate
HPLC	High performance liquid chromatography
Hs	*Homo sapiens*
IRS	Indoor residual spraying
ITNs	Insecticide treated nets
MALDI	Matrix assisted laser desorption ionisation
MBP	Myelin basic protein
MLKs	Mixed lineage kinases
mRNA	Messenger ribonucleic acid
MS	Mass spectrometry
NHS	N-Hydroxysuccinimide
Ni-NTA	Nickel nitrilotriacetic acid
NMR	Nuclear magnetic resonance
OD	Optical density
PAGE	Polyacrylamide gel electrophoresis
Pf	*Plasmodium falciparum*
PK	Protein kinase

PKA	Protein kinase A
PLK	Polo-like kinase
PNACL	Protein Nucleic Acid Chemistry Laboratory
PP1	1-(1,1-Dimethylethyl)-3-(4-methylphenyl)-1H-pyrazolo[3,4-d]pyrimindin-4-amine
PROTEX	Protein expression laboratory
RDTs	Rapid diagnostic tests
RNA	Ribonucleic acid
rRNA	Ribosomal ribonucleic acid
SDS	Sodium dodecyl sulphate
Tb	*Trypanosoma brucei*
TBB	4,5,6,7-Tetrabromobenztriazole
TCA	Trichloroacetic acid
TFA	Trifluoroacetic acid
TK	Tyrosine kinase
TKL	Tyrosine kinase-like kinase
TOF	Time of flight
Tris	Tris(hydroxymethyl)aminomethane
tRNA	Transfer ribonucleic acid
UV	Ultra-violet
WHO	World Health Organisation
Wt	Wildtype
Zm	*Zea mays*

Contents

1 Introduction

According to the WHO, half of the world's population live in areas at risk of malaria transmission. With growing resistance to current antimalarial agents, a challenge is placed on the scientific community to provide efficacious and cost effective methods for the diagnosis and treatment of malaria. For this to be possible a better understanding of the key biological processes of the malarial parasites is required. Protein phosphorylation regulates most aspects of cell life. Therefore, understanding the function of protein kinases in malaria parasites has the potential to uncover novel drug targets. The conserved nature of the ATP binding site across the kinome requires the development of methodologies for specifically targeting the kinase of interest in order to discover its substrates. To this end, the objective of this thesis was to develop methodologies for the study of phosphorylation processes occurring within the malarial parasite *Plasmodium falciparum*, the most deadly species of the parasite. In particular, this work focused on three essential kinases using two different chemical genetic approaches: γ-modified ATP analogues for the investigation of CK2; and covalent complementarity for the study of CLK1 and CLK3. Due to the importance of phosphorylation in the cellular environment, the development of these methodologies and the knowledge gained on these kinases will have beneficial impacts across a wide range of diseases, such as cancer and diabetes, as well as the target of this study, malaria.

1.1 Malaria

In 2010 there were an estimated 219 million cases of malaria worldwide, accounting for approximately 0.66 million deaths.[1] With half the world's population living in areas at risk of malaria transmission, one fifth (1.2 billion) in areas of high risk,[2] and the most widely affected areas being poorer nations, a challenge is placed on the scientific community to provide efficacious and cost effective methods for the diagnosis and treatment of malaria.

1.1.1 A tale as old as time

From periodic fevers in 2700 BC China to detailed descriptions of symptoms from Hippocrates in the 5th century to the work of European physicians in the 19th century, the characteristic signs of malaria have been described throughout history, highlighting the plight of mankind against this disease. Due to their small size, it was not possible to recognise protozoa until the invention of the microscope followed by its development for studying living things by Anton van Leeuwenhoek in the 16th century. Instead, the understanding of malaria was based on miasmatic theory, the idea that some diseases originated from corrupted environments.[3] The study of parasitic protozoa did not really begin until the establishment of the germ theory at the end of the 19th century[4] with Charles-Louis Alphonse Laverán first viewing the *Plasmodium* parasites in 1880 in blood samples taken from soldiers with malaria.[3]

The discovery of the transmission of malaria by the *Anopheles* mosquito by Sir Ronald Ross in 1897[5] explained the prevalence of this disease in tropical and sub-tropical climates, where the rainfall and temperature are ideal for *Anopheles* mosquitos.[6] Today malaria is thought of as both a disease of poverty and a cause of poverty that is

constraining economic growth in endemic countries through its direct and indirect costs (**Figure 1.1**).[7]

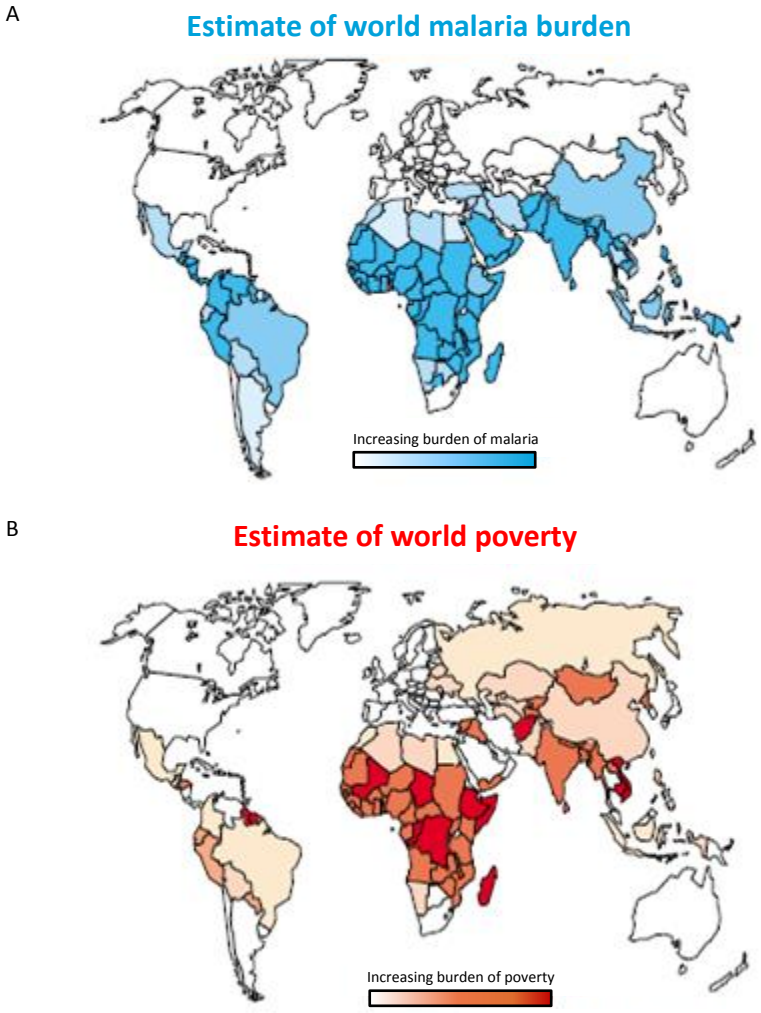

Figure 1.1: The startling correlation between malaria and poverty. A: the estimate of world malaria burden, where white represents no incidence of malaria and bright blue represents high incidence of malaria; B: the estimate of world poverty with the richest countries in white and the poorest in red.[7]

1.1.2 The life cycle of the malaria parasite

Malaria is caused by the eukaryotic unicellular protozoan parasite of the genus *Plasmodium*. By infecting red blood cells and eventually causing their rupture, malaria causes fever, severe anaemia, cerebral malaria and, without treatment, death. Of the ~170 species of malaria described,[8] the four main species of malaria known to infect humans are *P. falciparum*, *P. vivax*, *P. ovale* and *P. malariae. P*reviously thought to only infect monkeys, *P. knowlesi*, has also been found to infect humans.[9] Of the species of parasite that can infect humans, *P. falciparum* and *P. vivax* are the most common, with *P. falciparum* being the most prevalent in Sub-Saharan Africa and the most virulent.[10]

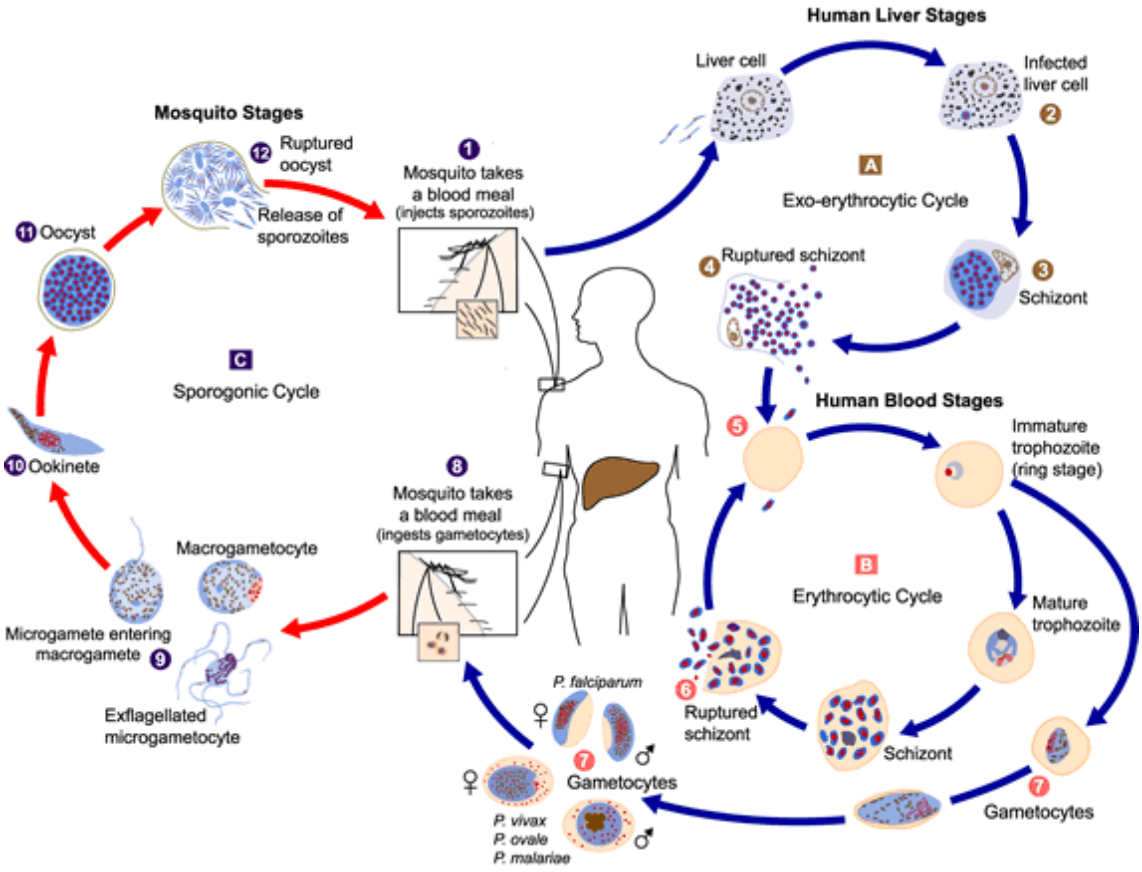

Figure 1.2: The life cycle of the malaria parasite[289] A) The exo-erythrocytic cycle, or human liver stages. Upon invasion of the human host, the parasites enter liver cells where they multiply before being expelled into the blood stream. B) The erythrocytic cycle, where the parasites multiply via trophozoites, ready for the invasion of more erythrocytes. Immature trophozoites can instead form gametocytes (7) ready for sexual reproduction in an *Anopheles* mosquito. C) The sporogonic cycle, which occurs within the mosquito, includes the completion of sexual reproduction.

The life cycles of plasmodia are complex with several stages in both humans and the *Anopheles* mosquitoes (**Figure 1.2**). An infected female *Anopheles* mosquito inoculates *Plasmodium* sporozoites into the human host from its salivary glands during feeding and these sporozoites migrate through the skin to a blood vessel. In the *P. falciparum* species, as little as ten sporozoites are required to result in infection.[11] Once in the blood stream, these sporozites travel to the liver where they invade hepatocytes and form tissue schizonts (**Figure 1.2 exo-erythrocytic cycle, cycle A**). Upon lysis of the infected hepatocytes, tens of thousands of merozoites are released into the circulation where they invade erythrocytes.[6, 12] The parasites rapidly transform into immature trophorozites and ingest the cytoplasm of the erythrocytes, producing the pigment haemozoin.[13] During asexual reproduction in the erythrocytic cycle (**Figure 1.2, cycle B**) the nuclear material of the parasite increases and multiple mitotic divisions occur, resulting in many nuclei, ready for the formation of merozoites in the mature schizont stage. These blood schizonts form and release another generation of merozoites upon rupture. It is this lysis of erythrocytes that causes most of the clinical symptoms of malaria and the time frame of this erythrocytic cycle is indicative of the *Plasmodium* species: *P. knowlesi 24 hr,*[14] *P. falciparum*, *P. ovale* and *P. vivax* 48 hr, *P. malariae* 72 hr.[6, 12]

During the erythrocytic cycle approximately 0.2-1%[15] of the immature trophozoites differentiate into gametocytes rather than continuing in the asexual cycle. Although gametocytes do not contribute to pathology, when ingested by another female *Anopheles* mosquito they enter the sporogonic cycle (**Figure 1.2, cycle C**) and continue sexual reproduction. In the midgut of the mosquito fertilisation and formation of zygotes occurs. Upon developing into an ookinete, the parasite passes through the

endothelium of the gut and forms an oocyst,[16] which produces thousands of sporozoites over 7-12 days.[17] These sporozoites are released and accumulate in the salivary glands of the mosquito ready to infect another human and thus completing their life cycle.[18]

Due to being the most lethal species of malaria, *P. falciparum* is regarded as the most important drug target. This virulence is mainly due to the high merozoite load and, unlike other species, it can bind to the endothelium during the blood stage[6] and sequester in organs, including the heart and brain.[19] This prevents the removal of infected erythrocytes by the spleen, leading to organ failure and severe malaria.[20]

1.1.3 Malarial chemotherapeutic agents

Throughout the complex, multi-stage lifecycle, the malaria parasite uses over 5000 protein-encoding genes[21] in order to adapt to the numerous environments it meets. This provides numerous potential drug targets at the three stages of its lifecycle. The main advantage of tackling the sporogonic cycle (**Figure 1.2, cycle C**) is the ability to prevent the spread of malaria without the need for medication to be given to humans. Although, there is widespread resistance to some insecticides, drugs that target the early mosquito stages of the parasites would need to only eliminate 5×10^3 parasites compared to 10^8-10^9 gametocytes in humans. This would reduce the number of parasite genomes exposed to the drug and hence, provide less opportunity for drug resistance to occur. The elimination of liver-stage malaria (**Figure 1.2, cycle A**) using vaccination is a particularly attractive potential target due to the presence of a small number of parasites[22] (only a few dozen of the sporozoites are transmitted from the mosquito and infect the liver).[6] The majority of antimalarial agents currently target the

erythrocytic cycle (**Figure 1.2 , cycle B**) due to this being the stage responsible for the clinical symptoms of malaria and the ease with which these can be studied in cell culture. Current antimalarial agents target four physiological pathways in plasmodia: haem metabolism, electron transport, protein translation, and folate metabolism.

1.1.3.1 *Interrupting haem metabolism*

Due to their limited ability to produce amino acids, plasmodia break down 60-80%[23] of the haemoglobin present in the red blood cell into its amino acid constituents. This degradation is performed by proteases within the parasite's acidic digestive vacuole (**Figure 1.3**) and results in the formation of the toxic metabolite haem (ferriprotoporphyrin IX). Plasmodia convert ferriprotoporphyrin IX to non-toxic crystalline heamozoin, containing cyclic dimers of ferriprotoporphyrin IX.[24] Also known as malaria pigment, these golden-brown/black granules are a distinctive feature of blood-stage malaria.[25] For this reason, compounds that disrupt haem metabolism have important antimalarial properties that have been exploited.

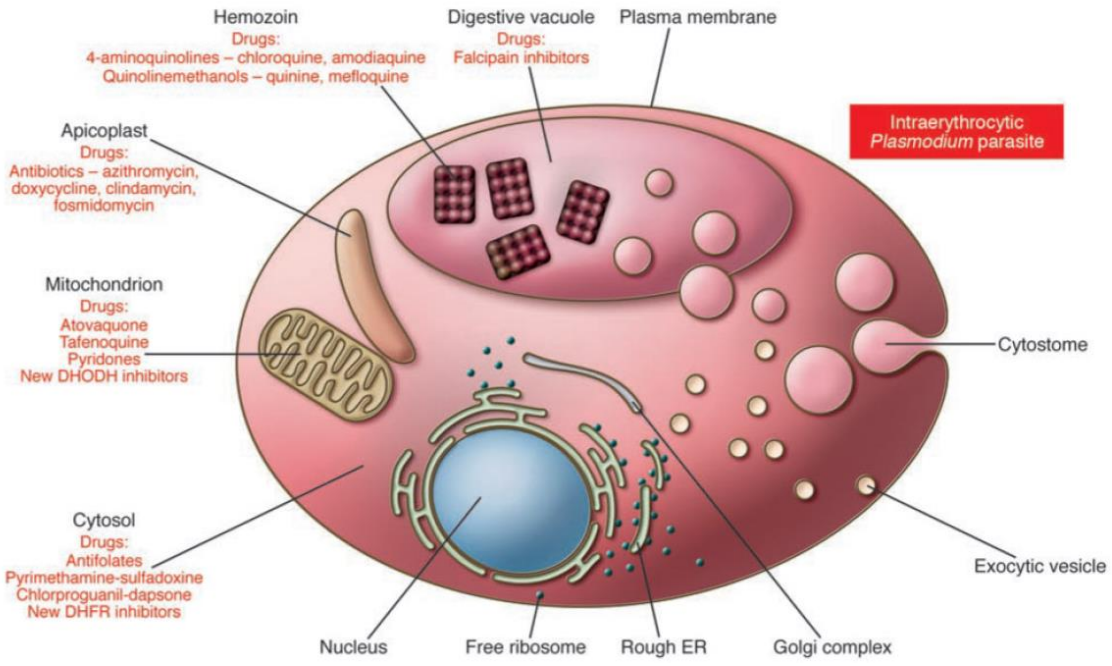

Figure 1.3: An intraerythrocytic *Plasmodium* parasite highlighting key parasitic intracellular compartments and the target areas of some antimalarial drugs.[6,290]

The traditional treatments for malaria were found to contain the antiplasmodial agent quinoline. Quinoline drugs include chloroquine (**1**), quinine (**2**), quinidine (**3**) and mefloquine (**4**). Chloroquine (**1**) acts by defusing into the digestive vacuole, where it is protonated by the acidic environment, rendering it unable to diffuse out of the vacuole. High localised concentrations of chloroquine develop, which inhibit the formation of heamozoin, resulting in an accumulation of ferriprotoporphyrin IX, which causes oxidative damage and therefore, death of the parasite. Mefloquine (**4**), quinine (**2**) and quinidine (**3**) are thought to act in the same way as chloroquine (**1**); although, as they are not as concentrated in the digestive vacuole as chloroquine (**1**), other modes of action might also be involved.[26] Quinine (**2**) has also been shown to intercalate DNA through hydrogen bonding, inhibiting transcription.[18]

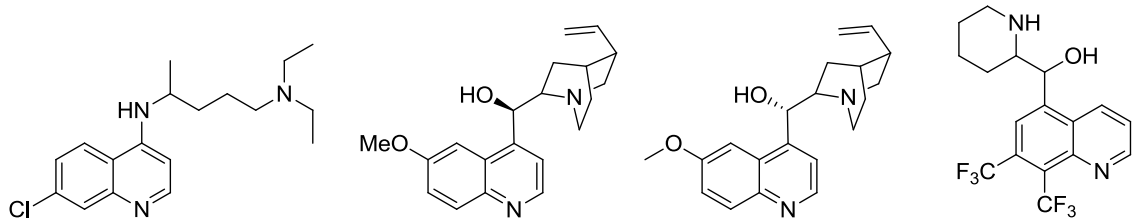

Figure 1.4: Four quinoline based antiplasmodial agents: chloroquine (1), quinine (2), quinidine (3) and mefloquine (4).

Chloroquine resistance is associated with a reduction in the amount of chloroquine accumulated in the digestive vacuole. It is thought that this is due to an increase in drug efflux caused by mutation to the gene encoding the *Pf*CRT transmembrane protein;[27] however, mutations to other genes are also thought to contribute to resistance.[28]

1.1.3.2 *Interrupting the electron transport chain*

Plasmodia rely upon electron transport for the oxidation of key enzymes in nucleotide synthesis. An early stage in pyrimidine synthesis is mediated by dihydroorodate dehydrogenase (DHOD), which is reduced during this synthesis. DHOD must therefore be re-oxidised in order to restore its catalytic activity. This oxidation is performed by ubiquinone, a membrane protein early in the electron transport chain (**Figure 1.5**). Thus, preventing ubiquinone oxidising DHOD disrupts plasmodial DNA replication and is the proposed method of action of the antimalarial drug primaquine (**5**). Another inhibitor of the electron transport chain, atovaquone (**6**), is known to inhibit the interaction between ubiquinone and the cytochrome bc_1 complex with ~100-fold selectivity for the plasmodial cytochrome bc_1 complex over the human analogue.[18] However, due to relatively quick emergence of resistance (this can be caused by a single point mutation in the gene encoding the cytochrome bc_1 complex) it is essential that this is not used as a single agent.[29]

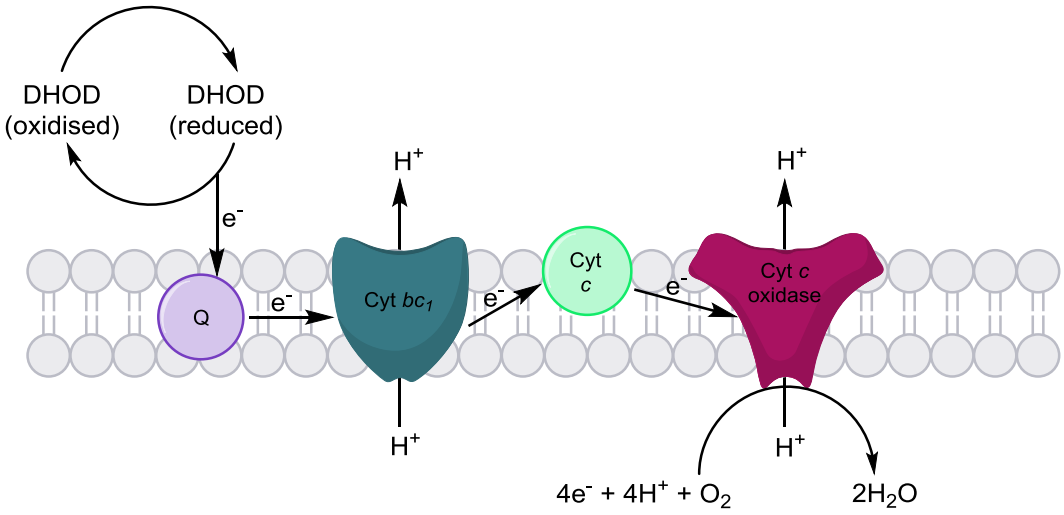

Figure 1.5: The mitochondrial electron transport chain in plasmodia. In plasmodia the electron transport chain is essential for the reduction of DHOD, used in pyrimidine synthesis. In this cascade, ubiquinone (Q) accepts electrons from reduced DHOD and passes them on to the cytochrome *bc₁ complex* (Cyt *bc₁*), which passes electrons to cytochrome *c* (Cyt *c*) and, finally, to cytochrome *c* oxidase (Cyt *c* oxidase). Cytochrome *c* oxidase then oxidises molecular oxygen, forming water inside the mitochondria. H^+ ions are also pumped out of the mitochondria.

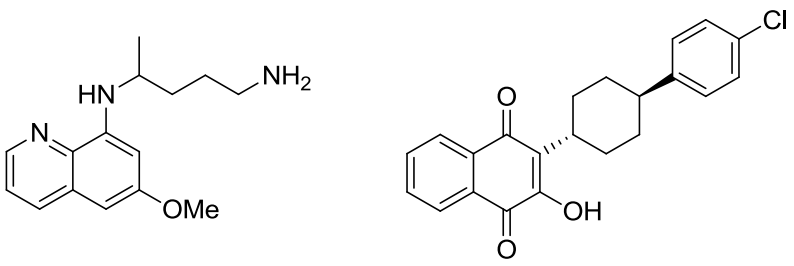

5 **6**

Figure 1.6: Two antimalarial agents thought to interrupt the electron transport chain are primaquine (5) and atovequone (6).

1.1.3.3 *Interrupting folate metabolism*

Folic acid is an essential vitamin in humans whereas parasites synthesise folic acid *de novo*. As folic acid is used in many biosynthetic pathways, including DNA and RNA precursor synthesis, a selective drug target is provided.[18] Anti-folate drugs are classified into type 1 and type 2 compounds. Type 1 anti-folates, such as sulfadoxine (**7**), inhibit the synthesis of folate. Type 2 anti-folates, e.g. pyrimethamine (**8**), prevent the utilisation of folate by dehydrofolate reductase.[26]

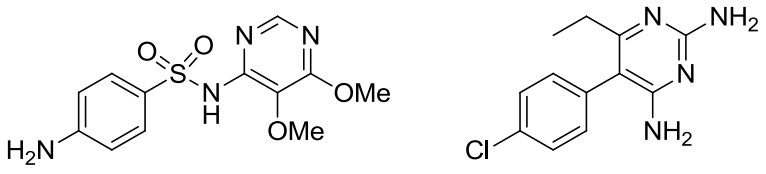

7 **8**

Figure 1.7: Sulfadoxine (7), a type 1 anti-folate and pyrimethamine (8), a type 2 anti-folate.

1.1.3.4 *Interrupting protein translation*

Agents that inhibit protein synthesis include doxycycline (**9**), tetracycline (**10**) and clindamycin (**11**). Doxycycline (**9**) and tetracycline (**10**) inhibit parasite protein synthesis by binding to the 30S ribosomal unit, blocking the binding of tRNA to

mRNA;[18] clindamycin (**11**) binds to the 50S ribosome and prevents the proper orientation of tRNA.[30]

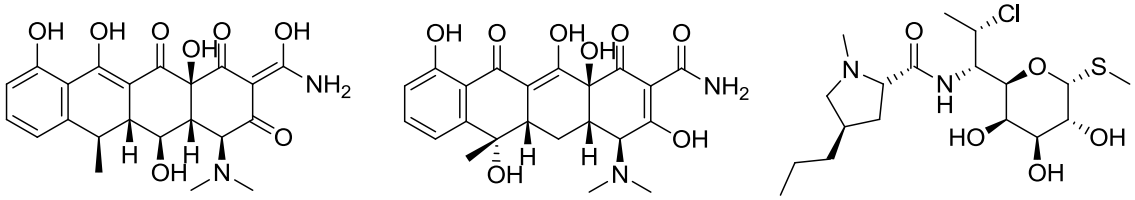

9 **10** **11**

Figure 1.8: Three agents which inhibit protein synthesis are doxycycline (9), tetracycline (10) and clindamycin (11).

1.1.3.5 *Other antimalarial agents*

Artemisinin (**12**) is a cyclic endoperoxidase, which is activated by free or haem-bound iron to form a carbon-centred free radical capable of causing damage to specific intracellular targets through alkylation.[31] The exact mechanism of specificity of artemisinin (**12**) and its derivatives for plasmodia-infected red blood cells is unknown; however, artemisinin-haem adducts have been found in parasite cultures[32] and artemisinin derivatives have been shown to alkylate six specific malaria proteins.[33] These compounds are associated with a rapid decrease in the level of parasites in the blood of infected individuals[18] – they reduce the parasitic load 10000-fold per asexual cycle (2 days) compared to between 100-fold and 1000-fold for other antimalarials.[34]

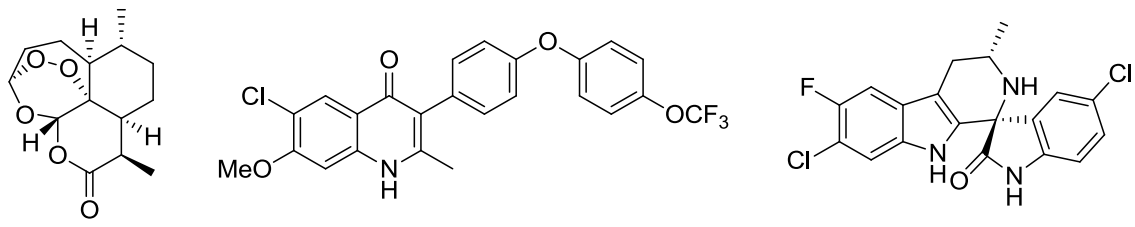

12 **13** **14**

Figure 1.9: The endoperoxidase artemisinin (12) causes damage to specific intracellular targets through alkylation. ELQ-300 (13) targets parasite mitochondria. The spiroindolone NITD609 (14) is in clinical trials.

An antimalarial has been developed that is effective across various stages of the parasite's lifecycle. ELQ-300 (**13**) targets parasite mitochondria, preventing the synthesis of thymine and cytosine (the primary function of *Plasmodium* mitochondria, compared to ATP synthesis in most organisms) needed for DNA synthesis; consequently, the parasite cannot reproduce and dies.[35] Another compound, the spiroindolone NITD609 (**14**), which rapidly inhibits *P. falciparum* protein synthesis, is in clinical trials.[36,37]

Despite many antimalarial agents having adverse side effects such as nausea, hypoglycaemia, hallucinations, fatal haemolysis and photosensitivity, the main problem is ever increasing resistance. Thus, there is a high level of interest in understanding the parasite in order to develop new highly specific molecules with novel modes of action.

1.1.4 Immunity and a potential vaccine

In endemic areas a degree of immunity is acquired through continued exposure;[38] however, immunity is slow to develop and requires multiple and frequent exposures.[25,39] This, therefore, is the reason why the majority of reported malaria cases are in children under five years of age. The attainment of protective immunity against the asexual blood stages of the parasite is complex and specific to each species. In areas with less stable malaria transmission, the population is less likely to be immune and people of all ages are at risk, resulting in epidemics.[38]

There is much interest in developing a vaccine against malaria. A vaccine would be hugely cost effective but requires the understanding of the immune mechanisms involved in conferring protection and then identifying target candidates and their

genes. Developments such as the sequencing of the *P. falciparum* genome[21] have greatly advanced this area of research and although a licenced vaccine is not currently available, research towards this has been pursued since the 1970s, with several found to be only partially effective in field trials.[38] There is currently one candidate vaccine in Phase 3 clinical trials and ~20 others in Phase 1 or Phase 2 clinical trials. The full Phase 3 trial results for the RTS,S/AS01 *P. falciparum* vaccine will not be available until late 2014 and other vaccine candidates are 5-10 years behind RTS,S/AS01.[1]

1.1.5 The fight against malaria

Following the discovery of DDT (dichlorodiphenyltrichloroethane) and the establishment of the World Health Organisation, malaria eradication was identified as a priority.[38] Soon after, the Global Malaria Eradication Programme was launched and depended upon chloroquine (**1**) for treatment and DDT for vector control.[6] Malaria was successfully eradicated in some areas e.g. southern Europe, North America, the Caribbean and some islands such as Mauritius and Singapore.[39] However, parasite resistance to chloroquine (**1**) developed, DDT-resistant *Anopholes* mosquitos occurred, concerns of the safety of DDT emerged, global funding was scaled back and the programme eventually abandoned in 1972.[40]

Although not included in the efforts of The Global Malaria Eradication Programme[6, 38] (at that time only approx. 10% of the world malaria death rate occurred in Africa[39]), many national malaria control organisations operated in many African countries from the 1950s. However, there was a fear that even powerful insecticides such as DDT would not be successful in eradicating malaria in Africa due to the intensity of transmission.[41] Fears over the consequential loss of immunity due to lack of exposure

to the parasite came true in 1986 with the outbreak of a severe two year epidemic in the highlands of Madagascar, where malaria had been almost eradicated for 20 years.[39]

By the turn of the 21st century, outside Africa, the chances of dying from malaria were 1% of what they had been 100 years previously.[39] Nevertheless, since the end of the Global Malaria Eradication Programme, the incidence of malaria has increased dramatically in many parts of the world.[6] In 2000 malaria was responsible for 2% of deaths worldwide; however, this was unevenly dispersed with <0.01% in Europe compared with 9% in Africa.[42] This was partly fuelled by the spread of chloroquine (**1**) resistance and the emergence of resistance to pyrimethamine-sulfadoxine (PSD) (a mixture of **7** and **8**), used as the replacement for chloroquine (**1**) as a first-line therapy. Chloroquine (**1**) and PSD cost less than US$0.20 per adult treatment course but drugs to treat multi-resistant strains (e.g. mefloquine (**4**)) cost over ten times as much and are not affordable for most people in Africa, where 90% of malaria deaths occur.[43] This and the decline of malaria transmission in Thailand that has occurred alongside economic development and an improved healthcare infrastructure further highlight the link between malaria and poverty.[44]

In light of the terrifying malaria statistics of the late 1990s and early 2000s, experts warned of an impending disaster.[45] This lead to an increase in the international solidarity for combat against malaria and resulted in the development of the WHO's Roll Back Malaria Partnership in 1998.[2] However, it was not until October 2007 after thought-provoking speeches at the Gates Foundation Malaria Forum[46, 47] that the WHO pledged to work with funding bodies towards a global attempt at eliminating malaria.[48]

The World Malaria Report 2012 describes malaria as 'an entirely preventable and treatable disease provided the currently recommended interventions are properly implemented'. These recommendations are: vector control through the use of insecticide treated nets (ITNs); indoor residual spraying (IRS); chemoprevention for the most vulnerable populations, e.g. pregnant women; confirmation of malaria diagnosis through microscopy or rapid diagnostic tests (RDTs) for every case; timely treatment with appropriate antimalarials.[1] This includes treating uncomplicated *P. falciparum* with an artemisinin combination therapy (ACT).[2] This involves giving an artemisinin derivative in combination with an antimalarial that has a much longer half-life but also a different target within the parasite. First used in the treatment of tuberculosis, the rationale behind this approach is that resistance arises from mutations. The probability that a mutant will occur that is simultaneously resistant to two drugs that have different targets is substantially less than a parasite with resistance against one drug developing a subsequent mutation that offers resistance to a second drug.[43]

The work of the WHO and other bodies is on-going. On World Malaria Day 2012, WHO launched a new initiative, T3: Test. Treat. Track, in which every suspected case is tested, every confirmed case is treated and every case is tracked in a surveillance system. There are exciting new prospects with the development of vaccines and work to find new antimalarials; however, parasite resistance to artemisinin (**12**) has been detected in four South-East Asian countries (Cambodia, Myanmar, Thailand and Vietnam) as a consequence of poor treatment practices, inadequate patient adherence to prescribed antimalarials and the availability of artemisinin-based monotherapies.[49] As yet no genetic marker for artemisinin (**12**) resistance has been identified[50] and no new class of antimalarials has been introduced since 1996.[51] Different malarial drug

targets are required and therefore, a better understanding of the key biological processes of the malarial parasites is necessary if the long term ideal goal of the eradication of malaria is ever to be realised.

1.2 Protein kinase structure and inhibition

The first direct evidence of enzymatic phosphorylation of a substrate came from Burnett and Kennedy in 1954.[52] Through the study of glycogen phosphorylase and subsequent discovery of phosphorylase kinase, the use of protein phosphorylation as a regulatory mechanism was identified by Krebs and Fischer later that decade.[53, 54] It is now understood that, partnered with protein phosphorylases,[55] protein kinases (PKs) mediate the majority of signalling and coordinate complex events in eukaryotes.[56, 57, 58] Eukaryotic protein kinases (ePKs) fall into two super-families: serine/threonine kinases, ubiquitous in eukaryotes; and tyrosine kinases, found in metazoa but missing in most unicellular eukaryotes.[59, 60]

1.2.1 Structure

With the first crystallisation of a protein kinase (PKA),[61, 62] it was possible to observe the overall architecture of the protein kinase superfamily. This allowed the conserved sequence motifs identified by Hanks and Hunter using the sequences of amino acids in kinase domains[63] to be mapped on to a three-dimensional structure, revealing their location and allowing for their functional identities, such as the recognition of substrates,[61] to be unveiled.

Kinase domains of ePKs have three separate roles: 1. Binding and orientation of the phosphate donor ATP, or sometimes GTP;[64,65] 2. Binding and orientation of the peptide substrate; and 3. transfer of γ-phosphate of ATP to the acceptor amino acid residue

(serine, threonine or tyrosine) of the peptide substrate. These kinase domains consist of twelve subdomains across two distinct lobes (**Figure 1.10**), which are well conserved across >95% of ePK sequences. The smaller N-terminal lobe, containing subdomains I to V, anchors the nucleotide whilst the larger C-terminal lobe, containing subdomains VIA to XI, is responsible for the binding of the substrate and initiating phosphorylation. Subdomain V spans the two lobes and the cleft between the two lobes is the catalytic site.[63]

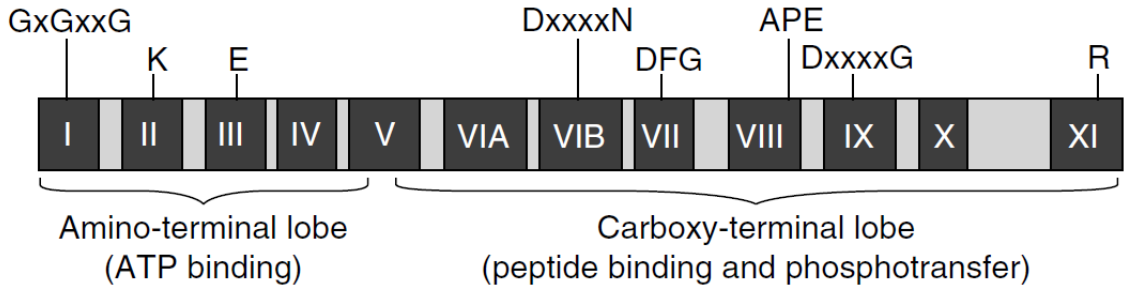

Figure 1.10: The ePK catalytic domain showing the twelve conserved subdomains (I-XI). The locations of highly conserved amino-acid residues and motifs throughout the ePK superfamily are indicated above the domains.[291]

Subdomain I at the N-terminus of the catalytic subunit contains the conserved motif GxGxxG and is predominantly β-strand in structure. These β-strands act as a flap to anchor the α- and β-phosphates of ATP and provide a hydrophobic pocket for the enclosure of the adenine ring. Subdomain II contains a lysine essential for maximal activity due to it orientating ATP by interacting with the α- and β-phosphates. Subdomain III is made up of a large α-helix containing a conserved glutamate, which forms a salt bridge with the lysine in subdomain II, thereby stabilising the interactions of subdomain II with ATP. Subdomain IV contains almost no conserved residues and has no direct involvement in catalysis or substrate recognition. Subdomain V links the small and large lobes of the catalytic subunit and three residues in this linking strand

form hydrogen bonds with the adenosine of ATP, which help to anchor it into position.[63]

Subdomain VIA in the C-terminus lobe is thought to support subdomain VIB, which is folded into two β-strands with a joining loop. This loop has been coined the catalytic loop because it contains a conserved aspartate that acts as the catalytic base – accepting a proton during phosphotransfer. The conserved aspartate residue is part of the conserved sequence DxxxxN, where the conserved asparagine residue chelates the Mg^{2+} that bridges the α- and γ-phosphates of ATP.[63]

Subdomain VII contains the highly conserved DFG triplet, the aspartate of which chelates the Mg^{2+} that bridges the β- and γ-phosphates of ATP; therefore, this residue helps to orientate the γ-phosphate for transfer to the serine/threonine/tyrosine residue of the substrate. The phenylalanine interacts with two hydrophobic residues in the small lobe.[66] Subdomain VIII is known to play a role in the recognition of peptide substrates and contains a highly conserved sequence, APE. Together these subdomains are known as the activation segment[54,67] and phosphorylation of one or more residues in this segment converts the kinase from its inactive to its active form. This can be by causing changes in the orientation of catalytic groups and substrate binding groups as well as the re-positioning of bulky R-groups that may block the catalytic site in the inactive conformation.[68] Control by phosphorylation is a feature of most but not all protein kinases;[67,69] this can be by autophosphorylation, particularly of tyrosine kinases, or as part of an enzyme cascade.[68]

Subdomain IX forms an α-helix, which helps to define the internal architecture of the ePK and contains an almost invariant aspartate residue.[54] Subdomain X is the most

poorly conserved subdomain. Subdomain XI contains a conserved arginine that forms an ion pair with the highly conserved glutamate of the APE sequence in subdomain VIII, thus stabilising the large c-terminal lobe.[63]

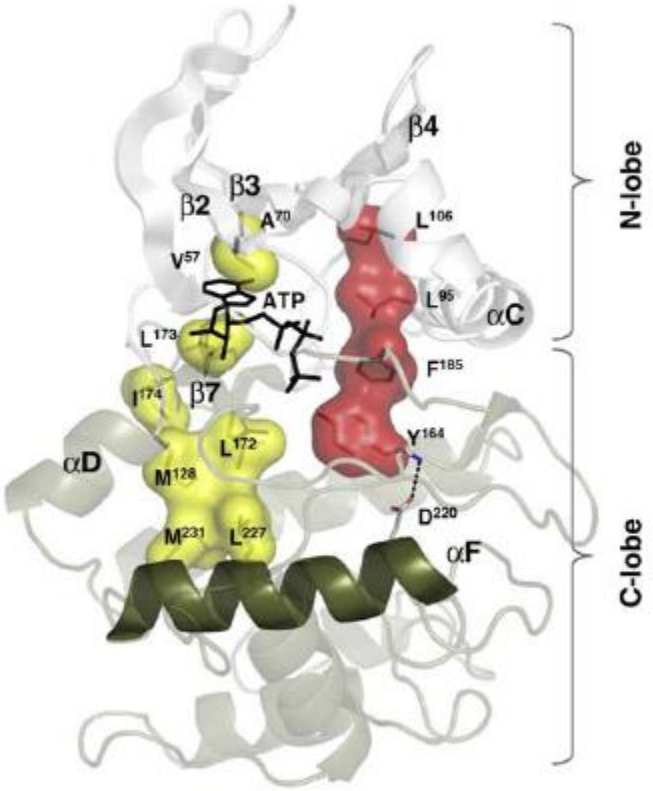

Figure 1.11: The R-spine (red) and C-spine (yellow), which is completed by the ATP molecule, are anchored to the α-helix of subdomain IX (green). Together these spines span the whole kinases domain, providing a connection between the two lobes.[54]

There are other features of ePKs that are not evident from the sequence of amino acid residues alone; for example, the regulatory spine (R-spine) and the catalytic spine (C-spine) consists of non-consecutive residues (**Figure 1.11**). The R-spine comprises four hydrophobic residues, two from the N-terminal lobe and two from the C-terminal lobe, and is anchored to the α-helix of subdomain IX. [54] The C-spine is also bound to the α-helix of subdomain IX and consists of residues from both lobes but is completed by the adenine ring of ATP.[70] The gate keeper residue is positioned between the C-spine and the R-spine and plays an important role in kinases activation[71] through

stabilisation of the R-spine[72] and its steric bulk controls the size of inhibitors able to bind to the active site.[73]

1.2.2 The evolution of eukaryotic protein kinases and the human kinome

Eukaryotic protein kinase superfamily members have been identified and characterised from a wide variety of animal phyla, plants, fungi and protozoa; hence, the ancestor of PKs can be traced back to before the evolutionary separation of the major eukaryotic kingdoms.[63] The evolution of ePKs occurred in a divergent manner from eukaryotic-like kinases[54] that are abundant in prokaryotes. This is evident by, among other things, their shared DFG motif;[74] however, unlike eukaryotic-like kinases, ePKs are highly regulated. Typically regulation is initiated by an extracellular signal,[54] e.g. a hormone or neurotransmitter, which causes a chain of events resulting in the conformational change to the ePK, causing it to become activated or deactivated. Examples of this control are (de)phosphorylation of the kinase, the binding of a secondary messenger (e.g. calmodulin binding to calmodulin-dependant protein kinases) and altering the level of expression of a regulatory subunit of the kinase.[68]

Advancements such as the sequencing of whole genomes, particularly the human genome project, have led to vast progressions in the field. The cataloguing of the protein kinase compliment of the human genome, the kinome, revealed that approximately 2% of genes in the human genome encode for ePKs.[57] This makes them among the largest families of genes in eukaryotes and illustrates their importance in regulating biological processes.[58, 63, 75]

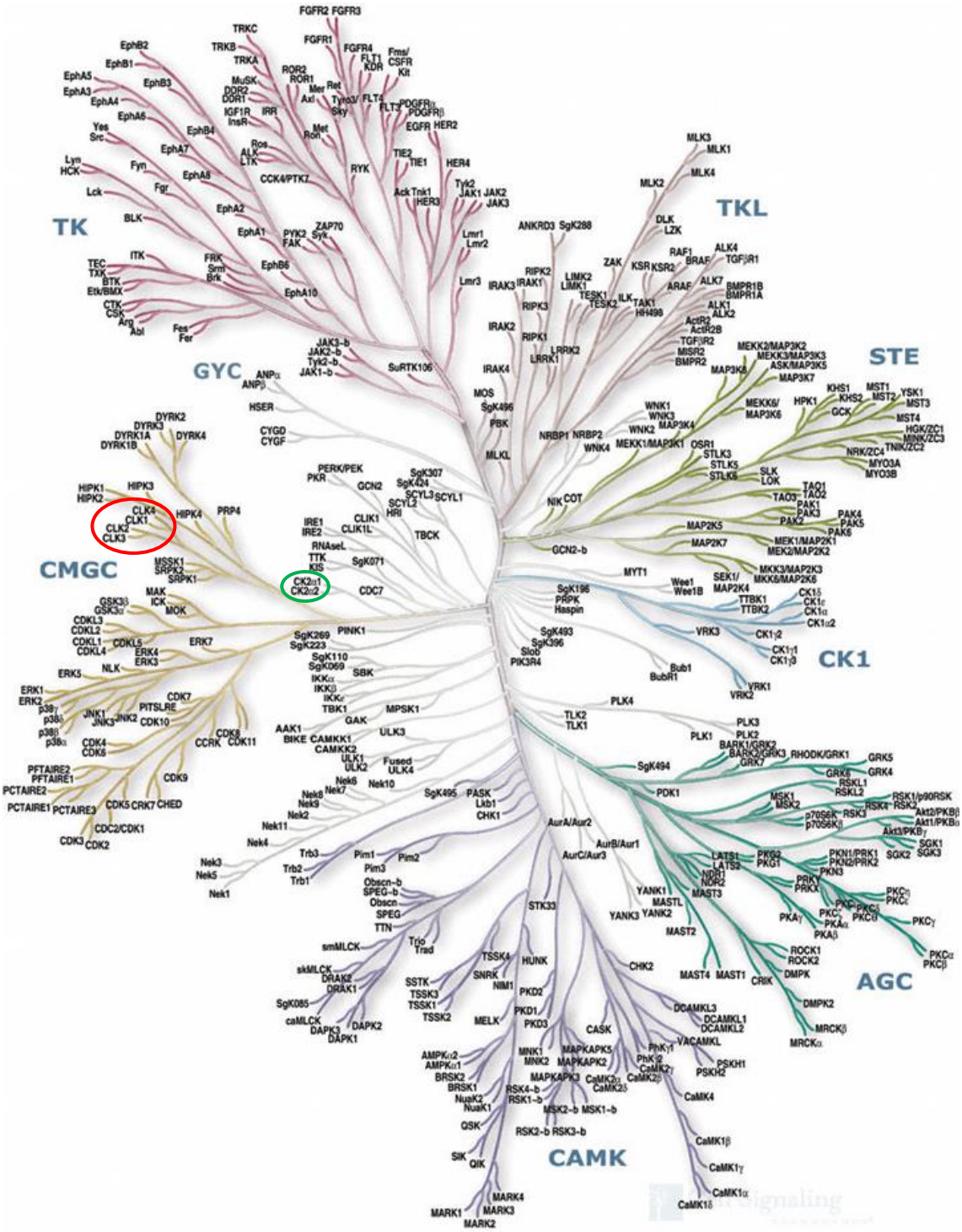

Figure 1.12: Phylogenetic tree of the complete human kinome showing the relationship between the kinase families. Each kinase is at the tip of a branch; the greater the similarity between the kinases the closer they are on the tree. The CLKs are circled in red and CK2α in green. Adapted from http://www.kinase.com[57]

Categorised by the amino acid sequence of their catalytic domain, the sequence similarity and structure of non-catalytic domains and the known biological functions, along with similar classifications made in other organisms,[58] the 518 (478 typical and 40 atypical) protein kinases of the ePK superfamily are divided into eight distinct groups. The human kinome has been mapped on a phylogenetic tree to show the relationship between the groups of kinases and families within those groups (**Figure 1.12**); the closer kinases are on the tree the more similar their structure and function. The eight groups are:

- AGC
- CAMK
- CK1
- CMGC
- RGC
- STE
- TK
- TKL

The AGC group, named after the kinases PKA, PKG and PKC, holds 60 of the 518 human protein kinases. Activation often involves phosphorylation of two highly conserved regulatory motifs; one is located in the activation segment (subdomains VII and VIII) and the other in a hydrophobic motif common in the non-catalytic domain of members of the AGC group. This group has a preference for the phosphorylation of Ser/Thr residues near Arg and Lys. Secondary messengers, such as cAMP for PKA, are required to induce activity in many kinases of the AGC group.[57, 76]

The CAMK group are also basophilic Ser/Thr kinases;[77] their relationship with the AGC group is depicted by their closeness on the phylogenetic tree (**Figure 1.12**). Most members of the group are activated following binding of Ca^{2+} or calmodulin to a small domain that is C-terminal to the catalytic domain.[78]

The CK1 group is small but these ePKs are essential, found in all eukaryotes and do not contain the APE in subdomain VIII or the arginine in subdomain XI that form a salt bridge in other ePKs.[79] Activity is controlled by extra cellular stimuli, the subcellular localisation of the kinases, interaction with cellular structures and proteins, inhibitory phosphorylation of the C-terminal regulatory domain and dephosphorylation or cleavage of this domain to restore activity. Functions of this group include the phosphorylation of proteins involved in the control of cell differentiation, proliferation and chromosome segregation. Mutations in CK1 kinases are linked to cancer and neurodegenerative diseases, e.g. Parkinson's disease.[80, 81]

The CMGC group is a large group of kinases found in all eukaryotes and includes CDKs, MAP kinases, GSKs and CDK-like kinases. CDKs, or cyclin-dependent kinases, regulate progression through different stages of the cell cycle. Thus, genetic or epigenetic alterations in CDKs/CDK control factors resulting in sustained proliferation devoid of control by external signals and thus, are associated with tumour progression.[82] MAP kinases, or mitogen-activated protein kinases, have key roles in the regulation of processes such as cell proliferation, differentiation and cell death. MAP kinases are abundant in the central nervous system and links between these kinases and psychiatric disorders are beginning to materialise. GSKs, glycogen synthase kinases, are involved in the insulin signalling pathway, which regulates glycogen synthase; the *Wnt* pathway, which is essential in embryonic development; and are also thought to play a role in neurodegenerative diseases.[83] The CLK family and CK2, highlighted in (**Figure 1.12**) are also part of this group and discussed in more detail separately.

The RGC group, or receptor guanylate cyclases, is a small group of ePKs that are similar in sequence to the TK group and are often grouped with soluble guanylyl cyclase receptors located in the cytoplasm. Found in metazoan but not fungi, plants and protists, these enzymes have some properties that are different to other Ser/Thr kinases. They function as receptors for peptide ligands and have four characteristic domains: an amino-terminal extracellular domain, a transmembrane region, an intracellular protein kinase-like domain and a carboxyl terminal guanylate cyclase catalytic domain. When a peptide ligand binds to the extracellular domain, the catalytic domain is activated and cGMP produced.[84, 85]

The STE group includes a large number of protein kinases involved in MAP kinase cascades and therefore, they have a central role in cell signalling and are vital in the amplification of signals from extracellular stimuli and the response of a cell to changes in its environment.[86]

The tyrosine kinase (TK) group is a set of ePKs that specifically phosphorylate tyrosine residues; this makes them distinct from dual specificity kinases, which also phosphorylate Ser/Thr resides. This branch of the phylogenetic tree can be divided into receptor[87] and non-receptor tyrosine kinases. TKs are not ubiquitous across eukaryotes; however, tyrosine phosphorylation in metazoans is essential for processes such as organ development, transcriptional control, maintenance of stem cells (e.g. vascular growth factor receptors) and tissue homeostasis. Abnormalities in tyrosine phosphorylation are closely related to various forms of cancer and congenital syndromes such as dwarfism.[59, 88]

The tyrosine kinase-like (TKL) group are Ser/Thr protein kinases that have close sequence similarity to tyrosine kinases. They are virtually absent in fungi but strongly represented in metazoans and photosynthetic organisms. In animals they are tightly integrated with signalling pathways and consequently, have significant roles; for example, mixed lineage kinases (MLKs) are involved in MAP kinases cascades and are responsible for activating apoptotic pathways implicated in Parkinson's disease.[89]

There are also small families of atypical protein kinases (aPKs), which are not closely related in sequence to ePKs and lack the twelve subdomains that define ePKs; however, they show kinase activity.[57, 90, 91]

1.2.3 The malarial kinome

In 1996 an international effort to sequence the *P. falciparum* genome was launched[92] and in 2002 the full genome sequence was published.[21] Initial comparisons of the *P. falciparum* genome with other genomes showed that 60% of the predicted genes could not be assigned functions.[93] This paved the way for exciting new opportunities in the study of biological processes involved in the life-cycle of *P. falciparum*, providing hope of the discovery of new drug targets. As a consequence of this work, it was possible to map the entire *P. falciparum* kinome and classify the kinases into the ePK groups.

Within *P. falciparum* 65 ePKs and 21 FIKK kinases (**Section 1.2.3.3**) have been identified.[90] Although much smaller than the 518 human ePKs identified, as with humans,[57] this figure represents 2% of genes in the malarial genome.[94] The primary sequences of these kinases have been used to assign them into groups according to the characteristics of their twelve catalytic domains. Although many of these proteins

conform to the model described by Hanks and Hunter,[63] there are often large insertions of charged or polar residues present both within and in between these domains.[95] This diversity provides the potential to selectively target *P. falciparum* kinases over their human counterparts not only as antimalarial agents but also for investigating their roles in the cellular processes of the parasite. Comparing human and *P. falciparum* ePKs using a phylogenetic tree (**Figure 1.13**) not only highlights that this species of the parasite is missing members of the STE and TK groups but also draws attention to the presence of orphan kinases.[90]

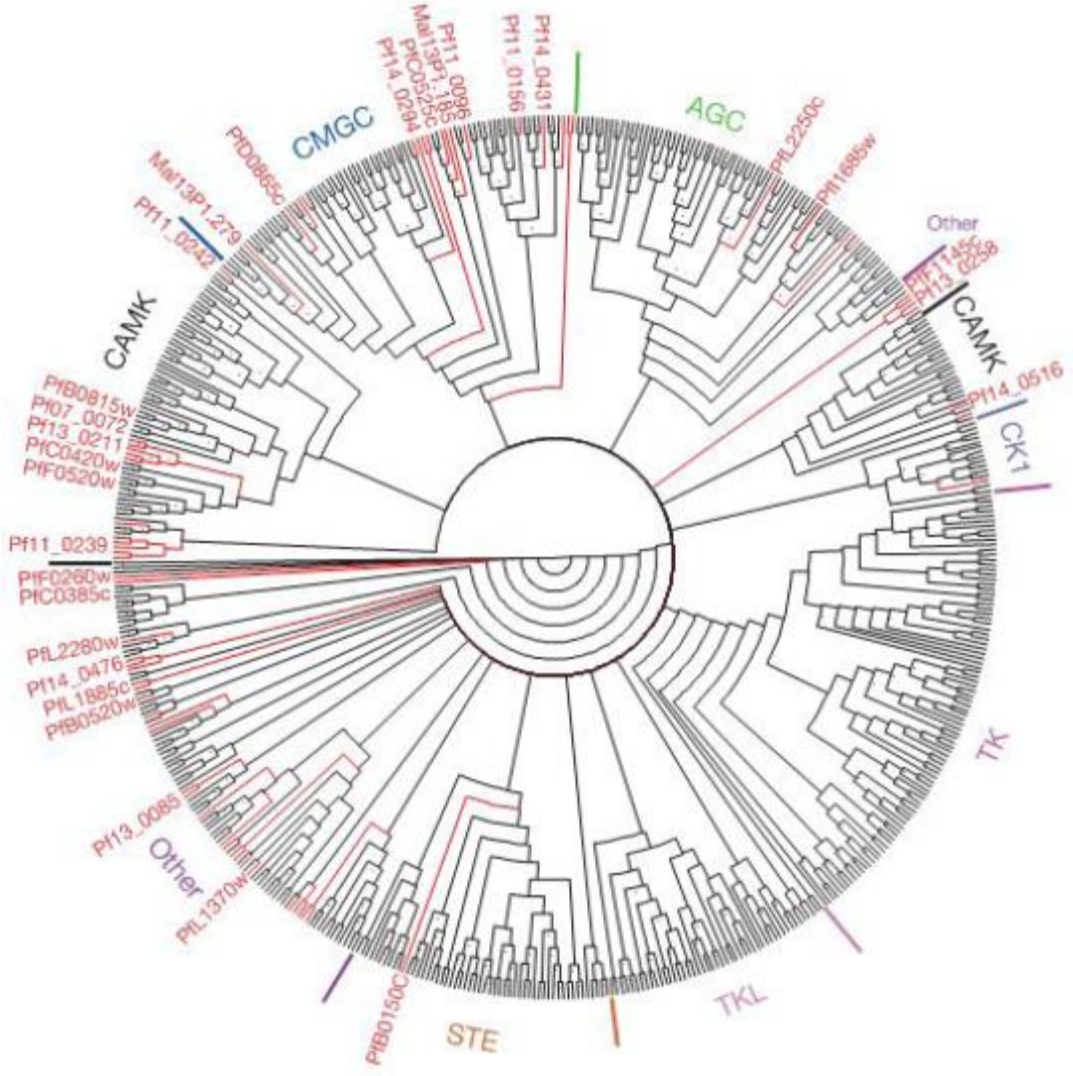

Figure 1.13: Phylogenetic tree of combined human and *P. falciparum* kinomes. Human lineages are coloured black and *P. falciparum* red.[292]

1.2.3.1 *The ePk groups present in P. falciparum*

There are five malarial kinases in the AGC group. Two PKA homologues have been identified and the PKG homologue has been shown to be expressed in the intraerthrocytic asexual stage of the parasite. However, there seems to be no clear PKC analogue.[96] The CAMK group is well represented in the malarial kinome with 13 kinases, indicating the importance of calcium signalling in the parasite.[97] CAMK activity has been shown to be essential for ookinete development in the mosquito vector and the CAMK kinase *Pf*CDPK4 has been found to be crucial for the development of the male gametocyte in the mosquito.[98]

The CK1 group only has one member in the *P. falciparum* kinome, which shows high sequence similarity with human CK1.[95,99] A dramatic example of the expansion of some ePK families in some organisms compared to others is the contrast in the size of the CK1 group between *P. falciparum* (1 gene) and *C. elegans* (85 genes).[90]

With 18 kinases, the CMGC group is the largest ePK group in *P. falciparum*. This includes six enzymes related to the CDKs,[100,90] two related to the MAP kinases[101,102,103] and three related to the GSK3 kinases.[104,105] In other eukaryotes most CMGC kinases are involved in the control of cell proliferation and development; therefore, their abundance in the *P. falciparum* kinome could be due to the variety of proliferation processes that occur during the complex malarial life-cycle. Also within the CMGC group is the single orthologue of CK2α [PF11-0096]. Most eukaryotes have two or more α-subunit encoding genes, highlighting the relative simplicity of the *P. falciparum* kinome.[90]

After further analysis, the five[90] *P. falciparum* enzymes originally constituting the TLK group have been reduced to four with *Pf*TKL3 being characterised as a semi-orphan kinase because it lacks a clear human orthologue.[106]

1.2.3.2 *The ePK groups missing from P. falciparum*

The RGC group is missing from protists and no *P. falciparum* protein kinases have been found within the STE group.[90] This supports the failure in *in vitro* and *in silico* work to establish the presence of MAPKK malarial homologues; however, the NIMA-related enzyme *Pf*nek-1 (*vide infra*) acts with *Pf*map-2 for the phosphorylation of exogenous substrates.[107] As is the case with most unicellular eukaryotes, the TK group is missing from *P. falciparum*.[59]

1.2.3.3 *Other kinases of P. falciparum*

There is a group of five *P. falciparum* genes that form the NIMA-related (Nrk) cluster, which are related to the Nek family, including the well characterised *Pf*Nek1 kinase. These enzymes are important in mitotic control.[90, 108, 107] There are several kinases that do not fit within any defined group or form small satellite clusters. Known as orphan kinases, two examples are three enzymes at the base of the CAMK and AGC branches, including *Pf*KIN [PF140516], which is known to be expressed in gametocytes;[109] and a group of three malarial kinases, including *Pf*PK4 [MAL6P1.416], which is expressed during intraerythrocytic development,[110] that form a distinct cluster associated with the NIMA group.[90]

Within the *P. falciparum* kinome there are several composite enzymes, that is enzymes with features from more than one established ePK family. For example, *Pf*PK6 and *Pf*crk-4 are composite enzymes with features of both CDKs and MAP kinases; *Pf*PK7 has

a C-terminal analogous to those conserved in MAPKKs and an N-terminal analogous to PKA but does not display the expected MAPKK activation site.[90, 111]

A novel group of 21 ePK-related proteins form a tight cluster in *P. falciparum*. Due to the Phe-Ile-Lys-Lys motif found in subdomain II of their catalytic domain, the cluster is named the FIKK group. These kinases all have a highly variable N-terminal extension and contain a region similar to the ePK catalytic domain that, despite large insertions in the catalytic domain typical of *P. falciparum* ePKs, has most of the conserved residues of ePKs. However, none of the FIKK enzymes possess the full GxGxxG motif present in subdomain I of ePKs.[90] Although this motif is involved in the positioning of the ATP molecule in the active cleft,[63] there are several enzymes throughout eukaryotes that have only one or two of these glycine residues but remain active; thus, this is unlikely to be detrimental to FIKK catalytic activity. There are also motifs that are fully conserved throughout the FIKK kinase group of *P. falciparum* and these were therefore used by Ward *et al.* to search for members of the FIKK group in other organisms. Sequences containing these motifs were only identified in *Apicomplexan* species.[90] Studies have shown FIKK proteins to be exported from the parasite to the host.[112]

A handful of aPKs have also been identified in *P. falciparum* using sequence comparisons with aPKs found in humans. These include two members of the ROI kinase family that are known to be involved in rRNA processing in *S. cerevisiae*.[90]

1.2.4 Kinases as potential antimalarial drug targets

Traditional searches for antimalarial drugs involve the screening of chemical libraries against erythrocytes infected with the parasite. Once a molecule has been identified that kills the parasite, the compound can be optimised and the molecular target searched for using resistance studies. The optimised drug can then be put into pre-clinical trials.[113] This approach can lead to the selection of compounds with multiple targets, reducing the possibility of parasites developing drug-resistance but potentially having greater toxicity to the host.

The sequencing of full genomes, including *P. falciparum*,[21] and the availability of high throughput screening methods led to the rational design molecular screening approach being favoured for the discovery of new drug targets for a wide range of diseases, including malaria. In this approach genomic data is used to identify a molecular target and knock-out parasites are developed to prove the target is crucial for parasite survival/proliferation. The target proteins are then expressed and purified for *in vitro* screening with chemical libraries. Hit compounds can then be optimised and put into pre-clinical trials. With this approach it is easier to ascertain the mode of action of the compound and therefore, gain a better understanding of the parasite.[113]

Protein phosphorylation regulates most aspects of cell life; consequently, abnormal levels of protein phosphorylation are a cause or consequence of diseases ranging from cancer to diabetes.[114] Therefore, there is a wide interest in the study of kinases, phosphatases and the phosphorylation pathways they are part of in order to obtain a better understanding of the mechanisms of many diseases. With a better understanding of a disease comes the ability to design effective new treatments. This

high research interest provides a bank of protein kinase knowledge from various fields to draw upon, including protein kinase inhibitors that can be used as reagents for the study of the physiological roles of protein kinases.

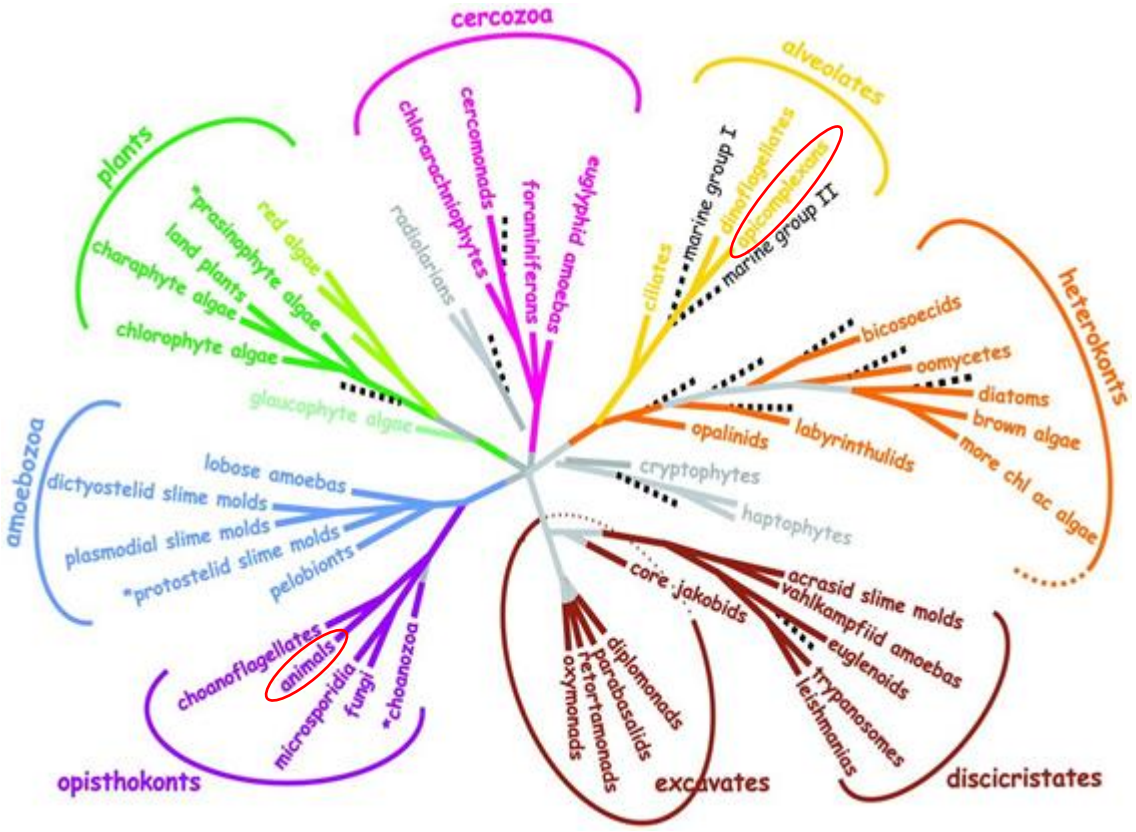

Figure 1.14: Phylogenetic tree showing the relationships between the major eukaryotic phyla. The animals and apicomplexans are circled in red to illustrate the distance between human and malarial kinomes. Adapted from Baldauf[293]

The large phylogenetic distance between *Plasmodium sp.* and animals (**Figure 1.14**) illustrates the divergence of the *Plasmodium* and human kinomes and thus, the potential of the *Plasmodium* kinome as a new antimalarial drug target. Some of these important divergences include: the absence of the TK, STE and RGC groups; the presence of orphan PKs, composite PKs and the FIKK PK family with no orthologues in humans; and the presence of a family of CDPKs fused to a calmodulin-like domain, which are found in plants but not metazoans.[16, 115]

Studies of the structures of a *P. falciparum* CDK, *Pf*PK5, and human CDK2 with a small molecule inhibitor (NU6102, **15**) bound to their respective ATP-binding pockets have revealed that, despite the general orientation of the inhibitor being similar in both kinases, there are subtle differences in the binding mode of the two enzymes.[116, 117] In spite of the inhibitor having a higher *in vitro* IC_{50} value for *Pf*PK5 over human CDK2 (215 nM and 5 nM respectively),[118] this has confirmed the idea that there is enough difference in the primary structure of most *Plasmodium* kinases compared to mammalian enzymes for species selective inhibition to be possible.[115]

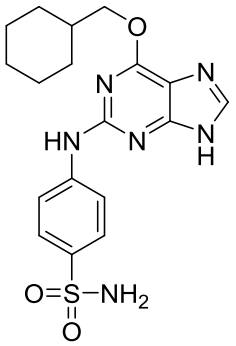

15

Figure 1.15: NU6102 (15), a small molecule kinase inhibitor.

1.2.5 Kinase inhibition

The conserved nature of the ATP binding site makes the interrogation of each kinase and the development of specific inhibitors challenging. However, due to the prevalence of abnormal phosphorylation in a wide variety of disease, kinases represent approximately one third of all protein targets under investigation by the pharmaceutical industry. This correlates to more than 130 protein kinase inhibitors in clinical development and many more in preclinical stages. To date, eleven kinases inhibitors have been launched as cancer chemotherapeutic agents and the only kinase inhibitor registered for non-oncology use is the immunosuppressant everolimus

(Certican®)[119] for the prophylaxis of organ rejection. All of these inhibitors target the ATP binding site except for everolimus.[120]

Most kinase inhibitors developed to date are ATP competitive inhibitors. Due to the conserved nature of the ATP binding site, most kinase inhibitors are not highly selective. Thus, kinase inhibition found through *in vitro* screening should be treated with caution.[121] Large-scale kinase selectivity screens have shown that selective inhibitors usually bind kinases that are grouped together on the kinome phylogenetic tree compared to more distant kinases.[122, 123] This lack of selectivity is one of the reasons why protein kinases inhibitors are currently predominately used in cancer chemotherapeutics; there is a greater tolerability for side effects during cancer treatment than for other conditions where treatment maybe lifelong.[120] As discussed earlier (**Section 1.2.1**), the cleft between the two N-terminal and C-terminal lobes forms the catalytic site of the kinase. Within this area is the conserved DFG motif of the activation loop, which helps to orientate the γ-phosphate for transfer. The activation loop can adopt different conformations from fully active to fully inactive, altering the state of the kinase.[120]

1.2.6 Types of kinase inhibitor

The original focus in the discovery of kinase inhibitors was to identify highly potent and specific compounds aimed at targeting a single kinase by imitating ATP binding; however, the lack of specificity of this approach can often be problematic. This has led to the optimisation of known inhibitors to fully exploit the target within the kinase, whether that is the ATP binding site or another region. The binding modes of these compounds can be broadly classified into covalent and non-covalent kinase inhibitors.

1.2.6.1 *Non-covalent kinase inhibitors*

Through the discovery of kinases inhibitors, serendipitously or otherwise, four types of non-covalent inhibitor have been identified type I, type I ½, type II and type III. The first group of small molecules found to target the ATP binding site are known as type I inhibitors. Although these inhibitors do not require a specific conformation of key structural elements, such as the DFG motif and the αC-helix,[124] they typically bind to an enzyme in the active "DFG in" conformation (**Figure 1.16**). Type I inhibitors mimic the interactions of the adenine ring with the hinge residues of the kinase through the formation one, two or three hydrogen bonds (**Figure 1.19**).[125]

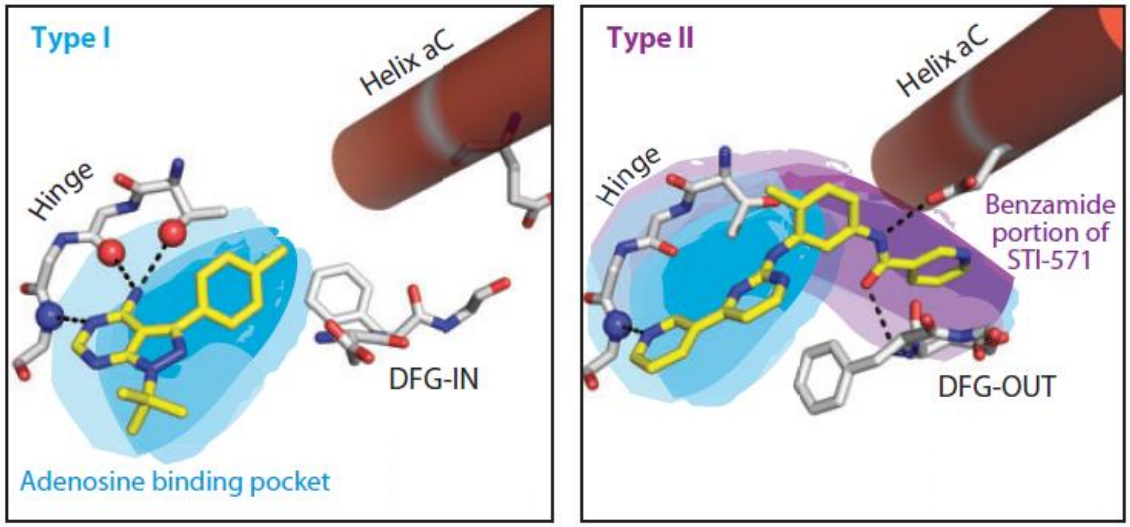

Figure 1.16: Type I and type II kinase inhibitors. Type I inhibitors do not require the αC-helix or the DFG motifs to be in a specific conformation for binding. Here PP1 (16) is shown in complex with HCK. These inhibitors sit in the ATP binding site (blue) and form hydrogen bonds with the hinge region. Type II inhibitors require the "DFG out" conformation for binding; this provides an extending binding pocket (purple). Here STI-571 (17) is shown in complex with Abl. Adapted from Da *et al.*[124]

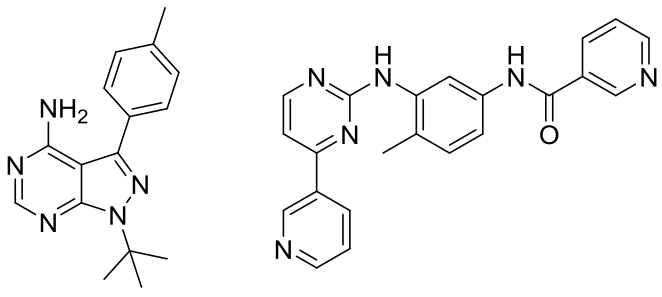

16 **17**

Figure 1.17: The type I inhibitor PP1 (16) and the type II inhibitor STI-571 (17).

The first kinase inhibitor on the drug market, imatinib (or Gleevec) (**18**), was found to bind to and stabilise the inactive "DFG out" form of the target kinase; these kinase inhibitors are referred to as type II inhibitors.[125] In the "DFG out" form the aspartate residue is flipped 180° compared to the "DFG in" conformation.[124] This results in the opening of an additional cavity, the allosteric site, which is hydrophobic (**Figure 1.16**).

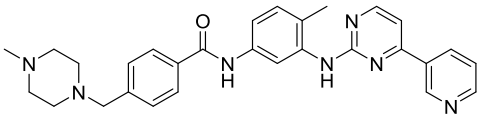

18

Figure 1.18: Imatinib (or Gleevec) (18) was the first kinase inhibitor on the drug market.

Not only do type II compounds bind to the hinge region in an analogous way to type I inhibitors, they also exploit hydrogen bonding and hydrophobic interactions in the allosteric site (**Figure 1.19**), including hydrogen bond formation with the conserved αC-helix. With this extra target site, type II inhibitors are usually more selective and potent than type I inhibitors. As kinases in the "DFG out" form have a higher K_m for ATP, type II inhibitors also face weaker competition from the high cellular ATP concentrations, resulting in enhanced *in vivo* activity.[126] Conversely, type II inhibitors have a higher molecular weight and thus, are likely to have reduced cell permeability and lower ligand efficiency.[125]

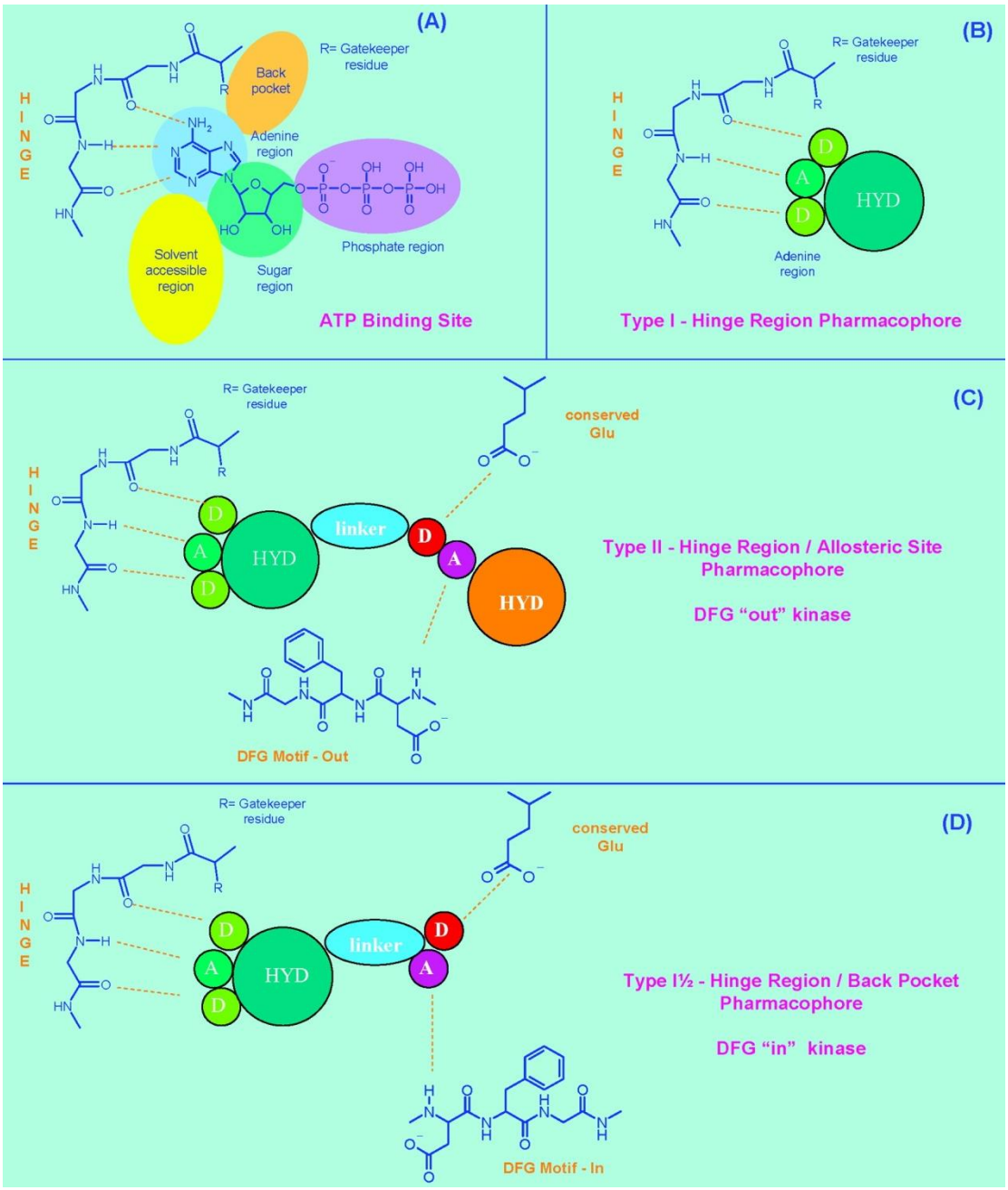

Figure 1.19: The interactions of ATP and type I, type I ½ and type II inhibitors with the ATP binding site. A: The regions of the ATP binding site – the adenine region (blue), the sugar region (green), the phosphate region (lilac), the back pocket (orange) and the solvent accessible region (yellow) – and the hydrogen bonds between the adenine ring and the hinge region are shown; B: Type I inhibitors form hydrogen bonds with the hinge region; C: Type II inhibitors form hydrogen bonds with the hinge region as well as interact with the allosteric region that is available in the "DFG out" conformation; D: Type I ½ inhibitors form hydrogen bonds with the hinge region and can extend into the back pocket due to the presence of smaller gatekeeper residue.[125]

The type III kinase inhibitors are non-ATP competitive inhibitors; i.e. they block kinase activity without displacing ATP and bind exclusively to the allosteric site.[124] Areas outside the catalytic domain are far more divergent than the catalytic site, offering the prospect of high selectivity;[127] however, it is difficult to know which sites to target and consequently designing inhibitors is problematic. Analysis of more recently published kinase inhibitors identified a new type of compound, which have been coined type I½ inhibitors owing to them exhibiting some properties of both type I and type II inhibitors.[125] These compounds target the back cavity of the ATP binding site in either the active "DFG in" and "αC-helix in" conformation or in the inactive "DFG in" and "αC-helix out" conformation. The back cavity is mainly hydrophobic and is not occupied by ATP. Access to this cavity is controlled by the gatekeeper residue, which is the first residue of the hinge connecting the C-terminal and N-terminal lobes (**Figure 1.19**). When the gatekeeper residue is large, e.g. phenylalanine, access to the cavity is blocked; when the gatekeeper is smaller, e.g. threonine, the R-group of the gatekeeper does not restrict access to the cavity. Therefore, kinases with a small gatekeeper can be targeted with bulky substituents to provide potent and selective inhibition.

An example of selectively targeting a kinase of a protozoan is the inhibition of CDPK1 in *T. gondii* and *C. parvum* using pyrazolopyrimidine compounds containing bulky substituents (e.g. **19a-c**), which do not prevent proliferation in human cell lines[128] and are not toxic to mice.[129] This is possible due, not only to CDPKs not being present in humans, but also to the presence of glycine at the gatekeeper residue of CDPK1 in *T. gondii* and *C. parum* compared to larger gatekeeper residues in all known human kinases.[130,131] This work led to the study of bulky pyrazolopyrimidine analogues, such

as BKI-1 (**20**) and NA-PP2 (**21**), as inhibitors of *Pf*CDPK4,[132] a kinase required for exflagellation in *P. falciparum* microgametes.[133] *Pf*CDPK4 has a serine gatekeeper residue, smaller than that of most mammalian kinases, and a binding pocket very similar to those found in *Cp*CDPK1 and *Tg*CDPK1.[129] The high selectivity, low toxicity and the high oral bioavailability of these compounds, as well as the ability to readily generate them from simple starting materials, holds promise that these drug molecules could be used to prevent malaria transmission to humans.[132]

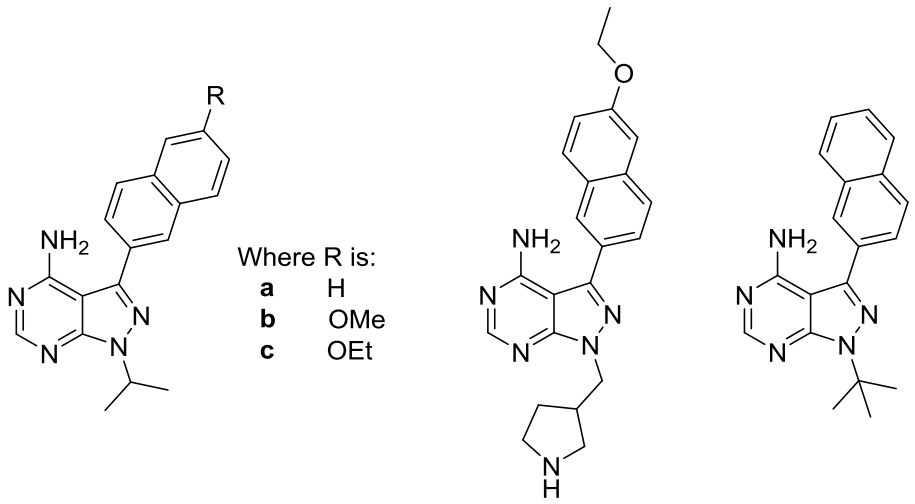

19 **20** **21**

Figure 1.20: Pyrazolopyrimidine compounds containing bulky substituents such as 19a-c, 20 & 21 selectively inhibit CDPKs due to the presence of a glycine gatekeeper residue.

1.2.6.2 *Covalent kinase inhibitors*

Covalent inhibitors usually form a bond to a cysteine residue in or around the active site and thus, prevent the binding of ATP to the protein kinase.[120] A kinase inhibitor is only efficacious when bound to the kinase; hence, the dissociation constant (K_d) plays an important role in the efficacy of an inhibitor. Kinase inhibitors with covalent irreversible binding can, therefore, achieve the ultimate goal; they can maintain efficacy until *de novo* synthesis of the target protein. However, irreversible inhibitors

have only been developed for a small number of kinases.[134] Protein kinases do not use active site cysteine residue in their catalytic cycle; hence, irreversible kinase inhibitors depend upon non-catalytic cysteine residues adjacent to the ATP binding site.[135] Kwarcinski *et al.* exploited the non-conserved cysteine (present in 1.4% of kinases) in the glycine rich loop of c-Src, a tyrosine kinase frequently overexpressed in cancerous tumours and linked to Herceptin resistant breast cancer cell lines,[136] to irreversibly inhibit c-Src. Kwarcinski's work showcases the ability of irreversible inhibitors to have a greater potency and selectivity than their reversible counterparts. [135]

1.2.7 Resistance to kinase inhibitors

The most common single amino acid residue mutation leading to drug resistance occurs at the gatekeeper residue of the kinase because, although this residue plays no part in the binding of ATP, it is often in close contact with type I and type II inhibitors. This gatekeeper mutation usually prevents the inhibitor binding by sterically blocking the site.[120]

As a result of the ever increasing resistance to current antimalarial agents, new drugs with novel modes of action are required. A better understanding of the key biological processes of the malarial parasites is necessary to achieve this. Protein kinases, in partnership with proteases, mediate the majority of signalling in eukaryotes[56,57,58] and thus, understanding the function of kinases in *P. falciparum* would provide innovative targets for drug molecules. Methods for the study of phosphorylation processes within *P. falciparum* are, therefore, required.

1.3 Chemical genetics

Chemical genetics is the use of small molecule tools for the study of biological systems. Classical genetics, which uses mutagenesis to investigate the relationship between genotype and phenotype, and chemical genetics can both be divided into the forward and reverse approach.

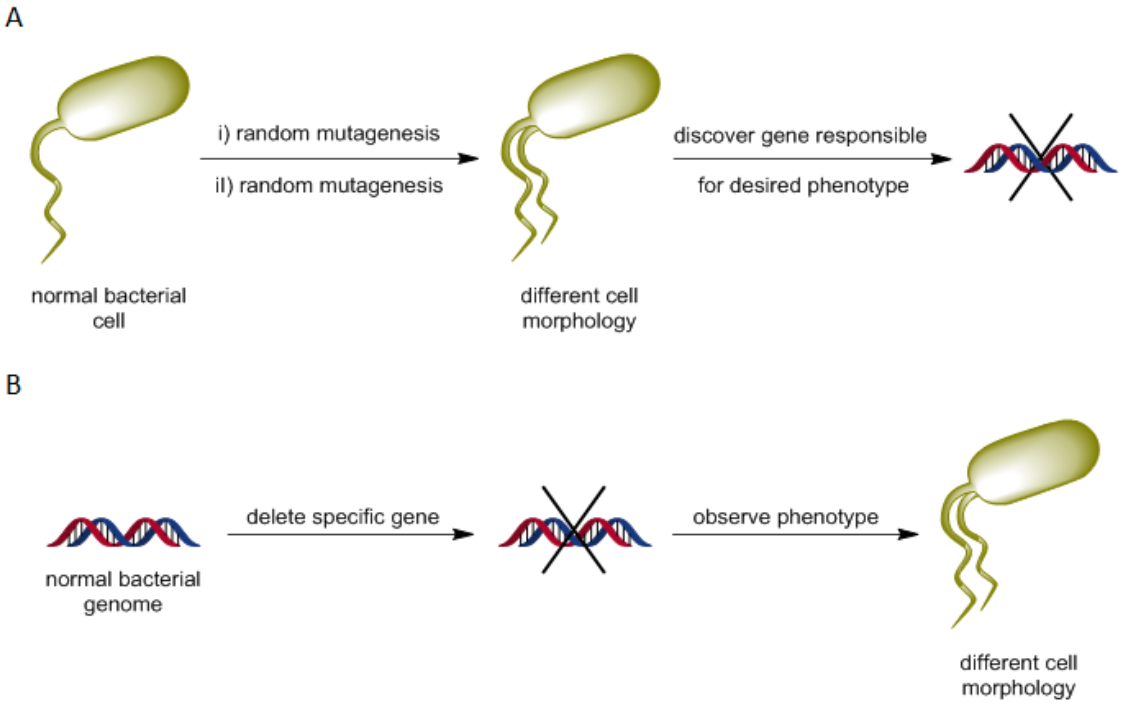

Figure 1.21: Classical genetics. A: Forward classical genetics uses random mutagenesis to produce a different cell morphology. The gene responsible is identified through mutation mapping; B: Reverse classical genetics mutates a specific gene and observes the resultant change(s) in phenotype.

Forward classical genetics (**Figure 1.21A**) aims to identify the genes responsible for the phenotype of interest. Through the use of DNA damaging agents or radiation, random mutant strains are formed and screened for the phenotype of interest. The gene responsible for the phenotype can then be found through mutation mapping. Reverse classical genetics (**Figure 1.21B**) aims to identify the role of a gene of interest. Firstly, a gene of interest is selected; secondly the gene is mutated; and thirdly the phenotypic differences between the mutant and wildtype are observed.[137]

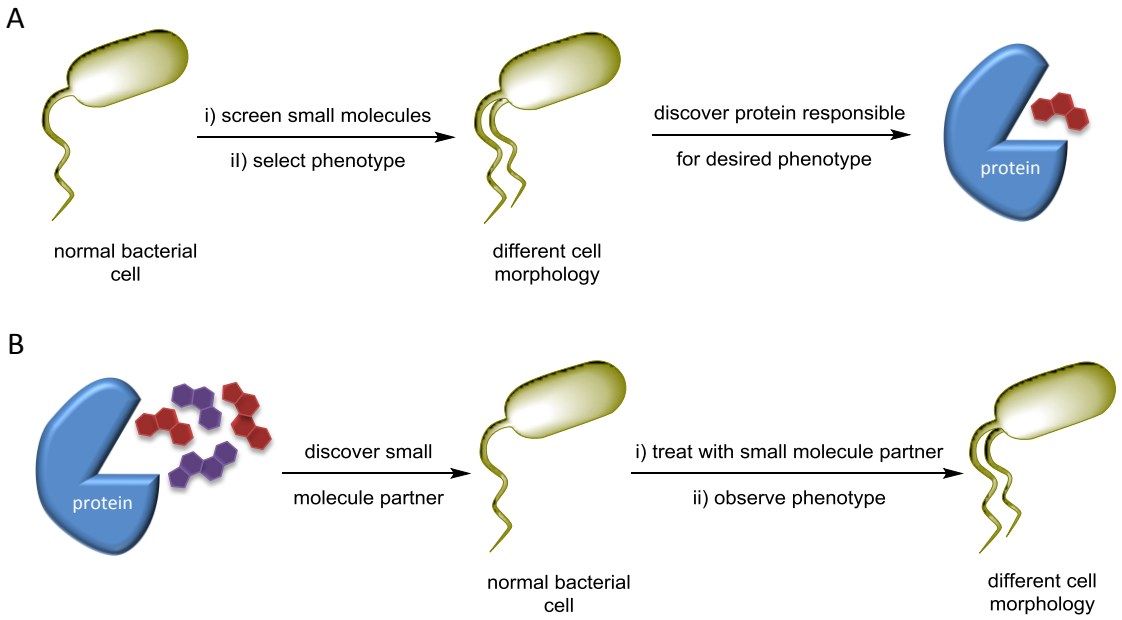

Figure 1.22: Chemical genetics. A: Forward chemical genetics uses small molecules to alter phenotype. The protein responsible for this phenotype is then identified. B: Reverse chemical genetics screens a library of small compounds against a target protein to identify a hit compound. This hit compound can then be introduced to a cell and the changes in phenotype observed.

Forward chemical genetics (**Figure 1.22A**) uses small molecules to alter phenotype. Compounds that induce a phenotype of interest are then selected and their target identified, providing insight into the function of the protein and the role of the gene. Reverse chemical genetics (**Figure 1.22B**) screens a library of compounds against a target protein to disrupt its function. Once a hit compound is identified it can be introduced into a cell and the phenotypic changes can be studied.[137]

Chemical genetics offers several advantages over classical genetics. The application of classical genetics is limited in higher organisms, particularly mammals, due to their diploid genome; physical size; and slow rate of reproduction. Chemical genetic studies can be applied at will to organisms, including mammals, allowing for dose dependant experiments to be carried out. Chemical genetic studies are particularly important for the analysis of the function of genes that are essential for survival of the organism and

thus, cannot be knocked out without causing lethality. Multi-functional proteins can have several binding partners; therefore, selective ligand binding has the potential to modulate individual functions. In classical genetics the knockout would delete the protein and remove the possibility of investigating its other functions.[137, 138, 139]

The main disadvantage of chemical genetics is the identification of a small molecule that is selective for the gene product of interest. Finding highly specific molecules, which do not yield off target effects, remains a significant challenge; hence, this approach has been combined with other tools for probing protein function, such as site directed mutagenesis (**Section 1.4.2.1**).[137, 138, 139]

1.4 Using a chemical biology toolkit to explore protein kinases

The interest in understanding disease to afford new treatments has required scientists to develop new techniques to aid in the unravelling of biological processes. A wide variety of biological and chemical techniques have been adopted to produce a chemical biology toolkit for exploring phosphorylation reactions catalysed by protein kinases. This requires not only using inhibitors to exploit naturally occurring differences between protein kinases but also engineering protein kinases, modifying protein/peptide substrates and the design of ATP derivatives and inhibitors.

1.4.1 Inhibitor design

Protein kinase inhibitors are not only important for the treatment of diseases but also in the probing of biological systems in order to gain a better understanding of the physiological roles of protein kinases in cellular networking.[56,120] By designing inhibitors that have bulky substituents in appropriate trajectories, the allosteric site and back pocket available in some kinases can be exploited.[140] For example, Cohen *et*

al. exploited the combined presence of a small threonine gatekeeper (present in ~20% of human kinases) and a cysteine in a position of the glycine rich loop of subdomain I usually occupied by a valine to selectively target three kinases: RSK1; RSK2; and RSK4, using bulky electrophilic inhibitors such as fmk (**22**).[131] This provided the ability to study the phosphorylation pathways of RSKs, which are poorly understood; however, mutations in the RSK2 gene are known to cause Coffin-Lowry syndrome, a human disorder characterised by severe mental retardation.[141]

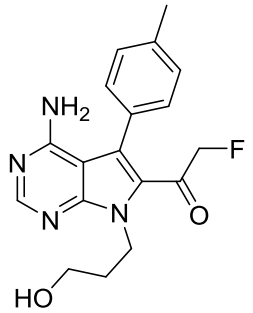

22

Figure 1.23: The bulky electrophilic inhibitor, fmk (22), designed to react with an uncommon cysteine reside present in RSKs.

1.4.2 Engineering protein kinases

Due to the conserved nature of the ATP binding pocket across the protein kinome, a number of methods have been developed that use genetic engineering to modify the kinase domain. These include site-directed mutagenesis, chemical ligation, nonsense suppression and cross-linking.

1.4.2.1 *Site-directed mutagenesis*

Site-directed mutagenesis can be used to modify specific amino acid residues within the ATP binding site, causing the ATP binding site to have different special properties and/or functional groups. This allows ATP derivatives and inhibitors to target the

kinase of interest with a high affinity and specificity, permitting the study of the kinase of interest and its substrates in complex mixtures such as cell lysates and *in vivo*.

Extensive work by Shokat *et al.* has shown that mutation of the gatekeeper residue from a medium sized gatekeeper residue (e.g. methionine (**27**), the most common gatekeeper) to a small amino acid residue (such as glycine (**23**) or alanine (**24**)) allows access to the back cavity of the ATP binding site.[142] This permits the binding of an ATP analogue with a bulky substituent in the N_6 position (e.g. compound **28**) or a bulky inhibitor (e.g. **16** and **29**), which is not possible in the wildtype kinase (**Figure 1.25**).[71] Initially developed for the study of v-Src in fibroblasts,[142] this approach has been used in the study of a variety of enzymes such as CDK2[143] and PKA[144] and has led directly to the identification of some kinase substrates; e.g. substrates of CDK1[145] and ERK2.[146]

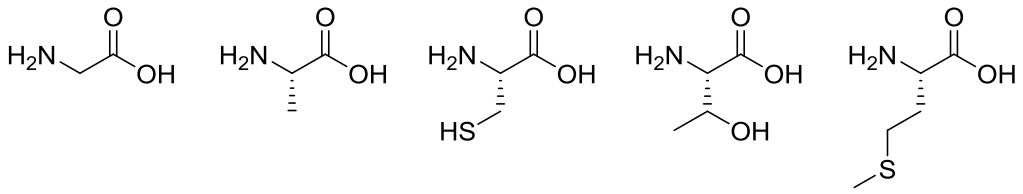

23 **24** **25** **26** **27**

Figure 1.24: The structures of the amino acids glycine (23), alanine (24), cysteine (25), threonine (26) and methionine (27). Methionine (27), the most common gatekeeper residue, is much larger than glycine (23) and alanine (24); therefore, forming the glycine or alanine gatekeeper mutant opens up access to the back pocket, which would otherwise be blocked by R-group of methionine (27). The relatively conserved geometry between threonine (26) and cysteine (25) can be readily seen.

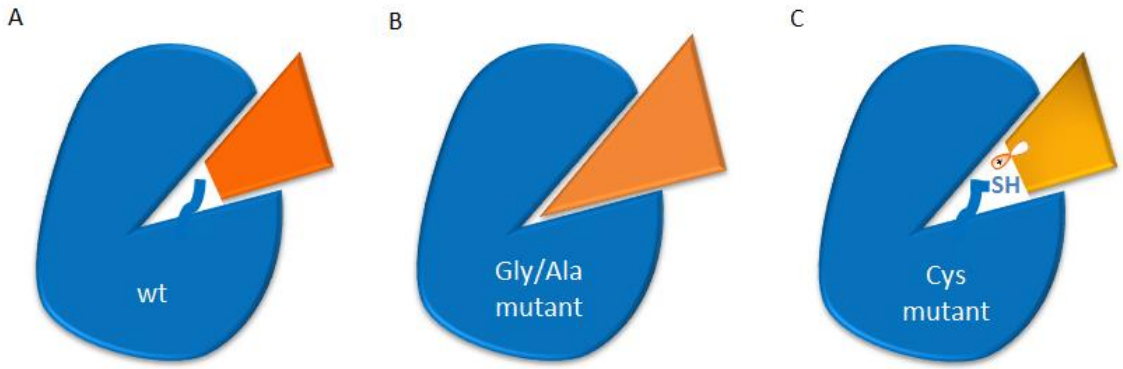

Figure 1.25: A schematic representation of an enzyme with different gatekeeper residue mutations. Enzymes are shown in blue and inhibitors in orange. A: wildtype kinases usually contain a medium sized gatekeeper residue (e.g. Met), which blocks access to the back pocket of the ATP binding site; B: Glu/Ala mutants allow much bulkier inhibitors to bind to the active site by allowing access to the back pocket; C: Cys mutants retain a similar geometry to the wildtype but can form covalent bonds with an electrophilic inhibitor.

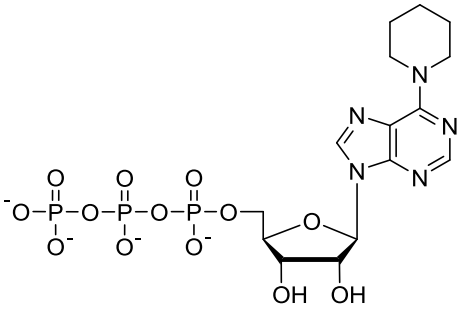

28

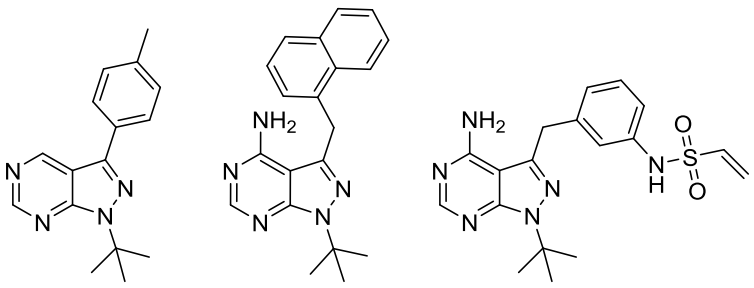

16 **30** **31**

Figure 1.26: An example of an N_6-modified ATP derivative (28); the inhibitor PP1 (16); a bulky analogue of PP1, 1-NM-PP1 (30); and an example of an electrophilic inhibitor (31).

Shokat *et al.* demonstrated that the binding of an N_6-modified ATP did not alter the phospho-acceptor binding site nor did it alter the site specificity of a range of peptide substrates for the tyrosine kinase c-Src.[147] The CDK2 gatekeeper study performed by Elphick *et al.*[143] showed the same to be true for serine/threonine kinases and further highlighted the ability of the mutant kinases to use ATP as a competing co-substrate. More importantly, this work found comparable K_m/V_{max} values for mutant CDK2 and the wild-type kinase. However, the enlarged binding pocket created through the mutation of the gatekeeper residue can lead to a near complete loss of kinase activity, such as that seen for Cdc5 (a member of the PLK family, involved in mitotic entry and exit); the <4% activity relative to wildtype for the glycine gatekeeper mutant of MEKK1 (a MAP3K involved in programmed cell death); and <20% activity observed for the glycine gatekeeper mutant of GRK2 (involved in GPCR signalling).[148] Sometimes this can be overcome by producing an alternative gatekeeper mutant; e.g. the T315G mutant of c-Abl was found to be unstable whereas the T315A mutant retained sufficient activity for *in vitro* inhibition studies.[149] Other times it is possible to restore activity with a second mutation.[148] These mutations are often in a β-sheet lying over the gatekeeper residue and usually introduce amino acid residues known to stabilise β-sheets and thus, promote the correct folding of the kinase into the active form.[150] Examples include the second-site mutation C57V in *Tb*PLK L118G (*vide infra*)[151] and S278V in GRK2 L271G.[148]

The covalent complementarity chemical genetic approach was developed by Shokat *et al.* as a further attempt to overcome the loss of activity often observed upon the formation of small gatekeeper kinase mutants. The Cys gatekeeper mutant (**Figure 1.25**) was introduced into c-Src PK, forming c-SrcT228C, in preparation for

inhibition with small molecule electrophiles, such as (**31**).[152] It was thought that because this strategy avoided enlarging the ATP binding pocket due to the similarity in size between threonine (**26**) and cysteine (**25**), it would preserve the geometry of the ATP-binding pocket and hence, prevent loss of kinase activity. The reaction of cysteine residues with small molecule electrophilic inhibitors had already been exploited for the study of RSKs (**Section 1.4.1**)[131] and double mutants created with small gatekeepers and a cysteine anchor residue for the study of Fyn, c-Src and EGFR.[153] Therefore, a cysteine gatekeeper mutant could result in selective irreversible inhibition with only one mutation to the kinase. Shokat *et al.* showed c-SrcT338C to have k_{cat} and K_m values, which closely mimicked the wildtype kinase and to have a catalytic activity (k_{cat}/K_m) 14-fold greater than that of c-SrcT338G. Using a panel of 20 electrophile containing inhibitors, Shaokat *et al.* proved that selective inhibition of the c-SrcT338G mutant over the wildtype kinase was possible.[152]

The selective inhibition of glycine/alanine or cysteine gatekeeper mutants for the investigation of phosphorylation in complex mixtures is only possible due to the rarity of these residues in the gatekeeper position of kinases. A study of 420 kinase sequences found ~23% of these kinases to have a small gatekeeper and ~16% to have a very large gatekeeper residue. However, the majority of kinases, ~61% have a medium gatekeeper residue, with Met being the most common ~40%.[154] When studying complex mixtures containing gatekeeper mutants the inhibitory effect of a bulky inhibitor (e.g. **16** and **30**) can be attributed to the gatekeeper mutant enzyme because gatekeeper residues as small as glycine and alanine occur naturally in <1% of kinases (**Table 1.1**). Cysteine residues are found as the gatekeeper in only two human kinases (SgK494 and MAPK/MAK/MRK overlapping kinase).[152]

Table 1.1: Gatekeeper residue distribution across 420 kinases.[125]

Gatekeeper	No. of kinases	Percentage	Size
Gly	1	0.24	S
Ala	1	0.24	S
Ser	3	0.71	S
Cys	2	0.48	S
Thr	76	18.10	S
Val	13	3.10	S
Ile	9	2.14	M
Leu	72	17.14	M
Met	169	40.24	M
Gln	8	1.90	M
Phe	63	15.00	L
Tyr	3	0.71	L

Work by Lozano-Núñez *et al.* produced an analogue sensitive mutant of PLK from the parasite *Trypanosoma brucei*. The *Tb*PLK contained two mutations: the gatekeeper mutation L118G; and a compensation mutation C57V, which restored sufficient activity to *Tb*PLK to support growth. *In vitro* testing of *Tb*PLK double mutant with a bulky analogue of PP1 (**30**) showed the wildtype was unaffected by the bulky inhibitor, whereas the mutant *Tb*PLK was inhibited (IC_{50} ~250 nM). As *Tb*PLK was found to tolerate these mutations and be sensitive to the bulky inhibitor, a *T. brucei* cell line was produced that expressed no wildtype *Tb*PLK, only mutant *Tb*PLK. The mutant parasites were found to be viable and had an almost identical growth rate to that of the wildtype. However, in the presence of the bulky inhibitor the growth of the mutant parasite was halted (with 500 nM of PP1 analogue the analogue sensitive cells grew at ~50% the rate of the control cells).[151]

1.4.2.2 *Chemical ligation*

Chemical ligation provides another method of monitoring the binding of inhibitors to the active site of kinases. As this chemical ligation can be made away from the ATP binding pocket, it can prevent loss of activity that is sometimes associated with mutations to the active site of the kinase. In this approach, kinase activity is stimulated by chemical or light stimuli, which are used to monitor phosphorylation and conformational changes associated with activity. An example is the monitoring of conformational changes of the p38α kinase, which is able to adopt the "DFG out" conformation (**Section 1.2.6.1**). This conformation can be monitored by placing a fluorophore, which is sensitive to the polarity of its surroundings, in the glycine rich loop of the Ser/Thr kinase p38α. The binding of an inhibitor, which stabilises the "DFG out" conformation can be detected by the resultant shift in the emission maximum (**Figure 1.27**).[155, 156]

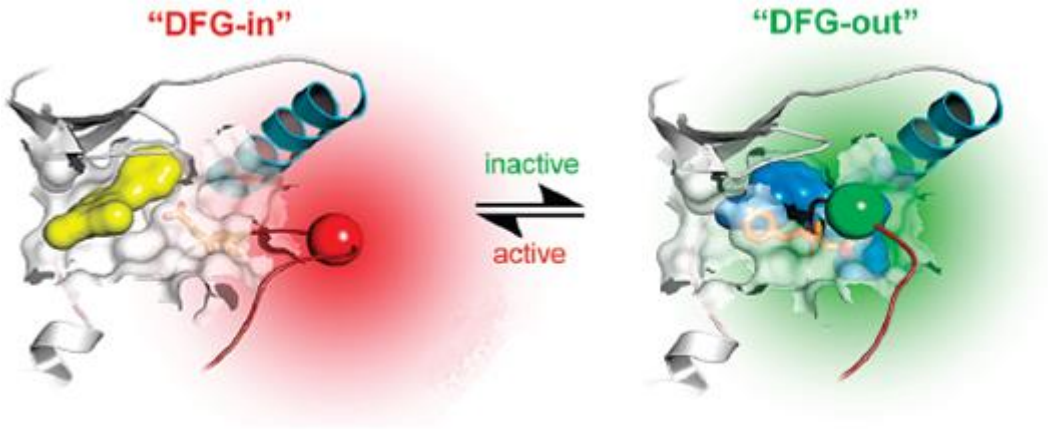

Figure 1.27: Type I inhibitors (yellow) can stabilise the DFG-in conformation, whereas Type II and III inhibitors (blue) can stabilise the DFG-out conformation. By introducing a polarity sensitive fluorophore into the glycine rich loop (blue α-helix) these conformational changes can be monitored by a shift in emission maximum between DFG-in and DFG-out conformations. Adapted from Simard *et al.*[294]

1.4.2.3 *Nonsense suppression*

Nonsense suppression allows the incorporation of phosphoamino acid mimics in a protein. The replacement of the phosphoamino acid with a mimic creates a phosphoprotein that is resistant to hydrolysis by phosphatases and hence, can simplify the search for phosphorylated targets.[155] A fluorescent dye can also be positioned on a residue near to a tyrosine phosphorylation site, allowing for detection of phosphorylation to be monitored by fluorescence.[157]

1.4.2.4 *Cross-linking*

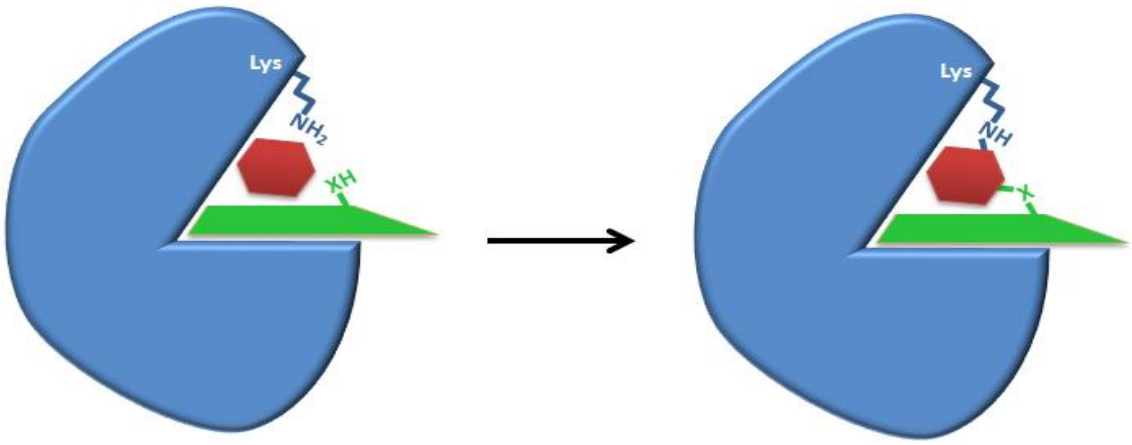

Figure 1.28: A schematic representation of substrate-kinase cross-linking reactions. The kinase is shown in blue, the ATP derivative/mimic in red and the peptide in green. X represents either the S of a Cys or the O of a Ser/Thr.

The cross-linking technique (**Figure 1.28**) is used to bind the substrate and kinase together via an ATP derivative (**Figure 1.29**). One method of cross-linking combines the use of a modified substrate (**Section 1.4.3**) with an ATP derivative or mimic (**Section 1.4.4**). The Ser/Thr to be phosphorylated is substituted with a Cys residue. The ATP derivative, *o*-phthaldialdehyde-benzoyl adenosine (**33**) binds to the ATP binding site and cross-links the Lys residue of the kinase to the Cys residue of the substrate[158] (**Figure 1.30**). Off target hits have been removed with the development of

naphthalene-2,3-dicarboxaldehyde adenosine (**34**) as a result of an improved structural fit in the ATP binding pocket.[159] Inhibitors with reactive groups have also been used in this manner to identify inhibitor-kinase matches; e.g. aminopyrazole *o*-phthaldialdehyde-benzoyl (**35**) and aminopyrazole thiophene-2,3-dicarboxaldehyde (**36**).[160]

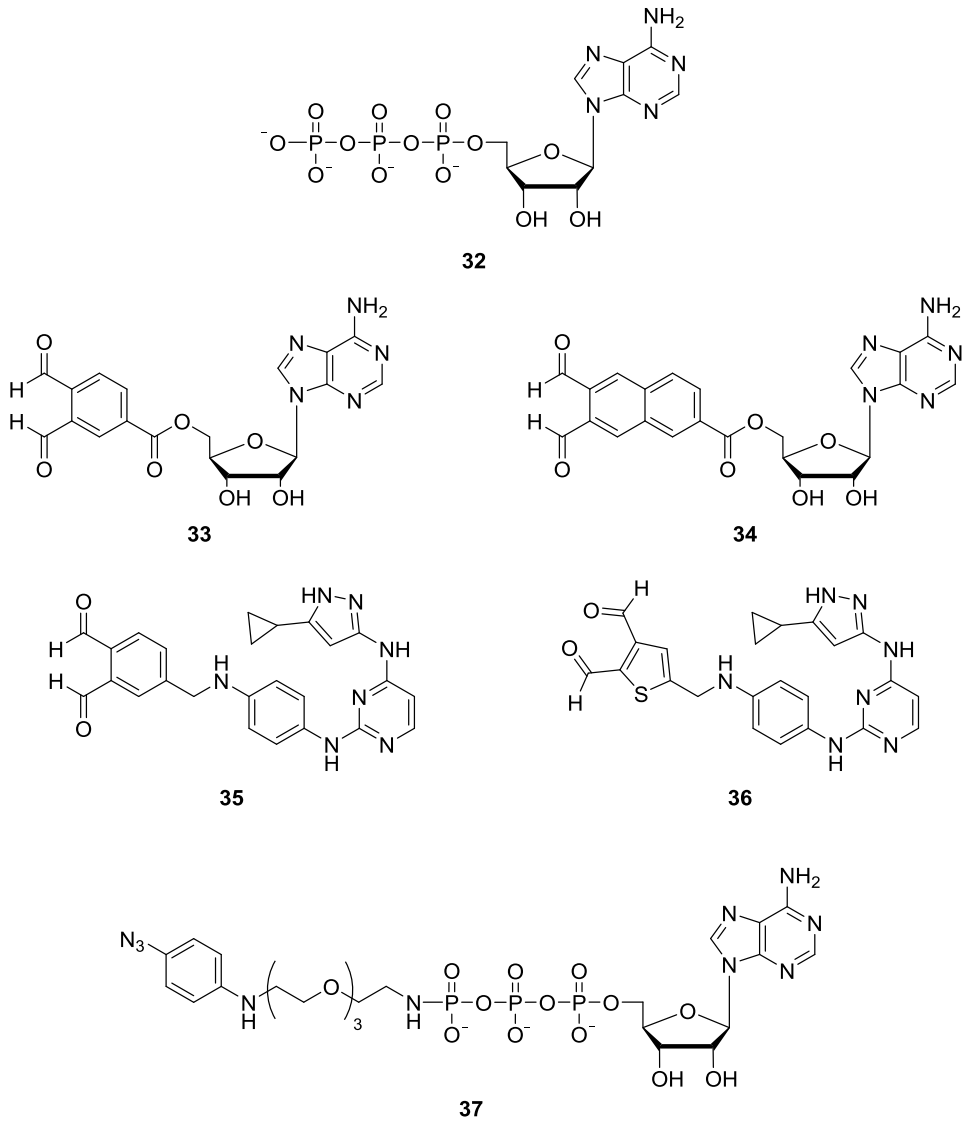

Figure 1.29: Examples of ATP derivatives and mimics used to cross link the substrate and kinase: ATP (32) *o*-phthaldialdehyde-benzoyl adenosine (33), naphthalene-2,3-dicarboxaldehyde adenosine (34), aminopyrazole *o*-phthaldialdehyde-benzoyl (35), aminopyrazole thiophene-2,3-dicarboxaldehyde (36) and a γ-aryl azide ATP analogue (37).

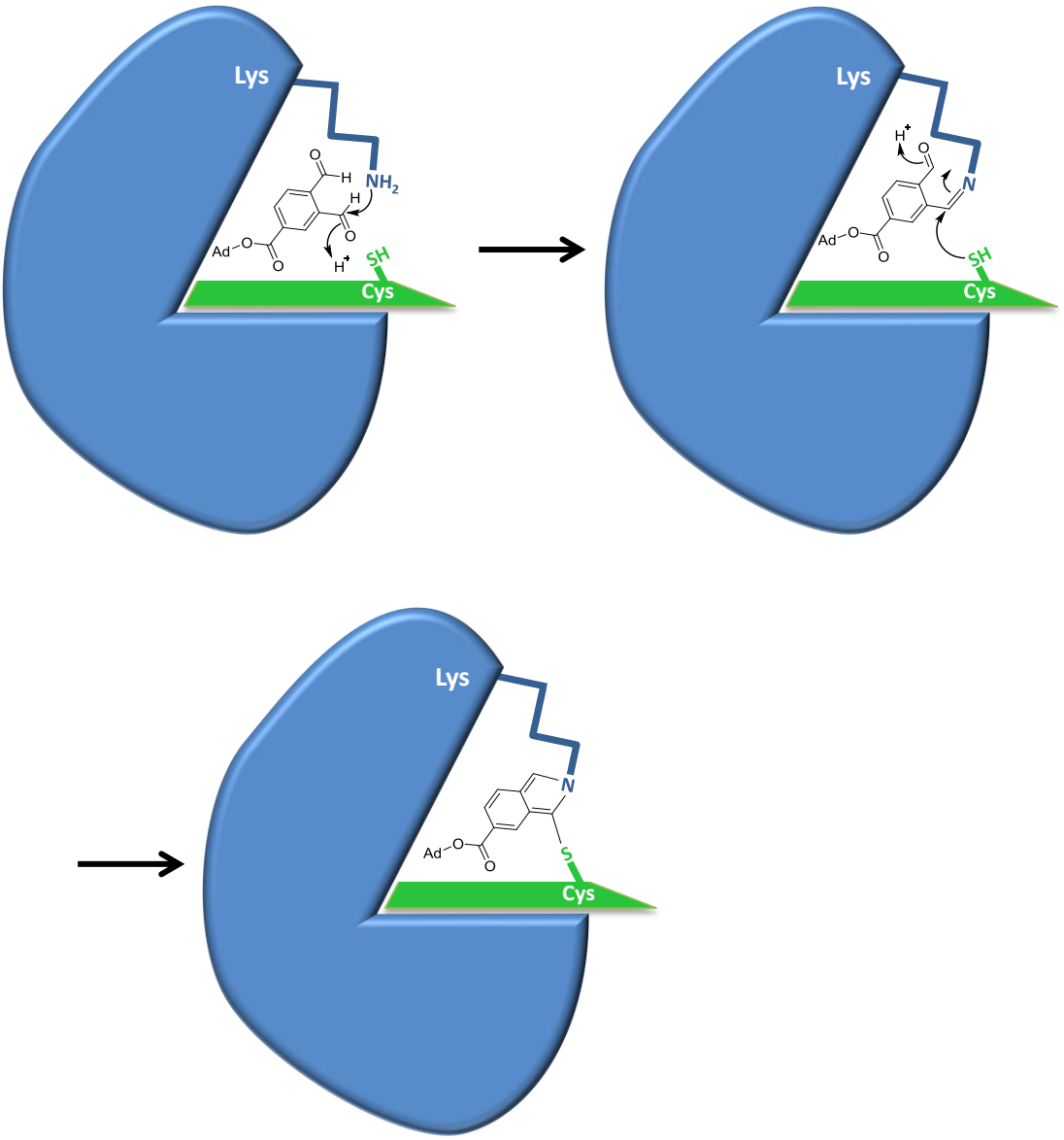

Figure 1.30: Schematic representation of the substrate-kinase cross-linking reaction using *o*-phthaldialdehyde-benzoyl adenosine (33) and a substrate in which the Ser/Thr has been replaced with a Cys. The kinase is shown in blue and the substrate in green.

Another method of cross-linking requires a photo-cross-linking moiety to be enzymatically introduced to the phosphate site of a substrate via phosphorylation with a γ-labelled ATP analogue. Pflum *et al.* demonstrated this by incubating CK2 and a rhodamine-labelled CK2 peptide substrate with a γ-aryl azide ATP analogue (**37**) whilst simultaneously irradiating the mixture with UV light (365 nm) to afford a covalent cross-link (**Figure 1.33**). Following phosphorylation in-gel fluorescence scanning

showed the presence of fluorophore labelled CK2, illustrating successful cross-linking.[161]

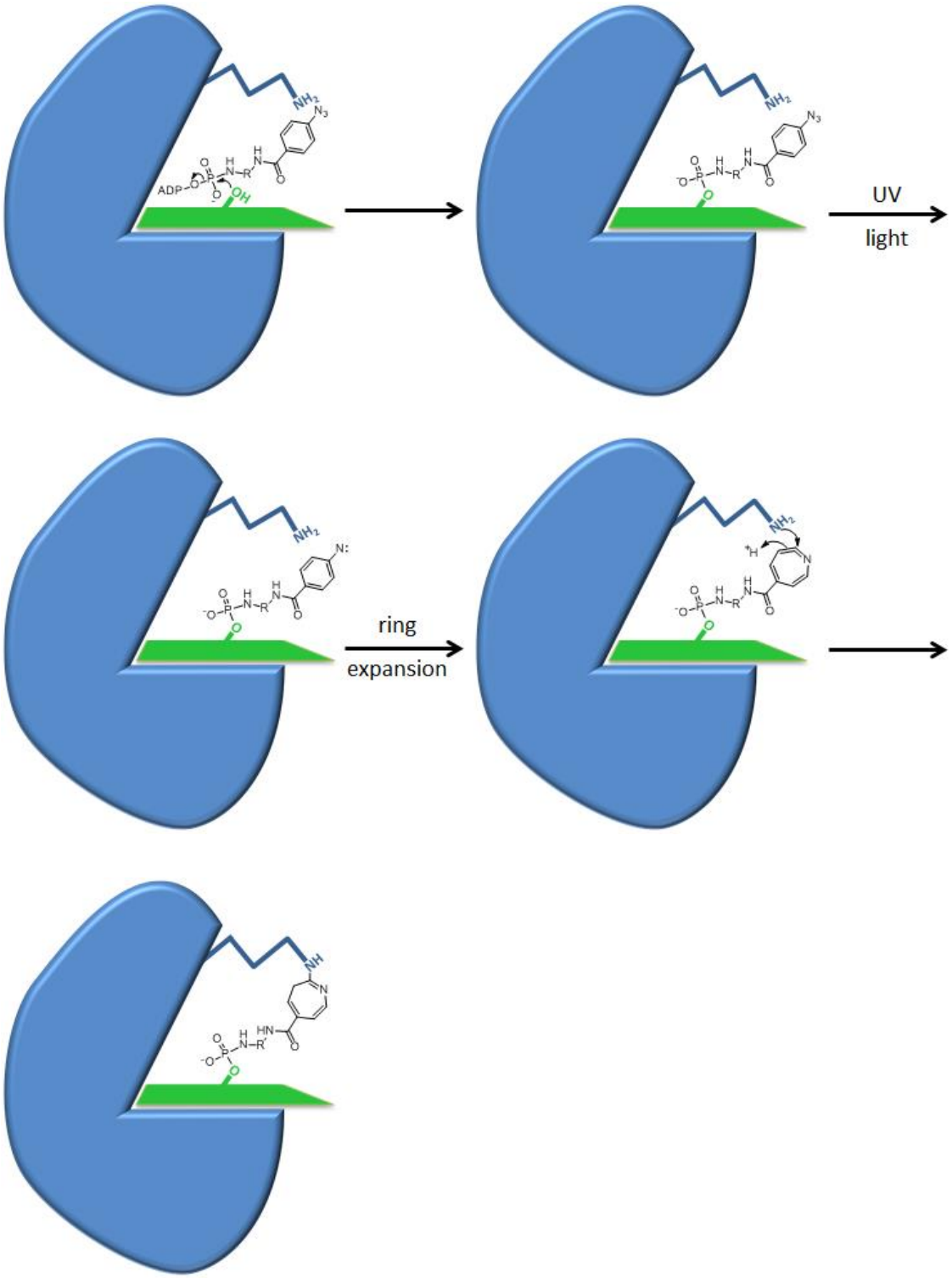

Figure 1.31: Schematic representation of the phosphorylation dependant substrate-kinase photo-cross-linking reaction using ATP-ArN_3 (37) and a substrate, which can be rhodamine-labelled for easy detection. Kinase mediated phosphorylation of a hydroxyl containing amino acid with ATP-ArN_3 in the presence of UV light leads to the formation of a nitrene, which causes ring expansion. This 7-membered ring readily reacts with nearby primary amines such as the Lys shown. The kinase is shown in blue and the substrate in green.

Cross-linking techniques have been used to conjugate a variety of Ser/Thr protein kinases to their substrates, including MAP kinases, PKA and CK2, as well as tyrosine kinases such as Abl.[155]

1.4.3 Modifying substrates

Kinase-substrate combinations are commonly studied using fluorescently labelled substrates. The conformational changes induced in a substrate upon phosphorylation turn on (or off) fluorescence, thereby giving rise to a direct and continuous method with which to monitor phosphorylation. Advantages include the ease of synthesis, a tuneable optical response and measurements in real time.[155]

Tyrosine phosphorylation can be observed using a proximal fluorophore, e.g. pyrene, to monitor the phosphorylation of the neighbouring Tyr residue (**Figure 1.32**). The nuclear Overhauser enhancements between the Tyr residue and the fluorophore are significantly stronger in the non-phosphorylated species than the phosphorylated species;[162] thus, phosphorylation prevents quenching and fluorescence is observed.[163] By using specific peptides containing fluorophores with non-overlapping emission properties, this principle has been used to simultaneously monitor Abl and Lyn activity; these TKs are implicated in imatinib resistant CML cell lines.[164]

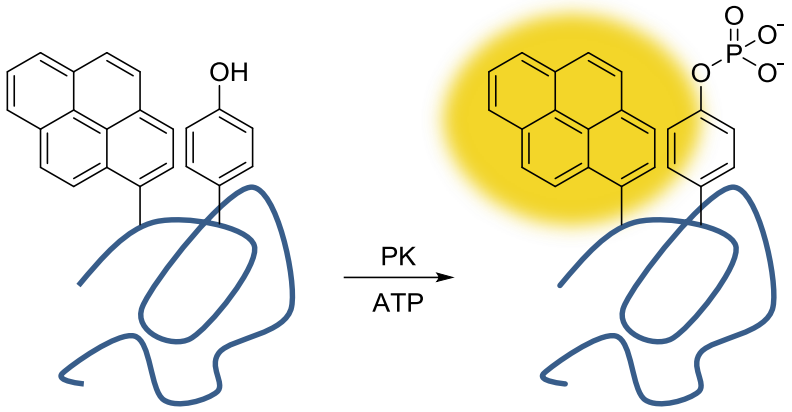

Figure 1.32: Schematic representation of pyrene as a proximal fluorophore. A pyrene residue can be positioned close to Tyr in the peptide (blue). Upon phosphorylation of the Tyr, quenching is prevented and fluorescence is observed.

The conformational changes that occur upon phosphorylation of a substrate can be used to alter the distance between two fluorophores and hence, change their physical properties (**Figure 1.33**). For example, in a study by Schults *et al.*, green fluorescence protein (GFP) was attached to the C-terminal of p47 and enhanced yellow fluorescence protein (EYFP) to the N-terminal. Upon phosphorylation by PKC *in vivo*, the conformational change induced FRET between GFP and EYFP, revealing that this phosphorylation occurred in the cytosol and not the nucleus.[165] An alternative to FRET probes is the split luciferase mechanism. The C-terminal and N-terminal fragments of luciferase are attached to either end of a target sequence. Upon phosphorylation, the two luciferase fragments are brought together, dramatically increasing fluorescence.[166] This method is advantageous over FRET because no excitation is necessary. Therefore, it can be used *in vivo* without phototoxicity.[155]

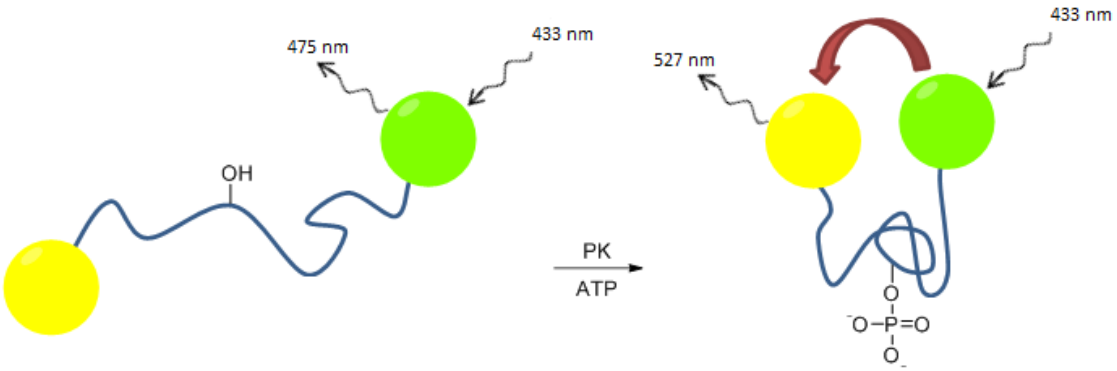

Figure 1.33: Schematic representation of FRET caused by the conformational change of a substrate. Upon phosphorylation a conformational change occurs in the substrate (blue). This brings the GFP and EYFP in close enough proximity for FRET to occur; therefore, a shift in emission wavelength is observed.

Photocaging allows control over the accessibility of the substrate during phosphorylation by introducing a light sensitive protecting group to the side chain of an amino acid of interest. These caged substrates can permeate the cell membrane and once inside the cell remain in a dormant/inactive state until the cage is removed by photocleavage, revealing the native substrate (**Figure 1.34**). The effects of the presence of the native substrate can then be measured.[155, 167, 168]

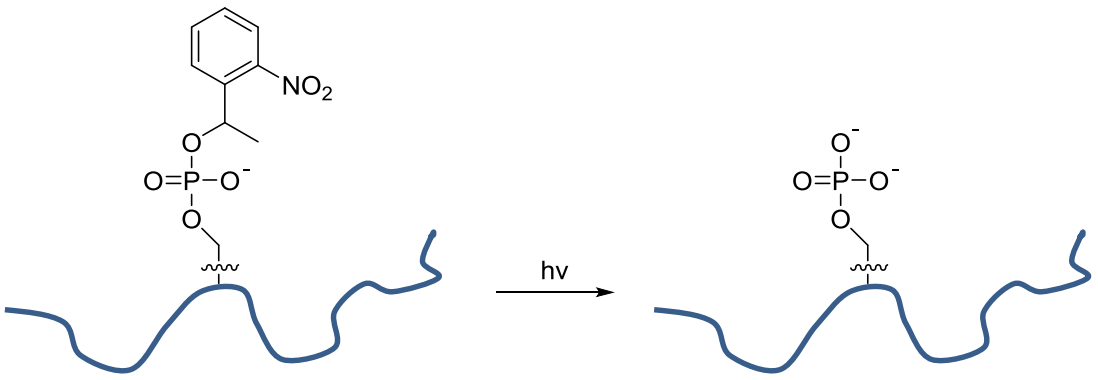

Figure 1.34: Schematic representation of a photocaged phosphopeptide. The photocaged phosphopeptide can cross cell membranes and remains caged until UV light is administered.

1.4.4 Designing ATP derivatives

ATP derivatives have been widely used for the study of the structure and mechanism of ATP-binding to a variety of enzymes. Modifications to the triphosphate fragment have resulted in ATP analogues that are commonly used as stable crystallographic probes.[169] ATP derivatives can be used to provide insight into protein kinase-catalysed transformations, kinase activity, inhibitor screening and *in vivo* targets. The most common modifications for the use in kinase studies are those at the exocyclic nitrogen N_6 of the adenine or at the γ-phosphate.[155]

1.4.4.1 *N_6-modified ATP*

As discussed *vide supra* (**Sections 1.2.6.1** & **1.4.1**), it is possible to exploit the hydrophobic back pocket of the ATP binding site in kinases with a smaller gatekeeper residue, resulting in potent and selective inhibition using bulky inhibitors. Bulky substituents can be placed at the N_6 position of ATP (**Figure 1.26** & **Figure 1.35**) to study the phosphorylations performed by a specific/reduced number of kinases capable of using the modified ATP substrate. Kinases with naturally large gatekeeper residues can be made to accept N_6 modified ATP substrates by mutating the large gatekeeper residue to a smaller one (**Section 1.4.2.1**). This approach has been used in several studies, including the identification of substrates of Abl and Arg kinases,[170] and it has been shown that N_6-substituents greater in size than an isopropyloxy group (**38**) are detrimental to the activity of wild-type kinases.[142]

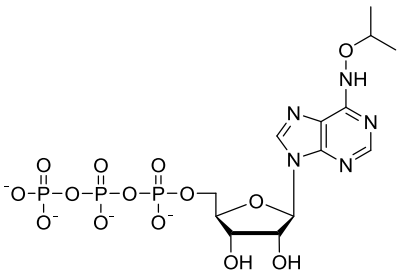

38

Figure 1.35: Isopropyloxy ATP (38), a N_6 modified ATP analogue.

1.4.4.2 *Modifications to the phosphate backbone of ATP*

A common modification to the phosphate backbone is to exchange the bridging oxygen between the β- and γ-phosphates for an NH (**39**) or a CH_2 (**40**) group. In these analogues the transfer of the γ-phosphate is prevented; thus, these analogues have been used in crystallisation studies to provide insight into binding states and reaction mechanisms.[171]

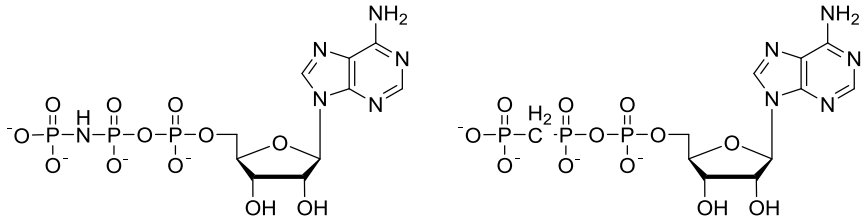

39 40

Figure 1.36: Structures of the non-hydrolysable ATP analogues AMPPNP (39) and AMPPCP (40).

Multiple γ-modified ATP derivatives have been synthesised and used by research groups. Upon phosphorylation, the γ-modification, or tag, is transferred to the substrate. Thus, these ATP derivatives can be used to provide insight into phosphorylation performed by kinases. The shallow, solvent exposed ATP binding pocket allows γ-derivatised ATP analogues to be readily tolerated by kinases.[172] The most common method of attaching a label to the γ-position is through a phosphoamide bond; however, phosphoesters, phosphothioesters and phosphonates have been reported (**Figure 1.37**).[155, 169, 173, 174, 175]

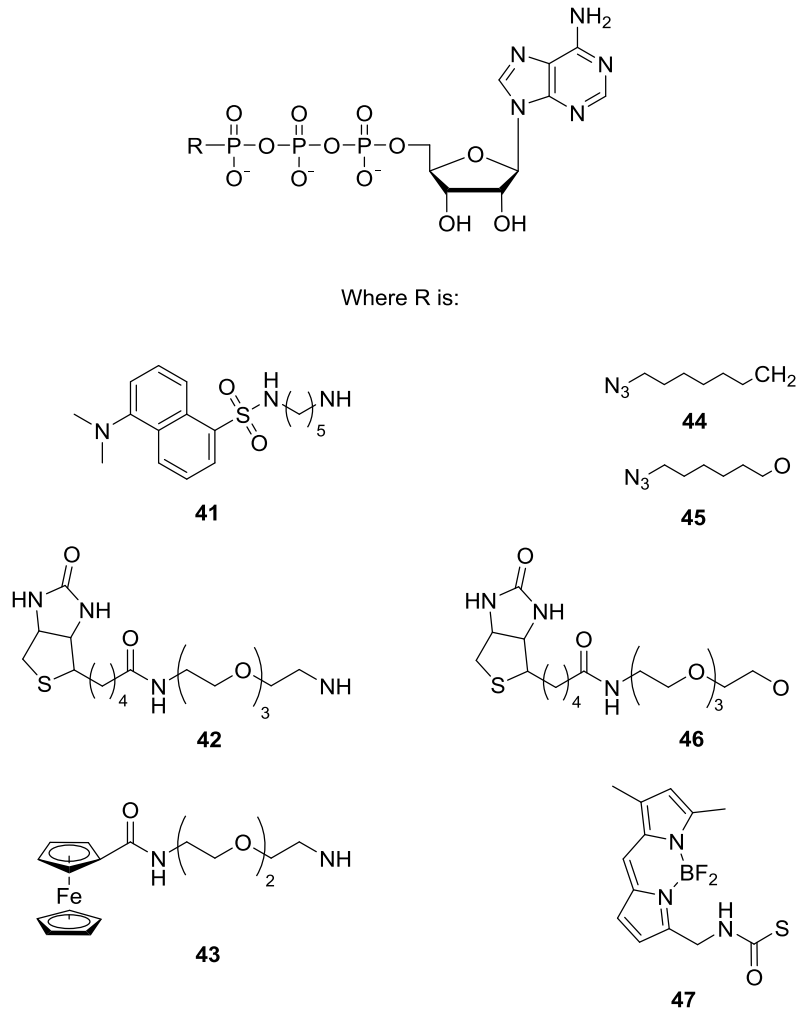

Figure 1.37: Examples of published ATP derivatives with modifications to the γ-phosphate.

Although ATPγS (**48**) is an unnatural co-substrate, it is a surprisingly good co-substrate for many kinases. As thiophosphorylated proteins are often resistant to phosphatases, ATPγS (**48**) can be useful for the study of substrate phosphorylation in complex mixtures. In addition, the large downfield shift of the ^{31}P NMR resonance of the thiophosphate and the difference in mass can be used to readily identify substrates phosphorylated by ATPγS (**48**) with NMR and MS.[176] Thiophosphorylated substrates can be subsequently alkylated with alkyl halides to further aid identification/isolation of phosphorylated substrates; however, alkylating agents also label other cellular nucleophiles.[177] Nevertheless, antibodies can be used to distinguish between

thiophosphate alkylation products and undesired alkylation products in complex protein mixtures.[178,179] Chemoselctive thio-alkylation in the presence of cysteine residues can be performed under pH control (Cys pK_a ~9 *vs* thiophosphorylated residue pK_a <3).[180] To introduce target selectivity, N_6-modified ATPγS (**49**) can be used in conjunction with gatekeeper mutation of the enzyme of interest.[145]

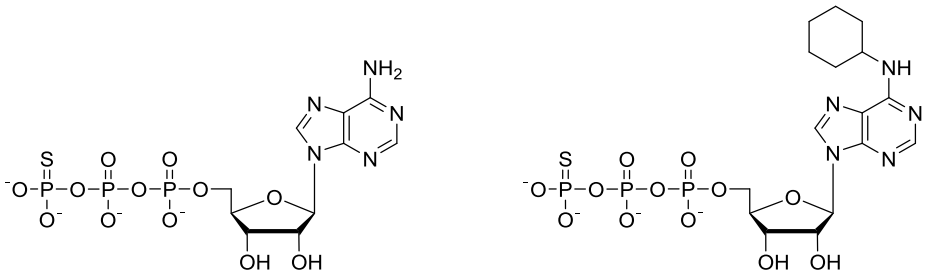

48 **49**

Figure 1.38: The structure of ATPγS (48) and an N_6 substituted ATPγS analogue (49).

Peptide biotinylation can be achieved using γ-biotin derivatised ATP (**42**). If the peptide substrate is bound to a gold nanoparticle, avidin-modified gold nanoparticles can be added after phosphorylation, which bind to the biotinylated nanoparticle and cause aggregation. This aggregation results in a colour change and hence, provides the possibility to measure the IC_{50} values of inhibitors through a colourimetric assay.[181] Analysis of peptide biotinylation can also be measured using MALDI-TOF MS.[172] An acyl analogue (**46**) of the phosphoamide ATPbiotin (**42**) has been found to react selectively and covalently with >75% of human protein kinases at one of the two conserved lysine residues known to be in the proximity of β- and γ-phosphates of bound ATP. Using this technique, IC_{50} values of ATP competitive inhibitors can be measured.[182]

Another γ-modified ATP analogue, ATP-dansyl (**41**), can be used to transfer a dansyl group to peptide and protein substrates. The study conducted by Green *et al.* highlights the ability of kinases to transfer the tagged γ-phosphate to serine, threonine and tyrosine residues. Substrate phosphorylation can be monitored by MALDI-TOF MS. If the peptide substrate contains rhodamine in close proximity to the residue to be phosphorylated, dansylation of the Ser/Thr/Tyr residue promotes FRET. Thus, phosphorylation can be analysed quantitatively by measuring the increase in emission fluorescence.[173]

Another example of a γ-modified ATP analogue in the literature is ferrocene-conjugated ATP (**43**). A peptide substrate is immobilised on the surface of a screen-printed gold electrode by mean of a sulphur bond. Phosphorylation with the γ-phosphate ferrocene group can be detected using electrochemical techniques, such as CV.[183,184] Anti-ferrocene antibodies have also been developed for the detection of proteins phosphorylated with a ferrocene tag using Western blot analysis.[185]

One of the major problems associated with the use of ATP analogues is that they must compete with ATP. As the *in vivo* level of ATP is ~1 mM, this can be a significant problem.[171] Attempts have be made to overcome this for N_6 analogues by reducing the size of the base, e.g. antiviral agent Ribavirin (**50**) and its derivatives (e.g. **51**), and developing kinases with ATP pockets that are restricted in size to hamper ATP binding (**Figure 1.40**).[186] However, these analogues are of limited use due to being less selective for mutant kinases than their N_6-derivatised counterparts. This is thought to be due to the flexibility of the kinase ATP binding region.[186, 187] Conversely, despite many N_6-ATP derivatives having a stronger binding affinity for the mutant kinases than

ATP itself,[188] this is not always the case.[143] Many ATP derivatives are also unlikely to cross the cell wall and therefore their use is limited to *in vitro* assays and cell lysate work.[171]

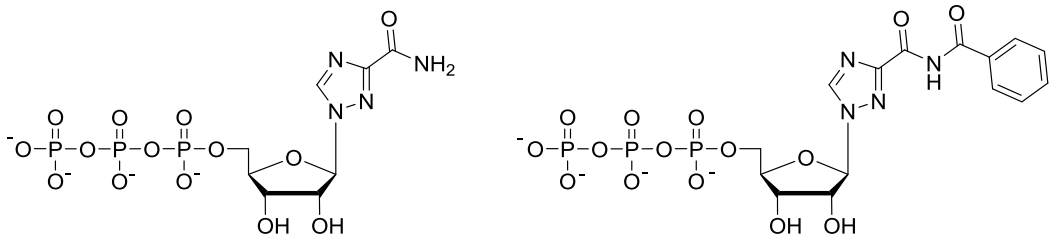

50 **51**

Figure 1.39: The antiviral ribavirin (50) and its bulky N_4 derivative (51).

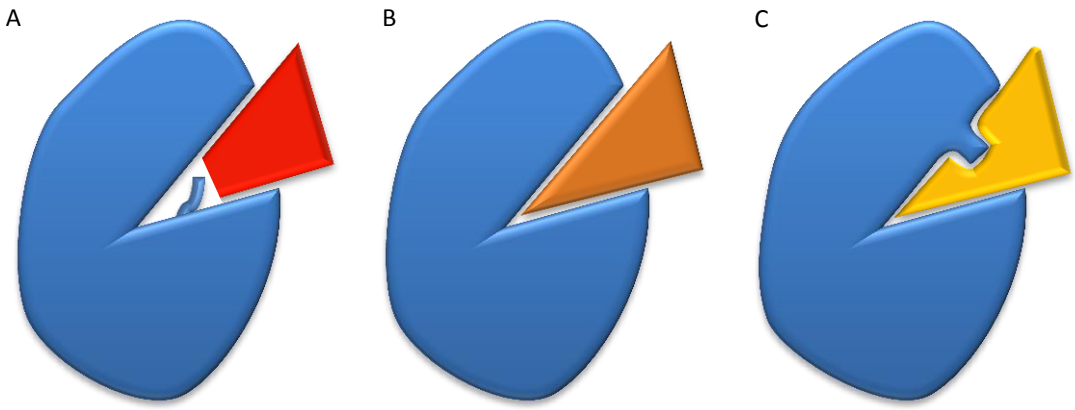

Figure 1.40: Schematic representation of an enzyme with different ATP binding site mutations. Enzymes are shown in blue and inhibitors orange. A: wildtype kinases usually contain a medium sized gatekeeper residue (e.g. Met), which blocks access to the back pocket of the ATP binding site; B: Glu/Ala mutants allow much bulkier inhibitors to bind to the active site by allowing access to the back pocket; C: mutations to bulky residues at the ATP binding region allow the enzyme to hamper ATP binding and have preference for ribavirin derivatives.

1.5 Aims

Understanding biological processes that are a cause or consequence of diseases is a key factor in the search for new treatments and overcoming resistance. As protein phosphorylation regulates most aspects of cell life, the objective of this thesis was to develop methodologies for the study of phosphorylation processes occurring within the malarial parasite *Plasmodium falciparum*, the most deadly species of the parasite. ATP-binding sites are well conserved among kinases and therefore identifying substrates of specific kinases through inhibition or using ATP derivatives can be challenging. Therefore, this thesis aimed to exploit and develop current chemical biology techniques to specifically study the substrates of *P. falciparum* kinases. In particular, this work focused on three kinases using two different chemical genetic approaches: γ-modified ATP/GTP analogues for the investigation of CK2; and covalent complementarity for the study of CLK1 and CLK3.

2 γ-modified ATP analogues for the study of CK2

2.1 Introduction

Protein kinase CK2, formerly casein kinase II, is ubiquitously expressed and highly conserved across eukaryotes. This serine/threonine kinase was the first protein kinase to be described and isolated upon its discovery in 1954.[52] Despite its original name, casein is not a substrate of CK2 *in vivo*.[189] Considerable work has been carried out to study the structure, substrates and function of CK2. It has been assigned >300 substrates and many more are predicted, resulting in CK2 being deemed the most pleiotropic protein kinase in eukaryotic organisms.[190] A common feature of these substrates is the presence of acidic amino acid residues surrounding the phosphoacceptor site.[190, 191] CK2 has documented roles across many cellular processes, including tRNA and rRNA synthesis,[192] apoptosis,[193] cell survival,[194] differentiation and cell cycle progression and is found in nearly all subcellular compartments;[191] mammalian CK2 has also been shown to phosphorylate several extracellular kinases.[195,] Its elevated activity in rapidly proliferating tissues and its potential to protect cells against apoptosis have evoked interest from the cancer research community to join the investigative attempts to comprehensively understand the ability of CK2 to regulate specific biological events, a feat which has eluded scientists for the past 60 years.[196]

2.1.1 The structure of CK2

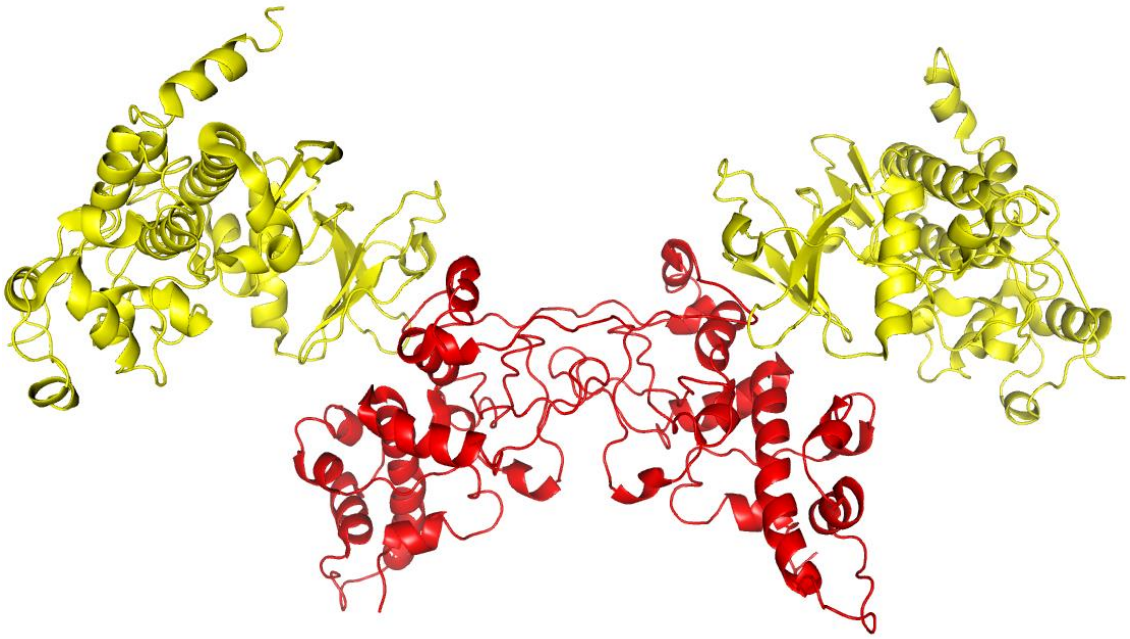

Figure 2.1: The crystal structure of the tetrameric CK2 holoenzyme. The two α-subunits are shown in yellow and the two β-subunits are shown in red (PDB file: 1JWH; resolution: 3.10 Å).[197]

The holoenzyme of CK2 is a tetramer consisting of two catalytically active α-subunits and two regulatory β-subunits[197] (**Figure 2.1**). In many species there are multiple isoforms of the subunits; for example, in yeast there are two catalytic subunits (α and α') and two regulatory subunits (β and β').[198] In humans there are two isoforms of the catalytic subunit (α and α')[199] and just one regulatory subunit (β), with the holoenzyme able to take the form $\alpha\alpha'\beta_2$, $\alpha\alpha\beta_2$ or $\alpha'_2\beta_2$.[200] The enzyme is found mainly as the holoenzyme *in vivo* but the isolated subunits have been found to exist *in vivo* in certain circumstances and could, therefore, have specific functions.[201] *In vitro* the tetrameric holoenzyme forms spontaneously by a self-assembly mechanism, which is mediated by the dimerization of the two β-subunits.[202] The α and α' catalytic subunits, which are encoded by distinct genes, exhibit ~90% identity within their catalytic domain with the main difference between the two being in their C-terminal chain.[196] These subunits are

also conserved across animals and birds (e.g. the β-subunit is identical in humans and chickens), suggesting that the functional properties of CK2 have been conserved throughout evolution.[200]

Unlike many other enzymes, the α-subunits of CK2 are constitutively active; i.e. control mechanisms common to other protein kinases (e.g. binding of secondary messengers, phosphorylation) are absent.[203] Despite this, there is evidence to suggest that the presence of the regulatory β-subunits tunes the catalytic activity of the α-subunits. For example, there are some substrates that require the presence of the β-subunit for phosphorylation to occur[204] and others, such as calmodulin,[205] which are phosphorylated by the α-subunit but not the holoenzyme. Mutants of CK2α with truncated N-termini have been found to have severely impaired catalytic activity, highlighting the importance of the interaction between the N-terminal and the activation loop for activity of the α-subunit. Interestingly, in some cases, the formation of the holoenzyme has been shown to restore wildtype levels of activity.[206] As the presence of the β-subunits do not turn off the catalytic activity of the enzyme, there must be specific interactions, whether steric or ionic, which prevent efficient binding of certain substrates.[203]

2.1.2 CK2 as a dual-specificity kinase

Tyrosine phosphorylation was thought to be exclusive to higher eukaryotes; however, there are reports of the presence of phospho-tyrosine signalling cascades in lower eukaryotes[207] despite a lack of *bona fide* tyrosine kinases. *Plasmodium falciparum* is one such organism. There are no *bona fide* tyrosine kinases within its kinome and TKL kinases have only been identified with serine/threonine phosphorylation thus far;

however, several phospho-tyrosine phosphatases have been found[208] and *in vitro* phospho-tyrosine phosphatase activity reported.[209] Work carried out in the Tobin lab has shown that tyrosine phosphorylation accounts for ~1% of the total phospho-proteome during the schizont stage of the parasite.[210] The presence of tyrosine phosphorylation can be explained by the activity of dual-specificity kinases and work carried out in the Tobin lab highlighted the ability of *Pf*CK2 to act as a dual-specificity kinase.[211] This is concordant with data showing other forms of CK2 to also have the ability to phosphorylate tyrosine residues.[212, 191]

2.1.3 Dual co-substrate specificity, a rare quality

Perhaps the most interesting feature of CK2 is its dual substrate specificity, that is, its ability to use not only ATP (**32**) but also GTP (**52**) to phosphorylate a substrate.[64, 65] This trait is not completely unique to CK2. Enzymes reported able to use GTP as a co-substrate include CaMKK,[213, 214] PKCδ,[215, 216] Nercc1[217] and mst3.[218] Despite not being unique, this unusual property enables the kinase responsible for phosphorylation to be drastically reduced from 518 human kinase to a mere handful. Hence, this quality has been exploited *in vitro* as a sensitive and specific diagnostic tool for the identification of CK2 activity to distinguish it from other protein kinases.[219] Indeed, this feature provided the first indication that CK1 and CK2, which had been co-purified during early casein kinase research, were two separate enzymes.[220, 221, 222]

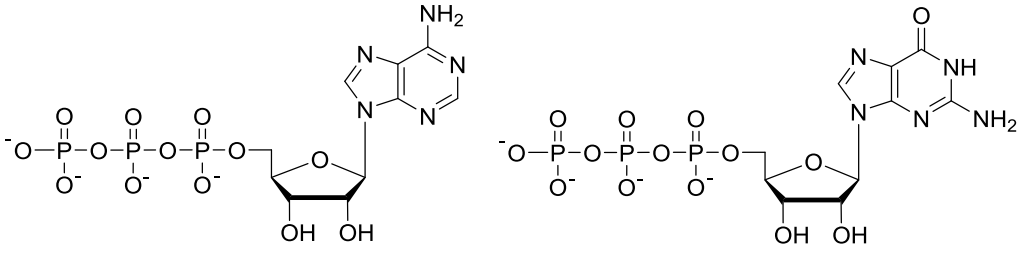

Figure 2.2: ATP (32) and GTP (52) are both co-substrates of CK2.

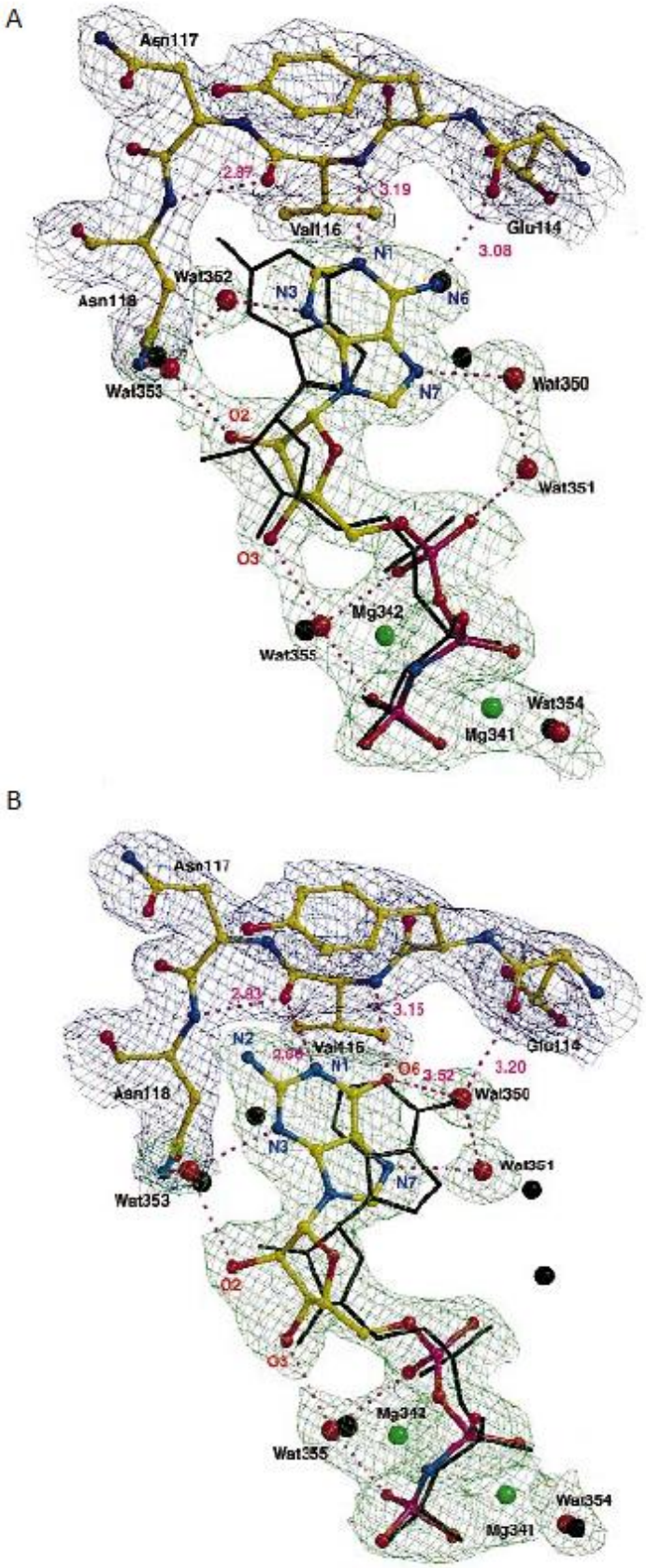

Figure 2.3: The binding site of the nucleotide purine base in ZmCK2. A: The AMPPNP-*Zm*CK2α complex, with GMPPNP in black for comparison; B: The GMPPNP-rmCK2α complex, with AMPPNP shown in black. N1 and N6 of adenosine are hydrogen bonded in a conserved way. GTP is incapable of following this same binding pattern and therefore, the guanine base is displaced along the backbone of the hinged region of CK2 until N1 and O6 can hydrogen bond correctly. A water molecule sits where the N6 of ATP would be, completing the hydrogen bonding with the backbone.[65]

Studies carried out to ascertain the residues responsible for the dual co-substrate specificity of CK2α have included: sequence alignment of CK2α with other eukaryotic protein kinases and mutation of residues usually occupied by other amino acids, which resulted in only small changes to the ratio K_m(GTP)/K_m(ATP);[223] deletion mutants, some of which were only stable as the holoenzyme and their affinity towards GTP was reduced;[224] and studies of the crystal structure of CK2α alone[197] or in complex with AMPPNP and GMPPNP,[65] which revealed how GTP binds in the active site. It has also been found that in the presence of Mn^{2+} GTP is the preferred co-substrate of CK2, whereas in the presence of Mg^{2+} ATP dominates.[225]

The explanation to this dual co-substrate specificity was revealed by studying the binding site of ATP/GTP in the CK2α subunit of recombinant *Zea mays* (*Zm*CK2α) (**Figure 2.3**). The atoms required for specific recognition of the adenine moiety (N1 and N6) are hydrogen bonded in a conserved way to the backbone of the hinged region (**Figure 2.3A**); however, GTP is incompatible with this hydrogen bonding pattern. The N1 acts as a hydrogen donor and O6 acts as a hydrogen acceptor (**Figure 2.3B**). In order for CK2α to utilise GTP, the guanine base is displaced along the backbone until hydrogen bond donors and acceptors match up correctly. The gap created at N6 is filled with water and therefore, the hydrogen-bonding potential of adenine is matched.[65]

2.1.4 CK2 in Plasmodium falciparum

The full sequencing of the *Plasmodium falciparum* genome[208] allowed for the discovery of the entire complement of *Plasmodium falciparum* protein kinases.[90,96] This revealed that, unlike the human genome, the *Plasmodium falciparum* genome encodes a single CK2α orthologue (PF11_0096). *Pf*CK2α has a 65% sequence identity with *Homo sapiens* and *Zea mays* CK2α as well as possessing the majority of features conserved among CK2α subunits.[226,227] In the study by Holland *et al.*,[227] *in vitro* tests revealed that *Pf*CK2α can utilise ATP and GTP as co-substrates with similar affinities; the K_m for ATP was recorded as 16.7 μM and the K_m for GTP was recorded as 34.9 μM. TBB (**53**), a known CK2 inhibitor, inhibits PfCK2α with an IC_{50} curve comparable to that of human CK2α (*Pf*CK2α IC_{50}: 2μM; *Hs*CK2α IC_{50}: 1.5μM). This study also provided strong evidence that *Pf*CK2α is essential to the viability of asexual erythrocytic stage parasites, validating it as a potential anti-malarial drug target.

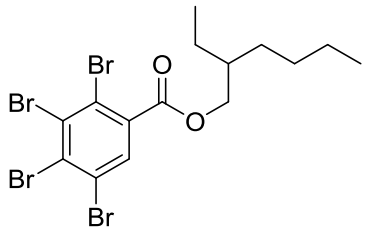

53

Figure 2.4: The CK2 inhibitor TBB, 4,5,6,7-tetrabromobenzotriazole (53).

Although humans have only one CK2 regulatory subunit, the *Plasmodium falciparum* genome encodes for two regulatory subunits: *Pf*CK2β_1 (PF11_0048) and *Pf*CK2β_2 (PF13_0232).[90,227] Respectively, these subunits bear 33% and 39% sequence identity with their human equivalent and both contain many features conserved amongst CK2β subunits. It has been found, through reverse genetics, that both *Pf*CK2β_1 and *Pf*CK2β_2

are required for the completion of the asexual erythrocytic cycle.[228] *Pf*CK2α is able to interact with both subunits *in vitro* to form the holoenzyme. Although interaction with the β-subunits does not drastically alter the K_m of ATP, it does reduce the activity of the kinase towards β-casein and therefore, is likely to have a functional significance *in vivo*.[227]

2.1.5 Inhibitors of CK2

Several ATP-competitive CK2 inhibitors, e.g. TBB (**53**) and its derivatives,[229] have been identified from screening programmes. Some, such as the pyrazolo[1,5-a][1,3,5] triazine derivatives,[230] have K_i values in the picomolar range; however, in all of these cases selectivity for CK2 was either poor or not defined. Nevertheless, there are some recent studies that show promise for the selective and potent inhibition of CK2.

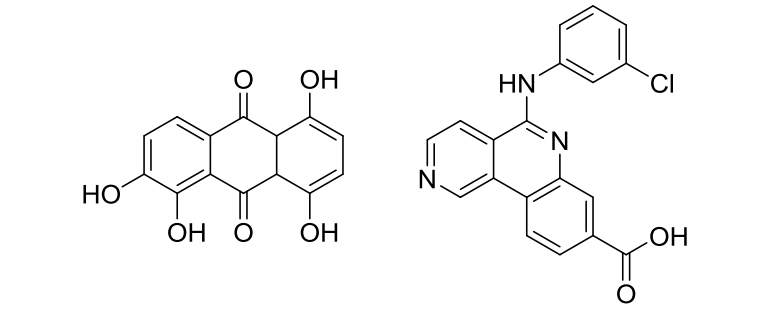

54 **55**

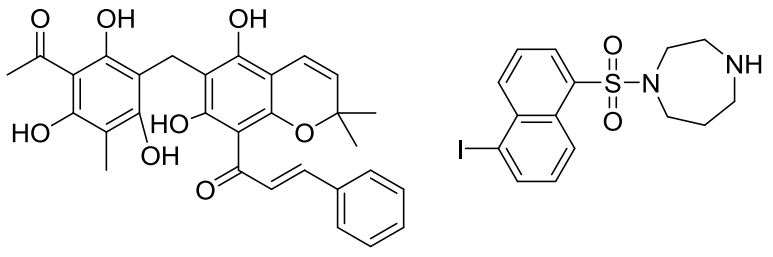

56 **57**

Figure 2.5: The structures of four CK2 inhibitors: quinalizarin (54), CX-4945 (55), Rottlerin (56) and ML-7 (57).

Quinalizarin (**54**) has been shown to have a K_i of 55 nM against human CK2, be cell permeable, cause apoptosis and be specific for CK2 across a panel of 75 kinases (at 1 μM CK2 activity had a residual activity of 7%; the second most inhibited kinase, PIM3, exhibited >50% residual activity).[231] Work carried out by another member of the group demonstrated that quinalizarin inhibits *Pf*CK2α as well as human CK2 (IC_{50} values of 2.0 μM and 0.8 μM respectively).[211]

CX-4945 (**55**) is a potent (K_i 0.38 nM), selective and orally bioavailable small molecule inhibitor of human CK2.[232] Developed by Cyclene Pharmaceuticals, it has been shown to be active against many cancer cell lines including prostate cancer,[233] to supress metastasis of lung cancer cells[234] and to reduce angiogenesis. As such, it was the first CK2 inhibitor to enter clinical trials.[232] This selectivity is thought to be possible due to a smaller than usual ATP binding pocket in CK2 than in other kinases.[235] The presence of three bulky residues gives rise to hydrophobic interactions, which stabilise the CK2-inhibitor complex.[236, 237]

Table 2.1: The IC_{50} values of two inhibitors, Rottlerin (56) and ML-7 (57), with PfCK2α and HsCK2α, illustrating the possibility to selectively inhibit PfCK2.[227]

	IC_{50} (μM)	
Inhibitor	***Pf*CK2α**	***Hs*CK2α**
ML-7	3-4	3-4
Rottlerin	7	>>20

Although *Pf*CK2α shows 65% sequence homology with *Hs*CK2α, it is hoped that the distance between these two organisms in the phylogenetic tree is enough to selectively target *Pf*CK2α. Encouragingly, there is data to show that is possible to selectively inhibit one homologue over the other (**Table 2.1**); however, Rottlerin (**56**) is a weak inhibitor with multiple targets and is, therefore, an unsuitable drug molecule.

This variance in IC_{50} values could be caused by the two differences within the active site of the two homologues; i.e. the replacement of Lys64 and Val116 of *Hs*CK2α with Pro and Ile respectively in *Pf*CK2α.[227]

2.2 Aims

Unravelling phosphorylation networks is a challenging task due to the complexity of phosphorylation patterns, the huge number of phosphorylation sites and the highly conserved ATP binding site of kinases. At present the analysis of protein phosphorylation in an enzyme pathway requires the substrate of interest to be isolated and then analysed by mass spectrometry to determine the peptide and the site of phosphorylation. Although generally successful, this procedure is laborious and requires optimisation.[171] Therefore, this thesis aimed to develop methodologies for the detection and analysis of *Pf*CK2 substrates specifically, even within cell lysates.

Kinases, including CK2, have been shown to transfer chemical tags to a peptide substrate upon phosphorylation using γ-modified ATP analogues, e.g. ATPγNH-linker-coumarin (**58**) (**Section 1.4.4.2**).[172] This study aimed to exploit the unusual ability of CK2 to utilise GTP as a co-substrate (**Section 2.1.3**) in order to specifically tag substrates of CK2 in the presence of other kinases using γ-modified GTP analogues (**Figure 2.6**). Through the transfer of a tagged phosphate, such as a fluorophore,[173] the phosphorylated substrates would be easily detected and isolated, allowing for their identification.

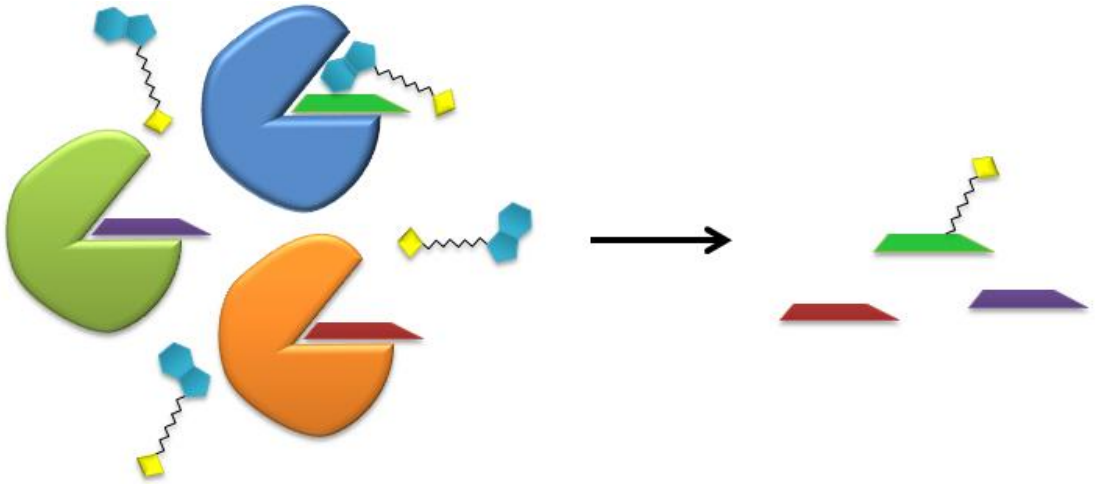

Figure 2.6: A schematic representation of CK2 (blue) being able to use a γ-modified GTP analogue to phosphorylate its substrate (green). Other kinases (green and orange), on the other hand, cannot use GTP as a co-substrate and, therefore, do not transfer a tagged phosphate to their substrates (purple and red).

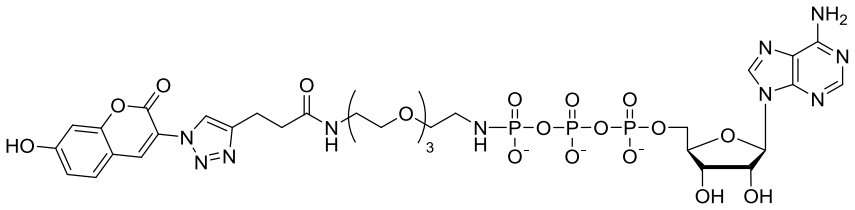

58

Figure 2.7: ATPγNH-linker-coumarin (58), an example of a γ-modified ATP analogue with a fluorescent coumarin tag.

Cyclene Pharmaceuticals would not supply a sample of the highly selective CK2 inhibitor CX-4945 (**55**); however the synthesis of this molecule and other derivatives has been published.[238] Therefore, it was decided to synthesise CX-4945 (**55**) and several of its analogues in order to ascertain whether they have the same inhibitory effect with *Pf*CK2 as with *Hs*CK2.

To summarise, the aims of this chapter were: to synthesis a selection of γ-modified ATP and GTP analogues such as (**58**) for use as a co-substrate with mammalian and *P. falciparum* CK2; to synthesise CX-4945 (**55**) and some of its analogues to screen them against *Pf*CK2; to express and purify *Pf*CK2α; to obtain proof of phosphorylation by the

modified co-substrates using MALDI-TOF MS; to establish the kinetic parameters of the co-substrates with both *Pf*CK2α and mammalian CK2; and to establish whether there is any selectivity between mammalian and *P. falciparum* CK2 with CX-4945 (**55**) and its derivatives.

2.3 Synthesis of ATP analogues

Protein kinases coordinate complex events in eukaryotes through the transfer of a phosphate group from ATP to a substrate. This phosphorylation event causes changes in the conformation of the substrate, altering its activity and consequently, has an effect on the subsequent events in a phosphorylation pathway. Mammalian CK2 has been shown to accept γ-modified ATP derivatives and transfer the tagged phosphate to CK2 substrates.[172] A tool box of these compounds was required to assess whether the same is true for *Pf*CK2. This was carried out with a view to synthesising γ-modified GTP derivatives to specifically tag CK2 substrates in the presence of other kinases. This was thought possible due to the unusual dual co-substrate specificity exhibited by CK2.[64, 65, 227]

A group of purine triphosphate analogues (**Figure 2.8**) with a range of chemical tags on the γ-phosphate were synthesised. A combinatorial synthetic approach was used to enable the same linker to be used where possible. Initially, the use of a phosphoramidate was envisaged for the formation of an ATP-linker-tag and, therefore, P-N analogues were synthesised (**58**, **59** & **60**). However, the acid liability of this bond[211,174] resulted in the search for a more stable method of attaching the linker and tag to the purine triphosphate. For this reason, a P-C analogue (**63**) and a P-S analogue (**62**) were synthesised and the synthesis of a P-O (**61**) analogue was attempted.

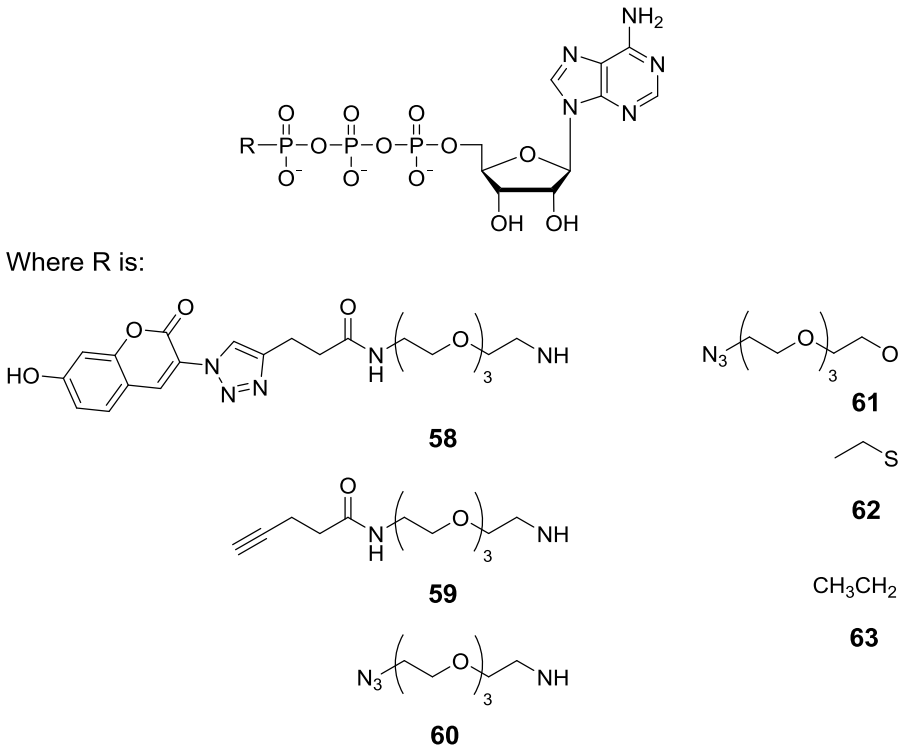

Figure 2.8: The ATP analogues synthesised in this work: ATPγNH-linker-coumarin (58), ATPγNH-linker-alkyne (59), ATPNH-PEG-N_3 (60), ATPO-PEG-N_3 (61), ATPγSEt (62), ATPγEt (63).

2.3.1 Initial proposed route for P-N analogues

The initial proposed synthetic route for P-N analogues (**Scheme 2.1**) involved the conversion of tetraethylene glycol (**64**) to the bis-azide analogue (**65**), which could then be converted to the N_3-PEG-NH_2 (**66**) for the formation of A/GTPNH-PEG-N_3 (**60** & **99**) or converted to the bis-amine analogue (**67**) for the synthesis of other analogues such as ATPalkyne (**59**).

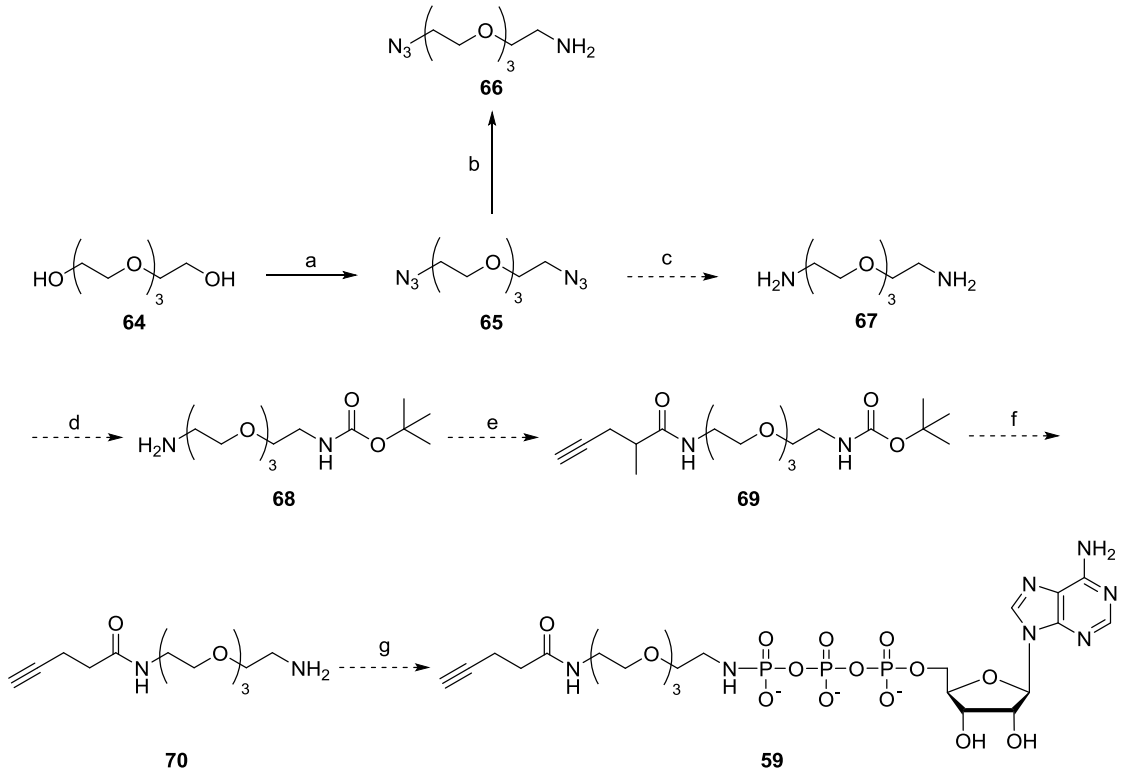

Scheme 2.1: Initial proposed synthesis for ATP analogues. Reagents and conditions: a) i) $MeSO_2Cl$, THF, TEA dropwise at 0° C, 12 hr RT ii) $NaHCO_3$, NaN_3, water, reflux 12 hr, 64% ; b) i) H_3PO_4, PPh_3, water, 0°C 45 min, 12 hr RT ii) KOH, 3 hr RT; c) Pd/C 10%, MeOH; d) BOC_2O, MeOH; e) 4-pentyoic acid, DCC, NHS, DIPEA, DMF; f) TFA, DCM; g) ATP, EDC, water, THF.

The synthesis of the bis-azide (**65**) from tetraethylene glycol (**64**) followed by the mono reduction to N_3-PEG-NH_2 (**66**) was facile and produced (**66**) in 45% yield over the two steps. However, reduction of the bis-azide (**65**) with 10% Pd/C resulted in the formation of predominately (**72**). Compound (**72**) is presumably formed by S_N2 attack of a bis-amine (**67**) or N_3-PEG-NH_2 (**66**), formed during the reduction, on a N_3-PEG-NH_2 (**66**) to eliminate azide (**Scheme 2.2**). This was, in part, due to concentration because under more dilute conditions less (**72**) was formed. To further reduce this formation an alternative route was sought (**Scheme 2.3**).

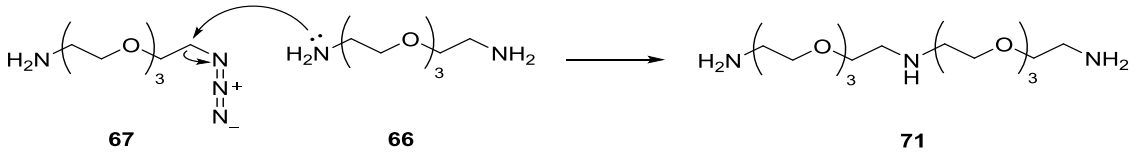

Scheme 2.2: S_N2 attack of bis-amine (67) on N_3-PEG-NH_2 (66) to afford (71).

2.3.2 Revised route for P-N analogues

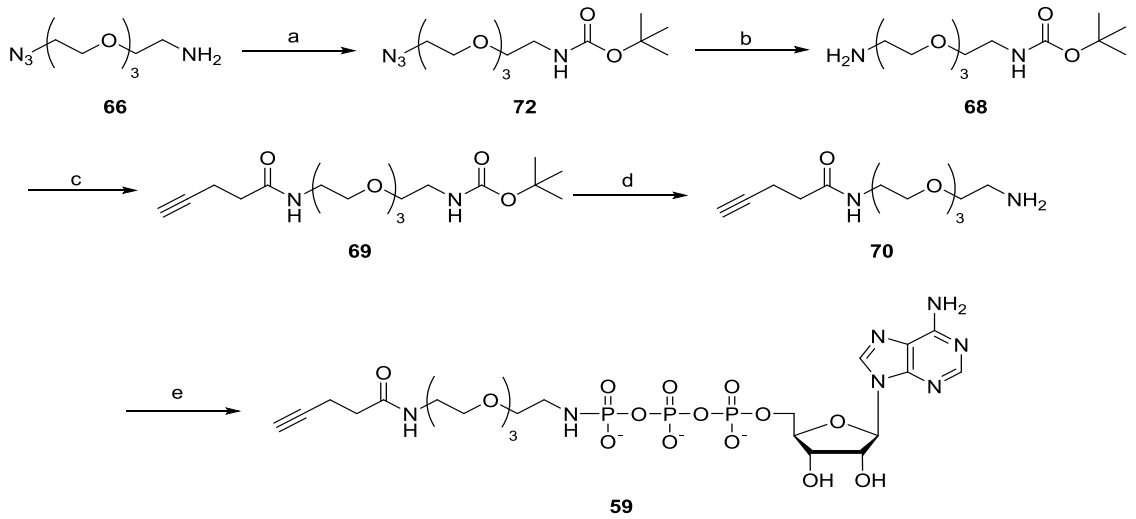

Scheme 2.3: Revised synthesis for ATP analogues. Reagents and conditions: a) BOC_2O, MeOH, RT, 12 hr, 34%; b) Pd/C 10%, MeOH, RT 88%; c) R-COOH, DCC, NHS, DIPEA, DMF, 40% when R-COOH was 4-pentynoic acid; d) TFA, DCM; e) ATP, EDC, water, THF.

The N_3-PEG-NH_2 (**66**) was BOC protected and purified by flash column chromatography to give N_3-PEG-NHBOC (**72**) in 34% yield. This was then further reduced using 10% Pd/C to yield NH_2-PEG-NHBOC (**68**) in 88% yield. Coupling of NH_2-PEG-NHBOC (**68**) to 4-pentynoic acid using DCC and NHS afforded NHBOC-linker-alkyne (**69**) in 4% yield following purification and was de-protected to give NH_2-linker-alkyne (**70**) in quantitative yield without further purification.

2.3.3 Nitrobenzofurazan as an alternative fluorescent tag

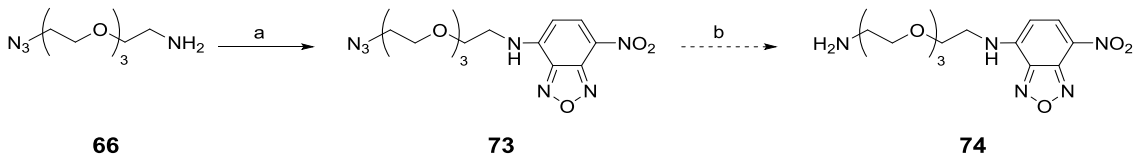

Scheme 2.1: Initial synthetic route for the nitrobenzofurazan tag & linker. Reagents and conditions: a) 4-chloro-7-nitrobenzofurazan, $NaHCO_3$, water, RT 12 hr, 69 %; b) i) H_3PO_4, PPh_3, water, 0°C 45 min, 12 hr RT ii) KOH, 3 hr RT.

Due to its proposed two step synthesis from the already synthesised N_3-PEG-NH_2 (**66**), the synthesis of nitrobenzofurazan bound to the linker was sought to form an alternative fluorescent ATP tag. Originally it was thought that the N_3-PEG-NH_2 (**66**) could be reacted with 4-chloro-7-nitrobenzofurazan and then reduced to give NH_2-PEG-Ar (**74**), ready to couple to ATP. N_3-PEG-Ar (**73**) was readily synthesised and purified in 69% yield from N_3-PEG-NH_2 (**66**). Staudinger reduction of N_3-PEG-Ar (**73**) was attempted but only starting material was identified.

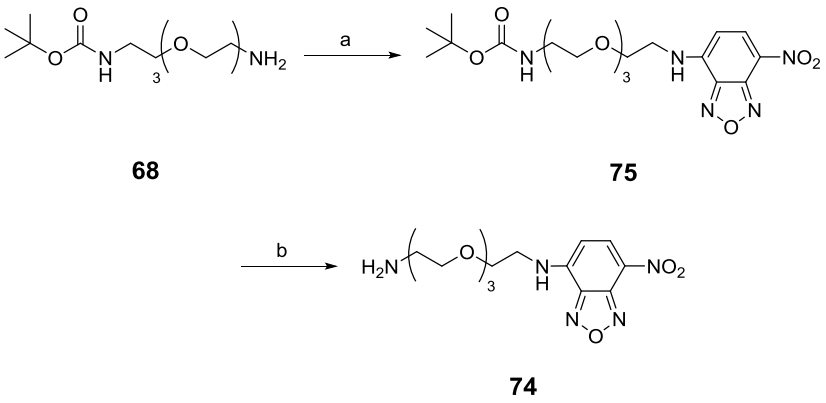

Scheme 2.4: Revised synthetic route for the nitrobenzofurazan tag & linker. Reagents and conditions: a) 4-chloro-7-nitrobenzofurazan, $NaHCO_3$, water, RT 12 hr, 60%; b) TFA, DCM, RT 2 hr.

An alternative route to NH_2-PEG-Ar (**74**) (**Scheme 2.4**) was to react BOCNH-PEG-NH_2 (**68**) with 4-chloro-7-nitrobenzofurazan to form BOCNH-PEG-Ar (**75**) followed by de-protection with TFA. Synthesis and purification of BOCNH-PEG-Ar (**75**) was readily

achieved in 60% yield and de-protection followed to give NH_2-PEG-Ar (**74**). However, comparison of the product to the NMR sample by TLC (10% [10% NH_4 in MeOH] in DCM) showed that the sample had degraded during NMR analysis. Despite attempted recovery by flash column chromatography, no product was isolated.

2.3.4 Coupling to ATP to form P-N analogues

ATPγNH-PEG-N_3 (**60**), GTPγNH-PEG-N_3 (**99**) and ATPγNH-linker-alkyne (**59**) were synthesised by coupling ATP to the relevant tagged linker, NH_2-PEG-N_3 (**66**) and NH_2-linker-alkyne (**70**), and purified by ion exchange chromatography. Further purification by RP-HPLC was required to remove A/GDP, which co-eluted with the analogues as these compounds have the same charge, and to ensure that no A/GTP was present. The low yield for the synthesis of GTPγNH-PEG-N_3 (**99**) can be attributed to adding EDC (**76**) to a mixture of GTP and NH_2-PEG-N_3 (**66**) rather than pre-activating the GTP with EDC. This resulted in the formation of (**77**), reducing the amount of NH_2-PEG-N_3 (**66**) available to react with GTP (**Scheme 2.5**).

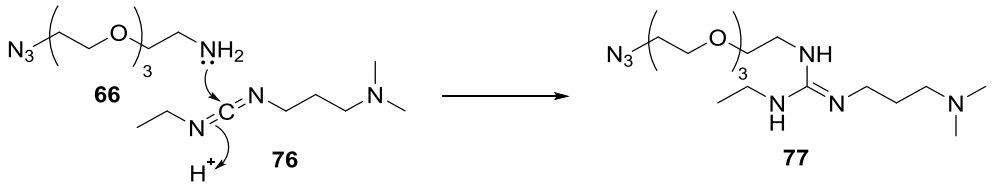

Scheme 2.5: If A/GTP is not pre-activated with EDC (76) or there is excess EDC present, it can react with the amine to be coupled to the ATP, in this case NH_2-PEG-N_3 (66), to give (77).

Crude ATPγNH-linker-alkyne (**59**) was stirred with coumarinazide (**78**) in a 1,3-dipolar Huisgencycloaddition "click" reaction. However, no product was obtained. As this has been previously synthesised by another lab member[211] and used in kinetic studies (**Section 2.5.9**), it is thought that this was due to the dilution of the reaction. ATPγNH-

PEG-alkyne (**59**) used was not pure, further decreasing the concentration of the reagent.

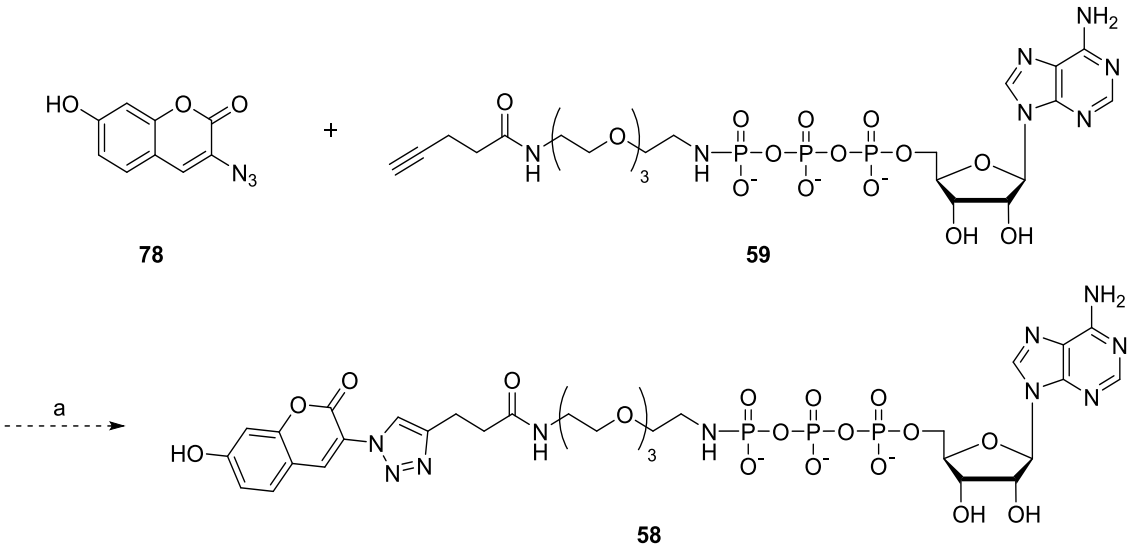

Scheme 2.2: Synthetic route for ATPγNH-linker-coumarin (58). Reagents and conditions: a) $CuSO_4$, sodium ascorbate, water, methanol, RT 3 hr.

These ATP phosphoramidate analogues (**58**, **59** & **60**) were previously synthesised and isolated by another group member.[211] These and the GTPγNH-PEG-N_3 (**99**), synthesised here, (as well as ATPγEt (**63**) (**Section 2.3.7**)) were purified using RP-HPLC with TEAA buffer as used in the initial analysis of these analogues as substrates for *Pf*CK2α (**Section 2.5**). However, it was decided to use TEAB buffer for the RP-HPLC purification[239] of the re-synthesised ATP analogues because it is easier to remove than TEAA and this buffer was already in use for ion exchange chromatography. However, degradation occurred during/after purification by RP-HPLC in this new buffer system for the P-N analogues. After this problem was discovered, investigations were undertaken using ATPγNH-PEG-N_3 (**60**).

Prior to RP-HPLC purification, the analytical RP-HPLC trace of ATPγNH-PEG-N_3 (**60**) showed predominantly two peaks (**Figure 2.9**) that were well resolved. The sample was

purified by semi-prep RP-HPLC and the fractions containing ATPγNH-PEG-N_3 (**60**) were pooled and concentrated *in vacuo* followed by several evaporations with methanol to remove excess TEAB. RP-HPLC analysis (**Figure 2.10**) showed the sample to contain the same ADP and ATP impurity peaks as before. As the separation was good (over 2 min) and small fractions (20 s) were collected, it was postulated that this was due to degradation. A further round of semi-prep RP-HPLC followed but afforded the same result.

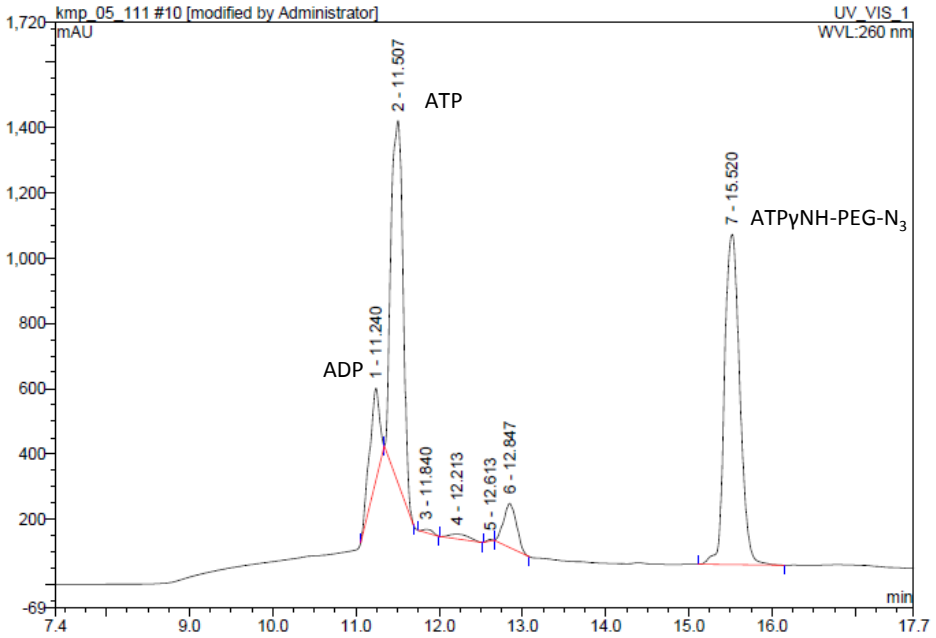

Figure 2.9: RP-HPLC trace of ATPγNH-PEG-N_3 (60) before purification by semi-prep RP-HPLC.

As the P-N bond is known to be acid labile[211, 174] and acidic buffers are often used in these RP-HPLC systems, tests were carried out to ensure the columns were being used at a suitable pH for the P-N analogues. The standard procedure for changing from the acidic buffer to the TEAB buffer was to wash the column with 100% water for a minimum of 10 min, followed by a minimum of 10 min equilibration with 100% Buffer A (50 mM TEAB in water). Therefore, the pH of the eluent from both the semi-

prep and analytical columns were tested after a 10 min water wash followed by 10 min equilibration with 100% Buffer A. The pH was found to be ~5.5 after the water wash and ~8.0 after equilibration with 100% Buffer A. It was therefore concluded that these wash and equilibration times were adequate.

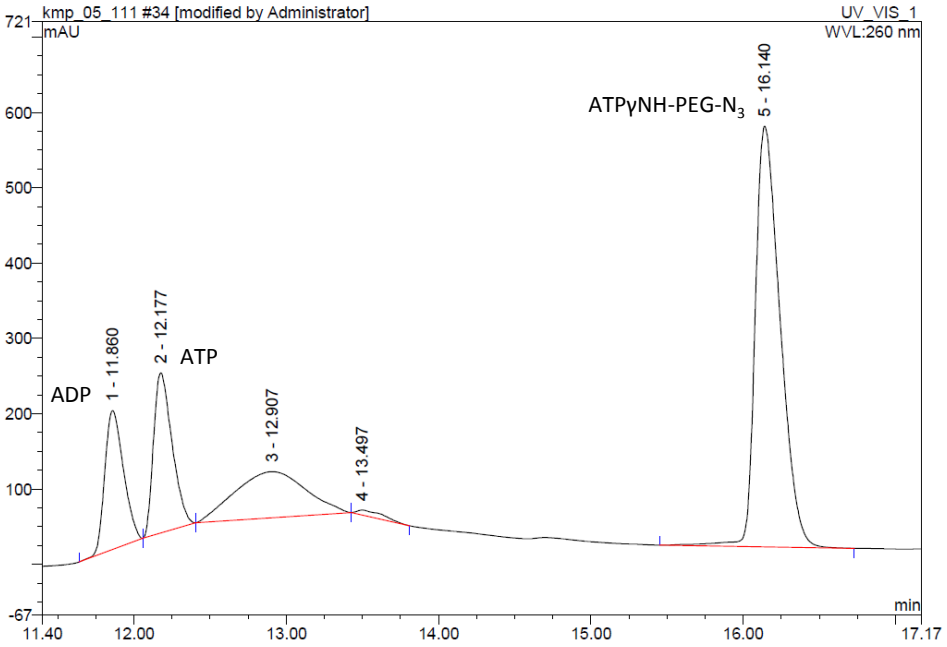

Figure 2.10: RP-HPLC trace of ATPγNH-PEG-N_3 (60) after first purification by semi-prep RP-HPLC.

ATPγNH-PEG-N_3 (**60**) was purified by analytical RP-HPLC, concentrated and subjected to several methanol evaporations before being analysed by analytical RP-HPLC (**Figure 2.11**). Only trace amounts of ATP/ADP were seen; the sample was predominantly ATPγNH-PEG-N_3 (**60**). This indicated that concentrating the sample and performing methanol evaporations was not the cause of degradation. It was, therefore, decided to purify more ATPγNH-PEG-N_3 (**60**) using analytical RP-HPLC ready for use in Caliper electrophoresis.

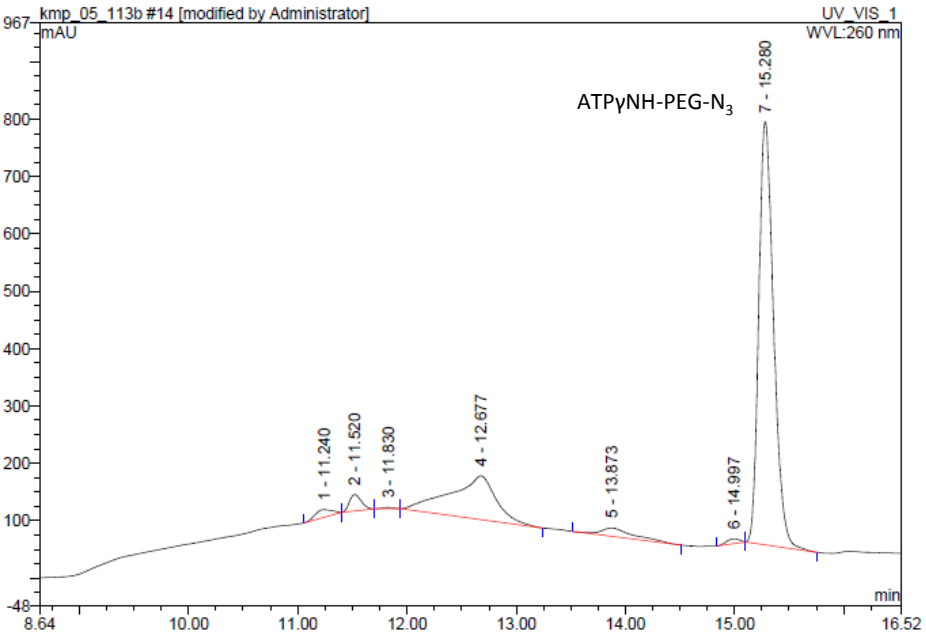

Figure 2.11: RP-HPLC trace of ATPγNH-PEG-N_3 (60) after purification using analytical RP-HPLC.

The default settings on the analytical RP-HPLC wash the loop with 80 µL (4 x loop volume) and overfill the loop by a factor of 2. Due to only a small amount of sample remaining, it was decided to reduce to wash volume to the recommended minimum of 40 µL and to only overfill the loop by a factor of 0.2. However, this caused the sample to be eluted in the dead volume due to trace amounts of acetonitrile in the loop from the loop cleaning method. Therefore, the default settings were used. Insufficient ATPγNH-PEG-N_3 (**60**) was collected for analysis by NMR or for kinetic studies using Caliper capillary electrophoresis. Due to time constraints, it was not possible to further investigate the problems experienced with degradation.

2.3.5 Synthetic routes for the synthesis of P-O analogues of ATP

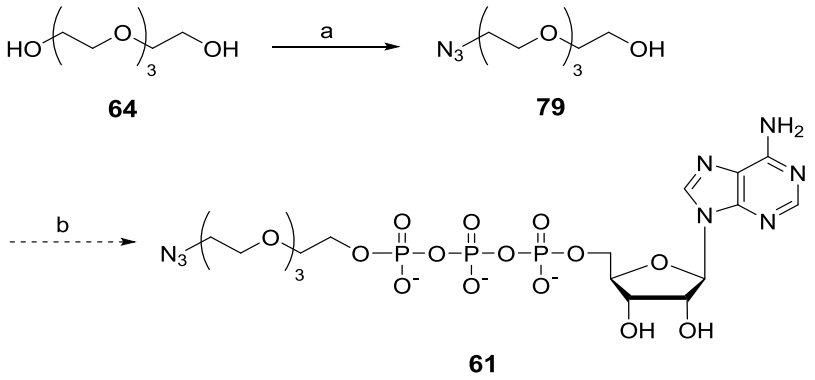

Scheme: 2.6: Initial synthetic route for ATPγO-PEG-N_3 (61). Reagents and conditions: a) i) $MeSO_2Cl$, TEA, DCM, 0°C 45 min, RT 12 hr ii) NaN_3, $NaHCO_3$, DCM, reflux 12 hr; b1) ATP, EDC, water, RT, 3 hr or b2) ATP, DCC, DMF, TEA, 40°C, 12 hr.

Tetraethylene glycol (**64**) was converted to N_3-PEG-OH (**79**) in 83% yield in a method analogous to that for bis-azide (**65**) synthesis (**Scheme 2.1**). Coupling of N_3-PEG-OH (**79**) to ATP was attempted with both EDC and DCC but only starting material was observed. Alternative routes for the synthesis of P-O ATP analogues were sought.

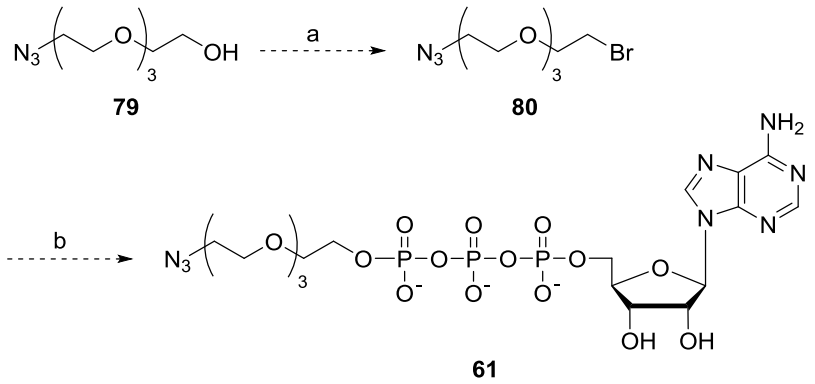

Scheme 2.7: Second synthetic route for ATPγO-PEG-N_3 (61). Reagents and conditions: a1) PBr_3, diethyl ether, RT, 12 hr or a2) PBr_3, diethyl ether, reflux, 12 hr, or a3) PBr_3, toluene, reflux 12 hr; b) ATP, DMF, RT, 12 hr.

Synthesis of N_3-PEG-Br (**80**) from N_3-PEG-OH (**79**) using PBr_3 was unsuccessful when stirred at room temperature or heated to reflux overnight in diethyl ether and when heated to reflux overnight in toluene (**Scheme 2.7**). An alternative method for the

synthesis of N_3-PEG-Br (**80**) was found (**Scheme 2.8**). N_3-PEG-Meso (**81**) was synthesised from N_3-PEG-OH (**79**) and readily converted to N_3-PEG-Br (**80**); however, the reaction of N_3-PEG-Br (**80**) with ATP was unsuccessful and only starting materials were observed by MS.

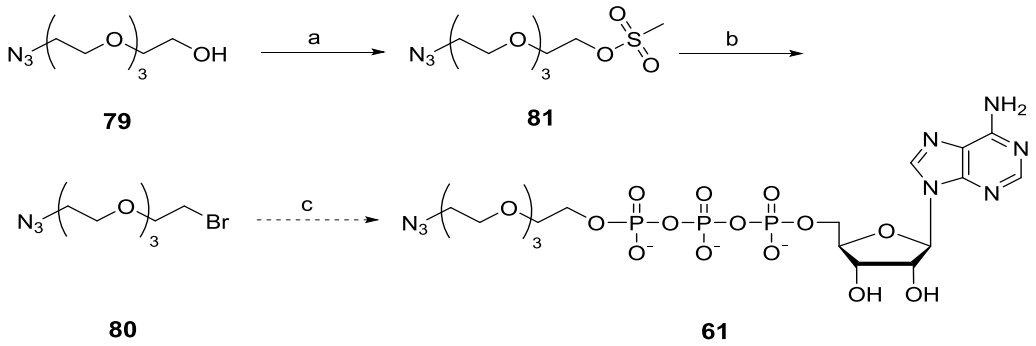

Scheme 2.8: Third synthetic route for ATPγO-PEG-N_3 (61). Reagents and conditions: a) i)$MeSO_2Cl$, TEA, DCM, 0°C, 45 min ii) RT 12 hr 38%; b) $(Bu)_4N^+$, acetonitrile, 50°C 12 hr 36%; c) ATP, DMF, RT, 12 hr.

N_3-PEG-OH (**79**) was converted to N_3-PEG-OPO_3H_2 (**82**) using $POCl_3$. The product was detected by LCMS and used without further purification. No product was observed by MS for the reaction of ADP with N_3-PEG-OPO_3H_2 (**82**); only ATP, ADP and AMP were evident. This suggested that H_3PO_4 made *in situ* during N_3-PEG-OPO_3H_2 (**82**) synthesis had reacted with ADP.

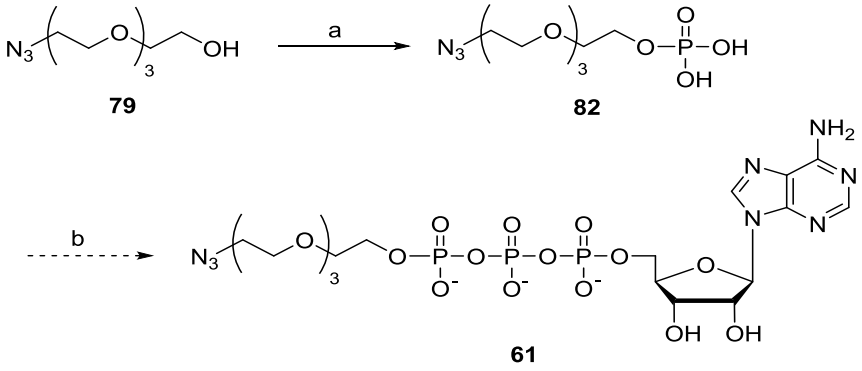

Scheme 2.9: Fourth synthetic route for ATPγO-PEG-N_3 (61). Reagents and conditions: a) $POCl_3$, TEA, ether, -78°C 30 min, RT, 12 hr; b) Pre-activated ADP (i) ADP, CDI, DMF, RT, 12 hr ii) MeOH, RT, 30 min), DMF, RT, 12 hr.

ATP P-O analogues were not prepared. As mesyl is a good leaving group,[240] the synthesis of (**61**) could be attempted by directly reacting N_3-PEG-Meso (**81**) with ATP, rather than going through N_3-PEG-Br (**80**). N_3-PEG-Br (**80**) could also be reacted directly with the ATP disodium salt in water.[241] Purification of N_3-PEG-OPO_3H_2 (**82**) to remove excess H_3PO_4 could result in successful synthesis of (**61**), instead of the synthesis of ATP, because there would no longer be phosphoric acid competing with N_3-PEG-OPO_3H_2 (**82**) to react with ADP.

2.3.6 Synthesis of ATPγSEt

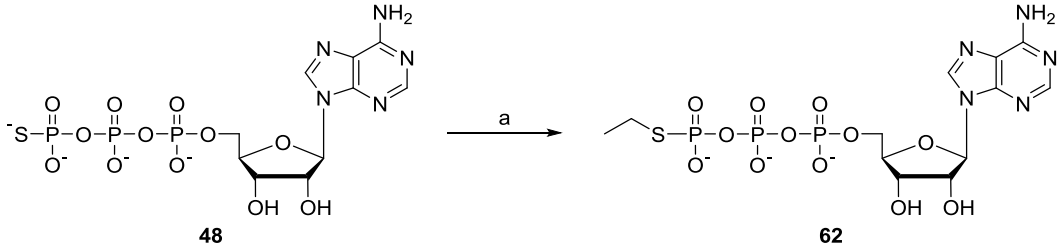

Scheme 2.10: Synthetic route for ATPγSEt (62). Reagents and condtions: a) iodoethane, MeOD, D_2O, RT, 48 hr.

ATPγS (**48**) was reacted with iodoethane in a 1:1 ratio to reduce the possibility of alkylation at multiple sites due to electrophilic attack on the adenosine (**Scheme 2.12**) instead of the desired electrophilic attack on the sulphur (**Scheme 2.11**). The reaction was monitored by ^{31}P & ^{1}H NMR. No product was afforded after 24 hr so additional iodoethane was added. After a further 48 hr ^{31}P NMR confirmed the presence of multiple ATP species. Purification by RP-HPLC followed by ESMS confirmed the presence of ATPγSEt (**62**). Although the 550 [M-H^+] ion only proves the presence of an alkylated ATPγS substance, the presence of the [ADP-H^+] fragment at 426 proves that the ethylation occurred on the S, rather than on the adenosine. Only 10 nmol were isolated after RP-HPLC; hence, it was not possible to perform NMR analysis on ATPγSEt

(**62**). Due to the poor conversion and price of ATPγS (**48**), it was decided not to continue with the synthesis. However, as RP-HPLC conditions were established during this initial synthesis, it would be possible to carry out the reaction under more concentrated conditions and monitor progress by RP-HPLC instead of NMR, potentially increasing the amount of product produced.

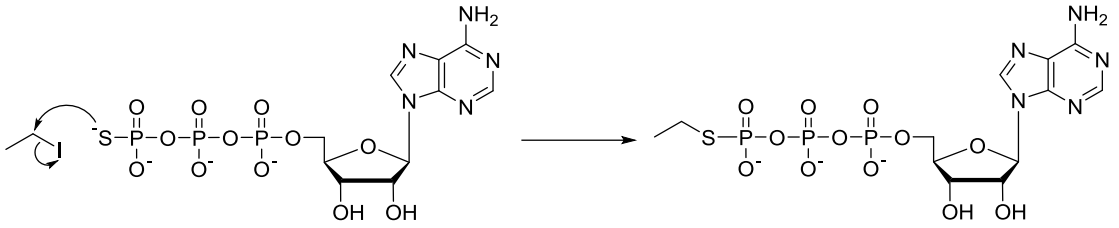

48 **62**

Scheme 2.11: The mechanism for the S_N2 reaction between the γS of ATPγS (48) and iodoethane.

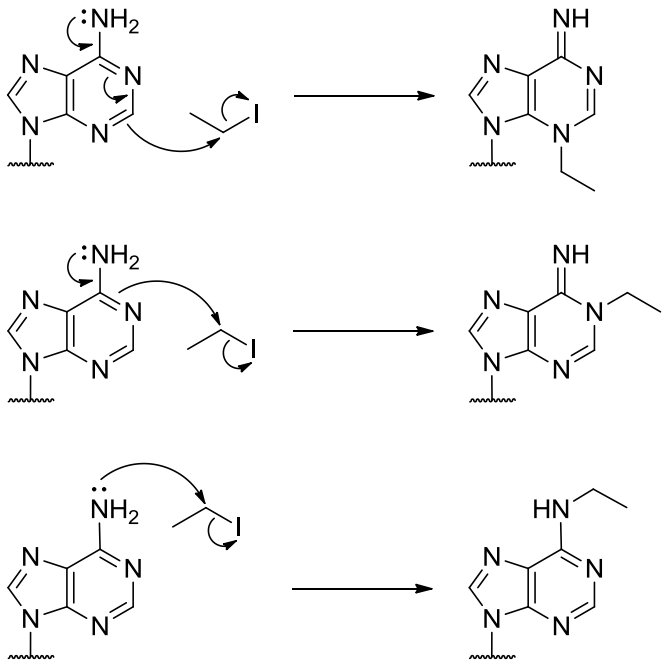

Scheme 2.12: S_N2 alkylation can occur at three positions on the adenine of ATPγS (48).

2.3.7 Synthesis of ATPγEt

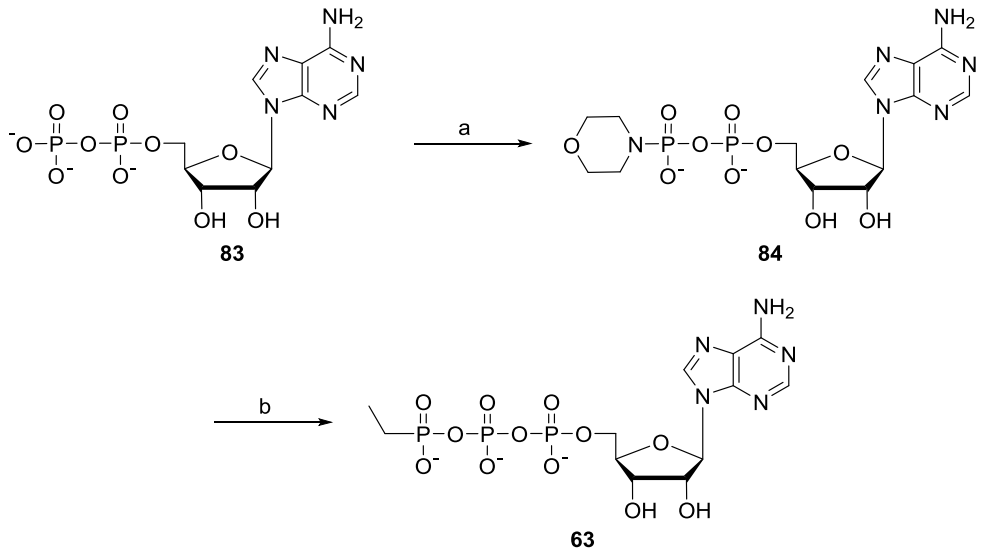

Scheme 2.13: Synthetic route for ATPγEt (63). Reagents and conditions: a) morpholine, DCC, ^{t}BuOH, water, reflux, 12 hr, 30% crude; b) ethylphosphonic acid, DMSO, 40°C, 48 hr, 9%.

ADP (**83**) was reacted with morpholine to produce ADP-morpholidate (**84**), which was purified by ion exchange chromatography. This afforded a mixture of ADP-morpholidate and AMP, due to their identical charge, which was then reacted with ethylphosphonic acid to produce ATPγEt (**63**). Purification by ion exchange chromatography was followed by HPLC to ensure the removal of ADP and ATP. The synthesis was relatively facile; however, a much shallower HPLC gradient was required than for the P-N analogues to ensure separation from ATP and ADP (**Figure 2.12**). There was no problem with degradation following RP-HPLC purification with TEAB buffer (**Figure 2.13**), unlike for the P-N analogues (**Section 2.3.4**).

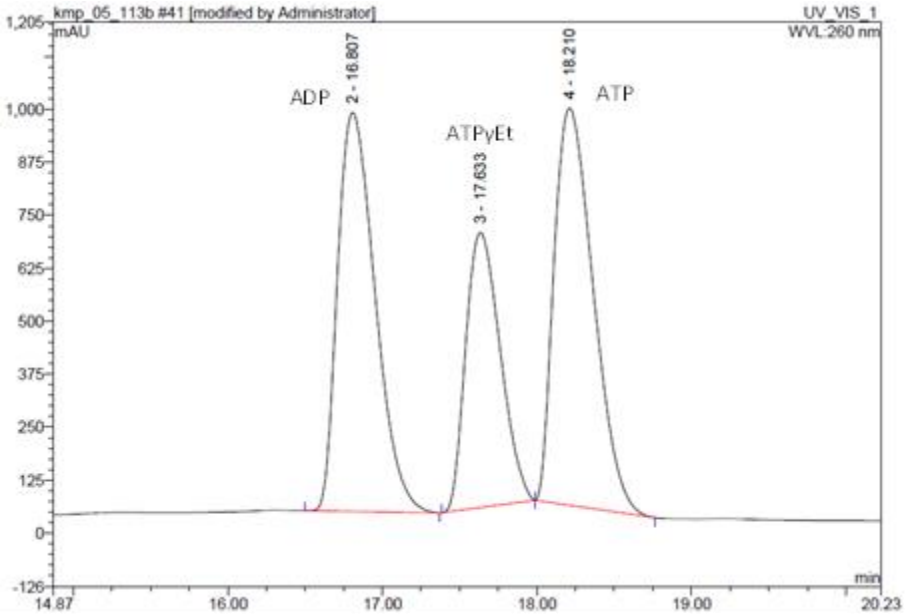

Figure 2.12: RP-HPLC trace of ATPγEt (63) spiked with ADP and ATP.

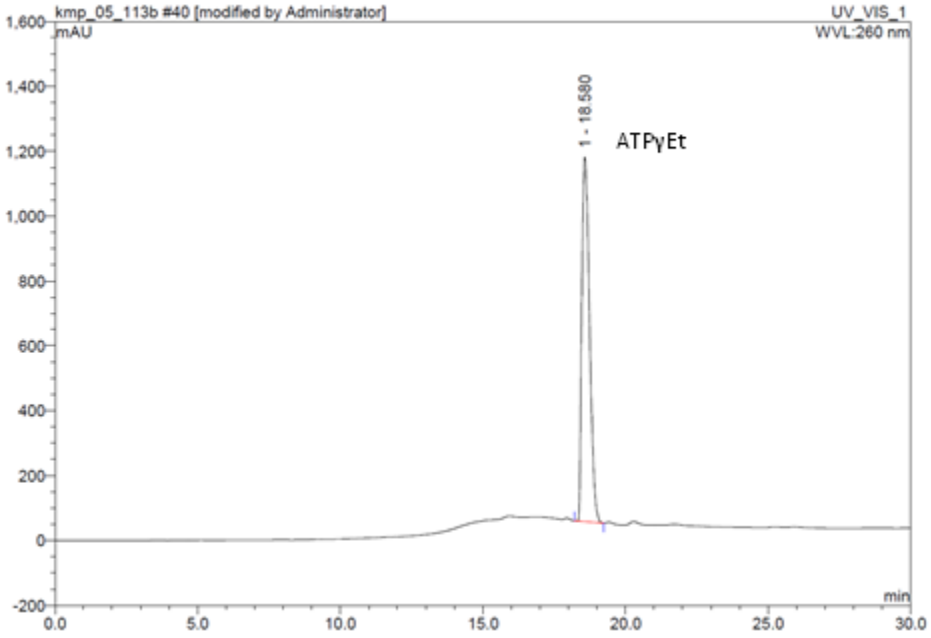

Figure 2.13: RP-HPLC trace of ATPγEt (63) after purification by RP-HPLC.

2.4 Synthesis of CX-4945 and analogues

The synthesis of CX-4945 (**55**) was sought for its potential to selectively inhibit *Pf*CK2 within the parasite. The potency and selectivity of the small molecule inhibitor CX-4945 (**55**) for human CK2 made it and its derivatives interesting molecular probes for the study of phosphorylation pathways of *Pf*CK2. As *Pf*CK2 is essential for sexual proliferation of the parasite,[115] Knock-out mutants cannot be used to study the cellular processes *Pf*CK2 is involved in. Inhibitors can be used in a dose dependent manner to study the effect of reduced kinase activity.

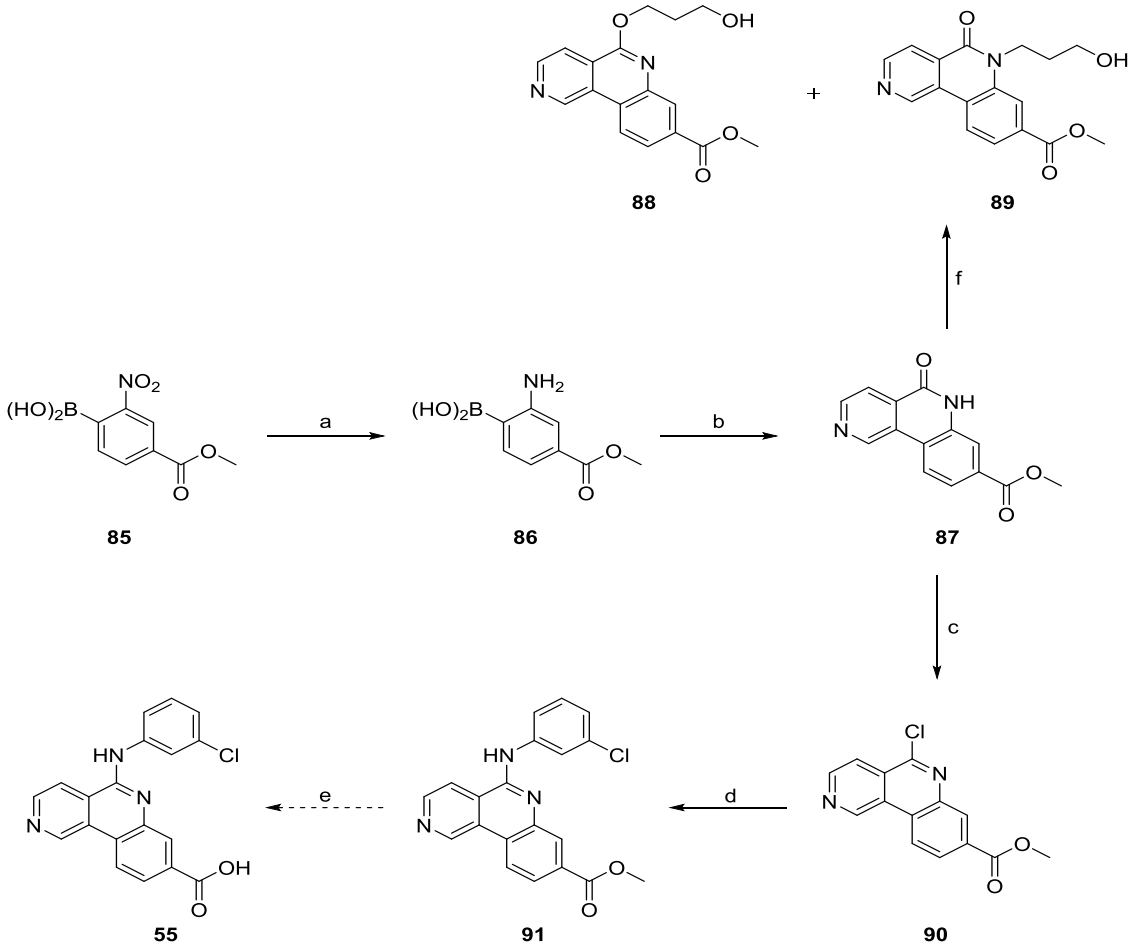

Scheme 2.14: Synthetic route for CX-4945 (55). Reagents and conditions: a) PD/C-10%, methanol, ethanol, RT, 2 hr 98%; b) ethyl 3-bromoisonicotinate, $PdCL_2$(dppf), NaOAc, DMF, 125 °C, 12hr, 64%; c) $POCl_3$, 110 °C, 72 hr, 50% purity by NMR; d) p-choloraniline, NMP, 80 °C, 12 hr, 2.5%; e) i) THF, $LiAlH_4$,- 40°C, 1 hr, ii) H_2O; f) iodopropanol, K_2CO_3, DMF, 100 °C, 1.5 hr.

The published synthesis of CX-4945 (**55**)[238] used 2-amino-4(methoxycarbonyl)phenyl) boronic acid (**86**) as the starting point; however, in this synthesis 2-amino-4(methoxycarbonyl)phenyl)boronic acid (**86**) was produced by the reduction of 2-nitro-4-(methoxycarbonyl) phenyl)boronic acid (**85**) with Pd/C-10%. It was found that if the solution was not dilute enough the starting material would precipitate out of solution during synthesis, reducing the yield. The CH protons are not well resolved in the ^{1}H NMR, resulting in a broad 2H singlet instead of two doublets. However, this concurs with an NMR spectra provided by Combi-blocks, from whom the starting material (**85**) was obtained, and it is likely this is caused by coupling to the boron.

5-Oxo-5,6-dihydrobenzo[c][2,6]naphthyridine-8-carboxylate (**87**) was synthesised from the Suzuki cross-coupling of (**86**) with ethyl 3-bromoisonicotinate using $PdCl_2$(dppf). In modification to the literature method,[238] after the product had been precipitated with water, it was collected by centrifugation, rather than filtration, and the process repeated twice more to remove the water soluble palladium catalyst, $PdCl_2$(dppf).[242] Compound (**87**) was then reacted with iodopropanol to afford two isomers (**88**) and (**89**), as confirmed by LCMS and TLC. In the interest of time these compounds were not isolated or further pursued. These compounds were of interest as their analogues (**92**) & (**93**) were found to have IC_{50} values for mammalian CK2 of approx. 1 µM.[238]

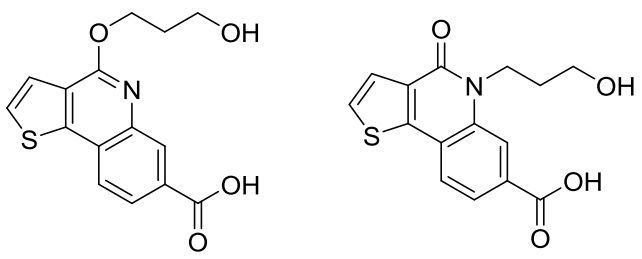

92 **93**

Figure 2.14: Two analogues of CX-4945, (92) & (93) inhibit mammalian CK2 with IC_{50} values of 1.50 and 0.99 µM respectively.[238]

5-Oxo-5,6-dihydrobenzo[c][2,6]naphthyridine-8-carboxylate (**87**) was reacted with $POCl_3$ to afford 5-methyl-5-chlorobenzo[c][2,6]naphthyridine-8-carboxylate (**90**) by LCMS and ^1H NMR; however, the crude sample was black and not very soluble. Extraction with DCM was unsuccessful; thus, the alternative workup, dissolving the crude sample in acetonitrile and precipitating with iced water, suggested in the literature,[238] was used. However, rather than giving only the product, this afforded two compounds by LCMS (R_t 1.93; m/z calculated 273.0431 $[M+H^+]$ observed 273.0427 & 275.0414 & R_t 1.38; m/z calculated 255.0770 $[M+H^+]$ observed 255.0778). Initially it was thought that this second compound was unreacted starting material but prior to the addition of water, this species was not detected by MS. It was, therefore, concluded that water could act as a nucleophile to displace the chlorine group, affording the starting material (**87**) (**Scheme 2.15**).

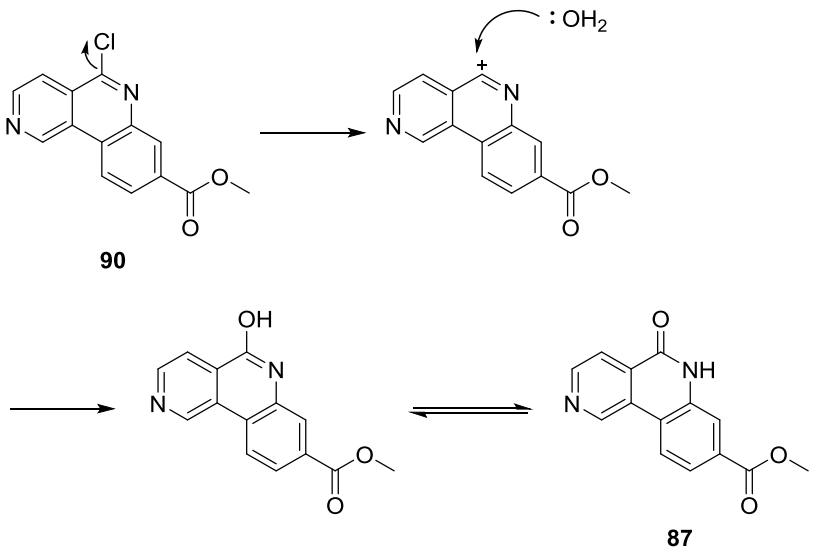

Scheme 2.15: Mechanism for the suggested S_N1 attack of water to displace chlorine, resulting in the reformation of the starting material (86).

Methyl 5-((3-chlorophenyl) amino)benzo[c][2,6]naphthyridine-8-carboxylate (**91**) was synthesised and purified in low yield (2.5%) from (**90**). Due to the difficulty in isolating (**90**) and time constraints, the synthesis of (**55**) was not completed.

2.5 Analysis of ATP analogues as substrates of CK2

2.5.1 Expression and purification of *Pf*CK2α

The pGRX-2T plasmid containing the coding sequence for the bacterial expression of *Pf*CK2α-GST fusion protein was transformed into BL21-CodonPlus (DE3)-RIPL competent cells and *Pf*CK2α-GST was successfully expressed and purified using glutathione affinity chromatography. The concentration of protein was measured using a Bradford assay and the percentage of *Pf*CK2α-GST calculated using densiometry. As the GST tag was at the N-terminus of the PfCK2α, truncated proteins eluted together with the full length protein during purification. It was hypothesised that if the tag used for purification were on the C-terminus, only the full length protein would be retained on the column and truncated proteins would be removed during the washes; hence, the purity would increase. A pLEICS-05 vector containing the coding sequence for the bacterial expression of *Pf*CK2α-His_6 fusion protein was, therefore, produced by PROTEX (University of Leicester). *Pf*CK2α-His_6 was indeed purer than *Pf*CK2α-GST, as can be seen in (**Figure 2.15**), with the *Pf*CK2α-His_6 being approx. 50% of the total protein content compared to 25% for *Pf*CK2α-GST.

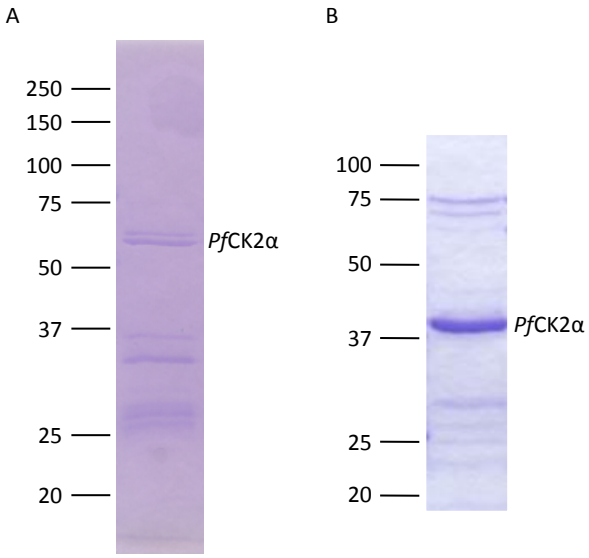

Figure 2.15: SDS-PAGE of *Pf*CK2 after purification. A: *Pf*CK2α-GST fusion protein where the tag is on the N-terminus; B: *Pf*CK2α-his$_6$ fusion protein where the tag is on the C-terminus.

2.5.2 Establishing activity – Quantitative analysis

Initial assays were performed to confirm the activity of *Pf*CK2α-GST and *Pf*CK2α-His$_6$ were active by measuring the cpm (representing phosphorylated peptide) with increasing enzyme concentration. The enzymes were shown to be active because as the concentration of enzyme increased so too did the phosphorylation of the peptide substrate until the concentration of peptide became a limiting reagent, resulting in the plateau observed (**Figure 2.16** & **Figure 2.17**). These curves were used to decide the quantity of *Pf*CK2α to be used in the subsequent assays for the determination of the kinetic parameters of these enzymes with ATP and GTP. A compromise was needed between a level of activity that provided a cpm at least an order of magnitude above the background level and a level that ensured the extent of phosphorylation was low enough to enable steady state assumptions to be made.

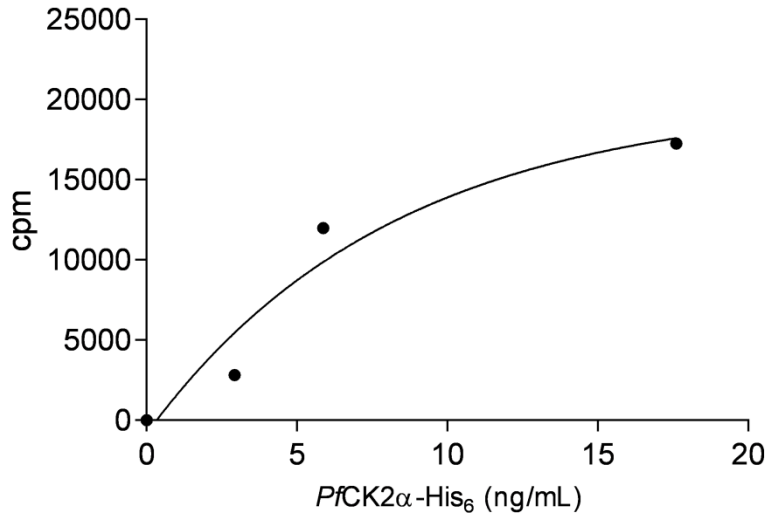

Figure 2.16: Dependence of rate on the concentration of enzyme. Increased rate (i.e. increased phosphorylated peptide) was observed with increasing enzyme concentration for *Pf*CK2α-GST.

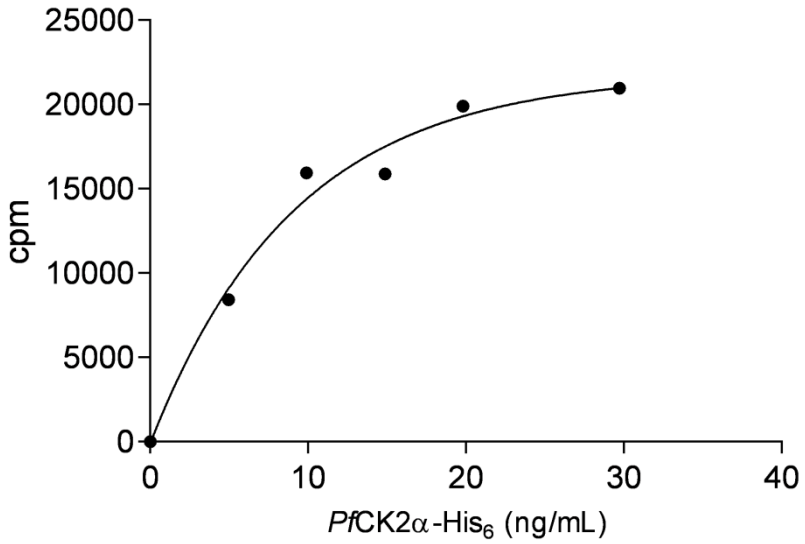

Figure 2.17: Dependence of cpm (i.e. increased phosphorylated peptide) on the concentration of enzyme. Increased phosphorylation was observed with increasing enzyme concentration for *Pf*CK2α-His_6.

When activity checks were performed periodically on the same batch of *Pf*CK2α-GST, it was found that *Pf*CK2α-GST activity diminished over time (**Figure 2.18**) despite being stored as aliquots at -80°C and not subjected to multiple freeze-thaw cycles. Hence, it was necessary to purify *Pf*CK2α in small batches and for kinetic assays to be performed as soon as possible thereafter. This instability could be a result of remaining enzyme impurities produced during protein preparation, the optimum buffer conditions not

being used, a change in pH upon freezing due to ice crystal formation, or inherent instability of the kinase. It has been found that some CK2 mutant kinases with truncated N-termini are unstable and inactive as the CK2α subunit but activity is restored upon formation of the holoenzyme.[206] It is therefore plausible that the *Pf*CK2α subunit is stabilised by the β-subunits and activity would be regained upon formation of the holoenzyme. During the conference Molecular Approaches to Malaria 2012, discussion with another researcher, who has worked on *Pf*CK2α, highlighted that this is a common problem with *Pf*CK2α and has resulted in it no longer being used in multi-enzyme drug screens by that group.

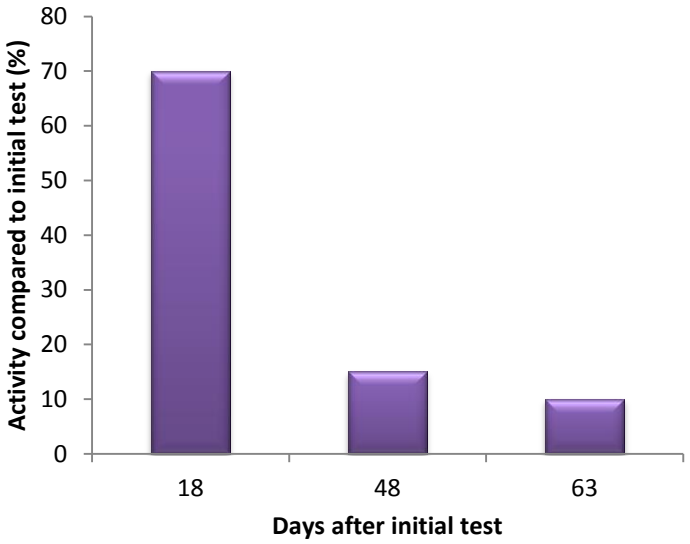

Figure 2.18 The activity of a batch of *Pf*CK2α-GST measured on different dates and compared to the activity of the same batch on 20/01/2011. Activity diminished over time.

2.5.3 Peptide phosphorylation analysis by MALDI-TOF MS

To demonstrate unequivocally the use of γ-modified ATP analogues by mammalian CK2 and *Pf*CK2α and the transfer of the intact phosphate tag to the peptide substrate, an assay using analysis by mass spectrometry was explored. The enzymes were

incubated with ATP or an ATP analogue and a known peptide substrate for CK2 for 2-18 hr. The sample was desalted by Zip Tip and analysed by MALDI-TOF MS. The mass of each tagged phosphorylated peptide should be unique to the analogue used (**Table 2.2**) rendering them readily identifiable by MS.

Table 2.2: Expected mass of peptides RRRADDSDDDDD (used with *Pf*CK2α) and RRREEETEEE (used with mammalian CK2) phosphorylated with different tags. Peptide masses prior to phosphorylation: RRRADDSDDDDD 1449.5716 Da & RRREEETEE 1361.6171 Da.

	Mass (Da)	
Co-substrate	**Phosphorylated RRRADDSDDDDD**	**Phosphorylated RRREEETEEE**
ATP (**32**)	1529.5380	1441.5835
GTP (**52**)	1529.5380	1441.5835
ATPγNH-PEG-N_3 (60)	1729.6653	1641.7108
ATPγEt (**63**)	1541.5744	1453.6199
ATPγS (**48**)	1545.5151	1457.5606
GTPγS (**94**)	1545.5151	1457.5606

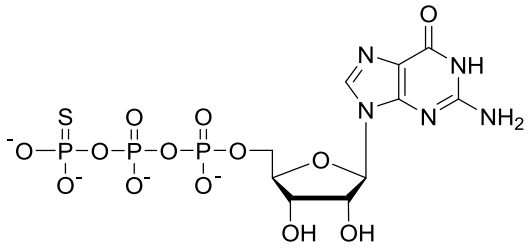

94

Figure 2.19: The structure of the GTP derivative, GTPγS.

For both mammalian CK2 and *Pf*CK2α the corresponding phosphorylated peptides were observed as expected when using ATP (**32**) as a co-substrate (**Figure 2.20**), validating their use as substrates for these enzymes. However, when GTP (**52**) was used as a co-substrate phosphorylation was only observed with mammalian CK2 (**Figure 2.21**). This was surprising due to work published by Holland *et al.*,[227] which

reported GTP as a substrate for *Pf*CK2α, but is supported by the kinetic studies carried out in Leicester (**Section 2.5.5**) and Grenoble (**Section 2.5.6**). Therefore, further investigation was required before embarking upon the synthesis of GTP analogues for the study of *Pf*CK2 phosphorylation pathways.

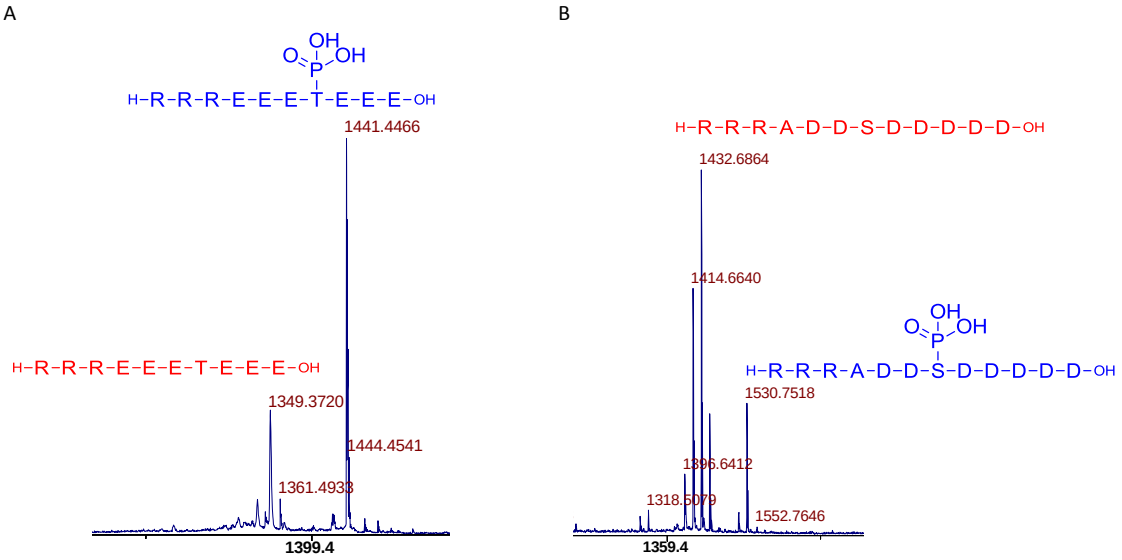

Figure 2.20: MALDI-TOF MS analysis of kinase assays with ATP (32) as the co-substrate. Peptide labelled in red and phosphorylated peptide in blue. A: Using mammalian CK2 with peptide RRREEETEEE; B: Using *Pf*CK2α with peptide substrate RRRADDSDDDDD. Phosphorylation was observed using both mammalian CK2 and *Pf*CK2α.

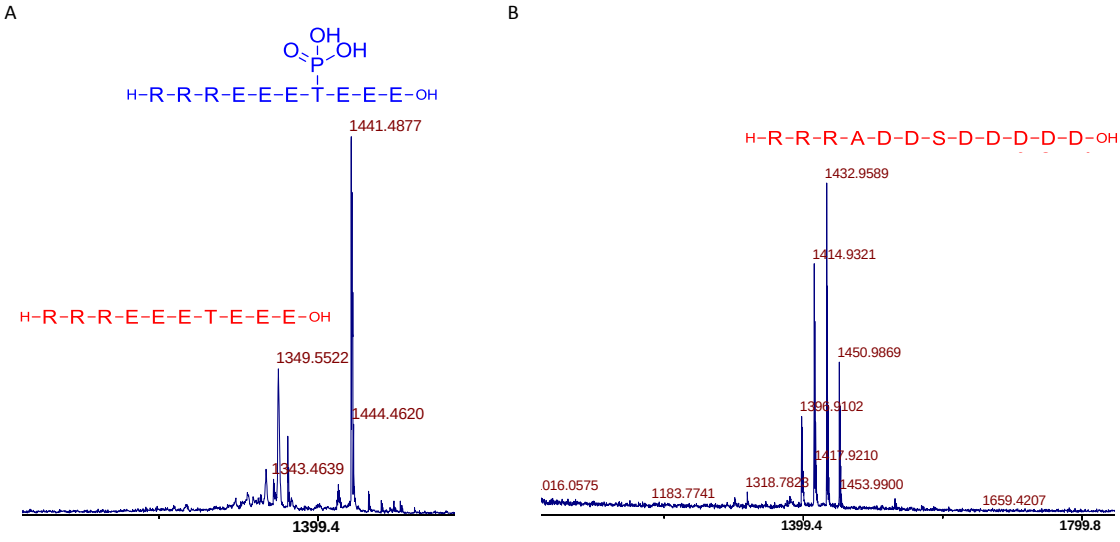

Figure 2.21: MALDI-TOF MS analysis of kinase assays with GTP (52) as the co-substrate. Peptide labelled in red and phosphorylated peptide in blue. A: Using mammalian CK2 with peptide RRREEETEEE; B: Using *Pf*CK2α with peptide substrate RRRADDSDDDDD. Phosphorylation was observed using mammalian CK2 but not *Pf*CK2α.

The expected masses of the azide-tagged phosphorylated peptide 1729.6653 Da (*Pf*CK2α) and 1641.7108 Da (mammalian CK2) were not observed for either kinase with ATPγNH-PEG-N_3 (**60**) or other P-N analogues;[211] only phosphorylated peptide was detected (**Figure 2.22**). Since the ATP analogues were established to be free from ATP by HPLC analysis prior to the assays (**Figure 2.23**) and analogues such as these were reported to be accepted by CK2 by Pflum *et al.*,[173, 172, 243] it was concluded that the P-N bond was unstable during the experimental conditions used. The analogues were shown to be stable during their purification, concentration and characterisation. The most likely cause of this P-N bond cleavage was the acidic conditions of the Zip Tip desalting procedure. This Zip Tip treatment was necessary to remove the high salt content present in the buffered sample prior to MALDI-TOF MS and therefore, this step was unavoidable.

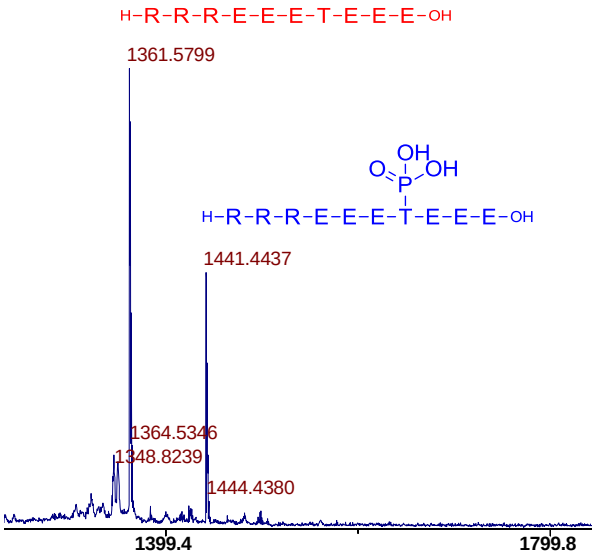

Figure 2.22: MALDI-TOF MS analysis of a kinase assay using mammalian CK2 with peptide RRREEETEEE with ATPγNH-PEG-N_3 (60) as the co-substrate. Peptide labelled in red and phosphorylated peptide in blue. No tagged phosphorylation was observed (expected mass 1729.6653) only untagged phosphorylation.

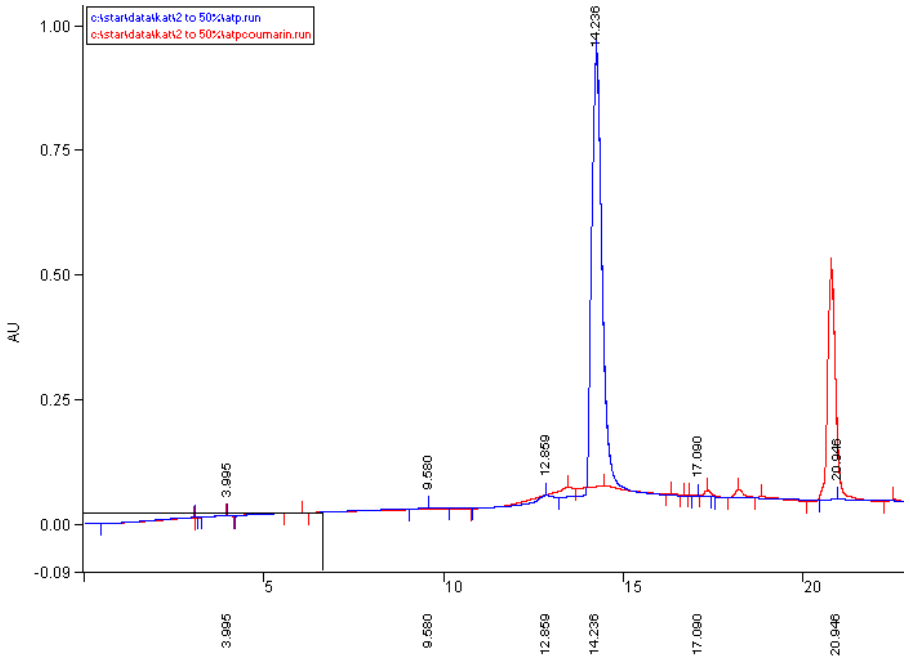

Figure 2.23: HPLC overlay of ATP (blue) and ATPγNH-linker-coumarin (58) (red), highlighting the lack of ATP present after purification of the analogues. Monitored at λ_{max} 260 nm.

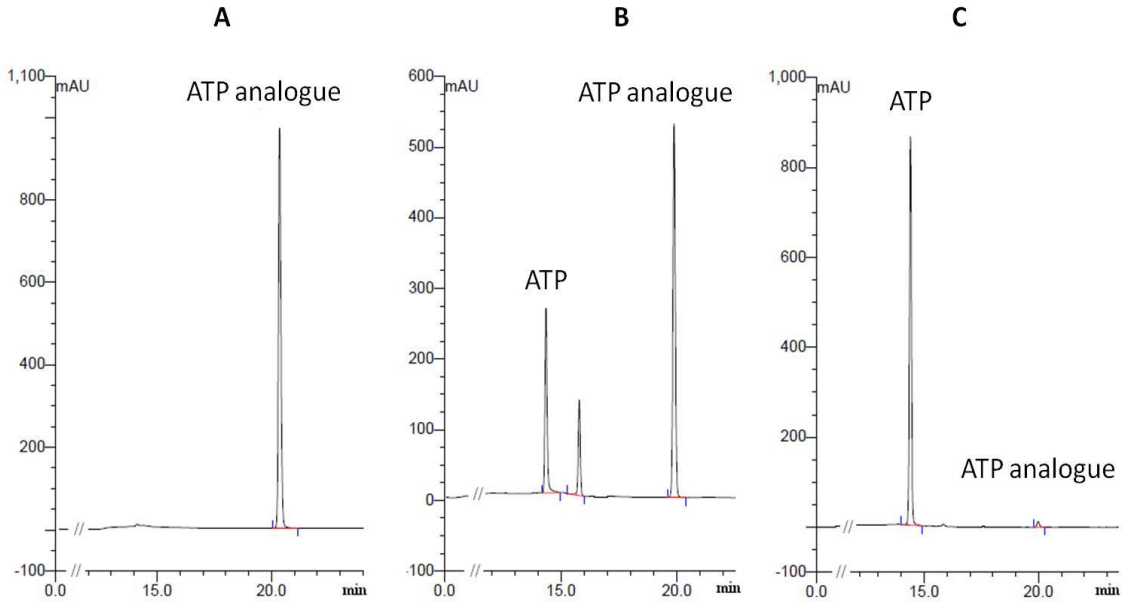

Figure 2.24: HPLC analysis for the stability of ATPγNH-PEG-N_3 (58), in acidic conditions, monitored at λ_{max} 260 nm. A: ATPγNH-PEG-N_3 (58) before being subjected to 0.1% TFA; B: ATPγNH-PEG-N_3 (58) after 5 min in 0.1% TFA. The degradation to ATP can be seen; C: ATPγNH-PEG-N_3 (58) after 1 hr in 0.1% TFA, showing very little ATPγNH-PEG-N_3 (58) remaining.[211]

Further study using HPLC showed that after 5 min incubation in 0.1% TFA 40% of ATP-N-linker analogue was hydrolysed and after 1 hr the whole sample had degraded (**Figure 2.24**).[211] Hacker *et al.*[174] have since confirmed this with a study of the stability

of a variety of modified ATP analogues over a broad pH range, which demonstrated that P-N-linkers show signs of degradation at pH 5.5 and are completely degraded at pH 2.0. P-C-linkers and P-O-linkers, on the other hand, were stable from pH 12.0 to pH 2.0. An alternative to the P-N-linker was therefore required.

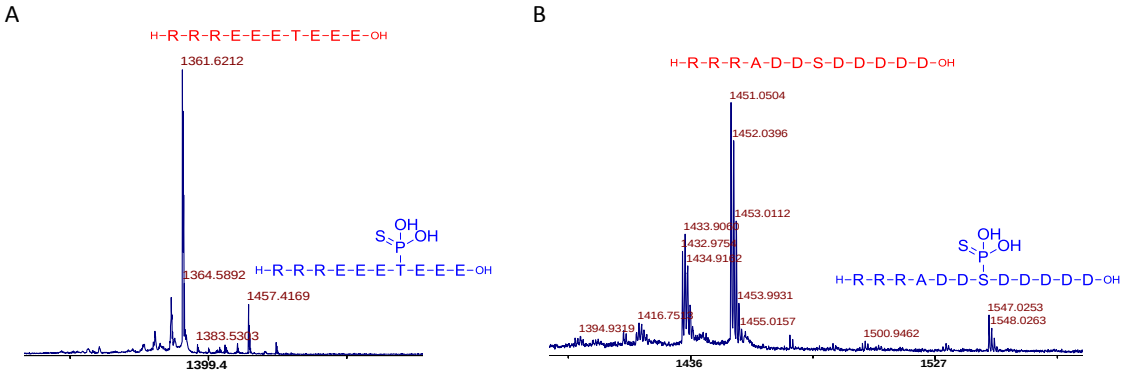

Figure 2.25: MALDI-TOF MS analysis of kinase assay with ATPγS (48) co-substrate. Peptide labelled in red and phosphorylated peptide in blue. A: Using mammalian CK2 with peptide RRREEETEEE; B: Using *Pf*CK2α with peptide substrate RRRADDSDDDDD. Phosphorylation was observed using both mammalian CK2 and *Pf*CK2α.

The use of ATPγS (**48**) as a co-substrate by both enzymes was illustrated by the addition of H_2PO_2S to the peptide substrates (**Figure 2.25**), demonstrating the stability of P-S bond under the assay conditions and during the acid Zip Tip desalting protocol. This data highlighted the potential to develop P-S-linker tags, which have been successfully produced by Cole *et al.* for the development of protein kinase A inhibitors[244] and the study of protein kinase-substrate interactions.[245] However, these were reported to be stable at neutral pH for >12 hr but unstable at pH 2, having a half-life of ~2 hr.[244] Unsurprisingly, given the results for GTP (**52**), when the co-substrate was GTPγS (**94**) peptide phosphorylation was only observed for mammalian CK2 (**Figure 2.26**).

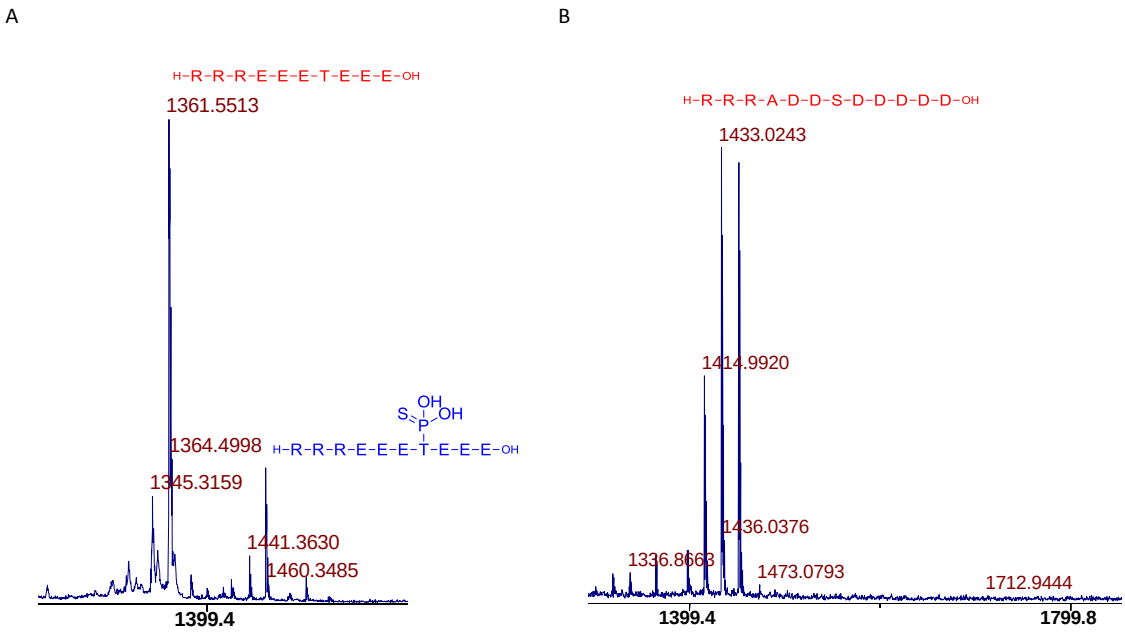

Figure 2.26: MALDI-TOF MS analysis of a kinase assay with GTPγS (94) as the co-substrate. Peptide labelled in red and phosphorylated peptide in blue. A: Using mammalian CK2 with peptide RRREEETEEE; B: Using *Pf*CK2α with peptide substrate RRRADDSDDDDD. Phosphorylation was observed using mammalian CK2 but not *Pf*CK2α.

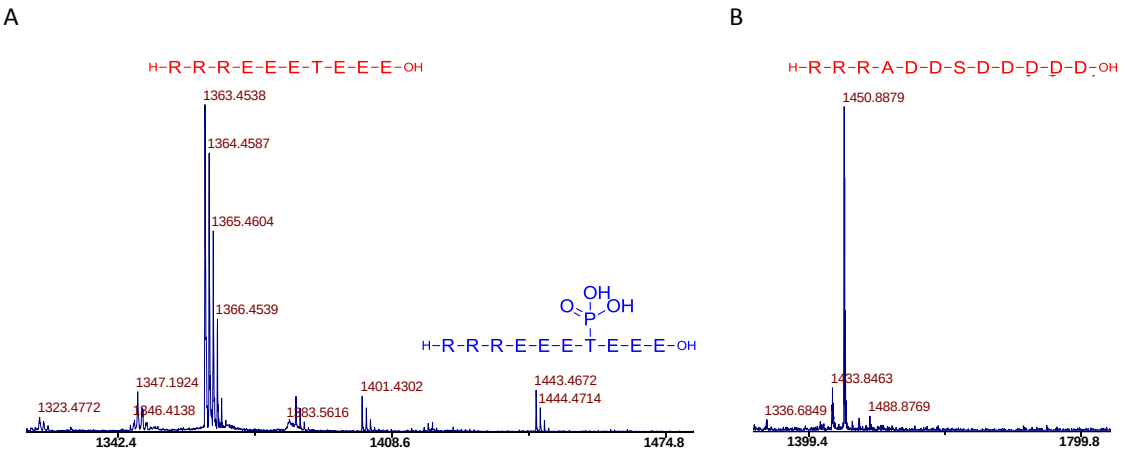

Figure 2.27: MALDI-TOF MS analysis of a kinase assay with ATPγEt (53) as the co-substrate. Peptide labelled in red and phosphorylated peptide in blue. A: Using mammalian CK2 with peptide RRREEETEEE; B: Using *Pf*CK2α with peptide substrate RRRADDSDDDDD. Tagged phosphorylation was not observed using either kinase. The phosphorylation observed with mammalian CK2 was thought to be due to trace amounts of ATP present in the commercial mammalian CK2 or simply background noise.

ATPγEt (**63**) was synthesised as an acid stable alternative to the ATP phosphoramidate analogues. However, no phosphorylation was observed for *Pf*CK2α-GST and only a very small amount of untagged phosphorylated peptide was detected for mammalian CK2 after overnight incubation (**Figure 2.27**). It is therefore hypothesised that ATPγEt (**63**) is

not a co-substrate for *Pf*CK2α or mammalian CK2 and that this trace amount of phosphorylation is due to trace amounts of ATP present in the commercial mammalian CK2 or is simply background noise. Further studies with ATPγEt (**63**) can be found later (**Section 2.5.8**).

There are relatively few examples of nucleotide triphosphate with a γ-phosphonate. 2'-Deoxythymidine triphosphate analogues, including phosphonates, have been synthesised by Krayevsky *et al.*[246, 247, 248] for the study of HIV and AMV. Krayevsky *et al.* found very little difference between the substrate properties of dTTPγMe and dTTP toward retro-viral reverse transcriptases.[247] However, when used by reverse transcriptases, the α-phosphate dTTPγMe is the reactive group; therefore, the γ-phosphate is not directly involved in the reaction. With kinases the γ-phosphate is the site of nucleophilic attack and, thus, the difference in the tolerance of the γ-P-C bond can be readily explained.

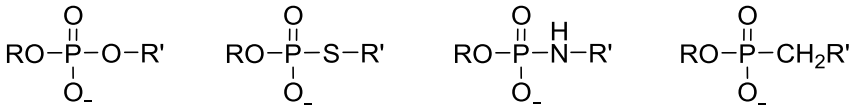

95 **96** **97** **98**

Figure 2.28: The four phosphate analogues: phosphoester (95); phosphothioester (96); phosphoramidate (97); and phosphonate (98) have different reactivities.

The acid lability of the P-N bond in the phosphoramidate compared to the other phosphate analogues can be explained by the electronegativity and basicity of the functional groups as well as the poor orbital overlap between the 3p orbital of phosphorus and the 2p orbital of oxygen.

The similarity in electronegativity between phosphorus and carbon or sulphur results in a less electrophilic phosphorus centre for attack by a nucleophile in phosphonates (**87**) and thiophosphates (**85**) than in phosphoramidates (**86**) and phosphoesters (**84**). Thus, phosphonates (**87**) and thiophosphates (**85**) are stable to acid catalysed hydrolysis compared to phosphoramidates (**86**) and phosphoesters (**84**).

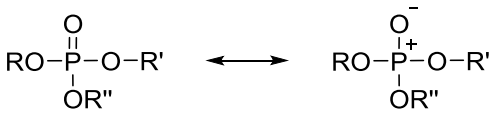

Figure 2.29: Resonance canonicals of phosphate groups. It is thought by many phosphorus chemists that there should not be a double bond in phosphates but rather a positive phosphorus and a negative oxygen due to poor orbital overlap.

The π-bond in phosphates is weak due to the poor orbital overlap between the 3p orbital of phosphorus and the 2p orbital of oxygen. Consequently, there is much debate and research among phosphorus chemists as to whether the P=O in phosphates should actually be regarded as having little π-character and should instead be seen to have considerable P^{+}–O^{-} character (**Figure 2.29**). Many have concluded that the bond should be regarded as an unusually short and strong single bond, with this strength attributed to back bonding.[249] This results in the phosphorus of a phosphate group being more electropositive than the carbon in a carboxylic acid derivative. Therefore, analogies between the reactivity of phosphates and carboxylic acid derivatives can be misleading; whereas acid catalysed hydrolysis of amides first requires the protonation of the carbonyl oxygen (**Scheme: 2.16**), the initial step in the acid catalysed hydrolysis of phosphoramidates is the protonation of the basic nitrogen (**Scheme: 2.17**). The protonation of the oxygen in the equivalent phosphoester is much more difficult due to its lower pKa; thus, in phosphates P=O is likely to be the

site of protonation (**Scheme 2.18**). Consequently, phosphoesters are more stable to acid hydrolysis than phosphoramidates.

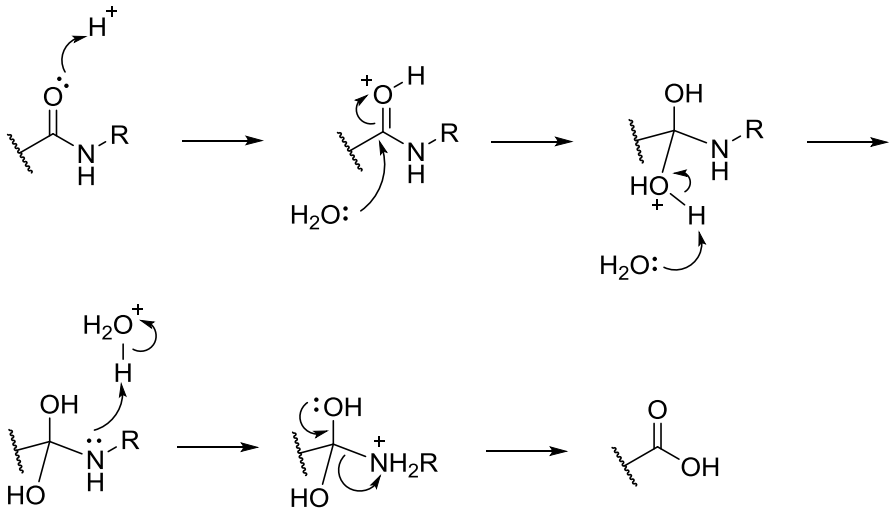

Scheme: 2.16: The acid catalysed hydrolysis of an amide. The initial step is the protonation of the carbonyl oxygen.

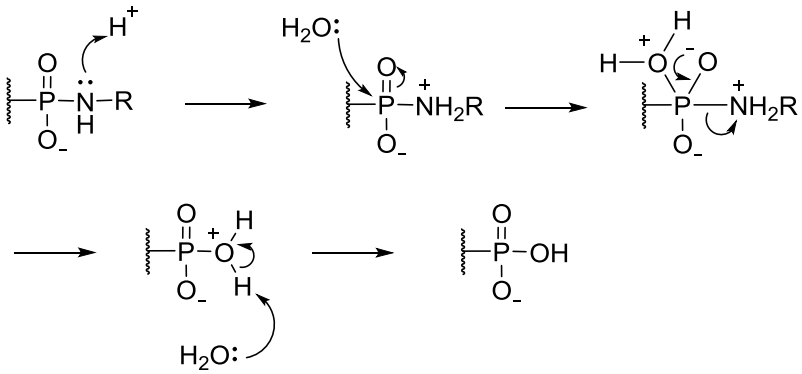

Scheme: 2.17: The acid catalysed hydrolysis of a phosphoramidate. The initial step is the protonation of the basic nitrogen.

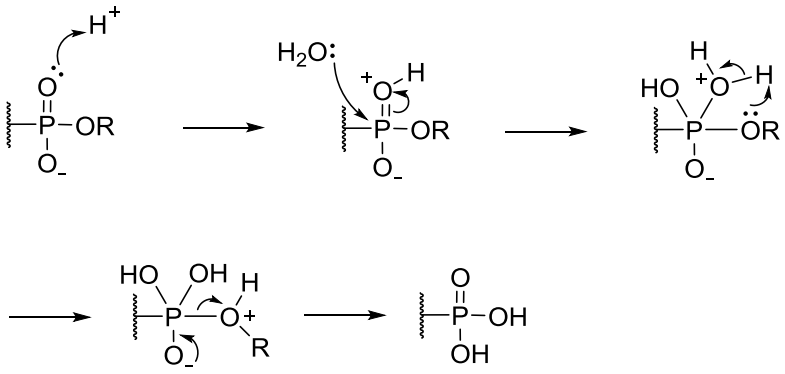

Scheme 2.18: The acid catalysed hydrolysis of a phosphoester. The initial step is the protonation of the phosphoryl oxygen.

2.5.4 Kinetic parameters, ATP Leicester

Studies on the kinetic parameters of *Pf*CK2α and mammalian CK2 were carried out with ATP and GTP as co-substrates in order to obtain the kinetic parameters of these natural co-substrates before looking at the kinetic properties of the ATP and GTP analogues proposed. Work by Holland *et al.*[227] that deemed GTP to have a similar K_m to ATP when used as a co-substrate of *Pf*CK2α (16.7 µM ATP, 34.9 µM GTP) used 100 µM, 25 µM, 6.25 µM and 1.56 µM ATP/GTP for the study of kinetic parameters. In order to emulate the study, the same concentrations were used with the addition of an extra point at 2.5 µM. Work with the Cochet lab, where the original study was carried out by Holland *et al.*, resulted in the use of 100, 50, 30, 20 and 10 µM ATP/GTP.

Table 2.3: Kinetic parameters measured for mammalian CK2 (1.12 µg/µL) with ATP using peptide RRREEETEEE.

Enzyme (µg/µL)	1.12
K_m (µM)	23.9
V_{max} (µmol min^{-1})	9.6 x10^{-6}
k_{cat} (min^{-1})	1.2 x10^{-6}
k_{cat}/K_m ($M^{-1}min^{-1}$)	0.05

The assay conditions were optimised for mammalian CK2 resulting in 25 U, or 1.12 µg/µL, of mammalian CK2 being used. This resulted in a K_m for ATP of 23.9 µM (**Table 2.3**), which is in the expected range and gave the desired curved plot (**Figure 2.30**) with only approx. 3% of the peptide being phosphorylated. Subsequently, this concentration of enzyme was also used for the study of mammalian CK2 with GTP (**Sections 2.5.5** & **2.5.6**).

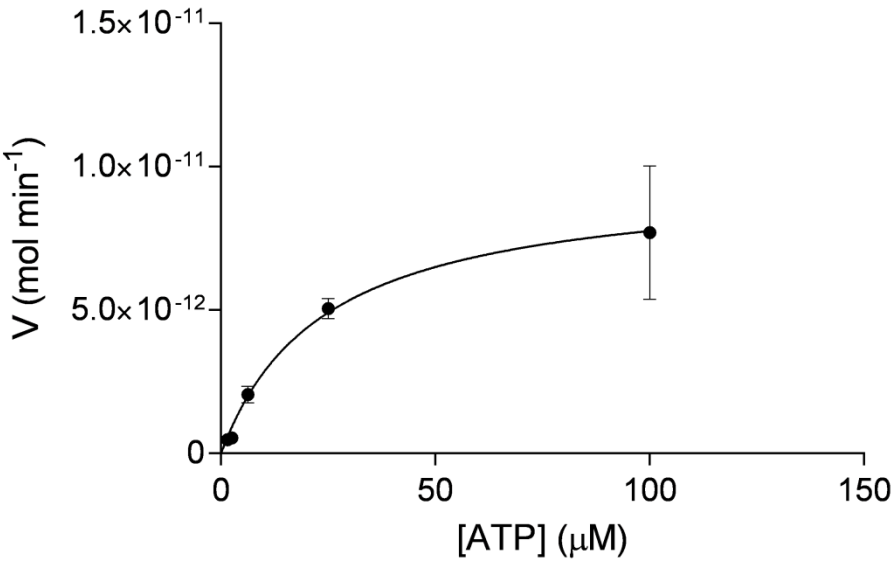

Figure 2.30: Mammalian CK2 kinetic parameters using 25 U CK2. Non-linear regression of [ATP] against rate of phosphorylation of peptide RRREEETEEE, allowing the calculation of K_m, V_{max} & k_{cat}.

The kinetic parameters of *Pf*CK2α-GST with ATP were measured using 7.0 ng/μL of enzyme. However, from the shape of the non-linear regression plot (**Figure 2.31**) and the comparison of the K_m (177.6 μM) (**Table 2.4**) compared to the literature value 16.7 μM,[227] it is thought likely that more ATP concentrations needed to be studied, including between 25 μM and 100 μM to better define the curve region and greater than 100 μM to give a more accurate representation of V_{max}.[250] This was not initially identified due to the original use of linear regression on a Lineweaver-Burk plot (**Figure 2.32**) to calculate kinetic parameters, which resulted in an expected K_m for *Pf*CK2α-GST (22.8 μM) (**Table 2.4**). This highlights the error that can occur with linear regression due to its ability to mask poorly defined kinetic parameters.

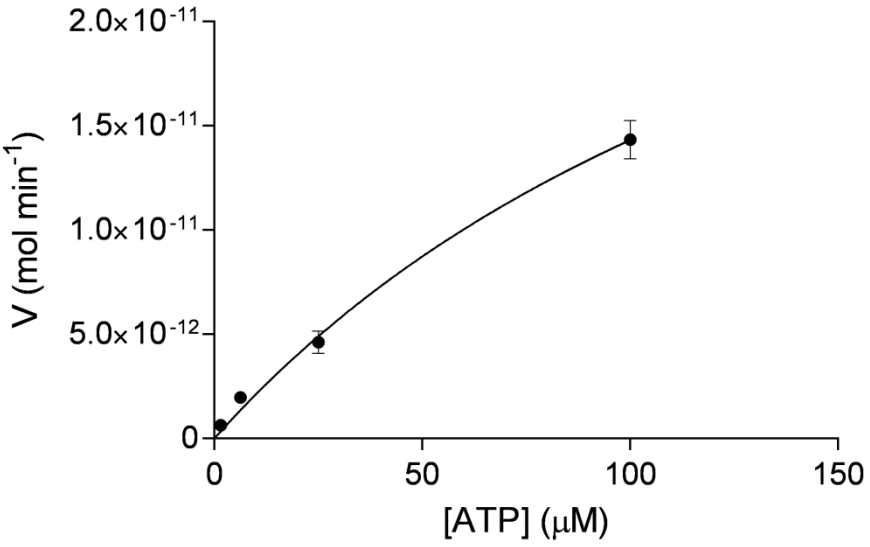

Figure 2.31: *Pf*CK2α-GST kinetic parameters. Non-linear regression of [ATP] against rate of phosphorylation of peptide RRRDADDSDDDDD, allowing the calculation of K_m, V_{max} & k_{cat}.

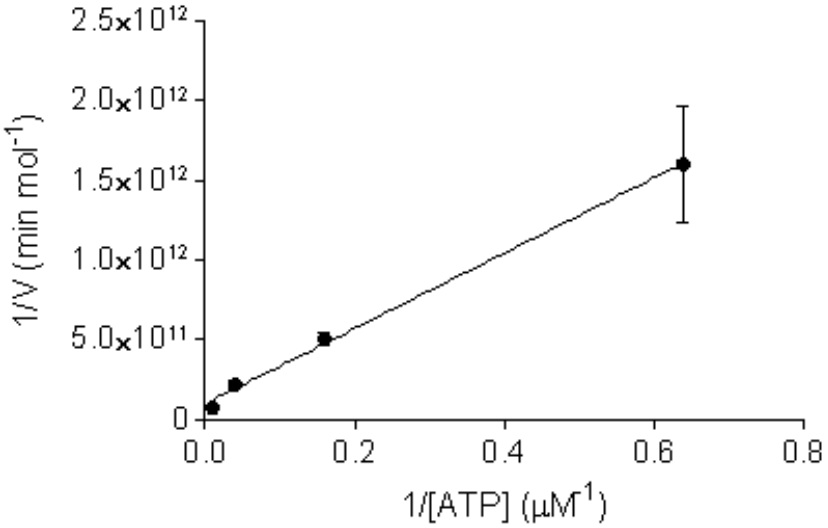

Figure 2.32: Kinetic parameters for *Pf*CK2α-GST. Lineweaver-Burk plot with of [ATP] against rate of phosphorylation of peptide RRRDADDSDDDDD, allowing the calculation of K_m, V_{max} & k_{cat} by linear regression.

Table 2.4: Kinetic parameters of *Pf*CK2α-GST for ATP using peptide RRRADDSDDDDD. Both sets of parameters are calculated from the same raw data using either non-linear regression or linear regression, highlighting the inaccuracy in calculating values using linear regression.

	Non-linear	Linear
K_m (μM)	177.6	22.8
V_{max} (μmol min^{-1})	4.0 $x10^{-5}$	4.0 $x10^{-6}$
k_{cat} (min^{-1})	3.7 $x10^{-3}$	9.4 $x10^{-5}$
k_{cat}/K_m ($M^{-1}min^{-1}$)	2.10	4.11

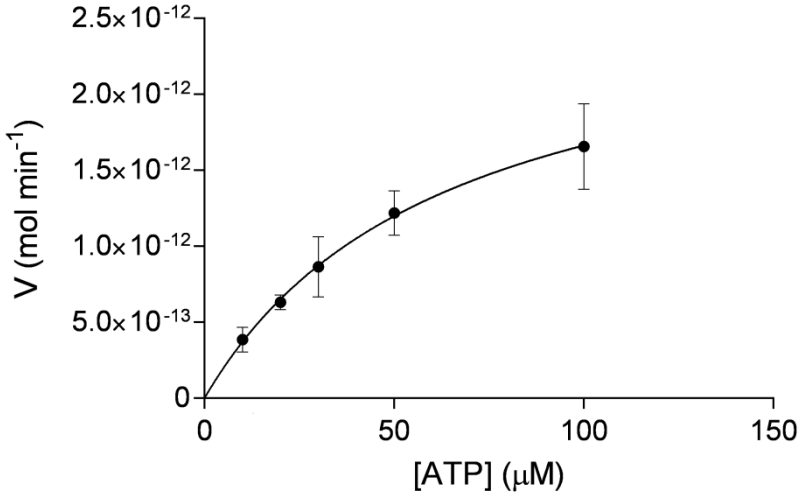

Figure 2.33: *Pf*CK2α-His$_6$ kinetic parameters. Non-linear regression of [ATP] against rate of phosphorylation of peptide RRREDEESDDEE, allowing the calculation of K_m, V_{max} & k_{cat}.

The kinetic parameters of *Pf*CK2α-His$_6$ with ATP were measured using 7.4 ng/μL of enzyme. It can be seen that there is good correlation between the data and the non-linear regression curve (**Figure 2.33**) and the kinetic parameters (**Table 2.5**) better concur with the literature value[227] than *Pf*CK2α-GST did.

Table 2.5: Kinetic parameters measured for *Pf*CK2α-His$_6$ using peptide RRREDEESDDEE.

	ATP
K_m (μM)	63.4
V_{max} (μmol min^{-1})	2.7 x10^{-7}
k_{cat} (min^{-1})	1.1 x10^{-5}
k_{cat}/K_m (M^{-1}min^{-1})	0.18

2.5.5 Kinetic parameters, GTP Leicester

The kinetic parameters of mammalian CK2 with GTP were defined (**Table 2.6** & **Figure 2.34**). The K_m of 63.4 µM corresponded to literature values of 20.8 µM[225] and 52.0 µM.[219] However, despite multiple attempts with different batches of enzyme (both GST and His_6 tagged) and different methodologies (the use of [γ-32P]-GTP, the use of GTP with [γ-32P]-ATP and analysis by MALDI-TOF MS (**Section 2.5.3**)), data was not found to support the evidence provided by Holland *et al.*[227] that *Pf*CK2α uses GTP as a co-substrate.

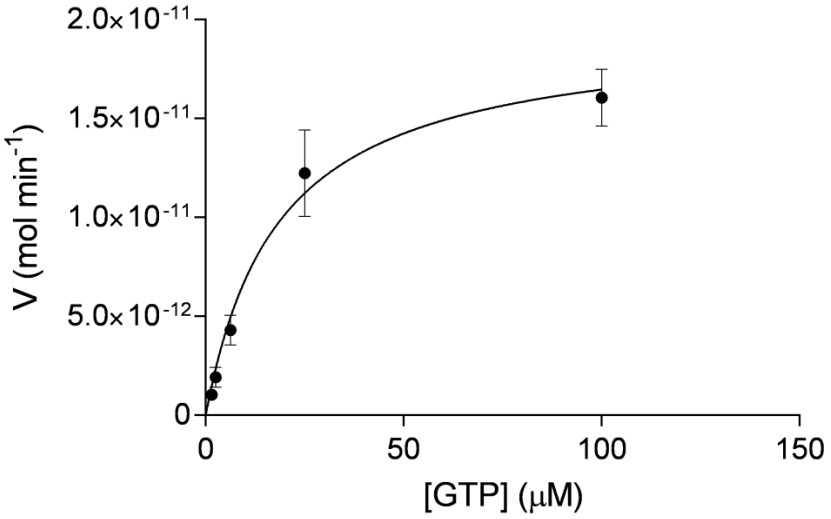

Figure 2.34: Mammalian CK2 kinetic parameters using 25 U (1.12 µg/µL) CK2. Non-linear regression of [GTP] against rate of phosphorylation of peptide RRREEETEEE, allowing the calculation of K_m, V_{max} & k_{cat}.

Table 2.6: Kinetic parameters measured for mammalian CK2 with GTP using peptide RRREEETEEE.

	GTP
K_m (µM)	18.4
V_{max} (µmol min^{-1})	1.9 x10^{-5}
k_{cat} (min^{-1})	2.4 x10^{-6}
k_{cat}/K_m ($M^{-1}min^{-1}$)	0.13

2.5.6 Kinetic parameters, Grenoble

In order to further investigate the inability to replicate work of Holland *et al.*[227] and demonstrate that *Pf*CK2α is able to use GTP as a co-substrate, a collaboration was set up with the lab where the original work was carried out. It was not possible to determine k_{cat} for *Pf*CK2α-GST, only K_m and V_{max}, because an accurate concentration of *Pf*CK2α-GST could not be determined due to problems experienced during the Bradford assays. Although the K_m of 17.2 μM (**Table 2.7**) for ATP concurs with that found for *Pf*CK2α-His_6 (63.4 μM (**Table 2.5**)), from the non-linear regression plot (**Figure 2.35**) it is possible to see that K_m/V_{max} is not well defined due to a lack of points on the initial slope of the curve. V_{max} would be better defined if higher concentrations of ATP had been used.[250] Therefore, the values could be misleading.

Table 2.7: K_m & V_{max} for ATP with *Pf*CK2α and peptide RRREDEESDDEE.

	K_m (μM)	V_{max} (μmol min^{-1})
ATP	17.2	5.6 x10^{-6}

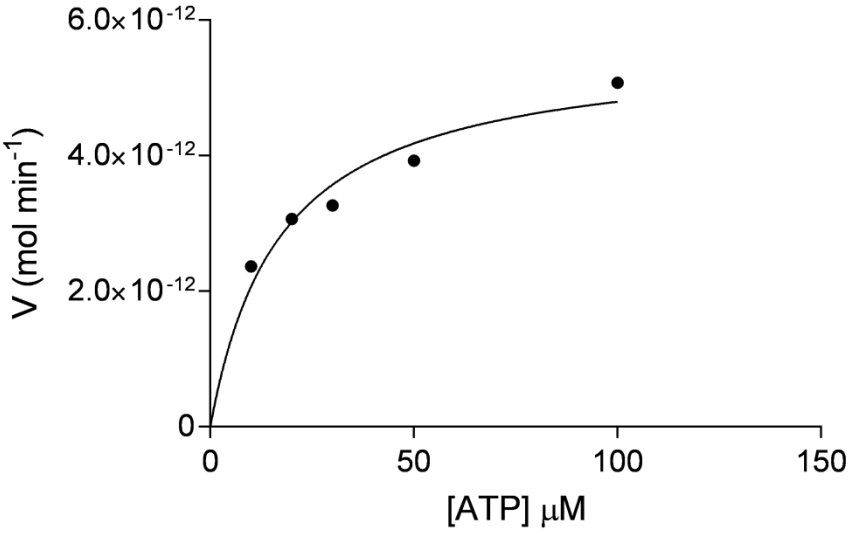

Figure 2.35: *Pf*CK2α kinetic parameters. Non-linear regression of [ATP] against rate of phosphorylation of peptide RRREDEESDDEE, allowing the calculation of K_m & V_{max}.

Kinetic parameters for the use of GTP as a co-substrate by mammalian CK2α were measured (**Table 2.8** & **Figure 2.36**); however, these values differ from that found in Leicester for the holoenzyme (**Table 2.3**). Although the activity of the α-subunits is altered slightly by the presence of the regulatory β-subunits, the main difference is that a substrate's phosphorylation can be promoted or inhibited by the presence of the β-subunit.[206, 204, 205] As a different peptide was used in the study in Leicester to that in Grenoble, it is possible that this could have had a knock on effect on the K_m of GTP observed for the holoenzyme (Leicester) and CK2α (Grenoble). However, the data collected in Grenoble was not carried out in duplicate/triplicate, reducing the reliability of the results and from the non-linear regression (**Figure 2.36**) it would appear that a much larger concentration of GTP should have also been studied in order to ensure that V_{max} was well defined.[250] These factors could be responsible for the difference in K_m and, more importantly, in k_{cat}/K_m for *hs*CK2α (Grenoble) and the holoenzyme (Leicester).

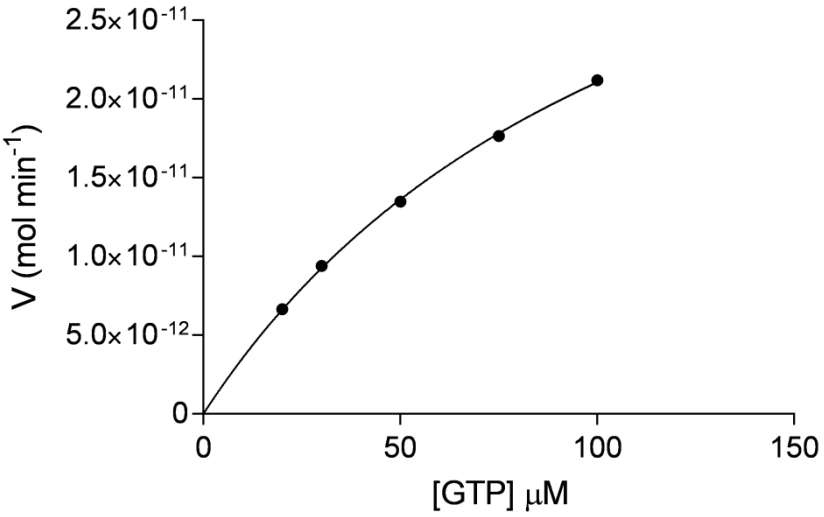

Figure 2.36: Mammalian CK2α kinetic parameters. Non-linear regression of [GTP] against rate of phosphorylation of peptide RRREDEESDDEE, allowing the calculation of K_m & V_{max}.

Table 2.8: Kinetic parameters for GTP with mammalian CK2α and peptide RRREDEESDDEE.

	GTP
K_m (μM)	120.6
V_{max} (μmol min^{-1})	4.6 $x10^{-5}$
k_{cat} (min^{-1})	1.4 $x10^{-2}$
k_{cat}/K_m ($M^{-1}min^{-1}$)	112.35

Once again, no evidence was found for the use of GTP as a co-substrate for *Pf*CK2α either when [γ-32P]-GTP or GTP with [γ-32P]-ATP was used. The latter would probe whether GTP can bind to *Pf*CK2α and, consequently, inhibit turnover with the [γ-32P]-ATP.

2.5.7 Summary of kinetic parameters for *Pf*CK2α and mammalian CK2 with ATP and GTP as co-substrates

The kinetic parameters for ATP with mammalian CK2 concurred with literature values.[206, 65, 219] However, it would have been beneficial to include a concentration far higher than 100 μM to ensure accurate determination of $V_{max,}$ and values between 50 μM and 100 μM for more accurate determination of K_m.[250]

The kinetic parameters for GTP with mammalian CK2 measured in Leicester (with peptide RRREEETEEE) differed greatly for those with the α-subunit measured in Grenoble (with peptide RRREDEESDDEE) (**Table 2.9**). Although data in Grenoble was not collected in duplicate/triplicate and a much larger concentration of GTP would be needed in order to better define the V_{max} obtained in Grenoble,[250] the difference in the kinetic parameters observed in each case could be caused by the regulatory effect of the β-subunit.[206] The β-subunit has been shown to tune the activity of the α-subunit

towards certain substrates through the formation of the holoenzyme. For example, calmodulin has been shown to be phosphorylated by the α-subunit and not the holoenzyme,[205] while the reverse is true for some other substrates.[204]

Table 2.9: Summary of kinetic parameters for GTP and ATP with mammalian CK2 when using peptide RRREEETEEE and with hsCK2α when using peptide RRREDEESDDEE.

	RRREDEESDDEE	RRREEETEEE	
	GTP	ATP	GTP
K_m (μM)	120.6	23.9	18.4
V_{max} (μmol min^{-1})	4.6 $x10^{-5}$	9.6 $x10^{-6}$	1.9 $X10^{-5}$
k_{cat} (min^{-1})	1.4 $x10^{-2}$	1.2 $x10^{-6}$	2.6 $X10^{-6}$
k_{cat}/K_m ($M^{-1}min^{-1}$)	1.12 $X10^{2}$	0.05	0.13

Table 2.10: Summary of kinetic parameters for ATP with *Pf*CK2α

	RRRADDSDDDDD	RRREDEESDDEE	
	*Pf*CK2α-GST	*Pf*CK2α-GST	*Pf*CK2α-His_6
K_m (μM)	177.6	17.2	63.4
V_{max} (μmol min^{-1})	4.0 $x10^{-5}$	5.6 $x10^{-6}$	2.7 $x10^{-7}$
k_{cat} (min^{-1})	3.7 $x10^{-3}$	-	1.1 $x10^{-5}$
k_{cat}/K_m ($M^{-1}min^{-1}$)	2.10	-	0.18

The kinetic parameters for ATP with *Pf*CK2α-His_6 and peptide RRREDEESDDEE measured in Leicester differed from those recorded with *Pf*CK2α-GST and peptide RRRADDSDDDDD (**Table 2.10**). The two most likely causes of this are: insufficient data points being collected for *Pf*CK2α-GST (**Figure 2.35**), resulting in poorly defined K_m and V_{max} values;[250] and the effect of a large N-terminal GST-tag compared to the much smaller C-terminal His_6-tag. The K_m value measured for *Pf*CK2α-His_6 for ATP concurred with that published by Holland *et al.*[227] (**Table 2.11**).

Table 2.11: Summary of kinetic parameters for ATP and GTP with *Pf*CK2α published by Holland *et al*.[227] The K_m and V_{max} values are taken directly from the journal article and k_{cat} and k_{cat}/K_m have been calculated from the information published.

	RRRADDSDDDDD	
	ATP	**GTP**
K_m (μM)	16.7	34.9
V_{max} (μmol min^{-1})	6.6 $x10^{-3}$	2.1 $X10^{-3}$
k_{cat} (min^{-1})	0.13	4.3 $X10^{-2}$
k_{cat}/K_m ($M^{-1}min^{-1}$)	8.04 $x10^{3}$	1.22 $x10^{3}$

Despite the data published by Holland *et al.* (**Table 2.11**)[227] and recent work by Engelberg *et al.*,[251] which uses the ability of *Pf*CK2 to tolerate GTP as a co-substrate as evidence to support the notion that *Pf*Rh2b is phosphorylated by *Pf*CK2, no evidence was found to support *Pf*CK2α accepting GTP as a co-substrate.

2.5.8 ATPγEt as an inhibitor of CK2

Although from kinase assays analysed by MALDI-TOF MS (**Section 2.5.3**) it was found that ATPγEt (**63**) was not an active co-substrate for *Pf*CK2α or mammalian CK2, it was hypothesised that ATPγEt (**63**) could be binding to the active site of the kinases without phosphorylating the peptide substrates. It was found that as the concentration of ATPγEt (**63**) increased the cpm decreased for both *Pf*CK2α-GST and mammalian CK2 (**Figure 2.37**); thus, ATPγEt (**63**) does bind to the active site of both kinases. The IC_{50} values are tabulated *vide infra* (**Table 2.12**) but it is important to note that the concentration of *Pf*CK2α-GST and mammalian CK2 were not identical and are, therefore, not directly comparable.

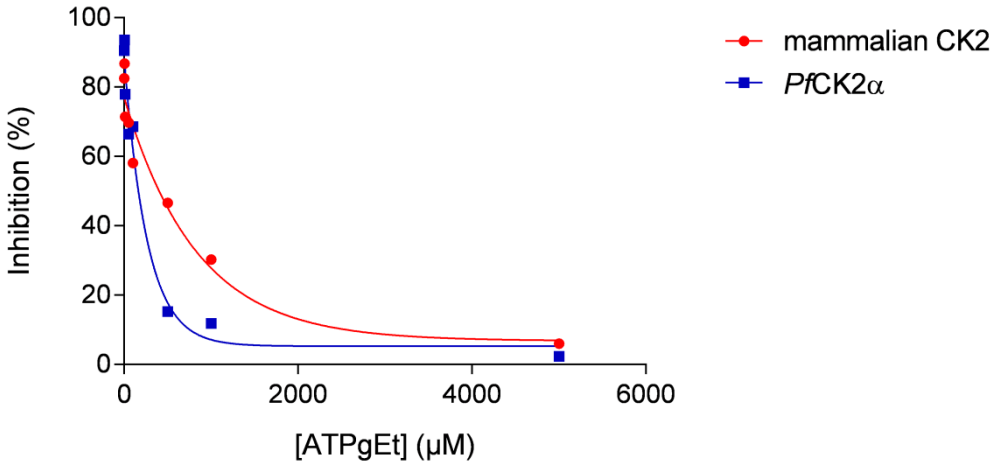

Figure 2.37: Scatter chart showing the percentage inhibition of mammalian CK2 with peptide RRREEETEEE (red) and *Pf*CK2α with peptide RRRADDSDDDDD (blue) by ATPγEt (63) in the presence of 50 µM ATP.

Table 2.12: IC_{50} values for the inhibition of mammalian CK2 with peptide RRREEETEEE and *Pf*CK2α with peptide RRRADDSDDDDD by ATPγEt in the presence of 50 µM ATP.

	***Pf*CK2α**	**Mammalian CK2**
IC_{50} (µM)	184	576

2.5.9 Apparent IC_{50} values for ATP analogues with PfCK2α

Without access to radio-labelled versions of the analogues, K_m and k_{cat} values could not be determined. Using [γ-^{32}P]-ATP these analogues were evaluated as inhibitors. Inhibition assays for *Pf*CK2α were performed with ATPγNH-linker-coumarin (**58**), ATPγNH-PEG-N_3 (**60**), ATPγS (**48**), and ATPγNH-linker-alkyne (**59**) to obtain some indirect information on the ability of *Pf*CK2α to use these ATP analogues as substrates relative to one another. Apparent IC_{50} values were obtained using a Dixon plot (**Figure 2.38**). The greatest inhibitory response was observed for ATPγS (**48**) (IC_{50} 20 µM), with ATPγNH-PEG-N_3 (**60**) having the lowest inhibitory effect (IC_{50} 360 µM) on *Pf*CK2α (**Table 2.13**). These assays were not carried out in duplicate and, ideally, they should have been repeated. However, the R^2 values are above 0.97

except for ATPγNH-PEG-N_3 (**60**) (0.87) and the assays were performed simultaneously, allowing for a reliable comparison between the analogues. Therefore, it can be deduced that ATPγS (**48**) and ATPγNH-linker-alkyne (**59**) are accepted into the active site of the kinase more readily than ATPγNH-linker-coumarin (**58**) and ATPγNH-PEG-N_3 (**60**).

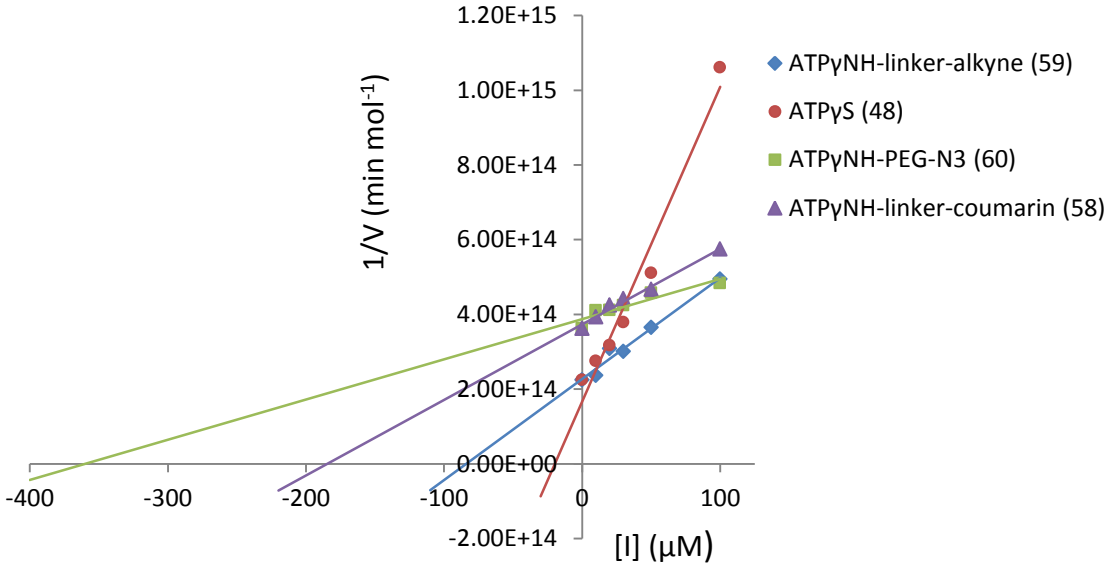

Figure 2.38: Dixon plot of the ATP analogues ATPγNH-linker-alkyne (59), ATPγS (48), ATPγNH-PEG-N_3 (60) and ATPγNH-linker-coumarin (58) allowing for the calculation of apparent IC_{50} values for the ATP analogues shown with *Pf*CK2α and peptide RRREDEESDDEE.

Table 2.13: IC_{50} values for the ATP analogues shown with *Pf*CK2α and peptide RRREDEESDDEE as calculated from the above Dixon plot.

Compound	IC_{50} (µM)
ATPγNH-linker-coumarin (**58**)	185
ATPγNH-PEG-N_3 (**60**)	360
ATPγS (**48**)	20
ATPγNH-linker-alkyne (**59**)	85

The values measured are apparent IC_{50} values because the analogues are also substrates of CK2 and, as such, are consumed during the assay; hence, the concentration of the ATP analogues does not remain constant throughout. Since IC_{50}

values are relative values that depend upon substrate concentration, all reaction conditions must be defined for these values to be compared with other data sets but the enzyme concentration used in these assays can only be estimated. However, according to the Cheng-Prusoff relationship[252,253] (**Equation 2.1**) when substrate concentration, [S], is vastly lower than K_m, $[S]/K_m$ approaches zero and IC_{50} approaches K_i.[252] As a very low substrate concentration (55.8 fmol, i.e. [γ-32P]-ATP as purchased) was used, these apparent IC_{50} values serve as an upper limit for the apparent K_i of the ATP analogues studied.

$$IC_{50} = K_i \left(1 + \frac{[S]}{K_m}\right)$$

Equation 2.1: Cheng-Prusoff relationship[252,253]

2.6 Conclusions

CX-4945 (**55**) was published by Pierre *et al.* as a potent and selective inhibitor for human CK2[254] and entered clinical trials for the treatment of cancer. The published synthetic route to this and two analogues (**88**) and (**89**) [238] was followed in order to test the efficacy of some of these analogues for *Pf*CK2α. The penultimate step in the synthesis of CX-4945 (**45**) and analogues (**88**) and (**89**) was reached. Their synthesis was not completed due to problems encountered during synthesis, low solubility and time constraints.

A range of γ-modified nucleotide triphosphates were synthesised for the study of phosphorylation by *Pf*CK2α and mammalian CK2. ATP phosphoramidate analogues (**58**, **59** & **60**) were re-synthesised for direct kinetic analysis by Caliper Capillary Electrophoresis (CE) (*vide infra*), which is performed at ~pH 7 and does not require

radio-labelled analogues. However, problems experienced with purification were not able to be overcome due to time constraints. These analogues had been previously synthesised by the group[211] and this batch of compounds was used in the studies with MALDI-TOF MS and kinetics studies using radiolabelled ATP reported in this thesis. GTPγNH-PEG-N_3 (**99**) was also successfully synthesised and purified.

ATPγSEt (**62**) was synthesised from ATPγS (**48**); however, due to very poor yield and high cost of ATPγS (**48**), this synthesis was not repeated to produce enough ATPγSEt (**62**) for use in enzyme studies. The synthesis of ATP-O-PEG-N_3 (**61**) was attempted by several synthetic routes without success. ATPγEt (**63**) was successfully synthesised and used for the study of mammalian CK2 and *Pf*CK2α.

*Pf*CK2α was found to rapidly lose activity, even when stored at -80°C. After two months the activity had dropped to just 10% of the activity of a freshly prepared batch. Therefore, it was necessary to carry out kinetic studies as soon as possible after enzyme purification.

From the MALDI-TOF MS study, it was concluded that for mammalian CK2 phosphorylation of the peptide substrate RRREEETEEE by ATP (**32**), ATPγS (**48**), GTP (**52**) and GTPγS (**94**) could be directly observed due to the specific mass of the phosphorylated peptide (**Table 2.2**). For *Pf*CK2α phosphorylation of peptide substrate RRRADDSDDDDD was observed for ATP (**32**) and ATPγS (**48**) but no phosphorylation was observed when using GTP (**52**) or GTPγS (**94**) as a co-substrate. The use of ATP-phosphoramidate co-substrates (**58**), (**59**) and (**60**) resulted in no detectable tagged phosphorylation; only the standard phosphopeptide was observed due to the instability of the P-N bond under the acidic conditions of the Zip Tip de-salting

procedure. ATPγEt (**63**) was developed as an acid stable analogue; however, no phosphorylation was detected when this was used a co-substrate for either enzyme.

The kinetic parameters measured for mammalian CK2 using ATP (**32**) and GTP (**52**) as a co-substrate supported the literature values, as did those measured for *Pf*CK2α when ATP (**32**) was used as a co-substrate. Despite the literature,[227,251] there was no evidence to support the acceptance of GTP (**52**) as a co-substrate by *Pf*CK2α during the kinetic studies.

Despite no evidence for the phosphorylation of peptide substrates by either kinase using ATPγEt (**63**) as a co-substrate, ATPγEt (**63**) was found to act as an inhibitor for both mammalian CK2 and *Pf*CK2α. This indicated the potential to develop these molecules further.

Using [γ-^{32}P]-ATP, K_m values for ATPγS (**48**), ATPγNH-PEG-N_3 (**60**), ATPγNH-linker-coumarin (**58**) and ATPγNH-linker-alkyne (**59**) analogues could not be measured directly because of a lack of detection method for the peptide containing the modified phosphate group. By treating them as inhibitors, apparent IC_{50} values were measured for each analogue with *Pf*CK2α. Although not true IC_{50} values due to the ability of the analogues to act as substrates, these values serve to compare the analogues with one another and show them all to be accepted into the active site of *Pf*CK2α.

2.7 Experimental

2.7.1 ATP analogue synthesis

2.7.1.1 *Synthesis of 1-azido-2-(2-(2-(2-azidoethoxy)ethoxy)ethoxy)ethane*[240]

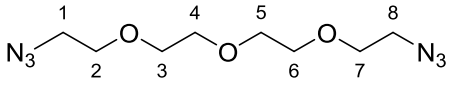

65

To a solution of tetraethylene glycol (**64**) (5.027 g, 25.8 mmol) in THF (30 mL) was added methane sulfonyl chloride (11.100 g, 7.5 mL, 96.9 mmol). The solution was cooled to 0 °C and triethylamine (6.523 g, 5.8 mL, 64.5 mmol) was added dropwise over 45 mins. The reaction mixture was allowed to warm to room temperature and stirred overnight. The reaction mixture was diluted with water (30 mL) and organic solvent was removed *in vacuo*. To the aqueous mixture $NaHCO_3$ (1.943 g, 23.1 mmol) and sodium azide (6.683 g, 102.8 mmol) were added and the mixture was heated to reflux overnight. Upon cooling, the reaction mixture was extracted with chloroform (3 x 75 mL), dried over anhydrous $MgSO_4$, filtered and concentrated *in vacuo*. Purification by flash column chromatography (1:1 ethyl acetate: petroleum ether (40-60 °C) yielded 1-azido-2-(2-(2-(2-azidoethoxy)ethyoxy)ethoxy)ethane (**65**) as a colourless oil (4.060 g, 16.6 mmol, 64% yield).

R_f 0.45 (1:1 ethylacetate:petroleum ether (40-60 °C)). IR (neat) ν_{max} (cm^{-1}): 2106 (N_3), 1300 (C-O). ^1H NMR (400MHz, $CDCl_3$) δ: 3.39 (4H, t, *J* = 5.1 Hz, CH_2 *1, 8*), 3.67 – 3.69 (12H, m, CH_2 *2- 7*). ^{13}C NMR (100MHz, $CDCl_3$) δ: 50.7 (CH_2 *1, 8*), 70.0 (CH_2 *2, 7*), 70.7 (CH_2 *3-6*).

2.7.1.2 *Synthesis of 2-(2-(2-(2-azidoethoxy)ethoxy)ethoxy)ethanamine*[240]

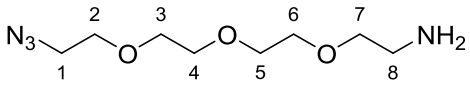

66

A solution of 1-azido-2-(2-(2-(2-azidoethoxy)ethyoxy)ethoxy)ethane (**65**) (2.0200 g, 8.3 mmol) and phosphoric acid (1.2 g, 700 µL, 12.2 mmol) in water (30 mL) was cooled to 0 °C under nitrogen. A solution of triphenyl phosphine (2.0256 g, 7.7 mmol) in diethyl ether (30 mL) was added dropwise with stirring over 45 min. The solution was allowed to warm to room temperature and stirred overnight. The biphasic solution was separated and the aqueous solution washed with diethyl ether (3 x 30 mL). A solution of potassium hydroxide (6 M, 12 mL) was added dropwise with stirring at 0 °C. The solution was allowed to warm to room temperature and stirred for 3 hr. The mixture was filtered and extracted with chloroform (3 x 70 mL), dried over $MgSO_4$, filtered and concentrated *in vacuo* to afford 2-(2-(2-(2-azidoethoxy)ethoxy)ethoxy) ethanamine (**66**) as a colourless oil (1.2863 g, 5.9 mmol, 71% yield).

R_f 0.10 (1:9 MeOH:DCM). HR-LCMS (ES): Rt 0.63 min; m/z calculated for $C_8H_{19}N_4O_3^+$ 219.2645 $[M+H]^+$observed 219.1458. IR (neat) ν_{max} (cm^{-1}): 3387 (N-H), 2101 (N_3), 1305 (C-O). ^{1}H NMR (400MHz, $CDCl_3$) δ: 1.61 (2H, s, NH_2), 2.86 (2H, t, *J* = 10.5 Hz, CH_2 *8*), 3.40 (2H, t, *J* = 5.2 Hz, CH_2 *1*), 3.51 (2H, t, *J* = 10.5 Hz, CH_2 *7*), 3.65-3.70 (10H, m, CH_2 *2 - 6*). ^{13}C NMR (100MHz, $CDCl_3$) δ: 41.8 (CH_2 *8*), 50.7 (CH_2 *1*), 70.1 (CH_2 *2*), 70.3 (CH_2 *6*), 70.7 (CH_2 *3-5*), 73.5 (CH_2 *7*).

2.7.1.3 *Synthesis of tert-butyl (2-(2-(2-(2-azidoethoxy)ethoxy)ethoxy)ethyl) carbamate*[255]

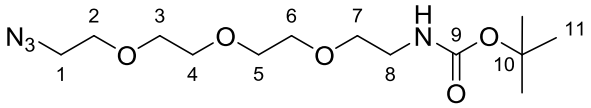

72

To a solution of 2-(2-(2-(2-azidoethoxy)ethoxy)ethoxy)ethanamine (**66**) (1.0131 g, 4.6 mmol) in methanol (30 mL) was added di-tert-butyl dicarbonate (1.0848 g, 5.0 mmol). The solution was stirred over night at room temperature. The reaction mixture was concentrated *in vacuo* and, dissolved in water (100 mL) and extracted with DCM (3 x 100 mL). The organic extract was dried over $MgSO_4$, filtered and concentrated *in vacuo*. Purification by flash column chromatography (3:1 ethyl acetate:hexane) afforded tert-butyl (2-(2-(2-(2-azidoethoxy)ethoxy)ethoxy)ethyl) carbamate (**72**) as a colourless oil (0.4904 g, 1.5 mmol, 34% yield).

R_f 0.50 (3:1 ethyl acetate:hexane). HR-LCMS (ES): R_t 1.83; m/z calculated for $C_{13}H_{26}N_4O_5Na^+$ 341.3632 $[M+Na]^+$ observed 341.1808, 285.1206 $[M-^tBu+Na]^+$, 219.1459 $[M\text{-}BOC+H]^+$. IR (neat) ν_{max} (cm^{-1}): 3360 (N-H), 2110 (N_3), 1710 (C=O). ^{1}H NMR (400MHz, $CDCl_3$) δ: 1.45 (9H, s, CH_3 *11*), 3.28-3.34 (2H, m, CH_2 *8*), 3.37-3.40 (2H, m, CH_2 *1*), 3.54 (2H, t, *J* = 5.1 Hz, CH_2 *7*), 3.60-3.69 (10H, m, CH_2 *2-6*), 5.01 (1H, s, NH). ^{13}C NMR (100MHz, $CDCl_3$) δ: 28.4 ($(CH_3)_3$ *11*), 40.4 (CH_2 *8*), 50.7 (CH_2 *1*), 70.1 (CH_2 *2*), 70.3 (CH_2 *3 & 7*), 70.7 (CH_2 *4-6*), 79.2 ($C(CH_3)_3$ *10*), 156.0 (C=O *9*).

2.7.1.4 *Synthesis of tert-butyl (2-(2-(2-(2-aminoethoxy)ethoxy)ethoxy)ethyl) carbamate*[256]

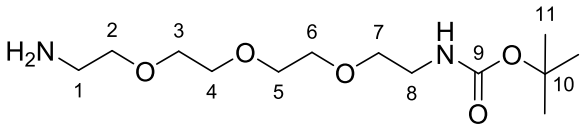

68

To a solution of tert-butyl (2-(2-(2-(2-azidoethoxy)ethoxy)ethoxy)ethyl) carbamate (**72**) (0.4904 g, 1.5 mmol) in methanol (250 mL) at 0 °C was added 10% Pd/C (49 mg). The solution was stirred and hydrogen gas was bubbled through the solution for 2 hr. The reaction mixture was filtered through celite and the filtrate concentrated *in vacuo* to afford tert-butyl (2-(2-(2-(2-aminoethoxy)ethoxy)ethoxy) ethyl)carbamate (**68**) as a colourless oil (0.3979 g, 1.4 mmol, 88% yield).

R_f 0.50 (1:9 acetone:DCM). HR-LCMS (ES): R_t 1.20; m/z calculated for $C_{13}H_{29}N_2O_5^+$ 293.2071 observed 293.2076 $[M+H]^+$, 237.1450 $[M-^tBu+H]^+$, 193.1541 $[M\text{-}BOC+H]^+$. IR (neat) ν_{max} (cm^{-1}): 1715 (C=O), 3368 (N-H). ^1H NMR (400MHz, $CDCl_3$) δ: 1.44 (9H, s, $(CH_3)_3$ *11*), 1.65 (2H, s, NH_2), 2.87 (2H, t, *J* = 5.2 Hz, CH_2 *1*), 3.28-3.35 (m, 2H, CH_2 *8*), 3.50-3.56 (4H, m, CH_2 *2 & 7*), 3.60-3.67 (8H, m, CH_2 *3-6*), 5.28 (1H, s, NH). ^{13}C NMR (100MHz, $CDCl_3$) δ: 28.4 (CH_3 *11*), 40.4 (CH_2 *8*), 41.7 (CH_2 *1*), 70.3 (CH_2 *3, 6 & 7*), 70.6 (CH_2 *4 & 5*), 73.4 (CH_2 *2*) 79.1 ($C(CH_3)_3$ *10*), 156.1 (C=O *9*).

2.7.1.5 *Synthesis of tert-butyl (13-oxo-3,6,9-trioxa-12-azaheptadec-16-yn-1-yl)carbamate*

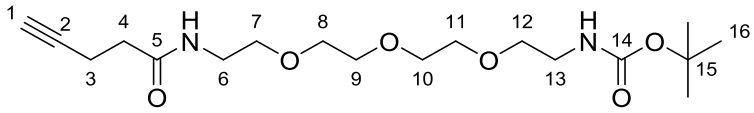

69

To a solution of pentynoic acid (40.0 mg, 0.41 mmol) in DMF (2 mL) was added DCC (81.5 mg, 0.41 mmol) and NHS (53.0 mg, 0.46 mmol). The reaction mixture was stirred for 30 min at room temperature. This reaction mixture was filtered into a solution of (2-(2-(2-(2-aminoethoxy)ethoxy)ethoxy) ethyl)carbamate (**68**) (116.1 mg, 0.40 mmol) and DIPEA (100 µL, 74.2 mg, 0.57 mmol) in DMF (2 mL) and stirred overnight. To a solution of 4-pentynoic acid (41.6 mg, 0.42 mmol) in DMF (2 mL) was added DCC (74.5 mg, 0.36 mmol) and NHS (51.2 mg, 0.44 mmol). The 4-pentynoic acid solution was stirred for 30 min before being filtered into the reaction mixture and stirred overnight at room temperature. The sample was filtered and concentrated *in vacuo*. Purification by flash column chromatography (100% ethyl acetate) afforded tert-butyl (13-oxo-3,6,9-trioxa-12-azaheptadec-16-yn-1-yl)carbamate, compound (**69**), as a colourless oil (0.0591 g, 0.16 mmol, 40% yield).

R_f 0.20 (100% ethyl acetate). HR-LCMS (ES): R_t; 163 min m/z calculated for $C_{18}H_{33}N_2O_6^+$ 373.2333 $[M+H]^+$ observed 373.2350, 395.2174 $[M+Na]^+$, 273.1812 $[M\text{-}BOC+H]^+$. IR (neat) ν_{max} (cm^{-1}): 3310 (N-H), 3087 (C≡C-H), 2121 (C≡C), 1709 & 1661 (C=O). ^1H NMR (500MHz, $CDCl_3$) δ: 1.37 (9H, s, CH_3 ^{16}), 1.94-1.98 (1H, app s, C≡CH ^{1}), 2.39 (2H, t, *J = 7.1*, CH_2 ^{4}), 2.50 (2H, td, $J^1 = 2.3$, $J^2 = 7.1$, CH_2 ^{3}), 3.24-3.25 (2H, m, CH_2 ^{13}), 3.44 (2H, app. q, *J = 10.0 & 5.2*, CH_2 ^{6}), 3.54 (4H, app. quin, *J = 5.2 & 4.8*, CH_2 $^{7\ \&\ 12}$), 3.56 (8H, s, CH_2 $^{8\text{-}11}$), 5.07 (1H, s, ROC(O)NH), 6.40 (1H, s, RC(O)NH). ^{13}C NMR (125 MHz, $CDCl_3$) δ:

14.8 (CH_2 [3]) 28.4 ((CH_3)$_3$ [16]), 35.1 (CH_2 [4]), 39.2 (CH_2 [6]), 40.3 (CH_2 [13]), 69.25 (H*C*≡CR [1]), 69.9 (CH_2 [12]), 70.1 (CH_2 [7]), 70.2 (CH_2 [8 & 11]), 70.4 (CH_2 [9 & 10]), 79.2 (C(CH_3)$_3$ [15]), 83.1 (HC≡*C*R [2]), 156.0 (C=O [14]), 171.1 (C=O [5]).

2.7.1.6 *N-(2-(2-(2-(2-aminoethoxy)ethoxy)ethoxy)ethyl)pent-4-ynamide*[257]

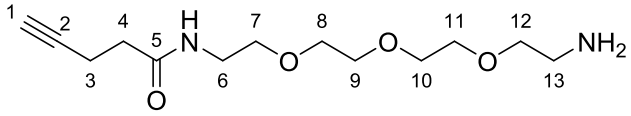

70

Tert-butyl(13-oxo-3,6,9-trioxa-12-azaheptadec-16-yn-1-yl)carbamate (**69**) (85.0 mg, 0.23 mmol) was stirred in 1:1 TFA:DCM (6 mL) for 1 hr. The sample was then concentrated *in vacuo*, followed by evaporations with DCM (3 x 10 mL). The sample was dissolved in water (10 mL) and dried using a freeze dryer. This afforded N-(2-(2-(2-(2-aminoethoxy)ethoxy)ethoxy)ethyl)-7-nitrobenzo[c][1,2,5]oxadiazol-4-amine (**70**) as a viscous oil in quantitative yield.

R_f 0.25 (1:9 MeOH:DCM). HR-LCMS (ES): Rt 0.27 min m/z calculated for $C_{13}H_{25}N_2O_4^+$ 273.1814 observed 273.1809 $[M+H]^+$.

2.7.1.7 *N-(2-(2-(2-(2-azidoethoxy)ethoxy)ethoxy)ethyl)-7-nitrobenzo[c][1,2,5] oxadiazol-4-amine*[258]

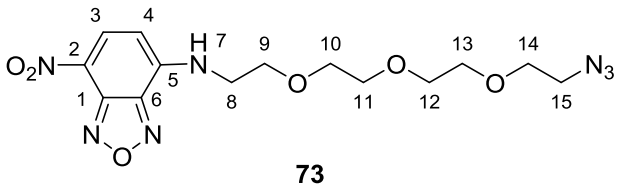

73

To a solution of 1-azido-2-(2-(2-(2-azidoethoxy)ethyoxy)ethoxy)ethane (**66**) (110.0 mg, 0.50 mmol) in aqueous $NaHCO_3$ (0.3 M, 5 mL) was added 4-chloro-7-nitrobenzofurazan (73.2 mg, 0.37 mmol) in methanol (10 mL). The solution was stirred overnight at room

temperature and concentrated *in vacuo* to give a brown oil. Purification by flash column chromatography (3:1 ethyl acetate:hexane) afforded compound (**73**), N-(2-(2-(2-(2-azidoethoxy)ethoxy)ethoxy)ethyl)-7-nitrobenzo[c][1,2,5]oxadiazol-4 amine, as a bright orange oil (96.7 mg, 0.25 mmol, 69%).

R_f 0.35 (3:1 Ethyl acetate:hexane). HR-LCMS (ES): R_t 1.83 min; m/z calculated for $C_{14}H_{19}N_7O_6Na^+$ 404.1289 [M+Na^+] observed 404.1314. UV-Vis (MeOH): λ_{max} (nm) 470, 338. Luminescence (MeOH): λ_{em} (nm) 538. ^{1}H NMR (400MHz, $CDCl_3$) δ: 3.36-3.40 (2H, m, CH_2 *15*), 3.65-3.74 (12H, m, CH_2 *8, 10-14*), 3.86-3.90 (2H, m, CH_2 *9*), 6.19 (1H, d, *J = 8.6*, CH *4*), 6.99 (1H, s, NH *7*), 8.49 (1H, d, *J = 8.6 Hz*, CH *3*). ^{13}C NMR (100MHz, $CDCl_3$) δ: 43.8 (CH_2 *8*), 50.8 (CH_2 *15*), 68.1 (CH_2 *9*), 70.0 (CH_2 *14*), 70.6 (CH_2 *10*), 70.68 (CH_2 *13*), 70.8 (CH_2 *11 & 12*), 96.5 (CH *4*), 136.4 (CH *3*), 144.2 (C_q).

2.7.1.8 *Synthesis of tert-butyl (2-(2-(2-(2-((7-nitrobenzo[c][1,2,5] oxadiazol-4-yl)amino)ethoxy)ethoxy)ethoxy)ethyl)carbamate*[258]

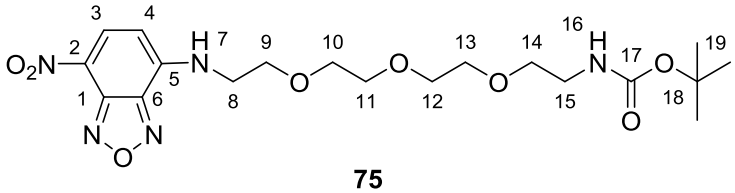

75

To a solution of tert-butyl (2-(2-(2-(2-aminoethoxy)ethoxy)ethoxy)ethyl)carbamate (**68**) (103.0 mg, 0.35 mmol) in aqueous $NaHCO_3$ (0.3 M, 5 mL) was added 4-chloro-7-nitrobenzofurazan (63.2 mg, 0.32 mmol) in methanol (15 mL). The solution was stirred overnight at room temperature and concentrated *in vacuo* to give a brown oil. Purification by flash column chromatography (3:1 ethyl acetate:hexane) afforded compound (**75**), tert-butyl (2-(2-(2-(2-((7-nitrobenzo[c][1,2,5]oxadiazol-4-yl)amino)

ethoxy)ethoxy)ethoxy)ethyl)carbamate, as a bright orange oil (94.3 mg, 0.21 mmol, 60% yield).

R_f 0.20 (3:1 ethyl acetate:hexane). HR-LCMS (ES): Rt 1.92 min; m/z calculated for $C_{19}H_{29}N_5O_8Na^+$ 478.1908 $[M+Na]^+$ observed 478.1905. IR (neat) ν_{max} (cm^{-1}): 1304 & 1586 (N-O), 1622 (C=C), 1709 (C=O), 3331 (N-H). UV-Vis (MeOH): λ_{max} (nm) 454, 329. Luminescence (MeOH): λ_{em} (nm) 516. ^{1}H NMR (400MHz, $CDCl_3$) δ: 1.35 (9H, s, CH_3 *19*), 3.20-3.26 (2H, m, CH_2 *15*), 3.45-3.49 (2H, m, CH_2 *14*), 3.55-3.69 (10H, m, CH_2 *8 & 10-13*), 3.80-3.84 (2H, m, CH_2 *9*), 4.98 (1H, s, NH *16*), 6.15 (1H, d, *J = 8.7*, CH *4*), 7.20 (1H, s, NH *7*), 8.38 (1H, d, *J = 8.7*, CH *3*). ^{13}C NMR (100MHz, $CDCl_3$) δ: 28.4 (CH_3 *19*), 40.3 (CH_2 *15*), 43.8 (CH_2 *8*), 68.2 (CH_2 *9*), 70.2 (CH_2 *10, 13 & 14*), 70.5 (CH_2 *11 & 12*), 79.2 ($C(CH_3)_3$ *18*), 98.9 (CH *4*), 123.5 (C *2*), 136.5 (CH *3*), 144.0 (CH *5*), 144.3 (CH *1 & 6*) 156.0 (C=O *17*).

2.7.1.9 *Attempted synthesis of N-(2-(2-(2-(2-aminoethoxy)ethoxy)ethoxy) ethyl)-7-nitrobenzo[c][1,2,5]oxadiazol-4-amine*[240]

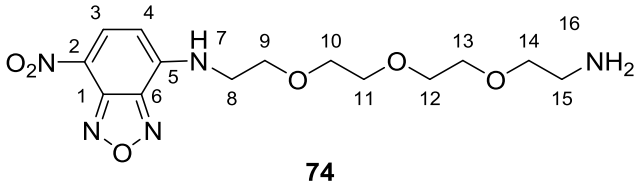

74

A solution of N-(2-(2-(2-(2-azidoethoxy)ethoxy)ethoxy)ethyl)-7-nitrobenzo[c][1,2,5] oxadiazol-4 amine (**73**) (90 mg, 0.24 mmol) and phosphoric acid (150 uL, 35 mg, 0.35 mmol) in water (5 mL) was cooled to 0°C under nitrogen. A solution of triphenyl phosphine (66 mg, 0.25 mmol) in diethyl ether (5 mL) was added dropwise with stirring. The solution was allowed to warm to room temperature and stirred overnight. The biphasic solution was separated and the aqueous solution washed with diethyl ether (3 x 10 mL). A solution of potassium hydroxide (6 M, 3 mL) was added and the

solution stirred for 3 hr. The mixture was filtered and extracted with chloroform (3 x 70 mL), dried over $MgSO_4$, filtered and concentrated *in vacuo.* No product was detected by ESMS.

2.7.1.10 *Synthesis of N-(2-(2-(2-(2-aminoethoxy)ethoxy)ethoxy) ethyl)-7-nitrobenzo[c][1,2,5]oxadiazol-4-amine*[257]

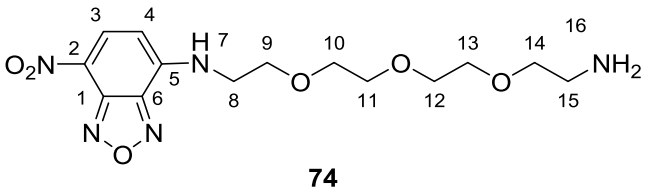

74

Tert-butyl (2-(2-(2-(2-((7-nitrobenzo[c][1,2,5]oxadiazol-4-yl) amino)ethoxy)ethoxy) ethoxy)ethyl)carbamate (**75**) (95.0 mg, 0.21 mmol) was stirred in 1:1 TFA:DCM (10 mL) for 3 hr. The sample was then concentrated *in vacuo*, followed by a further two evaporations with DCM. The sample was then finally dissolved in water (15 mL) and dried using a freeze dryer. This afforded N-(2-(2-(2-(2aminoethoxy)ethoxy)ethoxy) ethyl)-7-nitrobenzo[c][1,2,5]oxadiazol-4-amine, compound (**74**), as a very viscous bright orange oil (TFA salt) (83.2 mg, 0.18 mmol, 85%). Degradation occurred upon NMR and attempted purification by flash column chromatography.

R_f 0.25 (1:9 (10% NH_4^+ in MeOH):DCM). LCMS (ES): Rt 0.68 min m/z calculated for $C_{14}H_{22}N_5O_6^+$ 356.1565 $[M+H]^+$ observed 356.1562 & 378.1378 $[M+Na]^+$.

2.7.1.11 *Synthesis of 2-(2-(2-(2-azidoethoxy)ethoxy) ethoxy)ethanol*[240]

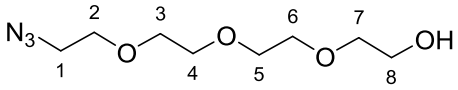

79

To a solution of tetraethylene glycol (11.8309 g, 60.9 mmol) in DCM (180 mL) at 0 °C was added triethylamine (3.057 g, 4.2 mL, 30.1mmol). A solution of methane sulfonyl chloride (2.2911 g, 1.6 mL, 20.1 mmol) in DCM (20mL) was added dropwise over 45 min. The reaction mixture was allowed to warm to room temperature and stirred overnight. The DCM was removed *in vacuo* and the resultant solid dissolved in water: ethanol solution (3:1, 100mL). Sodium azide (3.5837 g, 55.1 mmol) and $NaHCO_3$ (0.9408 g, 11.2 mmol) were added and the mixture heated to reflux overnight. Upon cooling, the reaction mixture was extracted with DCM (3 x 75 mL), dried over anhydrous $MgSO_4$, filtered and concentrated *in vacuo* to afford 2-(2-(2-(2-azidoethoxy)ethoxy)ethoxy)ethanol compound (**79**) as a colourless oil (3.6286 g, 16.6 mmol, 83% yield).

R_f 0.10 (4:1 ethyl acetate:petroleum ether 40-60°C). HR-LCMS (ES): R_t 1.22 min; m/z calculated for $C_8H_{18}N_3O_4^+$ 220.1292 observed 220.1290 $[M+H^+]$, 242.1116 $[M+Na]^+$. IR (neat) ν_{max} (cm^{-1}): 3473 (O-H), 2109 (N_3), 1303 (C-O). ^{1}H NMR (300MHz, $CDCl_3$) δ: 2.56 (1H, s, OH), 3.38 (2H, t, *J = 5.1*, CH_2 ^{1}), 3.58 (2H, t, *J = 5.*2, CH_2 ^{7}), 3.63-3.64 (10H, m, CH_2 $^{2-6}$), 3.70 (2H, t, *J = 5.2*, CH_2 ^{8}). ^{13}C NMR (100MHz, $CDCl_3$) δ: 50.7 (CH_2 ^{1}), 61.6 (CH_2 ^{8}), 70.0 (CH_2 ^{2}), 70.3 (CH_2 ^{3}), 70.5 (CH_2 ^{6}), 70.6 (CH_2 ^{4}), 70.6 (CH_2 ^{5}), 72.5 (CH_2 ^{7}).

2.7.1.12 *Synthesis of 2-(2-(2-(2-azidoethoxy)ethoxy)ethoxy)ethyl dihydrogen phosphate*[259]

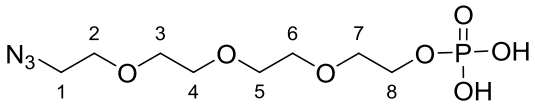

82

To a solution of phosphorus oxychloride (70 mg, 43 µL, 0.46 mmol) in dry diethyl ether (2 mL) under nitrogen at -78°C was added triethylamine (46 mg, 64 µL, 0.46 mmol). 2-(2-(2-(2-Azidoethoxy)ethoxy)ethoxy)ethanol (**79**) was added dissolved in diethyl ether (2 mL) and added dropwise. The sample was allowed to warm to room temperature overnight with stirring. Due to the presence of unreacted starting material by LCMS, more phosphorus oxychloride (250 µL) was added and the sample stirred overnight. The solution was quenched with TEAB (10 mL, 0.1 M) and concentrated to afford a colourless oil.

HR-LCMS (ES): Rt 1.04 min; m/z calculated for $C_8H_{19}N_3O_7P^+$ 300.0961 $[M+H]^+$ observed 300.0950 and 322.0780 $[M+Na]^+$.

2.7.1.13 *Synthesis of 2-(2-(2-(2-azidoethoxy)ethoxy)ethoxy)ethyl methanesulfonate*[240&260]

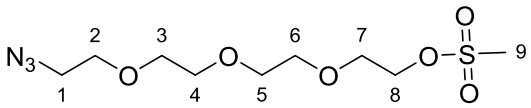

81

To a solution of 2-(2-(2-(2-azidoethoxy)ethoxy)ethoxy)ethanol (**79**) (308.0 mg, 1.41 mmol) in DCM (10 mL) at 0°C was added TEA (326.7 mg, 450 µL, 3.23 mmol) and methanesulfonyl chloride (266.4 mg, 180 µL, 2.33 mmol). The solution was allowed to

warm to room temperature overnight with stirring. DCM was removed *in vacuo* and the resultant oil was purified by flash column chromatography (3:1 ethyl acetate:petroleum ether 40-60°C) to afford compound (**81**), 2-(2-(2-(2-azidoethoxy) ethoxy)ethoxy)ethyl methanesulfonate, as a colourless oil (157.4 mg, 0.53 mmol, 38% yield).

R_f 0.25 (3:1 ethyl acetate:petroleum ether 40-60 °C). HR-LCMS (ES): R_t 1.487 min; m/z calculated for $C_9H_{19}N_3O_6SNa^+$ 320.0887 $[M+Na]^+$ observed 320.0898. IR (neat) ν_{max} (cm^{-1}): 2110 (N_3), 1352 (S=O), 1303 (C-O), 1175 (S=O). ^{1}H NMR (300MHz, $CDCl_3$) δ: 3.07 (3H, s, CH_3), 3.39 (2H, t, *J = 5.0 Hz*, CH_2 *1*), 3.64-3.70 (10H, m, CH_2 *2-6*), 3.75-3.79 (2H, m, CH_2 *7*), 4.36-4.39 (2H, m, CH_2 *8*). ^{13}C NMR (75MHz, $CDCl_3$) δ: 37.7 (CH_3), 50.7 (CH_2 *1*), 69.0 (CH_2 *7*), 69.3 (CH_2 *8*), 70.0 (CH_2 *2*), 70.6 (CH_2 *3 & 6*), 70.7 (CH_2 *4 & 5*).

2.7.1.14 *Attempted synthesis of 1-azido-2-(2-(2-(2-bromoethoxy)ethoxy) ethoxy)ethane*[261]

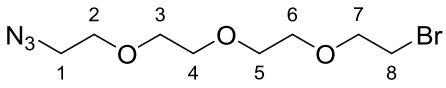

80

To a solution of 2-(2-(2-(2-azidoethoxy)ethoxy)ethoxy)ethanol (**79**) (115.0 mg, 0.52 mmol) **in dry diethyl ether** (5 mL) under nitrogen at 0°C was added phosphorus tribromide (576.0 mg, 200 µL, 2.13 mmol). **The solution was allowed to come to room temperature overnight with stirring**. Methanol (1 mL) was added on ice and the solution poured into water. The organic solution was washed with saturated $NaHCO_3$ solution (1 x 5 mL) and brine (1 x 5 mL). The aqueous layers were combined and back extracted with ethyl acetate (1 x 20 mL). The organic layers were combined, dried over $MgSO_4$ and concentrated. No product was evident by LCMS.

To a solution of 2-(2-(2-(2-azidoethoxy)ethoxy)ethoxy)ethanol (**79**) (119.0 mg, 0.54 mmol) **in dry diethyl ether** (5 mL) under nitrogen at 0°C was added phosphorus tribromide (576.0 mg, 200 µL, 2.13 mmol). **The solution was allowed to come to room temperature over 30 min and then heated to reflux overnight with stirring**. Methanol (1 mL) was added on ice and the solution poured into water. The organic solution was washed with saturated $NaHCO_3$ solution (1 x 5 mL) and brine (1 x 5 mL). The aqueous layers were combined and back extracted with ethyl acetate (1 x 20 mL). The organic layers were combined, dried over $MgSO_4$ and concentrated. No product was evident by LCMS.

To a solution of 2-(2-(2-(2-azidoethoxy)ethoxy)ethoxy)ethanol (**79**) (110.0 mg, 0.50 mmol) **in dry toluene** (5 mL) under nitrogen at 0°C was added phosphorus tribromide (576.0 mg, 200 µL, 2.13 mmol). **The solution was allowed to come to room temperature over 30 min and then heated to reflux overnight with stirring**. Methanol (1 mL) was added on ice and the solution poured into water. The organic solution was washed with saturated $NaHCO_3$ solution (1 x 5 mL) and brine (1 x 5 mL). The aqueous layers were combined and back extracted with ethyl acetate (1 x 20 mL). The organic layers were combined, dried over $MgSO_4$ and concentrated. No product was evident by LCMS.

2.7.1.15 *Synthesis of 1-azido-2-(2-(2-(2-bromoethoxy)ethoxy) ethoxy)ethane*[260]

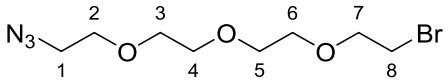

80

To a solution of 2-(2-(2-(2-azidoethoxy)ethoxy)ethoxy)ethanol (**79**) (126.0 mg, 0.42 mmol) in acetonitrile (10 mL) was added tetrabutylammonium bromide (248.0 mg, 0.75 mmol). The solution was heated overnight at 50 °C under nitrogen. Upon cooling acetonitrile was removed *in vacuo* to afford a red oil, which was dissolved in water (50 mL) and extracted with ethyl acetate (3 x 75 mL). The organic extracts were combined, washed with water (75 mL), dried over $MgSO_4$ and concentrated *in vacuo*. Flash column chromatography (1:1 ethyl acetate:petroleum ether 40-60°C) afforded 1-azido-2-(2-(2-(2-bromoethoxy)ethoxy)ethoxy)ethane (**80**) as a colourless oil (43.1 mg, 0.15 mmol, 36% yield).

R_f 0.60 (1:1 ethyl acetate:petroleum ether 40-60°C). LCMS (ES): R_t 1.74 min; m/z calculated for $C_8H_{16}BrN_3O_3Na^+$ 304.0267 & 306.0247 $[M+Na]^+$ observed 304.0265 & 306.0206. IR (neat) ν_{max} (cm^{-1}): 2870 (N-H), 2109 (N_3). ^1H NMR (300MHz, $CDCl_3$) δ: 3.32 (2H, t, *J = 5.1*, CH_2 ^{1}), 3.40 (2H, t, *J = 6.3*, CH_2 ^{8}), 3.60-3.62 (10H, m, CH_2 $^{2-6}$), 3.75 (2H, t, *J = 6.3*, CH_2 ^{7}). ^{13}C NMR (75MHz, $CDCl_3$) δ: 30.3 (CH_2 ^{8}), 50.7 (CH_2 ^{1}), 20.0 (CH_2 ^{2}), 70.5 (CH_2 ^{3}), 70.7 (CH_2 $^{4-6}$), 71.2 (CH_2 ^{7}).

2.7.1.16 *Synthesis of ATP-azide analogue*[262]

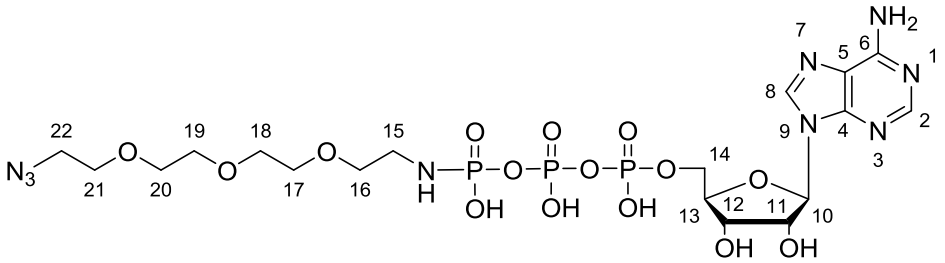

60

To a solution of ATP sodium salt (202.0 mg, approx. 0.37 mmol) in 1:1 THF:water (25 mL) was added EDC. HCl (72.9 mg, 0.38 mmol). The solution was made basic (approx. pH 9) using TEA and then stirred at room temperature for 60 min. 2-(2-(2-(2-Azidoethoxy)ethoxy)ethoxy)ethanamine (**66**) (160 mg, 0.73 mmol) was added and the reaction mixture stirred at room temperature overnight. The sample was concentrated *in vacuo* to remove THF and applied to a column of DEAE Sephadex. Elution was effected with a linear gradient of 1.8 L of triethylammonium bicarbonate from 50mM to 600 mM. $ATPN_3$ eluted at approx. 185-230 mM. These fractions were combined and evaporated to dryness. Residual triethylammonium bicarbonate was removed by evaporation with methanol (3 x 50 mL). Further purification by RP-HPLC (0-40 % B over 30 min; Buffer A: 50 mM TEAB ~pH 7.1, Buffer B: acetonitrile) followed and the relevant fractions were combined and evaporated to dryness. Residual triethylammonium bicarbonate was removed by evaporation with methanol (3 x 50 mL) before freeze-drying from water (1 mL). Pure product was not recovered from HPLC.

MS (ES): m/z 706 $[M-H]^-$. RP-HPLC: R_t 15.52 min (0-40% B over 30 min; Buffer A: 50 mM TEAB ~pH 7.1, Buffer B: acetonitrile).

2.7.1.17 *Synthesis of ATPγNH-linker-alkyne analogue*[262]

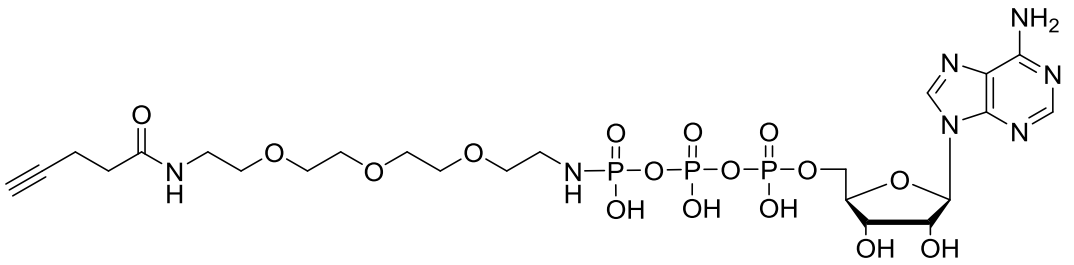

59

To a solution of ATP sodium salt (88.0 mg, approx. 0.16 mmol) in 1:1 THF:water (25 mL) was added EDC. HCl (31.1 mg, 0.16 mmol). The solution was made basic (approx. pH 9) using TEA and then stirred at room temperature for 60 min. N-(2-aminoethoxy)ethoxy)ethoxy)ethyl)-7-nitrobenzo[c][1,2,5]oxadiazol-4-amine (**70**) (30.0 mg, 0.11 mmol) was added and the reaction mixture stirred at room temperature overnight. The sample was concentrated *in vacuo* to remove THF and applied to a column of DEAE Sephadex. Elution was effected with a linear gradient of 1.8 L of triethylammonium bicarbonate from 50mM to 600 mM. ATPγNH-linker-alkyne (**59**) eluted at approx. 270-330 mM. These fractions were combined and evaporated to dryness to yield crude ATPγNH-linker-alkyne (**59**) (4.0 mg, 5.12 µmol, 5% crude yield). Residual triethylammonium bicarbonate was removed by evaporation with methanol (3 x 50 mL). Further purification by RP-HPLC (0-40% B over 30 min; Buffer A: 50 mM TEAB ~pH 7.1, Buffer B: acetonitrile) followed and the relevant fractions were combined and evaporated to dryness. Residual triethylammonium bicarbonate was removed by evaporation with methanol (3 x 50 mL) before freeze-drying from water (1 mL). Analysis by RP-HPLC showed degradation; therefore, pure product was not isolated.

MS (ES): m/z 760 $[M-H]^-$. RP-HPLC: R_t 15.93 min (0-40% B over 30 min; Buffer A 50 mM TEAB pH ~7.1, Buffer B acetonitrile); R_t 17.52 min (0-30% B over 30 min; Buffer A: 50 mM TEAB pH ~7.1, Buffer B: acetonitrile).

2.7.1.18 *Attempted synthesis of ATPγNH-linkier-coumarin* [263]

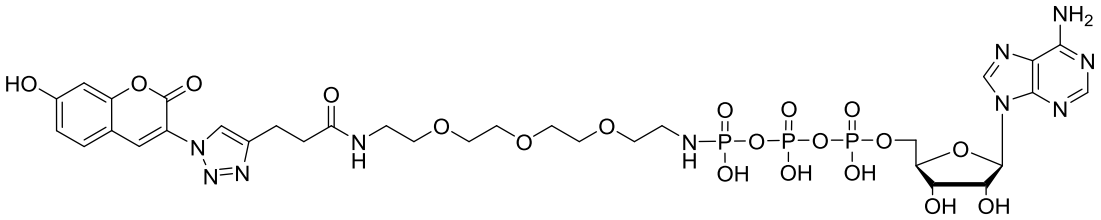

58

To a solution of crude ATPγNH-linker-alkyne (**58**) (2.0 mg, 2.63 µmol) and 7-Acetic-3-azidocoumarin (1.8 mg, 5.26 µmol) in 1:1 water:ethanol (400 µL) was added $CuSO_4$ (2 M, 2.6 µL, 5.26 µmol) and sodium ascorbate (10.0 mg, 0.42 µmol). The solution was stirred for 2 hr at room temperature. Analysis by MS and RP-HPLC showed no product.

2.7.1.19 *Attempted synthesis of ATP-azide analogue with P-O link*

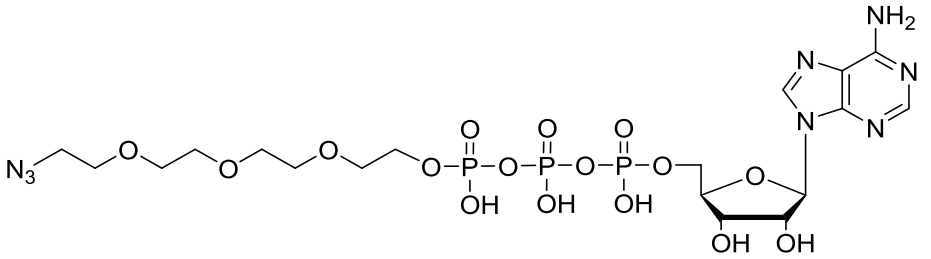

61

2.7.1.19.1 Using EDC[262]

A solution of ATP disodium salt (156.4 mg, 0.28 mmol) and EDC (47.8 mg, 0.25 mmol) in water (6 mL) was stirred at room temperature for 30 minutes to form the active ester. 2-(2-(2-(2-Azidoethoxy)ethoxy)ethoxy)ethanol (**79**) (49.9 mg, 0.23 mmol) was added and the solution stirred at room temperature for 3 hr. The reaction was

monitored by RP-HPLC (0-40% B over 30 min, Buffer A: 50 mM TEAB pH 7, Buffer B: acetonitrile). No product evident by HPLC, LCMS or MS.

2.7.1.19.2 Using DCC[264]

ATP disodium salt (54.1 mg, 98 µmol) was converted to the free acid form by shaking with Amberlyst 15 (50 mg) in water for 30 min. The Amberlyst 15 was removed by suction filtration and the filtrate evaporated to dryness. The free acid was converted to the triethylammonium salt by the addition of TEAB (3 mL, 1 M). Excess TEAB was removed by evaporation with methanol (3 x 5 mL) and the sample freeze dried from water (8 mL). ATP was rendered anhydrous by evaporation with dry pyridine (2 mL) and activated with DCC (20.8 mg, 98 µmol) in dry DMF (2 mL) for 1 hr. 2-(2-(2-(2-Azidoethoxy)ethoxy)ethoxy)ethanol (**79**) (107.1 mg, 0.49 mmol) was rendered anhydrous by evaporation with dry pyridine (2 x 2mL), dissolved in dry DMF (2 mL) with TEA (50 µL) and added to the ATP solution. The reaction mixture was stirred at 40 °C overnight. No product was detected by MS.

2.7.1.19.3 Using compound (**82**)[259]

ADP disodium salt (212.2 mg, 0.46 mmol) was converted to the free acid form by shaking with Amberlyst 15 (50 mg) in water for 30 min. The Amberlyst 15 was removed by suction filtration and the filtrate evaporated to dryness. The free acid was converted to the tributylammonium salt by the addition of TEAB (3 mL, 1 M). To a solution of the ADP salt in dry DMF (3 mL) was added CDI (74.6 mg, 0.46 mmol) and solution was left stirring overnight. Dry MeOH (20 µL) was added and the reaction mixture stirred for 30 min. Crude 2-(2-(2-(2-Azidoethoxy)ethoxy)ethoxy)ethyl

dihydrogen phosphate (**82**) was dissolved in dry DMF (2 mL) and added to the ADP solution. The reaction mixture was stirred overnight. No product was detected by MS.

2.7.1.19.4 Using compound (**80**)[174]

ATP disodium salt (100.6 mg, 0.18 mmol) was converted to the free acid form by shaking with Amberlyst 15 (50 mg) in water for 30 min. The Amberlyst 15 was removed by suction filtration and the filtrate evaporated to dryness. The free acid was converted to the triethylammonium salt by the addition of TEAB (3 mL, 1 M). Excess TEAB was removed by evaporation with methanol (3 x 5 mL) and the sample freeze dried from water (8 mL). ATP was dissolved in dry DMF (3 mL) and left over molecular sieves overnight. 1-azido-2-(2-(2-(2-bromoethoxy)ethoxy)ethoxy)ethane (**80**) was dissolved in dry DMF (2 mL) and left over molecular sieves overnight before being added to the ATP solution and stirred overnight. No product was detected by MS.

2.7.1.20 *Synthesis of ATPγSEt*[244]

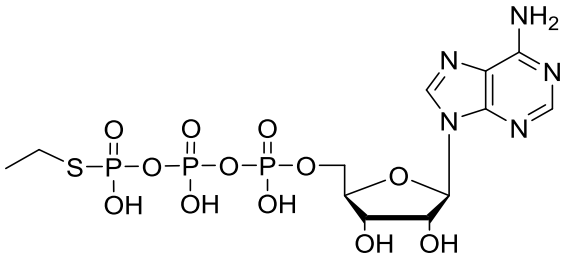

62

ATPγS (**48**) tetralithium salt (7 mg, 13 µmol) was dissolved in MeOD:D_2O (1:1, 1 mL) and placed in an NMR tube. Iodoethane (2.0 mg, 1 µL) was added and the reaction monitored by ^{31}P NMR. No change in NMR was seen after 24 hr therefore more iodoethane (4.0 mg, 2 µL) was added and the reaction mixture left for 48 hr. The sample was purified using RP-HPLC ((0-40% B over 20 min; Buffer A: 0.1 M TEAA in

water pH ~7.2; Buffer B: 0.1 M TEAA in 80:20 ACN:water pH ~7.2)) to yield ATPγSEt (**62**) (10 nmol).

ES MS: m/z 550 [M-H], 426 $[ADP-H]^-$. RP-HPLC: R_t 15.247 min (0-40% B over 25 min; Buffer A: 0.1 M TEAA in water ~pH 7.2; Buffer B: 0.1 M TEAA in 80:20 ACN:water ~pH 7.2).

2.7.1.21 *Synthesis of ADP-morpholidate*[265]

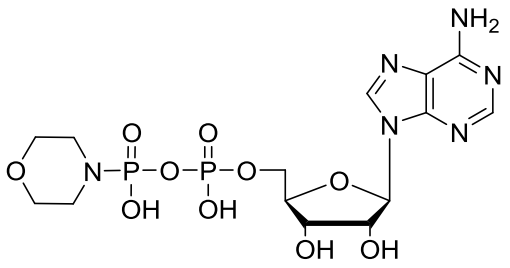

84

ADP mono sodium salt (402.9 mg, 0.90 mmol) was converted to the free acid form by shaking with Amberlyst 15 (100mg) in water for 1 hr. The Amberlyst 15 was removed by suction filtration and the filtrate freeze dried. The resultant free acid ADP was refluxed with morpholine (489.0 mg, 500 μL, 5.62 mmol) in 50% aqueous tertiary butanol (10 mL). DCC (1.1444 mg, 5.55 mmol) in tertiary butanol (5 mL) was added and the solution refluxed overnight. The sample was cooled, evaporated to half its volume and washed with ether (3 x 50 mL). The aqueous layer was filtered to remove dicyclohexylurea precipitate and applied to a column of DEAE Sephadex. Elution was effected with a linear gradient of 1.8 L of triethylammonium bicarbonate (50 mM to 600 mM). Three UV 260 nm absorbing peaks were obtained. ADP-morpholidate (**84**) was eluted at approx 200 mM to 340 mM. These fractions were combined and evaporated to dryness. Residual triethylammonium bicarbonate was removed by

evaporation with methanol (4 x 50 mL) and the sample freeze dried from water (10 mL) to yield the triethylammonium salt of ADP-morpholidate (**84**) (185.0 mg, 0.37 mmol, 30% crude yield).

HR-LCMS (ES): R_t: 0.39 min; m/z calculated for $C_{14}H_{21}N_6O_{10}P_2^-$ 495.0800 $[M-H]^-$ observed 495.0858. UV λ_{max} 259.3 nm.

2.7.1.22 *Synthesis of ATPγEt*[265]

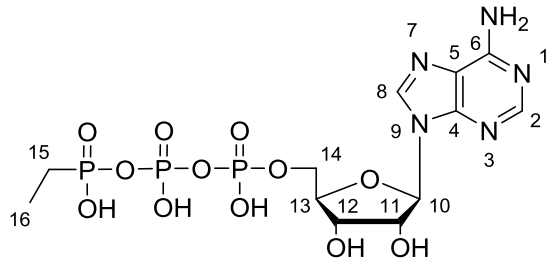

63

Crude ADP-morpholidate triethylammonium salt (**84**) (168.3 mg, 0.24 mmol) was rendered anhydrous by evaporation with dry pyridine (3 x 3 mL). Residual pyridine was removed by evaporation with dry toluene (3 x 2 mL). Ethylphosphonic acid (73.0 mg, 0.67 mmol) was placed in pyridine (1 mL). A cloudy suspension formed. Upon addition of Bu_3N (250 µL, 194.5 mg, 1.05 mmol) the solution became clear. This was evaporated to dryness by evaporation with dry pyridine (3 x 3 mL) and residual pyridine removed by evaporation with dry toluene (3 x 2 mL). This was dissolved in dry DMSO (3 mL) and added to the anhydrous ADP-morpholidate (**84**). The reaction mixture was stirred at 40 °C for 48 hr. This was then applied to a column of DEAE Sephadex. Elution was effected with a linear gradient of 1.8 L of triethylammonium bicarbonate from 50mM to 400 mM. ATPγEt eluted at approx 210-255 mM. These fractions were combined and evaporated to dryness. Residual triethylammonium bicarbonate was removed by

evaporation with methanol (3 x 50 mL). Further purification by RP-HPLC (0-10% B; Buffer A: 50 mM TEAB pH ~7.1, Buffer B: acetonitrile) followed and the relevant fractions were combined and evaporated to dryness. Residual triethylammonium bicarbonate was removed by evaporation with methanol (3 x 50 mL) before freeze-drying from water (1 mL) to yield ATPγEt (**63**) as the triethyl ammonium salt (17.6 mg, 21.46 µmol, 9% yield).

LCMS (Es): R_t 0.435; m/z Calculated for $C_{12}H_{21}N_5O_{12}P_3^+$ 520.0400 $[M+H]^+$ observed 520.0372 & 517.8624 $[M-H]^-$ &. MS (ES): m/z 518 $[M-H]^-$. RP-HPLC: R_t 18.580 min (0-10% B over 30 min; Buffer A: 50 mM TEAB ~pH 7.1, Buffer B: acetonitrile). UV λ_{max}: 259.00 nm. ^{1}H NMR (300MHz, D_2O) δ: 1.02 (3H, dt, *J = 20.0* & *J = 7.7*, CH_3 *16*), 1.69 (2H, dq, *J = 17.6* & *J= 7.7*, CH_2 *15*), 4.12-4.25 (2H, m, CH_2 *14*), 4.34 (1H, app quintet, *J =5.5 & 2.76* , CH *13*), 4.52 (1H, dd, *J = 5.1 & J = 3.4*, CH *12*), 4.72-4.76 (1H, m, CH *11*), 6.08 (1H, d, *J = 6.1*, CH *10*), 8.20 (1H, s, CH *8*), 8.48 (1H, s, CH *2*). ^{31}P {^{1}H} NMR (100MHz, D_2O) δ: -23.06 (1P, m, β), -11.43 (1P, d, *J = 18.6*, α), 22.43 (1P, d, *J = 21.8*, γ).

2.7.1.23 ***Synthesis of GTP-azide analogue***[262]

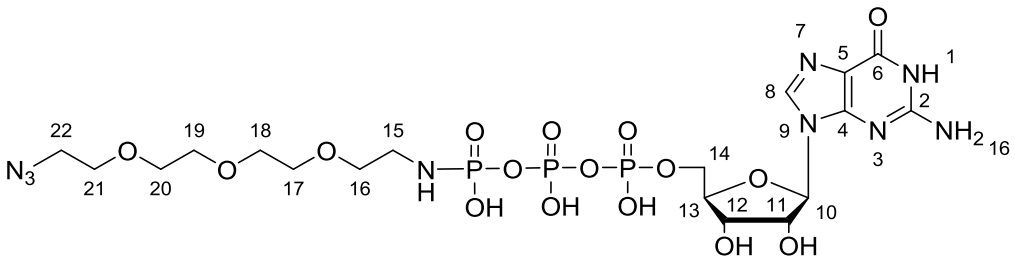

99

To a solution of GTP sodium salt (70.9 mg, approx. 0.14 mmol) in 1:1 THF:water (25 mL) was added EDC (118.4 µL, 103.9 mg, 0.54 mmol) and 2-(2-(2-(2-azidoethoxy)ethoxy)ethoxy)ethanamine (**66**) (68.4 mg, 0.313 mmol) and the reaction

mixture stirred at room temperature overnight. The sample was concentrated *in vacuo* to remove THF and applied to a column of DEAE Sephadex. Elution was effected with a linear gradient of 1.8 L of triethylammonium bicarbonate from 50mM to 470 mM. GTPγNH-PEG-N_3 (**94**) eluted at approx. 270-330 mM. These fractions were combined and evaporated to dryness. Residual triethylammonium bicarbonate was removed by evaporation with methanol (3 x 50 mL). Further purification by RP-HPLC (2-30% B over 20 min; Buffer A: 0.1 M TEAA in water ~pH 7.2; Buffer B: 0.1 M TEAA in 80:20 ACN:water ~pH 7.2) followed and the relevant fractions were combined and evaporated to dryness. Residual triethylammonium bicarbonate was removed by evaporation with methanol (3 x 50 mL) before freeze-drying from water (1 mL) to yield GTPγNH-PEG-N_3 (**99**) as the triethylammonium salt (1.4 mg, 1.36 µmol, 1%).

MS (ES): m/z 722 $[M-H]^-$. RP-HPLC: R_t 24.107 min (2-30% B over 25 min; Buffer A: 0.1 M TEAA in water pH ~7.2; Buffer B: 0.1 M TEAA in 80:20 ACN:water pH ~7.2). ^{1}H NMR (400MHz, D_2O) δ: 2.99-3.06 (2H, m, CH_2 ^{15}), 3.44 (2H, t, *J = 5.2*, CH_2 ^{22}) 3.51 (2H, t, *J = 5.8*, ^{16}), 3.60-3.69 (10H, m, CH_2 $^{17-21}$), 4.11-4.23 (2H, m, CH_2 ^{14}), 4.27-4.31 (1H, m, CH ^{13}), 4.50 (1H, dd, *J = 5.4* & *J = 3.1*, CH ^{12}), 5.87 (1H, d, *J = 6.5*, CH ^{10}), 8.05 (1H, s, CH ^{8}). ^{31}P NMR (400MHz, D_2O) δ: -11.40 (1P, d, *J = 18.2*, α), -22.86 (1P, t, *J = 20.3*, β), -1.36 (1P, m, γ).

2.7.2 Synthesis of CX-4945

2.7.2.1 *Synthesis of (2-amino-4-(methoxycarbonyl)phenyl)boronic acid*[266]

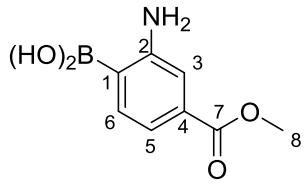

86

To a solution of 4-(methoxycarbonyl)-2-nitrophenyl)boronic acid (**85**) (0.9921 g, 4.41 mmol) in methanol (80 mL) and ethanol (170 mL) was added 10% Pd/C (95.5 mg). The reaction mixture was stirred under hydrogen at room temperature for 2 hr. The mixture was filtered through celite and concentrated *in vacuo* to afford crude 2-amino-4-(methoxycarbonyl)phenyl)boronic acid (**86**) as a yellow solid (0.8392 g, 4.30 mmol, 98% yield).

HR-LCMS (ES): R_t 1.04 min; m/z calculated for $C_8H_{11}NO_4B^+$ 196.0794 $[M+H]^+$ observed 196.0798. ^{1}H NMR (400MHz, $CDCl_3$) δ: 3.94 (3H, s, CH_3 ^{8}), 7.69 (1H, s, CH ^{3}), 7.73 (2H, br s, 2 CH $^{5\ \&\ 6}$).

2.7.2.2 *Synthesis of methyl 5-oxo-5,6-dihydrobenzo[c][2,6] naphthyridine-8-carboxylate*[238]

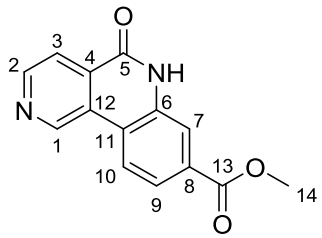

87

To a solution of (2-amino-4-(methoxycarbonyl)phenyl)boronic acid (**86**) (1.1508 g, 5.90 mmol) in DMF (30 mL) was added ethyl 3-bromoisonicotinate (888 µL, 1.4022 g,

6.49 mmol), $PdCl_2$(dppf) (0.2043 g, 0.29 mmol) and sodium acetate (3.4950 g, 41.31 mmol). The reaction mixture was placed under nitrogen and stirred at 125 °C overnight. The reaction mixture was cooled to room temperature and water added to precipitate the product. After centrifugation the supernatant was removed, the pellet re-suspended in water and dried *in vacuo* to afford methyl 5-oxo-5,6-dihydrobenzo [c][2,6]naphthyridine-8-carboxylate (**87**) (0.9599 g, 3.78 mmol, 64% yield).

HR-LCMS (ES): R_t 1.44 min; m/z calculated for $C_{14}H_{11}N_2O_3^+$ 255.0770 observed 255.0778 $[M+H]^+$. ^{1}H NMR (400 MHz, d_6DMSO) δ: 3.92 (3H, s, CH_3 *14*), 7.83 (1H, dd, *J = 8.4 & 1.6*, CH *10*), 8.02 (1H, d, *J = 1.6*, CH *7*), 8.15 (1H, d, *J = 5.1*, CH *3*), 8.72 (1H, d, *J = 8.4*, CH *9*), 8.89 (1H, d, *J = 5.16*, CH *2*), 9.94 (1H, s, CH *1*). ^{13}C NMR (100 MHz, d_6DMSO) δ: 52.5 (CH_3), 117.2 (CH), 122.6 (CH), 123.6 (CH), 136.9 (CH), 149.0 (CH).

2.7.2.3 *Synthesis of methyl 5-(3-hydroxypropoxy)-5,6-dihydrobenzo[c][2,6] naphthyridine-8-carboxylate & methyl 6-(3-hydroxypropyl)-5-oxo-5,6 dihydrobenzo[c][2,6]naphthyridine-8-carboxylate*[238]

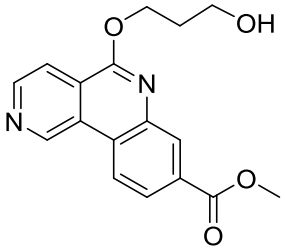

88

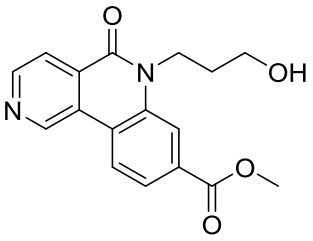

89

To a solution of (**87**) (39.1 mg, 0.15 mmol) in dry DMF (5 mL) was added potassium carbonate (158.1 mg, 1.14 mmol) and iodopropanol (200 µL, 468.1 mg, 2.52 mmol). The reaction mixture was stirred at 100 °C for 1.5 hr. The reaction mixture was diluted with water (15 mL) and extracted with DCM (3 x 50 mL). The extract was dried over $MgSO_4$, filtered and concentrated *in vacuo* to afford a crude mixture of methyl 5-(3-

hydroxypropoxy)-5,6-dihydrobenzo[c][2,6]naphthyridine-8-carboxylate (**88**) and methyl6-(3-hydroxypropyl)-5-oxo-5,6-dihydrobenzo[c][2,6]naphthyridine-8carboxylate (**89**) (82.5 mg in a 3:1 ratio by LCMS).

R_f 0.55 & 0.10 (100% ethyl acetate). HR-LCMS (ES): R_t 1.51 min; m/z calculated for $C_{17}H_{17}N_2O_4^+$ 313.1188 $[M+H]^+$ observed 313.12 and R_t 1.73 min; m/z calculated for $C_{17}H_{17}N_2O_4$ expected 313.1188 $[M+H]^+$ observed 313.12 $[M+H]^+$.

2.7.2.4 *Synthesis of methyl 5-chlorobenzo[c][2,6]naphthyridine-8 carboxylate*[238]

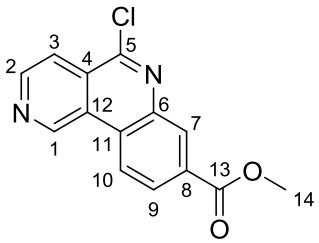

90

Compound (**87**) (0.1924 g, 0.76 mmol) and phosphorous oxychloride (2 mL) were combined in a Whatman vial and heated with stirring to 110 °C for 72 hr. Volatiles were removed *in vacuo* and acetonitrile added to the residue. The mixture was filtered to remove insoluble particulate matter and concentrated *in vacuo* to give crude methyl 5-chlorobenzo[c][2,6]naphthyridine-8-carboxylate, compound (**90**), (138.8 mg, 50% purity by NMR).

HR-LCMS (ES): R_t 1.93; m/z calculated for $C_{14}H_{10}N_2O_2Cl^+$ 273.0431 $[M+H^+]$ observed 273.0427 & 275.0414 & R_t 1.38; m/z calculated for $C_{14}H_{11}N_2O_3^+$ 255.0770 $[M+H^+]$ observed 255.0778. ^{1}H NMR (400MHz, d_6DMSO) δ: 4.03 (3H, s, CH_3 *14*), 8.35 (1H, d,

J = 5.5, CH [3]), 8.38 (1H, dd, *J = 8.6 & 1.7*, CH [10]), 8.63 (1H, d, *J = 1.6*, CH [7]), 9.15 (1H, d, *J = 5.5*, CH [2]), 9.22 (1H, d, *J = 8.6*, CH [9]), 10.43 (1H, s, CH [1]).

2.7.2.5 *Synthesis of methyl 5-(3-chlorophenyl)amino)benzo[c] [2,6]naphthyridine-8-carboxylate*[238]

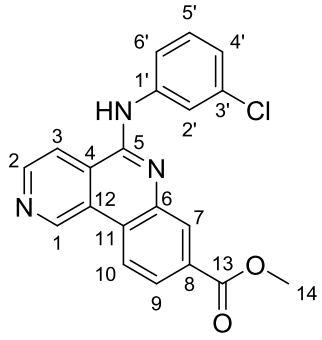

91

To a solution of crude compound (**90**) (300 mg, 1.10 mmol) in NMP (3 mL) was added p-chloroaniline (200 µL, 242 mg, 1.90 mmol). The reaction mixture was heated to 80 °C overnight. The solution was diluted with DCM (100 mL), washed with saturated $NaHCO_3$ solution (2 x 100 mL) and brine (1 x 100 mL). The DCM extract was dried over $MgSO_4$ and volatiles removed *in vacuo*. Purification by flash column chromatography (9:1 ethyl acetate: petroleum ether (40-60 °C)) yielded methyl 5-((3-chlorophenyl) amino)benzo[c][2,6]naphthyridine-8-carboxylate (**91**) as a yellow powder (10.1 mg, 0.03 mmol, 2.5% yield).

HR-LCMS (ES): R_t 2.25 min; m/z calculated for $C_{20}H_{15}N_3O_2Cl^+$ 364.0853 $[M+H]^+$ observed 364.0857 & 366.0832. ^{1}H NMR (400 MHz, d_6DMSO) δ: 3.95 (3H, s, CH_3 [14]), 7.16 (1H, ddd, *J = 8.1, 2.0 & 0.8* CH [4']), 7.47 (1H, t, *J = 8.1* CH [5']), 8.00 (1H, dd, *J = 8.4 & 1.8*, [10]), 8.11 (1H, ddd, *J = 8.1, 2.0 & 0.8*, CH [6']), 8.28-8.30 (1H, m, CH [2']), 8.61 (1H, d, *J = 5.4*, CH [3]), 8.91 (1H, d, *J = 8.4*, CH [9]), 9.03 (1H, d, *J = 5.4*, CH [2]), 9.71 (1H, s, CH [7]), 10.20 (1H, s, CH [1]).

2.7.3 Protein expression & purification

2.7.3.1 *Transformation & Expression*

BL21-CodonPlus (DE3)-RIPL competent cells (100 µL) were thawed on ice and placed into a pre-chilled 14 mL BD Falcon polypropylene round-bottom tube. The pGRX-2T or pLEICS-05 vector containing the coding sequence for the bacterial expression of *Pf*CK2α as a translational fusion with GST (former) or as a translational fusion with His_6 (latter) (~25 ng) was added; the tube was gently swirled to mix the sample and then incubated on ice for 30 min. Heat shock was performed by incubating the mixture in a 42 °C water bath for 20 s, followed by incubation on ice for 2 min. SOC medium (900 µL, 42 °C) was added and the transformation reaction mixture incubated at 37 °C, 220-250 rpm for 30 min. The cell culture (100 µL) was plated on LB agar petri dishes containing ampicillin (50 mg/L) and chloramphenicol (50 mg/L) and incubated at 37 °C overnight. A single colony was selected and grown in LB medium (100 mL) containing ampicillin (50 mg/L) and chloramphenicol (50 mg/L) overnight at 37 °C, 220-250 rpm. The culture was then diluted 1:9 in LB medium containing ampicillin (50 mg/L) and chloramphenicol (50 mg/L) and allowed to recover at 37 °C, 220-225 rpm for 30 min, or until the optical density at 600 nm (OD_{600}) reached 0.6-0.8. Protein expression was induced by the addition of IPTG (100 µM final concentration) at 22 °C, 220-250 rpm for 4 hr. The cells were collected by centrifugation (10 min, 10 000 rpm, 4 °C) and the pellets stored at -80 °C until required.

2.7.3.2 *Glutathione-affinity chromatography*

Cell pellets were re-suspended in ice-cold GST-lysis buffer (10 mL) and subjected to sonication (10 x 30 s with 30 s break at 4 °C). The cell free extract was obtained by

centrifugation (20 min, 20 000 rpm, 4 °C). The GST-fusion protein was purified from the supernatant using a glutathione sepharose column. The resin (500 µL) was equilibrated with GST-lysis buffer (5x column volumes) and the cell-free extract loaded on to the column. The column was then washed with GST-lysis buffer (10x column volumes) and the GST-fusion protein eluted in fractions of ~500 µL using GST-elution buffer. Fractions containing the GST-fusion protein (*Pf*CK2α), confirmed by SDS-PAGE, were pooled and dialysed for 2 hr, with stirring at 4 °C, against CK2-dialysis buffer (2 L).

2.7.3.3 *Ni-NTA-affinity chromatography*

Cell pellets were re-suspended in ice-cold lysis buffer (10 mL) (0.5%) and subjected to sonication (10 x 30 s with 30 s break at 4 °C). The cell free extract was obtained by centrifugation (20 min, 20 000 rpm, 4 °C). The His_6-fusion protein was purified from the supernatant using a nickel-nitrilotracetic acid (Ni-NTA) agarose column. The resin (2 mL) was equilibrated with Ni-NTA-lysis buffer (5x column volumes) and the cell-free extract loaded on to the column. The column was then washed with Ni-NTA-lysis buffer (10x column volumes) and the His_6-fusion protein eluted in fractions of ~500 µL using Ni-NTA-elution buffer. Fractions containing the His_6-fusion protein, confirmed by SDS-PAGE, were pooled and dialysed for 2 hr, with stirring at 4 °C, against CK2-dialysis buffer (2 L) to remove imidazole.

2.7.3.4 *Total protein content and purity*

2.7.3.4.1 SDS-PAGE

In order to confirm the presence of the required protein and its purity, SDS-PAGE was performed on fractions from the glutathione and Ni-NTA columns and the combined fractions after dialysis using polyacrylamide gels (10%, 0.75 mm thickness). Protein

samples were prepared for electrophoresis by adding an equal volume of 2x Laemmli buffer and heating at 60 °C for 3 min. Gels were run in SDS running buffer at 200 V for 45 min (or until the dye-front reached the end of the gel). The gels were stained by soaking in coomassie brilliant blue staining buffer and destained by soaking in destaining buffer. Precision plus unstained protein standards with protein markers of band sizes 250, 150, 100, 75, 50, 37, 25, 20, 15, & 10 kDa were used.

2.7.3.4.2 Bradford assay

The total protein content of the sample was measured using a Bradford assay. Protein sample (5 µL), water (995 µL) and Bradford reagent (1 mL) were mixed in a cuvette and allowed to react for 5 min. The absorbance of the sample at 595 nm was measured to give the concentration of the protein present. This was then used to calculate the amount of desired protein present from the densitometry of the SDS-PAGE (**Section 2.7.3.4.1**). For *Pf*CK2α the desired GST-fusion protein was deemed to be 25% of the total sample; i.e. 176 µg/mL for the batch used in kinetic studies in Leicester the desired His_6-fusion protein was deemed to be 50% of the total sample; i.e. 178 µg/mL.

2.7.4 Establishing activity

2.7.4.1 *Quantitative analysis*

For *PfCK2*α-GST kinase activity was tested in a final volume of 25 µL containing Tris HCl (20-22.4 mM), KCl (50 mM), $MgCl_2$ (10 mM), DTT (0-0.24 mM), NaCl (0-42 mM), Na_2EDTA (0-0.12 mM), peptide RRRADDSDDDDD (100 µM), ATP (100 µM, including [γ-^{32}P]-ATP 500-1000 cpm/pmol) and enzyme (0-21.2 ng/µL). For *Pf*CK2α-His_6 the activity was tested in a final volume of 18 µL containing TrisHCl (36 mM), $MgCl_2$ (18.6 mM), NaCl (62.5 mM), peptide RRREDEESDDEE (167 µM), ATP (100 µM, including

[γ-32P]-ATP 500-1000 cpm/pmol) and enzyme (0-29.7 ng/µL). The samples were incubated for 10 min at 37 °C before being quenched with H_3PO_4 (5 µL, 0.5 M). 10 µL of this solution was then spotted on to squares of P81 phosphocellulose paper and allowed to dry for 20 min. The samples were washed with H_3PO_4 (0.5%, 3 x 10 min washes) before being placed into Ultimate Gold scintillation fluid (5 mL) and the radioactive decay measured using a scintillator.

2.7.5 Enzyme kinetics

2.7.5.1 *Kinetic parameters Leicester*

Kinetic parameters for mammalian CK2 and *Pf*CK2α-GST were measured in a final volume of 25 µL containing Tris-HCl (20 mM), KCl (50 mM), $MgCl_2$ (10 mM), DTT (0.2 mM), NaCl (7 mM), Na_2EDTA (0.1 mM), peptide (mammalian CK2 RRREEETEEE 100 µM; *Pf*CK2α-GST RRRADDSDDDDD 100 µM), ATP (10-100 µM, including [γ-32P]-ATP 500-1000 cpm/pmol) and enzyme (mammalian CK2 250 U, 11.16 µg/µL & 25 U, 1.12 µg/µL & 8.3 U, 0.56 µg/µL; *Pf*CK2α-GST 7.0 ng/µL). Kinetic parameters for *Pf*CK2α-His_6 were measured in a final volume of 18 µL containing TrisHCl (36 mM), $MgCl_2$ (18.6 mM), NaCl (62.5 mM), peptide RRREDEESDDEE (167 µM), ATP (10-100 µM, including [γ-32P]-ATP 500-1000 cpm/pmol) and enzyme (7.4 ng/µL). Kinetic parameters for *Pf*CK2α-His_6 were measured in a final volume of 18 µL containing TrisHCl (36 mM), $MgCl_2$ (18.6 mM), NaCl (62.5 mM), peptide RRREDEESDDEE (167 µM), ATP (10-100 µM, including [γ-32P]-ATP 500-1000 cpm/pmol) and enzyme (7.4 ng/µL). In all three cases the samples were incubated for 10 min at 37 °C before being quenched with H_3PO_4 (5 µL, 0.5 M). 10 µL of this solution was then spotted on to squares of P81 phosphocellulose paper and allowed to dry for 20 min. The samples

were washed with H_3PO_4 (0.5%, 3 x 10 min washes) before being placed into Ultimate Gold scintillation fluid (5 mL) and the radioactive decay measured using a scintillator.

2.7.5.2 *Kinetic parameters, Grenoble*

Kinetic parameters for *Pf*CK2α-GST and mammalian CK2α were measured in a final volume of 18 µL containing TrisHCl (36 mM), $MgCl_2$ (18.6 mM), NaCl (62.5 mM), peptide RRREDEESDDEE (167 µM), ATP/GTP (10-100 µM, including [γ-32P]-ATP/GTP 500-1000 cpm/pmol) and enzyme (*Pf*CK2α-GST 3 µL - at 100 µM ATP & 167 µM RRREDEESDDEE 3 µL phosphorylated 0.02% peptide; mammalian CK2α 0.278 ng/µL). The samples were incubated for 5 min at room temperature before the reaction was quenched by the addition of TCA (60 µL, 4%) and casein (6 µL, 30 mg/mL). The samples were placed on ice for 15 min to encourage precipitation. Following centrifugation (15 min, 12 000 rpm) supernatant (60 µL) was spotted on to squares of P81 phosphocellulose paper and allowed to dry for 20 min. The samples were washed with H_3PO_4 (0.5%, 3 x 5 min washes) before being placed into Ultimate Gold scintillation fluid (2 mL) and the radioactive decay measured using a scintillator.

2.7.5.3 *Peptide phosphorylation analysis by MALDI-TOF MS*

Peptide phosphorylation assays were carried out in a final volume of 50 µL containing Tris HCl (20.4 mM), KCl (50 mM), $MgCl_2$ (10 mM), DTT (0.2 mM), NaCl (7 mM), Na_2EDTA (0.1 mM), peptide RRRADDSDDDDD (34.5 µM) for *PfF*CK2α-GST & RRREEETEEE (36.7 µM) for mammalian CK2, ATP analogue (1 mM) and enzyme (mammalian 250 U, 11.16 µg/µL; 7.0 ng/µL *Pf*CK2α).The samples were incubated for 2 hr or overnight before being placed on ice and TFA solution (5 µL, 1%) added. Purification to remove the high salt content prior to MALDI-TOF MS was performed using a Zip Tip. The Zip Tip

was permeabilised with acetonitrile and equilibrated with TFA (0.1% in water). A sample of the reaction mixture (10 µL) was loaded onto the Zip Tip and solution discarded. The Zip Tip was washed with TFA (3 x 10 µL, 0.1% in water) and the sample eluted with TFA (10 µL, 0.1% in 1:1 acetonitrile:water). The eluted sample (2 µL) was mixed with matrix (2 µL) and a portion (0.5 µL) loaded on to a plate and analysed by MALDI-TOF MS.

2.7.5.4 *ATPγEt as an inhibitor of CK2*

The inhibition of *Pf*CK2α-GST and mammalian CK2 with ATPγEt were measured in a final volume of 25 µL containing Tris HCl (20.4 mM), KCl (50 mM), $MgCl_2$ (10 mM), DTT (0.04 mM), NaCl (7 mM), Na_2EDTA (2 mM), peptide (RRREETEEE 117.6 µM for mammalian CK2; RRRADDSDDDDD 110.5 µM for *Pf*CK2α-GST), ATP (50 µM, including [γ-32P]-ATP 500-1000 cpm/pmol), ATPγEt (0-5mM) and enzyme (250 U (11.2 µg/µL) mammalian CK2; 7.0 ng/µL *Pf*CK2α). The samples were incubated for 10 min at 37 °C before being spotted on to squares of P81 phosphocellulose paper and allowed to dry for 20 min. The samples were washed with H_3PO_4 (0.5%, 3 x 10 min washes) before being placed into Ultimate Gold scintillation fluid (5 mL) and the radioactive decay measured using a scintillator.

2.7.5.5 *IC_{50} values for ATP analogues with PfCK2α*

Inhibition assays for *Pf*CK2α-GST were carried out in a final volume of 18 µL containing TrisHCl (36 mM), $MgCl_2$ (18.6 mM), peptide RRREDEESDDEE (167 µM), [γ-32P]-ATP (500-1000 cpm/pmol, including 55.8 fmol ATP), ATP analogue (10-100 µM) and enzyme (3 µL - at 100 µM ATP & 167 µM RRREDEESDDEE 3 µL phosphorylated 0.02% peptide). The samples were incubated for 5 min at room temperature before the reaction was

quenched by the addition of TCA (60 µL, 4%) and casein (6 µL, 30 mg/mL). The samples were placed on ice for 15 min to encourage precipitation. Following centrifugation (15 min, 12 000 rpm) supernatant (60 µL) was spotted on to squares of P81 phosphocellulose paper and allowed to dry for 20 min. The samples were washed with H_3PO_4 (0.5%, 3 x 5 min washes) before being placed into Ultimate Gold scintillation fluid (2 mL) and the radioactive decay measured using a scintillator.

3 Studying CLKs through gatekeeper mutations

3.1 Introduction

The CLK family belong to the CMGC group and have been identified as dual specificity kinases; in fact, CLK1 was one of the first dual specificity kinases to be discovered.[267,268,269] All four isoforms of CLK (CLK1, CLK2, CLK3 and CLK4) have a highly conserved structure with a signature amino acid motif in the subdomain X of the C-terminal lobe.[270,271] However, despite their overall highly conserved structure, the N-termini of the isoforms contain great variability.[270]

The CLK family are known to phosphorylate Ser residues in serine/arginine rich proteins (SR proteins),[272,273] which regulates the location and activity of the SR proteins. As SR proteins are a group of proteins that control alternative splicing, [274] CLK kinases are, therefore, key regulators of splicing.[275] This supports the findings that mutations in the *Drosophila* CLK homologue are embryonic lethal and result in defects in eye formation and neuronal development.[271] There is also evidence for their involvement in developmental processes; e.g. high levels of CLK3 were found in the cytoplasm of mature spermatozoa.[276]

3.1.1 CLK homologues in Plasmodium falciparum

The CMGC group is one of the major groups in the *Plasmodium falciparum* kinome, making up approximately a quarter of the *P. falciparum* kinome. Therefore, their abundance in *P. falciparum* is likely to reflect their importance in the cell proliferation and developmental processes of this parasite.[90] All four members of the CLK family are found in the *P. falciparum* kinome and are thought to perform crucial roles in asexual

proliferation because knockout vectors were not observed for the genes of any of the *Pf*CLKs after prolonged culture.[90,210]

3.1.2 Inhibition studies of the CLK family

In order to study the functions of the CLK family in more detail, there is now significant interest in identifying potent and highly selective CLK inhibitors with the sub-micromolar cellular activity required for *in vivo* experiments. Several efforts have been made to synthesise such inhibitors; however, due to the highly conserved nature of the kinase ATP site, the potent competitive inhibitors found have limited selectivity. That notwithstanding, several molecules have been developed, which go some way to providing insight into the function of CLKs.

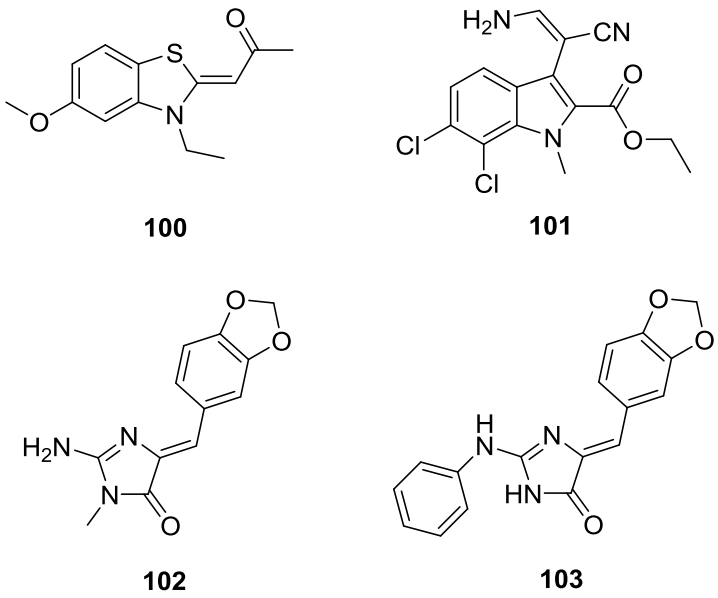

Figure 3.1: CLK inhibitors TG003 (100), KH-CB19 (101), leucettamine B (102) and leucettine L41 (103).

The cell permeable benzothiazole compound TG003 (**100**) synthesised by Muraki *et al.*[277] is highly potent for CLK1 and CLK4 (IC_{50} values 20 nM and 15 nM respectively); however, despite being selective against CLK3 (IC_{50} >10 μM), TG003 (**100**) targets CLK2

with an IC_{50} of 200 nM and a screening of TG003 (**100**) with 402 kinases revealed several off target effects (e.g. CK1δ and CK1ε).[278]

A dichloroindolyl enaminonitriles, KH-CB19 (**101**), developed by Fedorov *et al.*[275] was found to be a highly potent inhibitor of CLK1 (IC_{50} 19.7 nM) and CLK4 and to have a reduced affinity for CLK2 and CLK3 (IC_{50} 530 nM). When profiled against 176 kinases, KH-CB19 (**101**) only showed significant inhibition of one other kinase, PIM1.

Leucettines are derived from leucettamine B (**102**), a natural product found in the marine sponge *Leucetta microraphils*[279,280] known to inhibit CLKs.[281] Leucettine L41 (**103**) inhibits CLKs and has been shown to display neuroprotective properties in cells; however, due to its off target effects (e.g. CK2, GSK-3α and PIM1), it is not possible to attribute the observed neuroprotective effects to a specific kinase. In fact, the result could be due to a combination of interactions between leutticine L41 (**103**) and multiple kinases.[282]

The ability of CLK1, CLK2 and CLK3 to regulate splicing of adenovirus pre-mRNA *in vivo* and in human bronchial epithelial cells[283,284] and therefore, hold control over viral infection makes them intriguing targets for understanding viral infections, as well as cellular metabolism,[285] developmental processes,[271,276] and malaria.[90] However, in order to do this, the problem of off targeting must be conquered.

3.2 Aims

Although bioinformatics analysis has shown the *P. falciparum* CLKs to be involved in splicing and their role in cell proliferation and developmental processes have been implicated,[90] it has not been possible to investigate their exact functions using knock-out (KO) vectors because they are essential for asexual proliferation.[210] Thus, an alternative method for the study of CLKs was essential to widen knowledge on the spliceosomal machinery in the *Plasmodium falciparum* parasite. Consequently, this work aimed to use the covalent complementarity chemical genetic approach[152] (**Section 1.4.2.1**) to study the function and substrates of *Pf*CLK1 and *Pf*CLK3.

This work aimed to form the cysteine gatekeeper mutant of both *Pf*CLK1 and *Pf*CLK3, rendering the mutated kinases sensitive to electrophilic inhibitors. By screening these mutants with a panel of electrophilic inhibitors a hit compound would be found (**Figure 3.2A**). This would pave the way for the formation of a knock-in (KI) *P. falciparum* parasite that expresses the mutant kinase but not the wildtype (**Figure 3.2B**). Due to the rarity of cysteine residues in the gatekeeper position[125] (**Table 1.1, Section 1.4.2.1**), off target effects should be avoided; thus, allowing the effect of *Pf*CLK1 and *Pf*CLK3 inhibition on *P. falciparum* to be observed in turn.

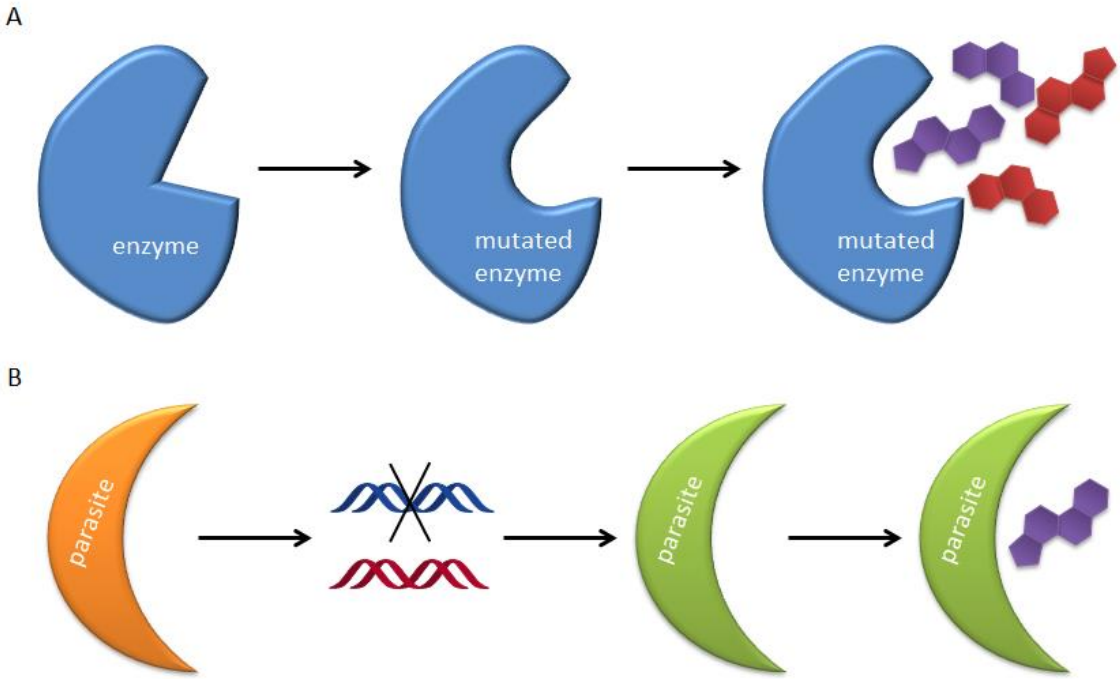

Figure 3.2: A schematic representation of the reverse chemical genetics planned for the study of *Pf*CLK1 and *Pf*CLK3. A: The gatekeeper residue of *Pf*CLK1 and *Pf*CLK3 can be altered from phenylalanine to cysteine through a single point mutation. The mutant enzyme (blue) can be expressed, purified and screened with electrophilic inhibitors (purple and red); B: The gene for the wildtype kinase (blue) can be removed from the wildtype parasite (orange) and replaced with the gene for the mutant kinase (red). The mutant parasite (green) can then be treated with a potent inhibitor (purple) in order to study the role of the enzyme within the parasite.

To summarise, the aims of this chapter were: to express and purify *Pf*CLK1, *Pf*CLK1F630C, *Pf*CLK3 and *Pf*CLK3F444C; to establish whether the gatekeeper mutation was detrimental to the activity of *Pf*CLK1F630C and *Pf*CLK3F444C; to establish the kinetic parameters of *Pf*CLK1, *Pf*CLK1F630C, *Pf*CLK3 and *Pf*CLK3F444C; and to screen a panel of electrophilic inhibitors against *Pf*CLK1, *Pf*CLK1F630C, *Pf*CLK3 and *Pf*CLK3F444C.

3.3 Results and Discussion

3.3.1 Expression of wild-type and mutant kinases

In order to validate the feasibility of *Pf*CLK1 and *Pf*CLK3 gatekeeper mutant kinases being used to study the phosphorylation pathways of these two kinases within the parasite, the mutant kinases first needed to be generated and their activity compared to their wild-type counterparts *in vitro*. PCR conditions were optimised to afford plasmids containing the genes for the kinase domain of *Pf*CLK1F630C and for full length *Pf*CLK3F444C through site directed mutagenesis. The plasmids were then amplified by growth in XL1-Blue supercompetent cells, extracted and purified before being analysed by PNACL (University of Leicester). These plasmids were then transformed into BL21-CodonPlus (DE3)-RIPL competent cells. Proteins *Pf*CLK1wt, *Pf*CLK1F630C, *Pf*CLK3F444C and *Pf*CLK3F444C were successfully expressed and purified using Ni-NTA-affinity chromatography. The His_6-fusion protein was deemed to be 10% of the total sample for *Pf*CLK1wt and *Pf*CLK1F630C; i.e. 74 μg/mL and 314 μg/mL respectively (**Figure 3.3**) and 30% of the total for *Pf*CLK3wt and *Pf*CLK3F444C; i.e. 246 μg/mL and 133 μg/mL respectively (**Figure 3.4**).

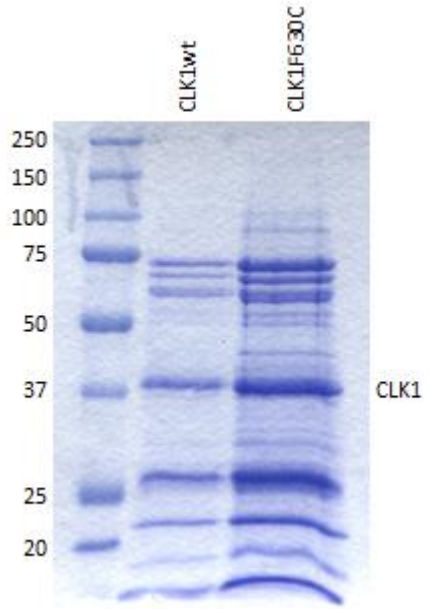

Figure 3.3: The pooled fractions from Ni-NTA affinity chromatography of *Pf*CLK1wt and *Pf*CLK1F630C analysed by SDS-PAGE and stained with coomassie.

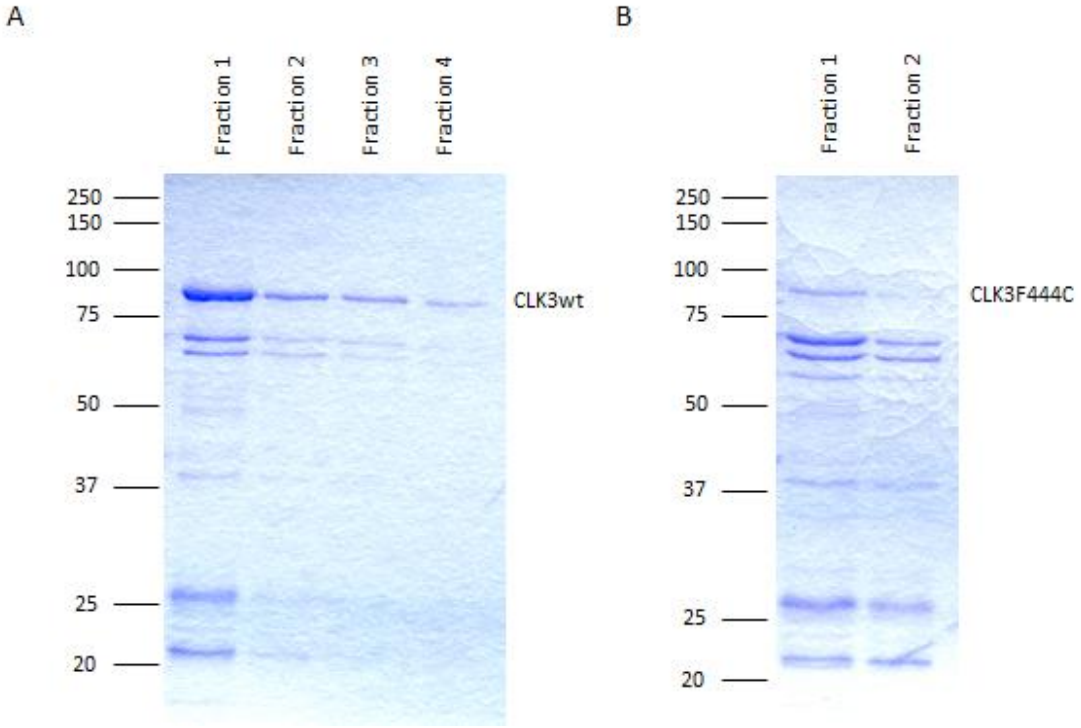

Figure 3.4: Fractions of *Pf*CLK3wt and *Pf*CLK3F444C from a Ni-NTA affinity column analysed by SDS-PAGE and stained with coomassie.

3.3.2 *The study of PfCLK3wt and PfCLK3F444C*

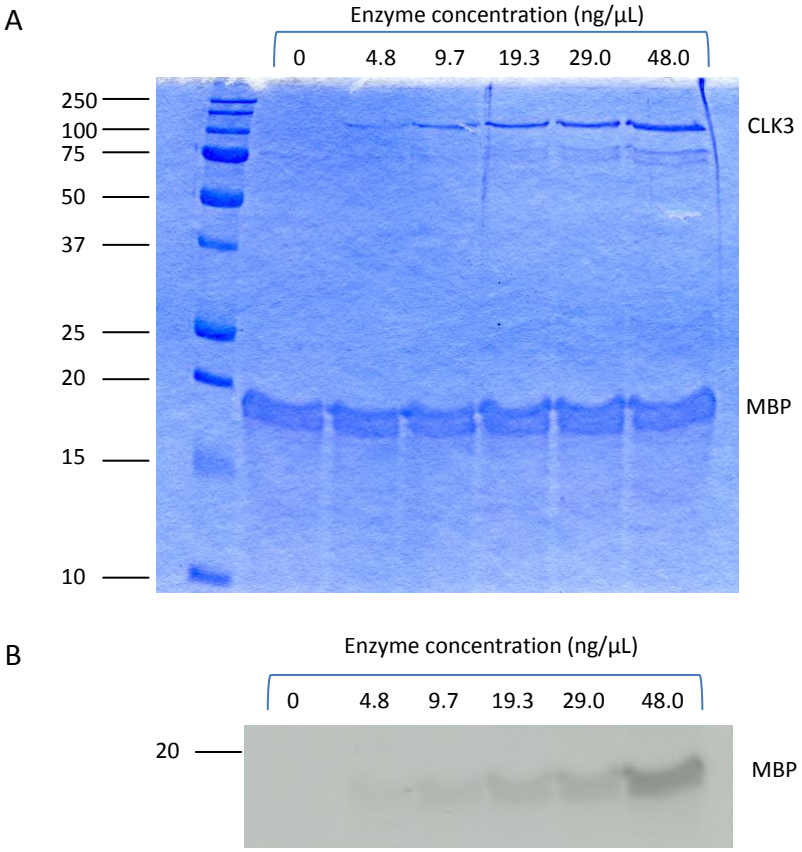

Figure 3.5: SDS-PAGE analysis of a kinase assay for *Pf*CLK3wt with ATP (50 µM), MBP (5.43 µM), and increasing concentrations of *Pf*CLK3wt from left to right. A: Protein bands visualised with coomassie; B: The corresponding autoradiograph, showing there to be increased phosphorylation with increasing amounts of kinase.

The activity of *Pf*CLK3wt was established by incubating the kinase with myelin basic protein MBP (5.43 µM), ATP (50 µM, including [γ-32P]-ATP 500-1000 cpm/pmol), and a range of enzyme concentrations (0-48 ng/µL). The resultant autoradiograph (**Figure 3.5B**) illustrated that *Pf*CLK3wt behaved as expected – as the concentration of enzyme increased so too did the phosphorylation of the protein substrate MBP. Hence, active *Pf*CLK3wt had been expressed.

To ensure kinetic parameters were being measured under steady state conditions, a time course assay was carried out (Error! Reference source not found.). It was decided that the 30 min reaction time already being used was adequate as this would

represent the initial velocity (~4% of the MBP present was phosphorylated), allowing for steady state assumptions to be made. All kinetic parameters for ATP and MBP with *Pf*CLK3wt were, therefore, measured after 30 min incubation.

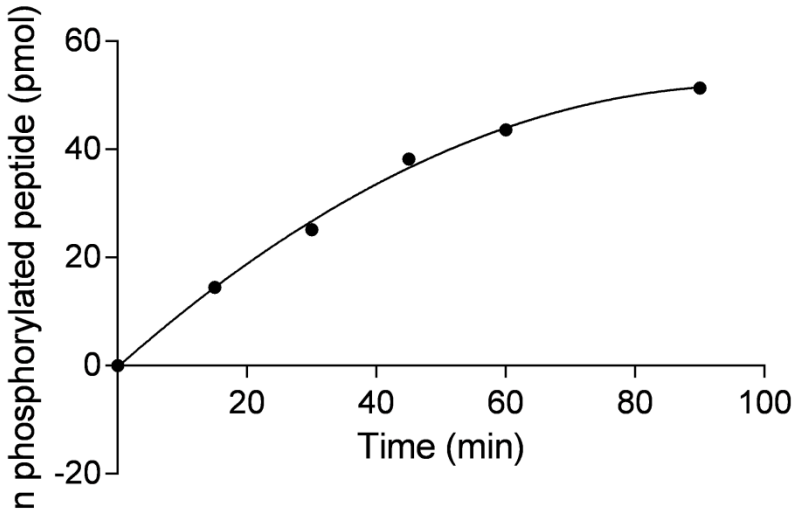

Figure 3.6: Time course assay for *Pf*CLK3wt illustrating the number of moles of phosphorylated peptide produced over time.

Table 3.1: Kinetic parameters measured for *Pf*CLK3wt.

	ATP	MBP
K_m (µM)	51.5	0.8
V_{max} (µmol min^{-1})	5.7 $x10^{-7}$	7.5 $x10^{-6}$
k_{cat} (min^{-1})	1.2 $x10^{-6}$	1.6 $x10^{-7}$
k_{cat}/K_m ($M^{-1}min^{-1}$)	0.02	20.69

When investigating K_m of MBP it was deemed that, a wide enough range of MBP concentrations were studied to give accurate information on both V_{max} and K_m due to the curve of the graph (**Figure 3.7**).[250] *Pf*CLK3wt was found to have a K_m of 0.8 µM and a k_{cat} of 1.6 x 10^{-7} min^{-1} for MBP (**Table 3.1**).

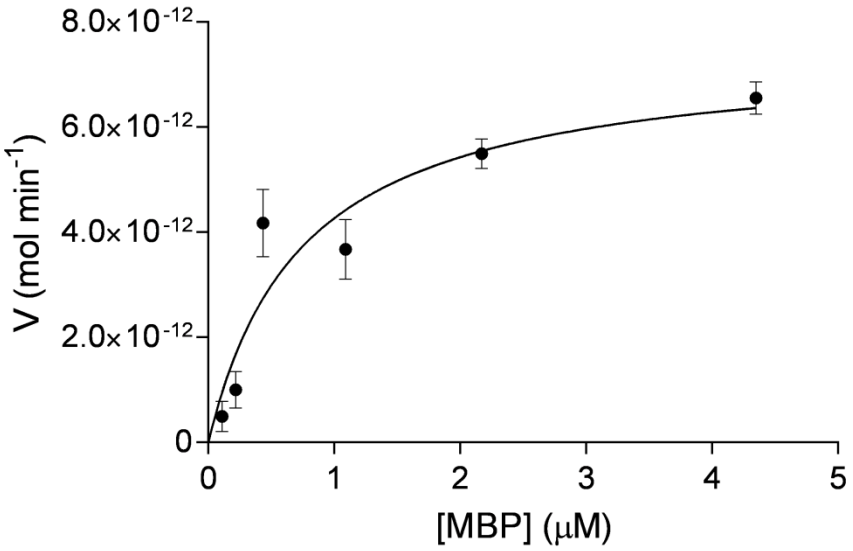

Figure 3.7: Assay to establish the kinetic parameter of PfCLK3wt for MBP. [MBP] plotted against rate of phosphorylation of MBP, allowing the calculation of K_m, V_{max} & k_{cat} of MBP using non-linear regression.

*Pf*CLK3wt was found to have a K_m of 51.5 μM and a k_{cat} of 1.2 x 10^{-6} min^{-1} for ATP (**Figure 3.8**). For these experiments 1 μL of [γ-32P]-ATP was added to each stock concentration of ATP; thus, the ratio of [γ-32P]-ATP:ATP changed as the concentration of ATP increased. This resulted in an increased sensitivity for lower concentrations of ATP used and, therefore, more accurate rate values for these lower concentrations. However, at high concentrations of ATP, e.g. 1 mM, the ratio of [γ-32P]-ATP:ATP was very low. This meant that only a small percentage of phosphorylation was observed compared to what was actually occurring, causing the radioactive decay counts to be much closer to the background level. Often this resulted in negative and, therefore, unusable values above 1 mM ATP. In order to include higher concentrations of ATP in the studies and improve the accuracy of V_{max},[250] more [γ-32P]-ATP could have been added to the more concentrated ATP stock solutions.

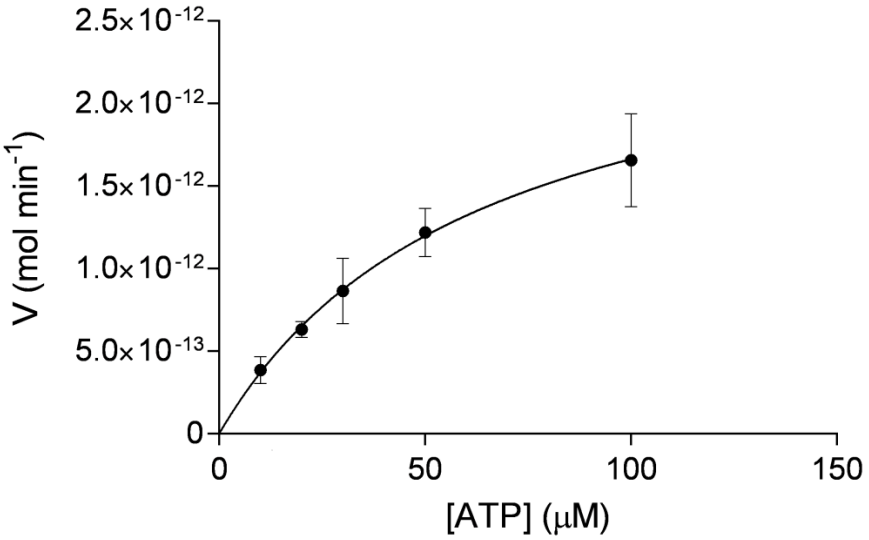

Figure 3.8: Assay to establish the kinetic parameter of *Pf*CLK3wt for ATP. [ATP] plotted against rate of phosphorylation of MBP, allowing the calculation of K_m, V_{max} & k_{cat} of MBP using non-linear regression.

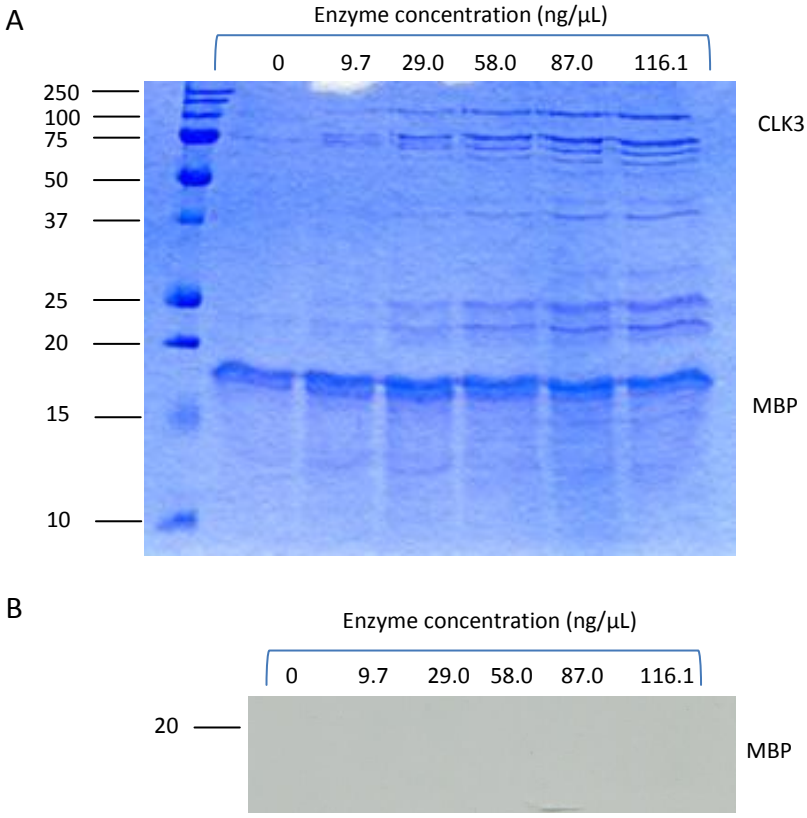

Figure 3.9: SDS-PAGE analysis of a kinase assay for *Pf*CLK3F444C with ATP (50 μM), MBP (5.43 μM), and increasing concentrations of *Pf*CLK3wt from left to right. A: Protein bands visualised with coomassie; B: The corresponding autoradiograph, showing *Pf*CLK3F444C to be inactive.

The activity of *Pf*CLK3F444C was investigated by incubating the kinase with MBP (5.43 µM), ATP (50 µM, including [γ-32P]-ATP 500-1000 cpm/pmol), and a range of enzyme concentrations (0-116 ng/µL). The resultant autoradiograph (**Figure 3.9B**) showed no phosphorylation; the mutation of the gatekeeper residue from phenylalanine to cysteine, therefore, rendered the kinase inactive. The presence of a cysteine residue in changes properties such as the pH of the microenvironment of the binding pocket and, consequently, may disrupt phosphorylation. This suggests that, perhaps, the cysteine gatekeeper mutant has much the same effect as a glycine/alanine mutation and, hence, its effect on activity must be judged on a case by case basis.

3.3.3 *The study of Pf*CLK1

Qualitative analysis was performed to establish whether *Pf*CLK1wt and *Pf*CLK1F630C were active by increasing the enzyme concentration. The autoradiographs (**Figure 3.10**) illustrate that *Pf*CLK1F630C displays activity, albeit at a much reduced level compared to that of *Pf*CLK1wt. However, whereas *Pf*CLK1wt behaved as expected (increased concentration of enzyme resulted in increased phosphorylation of the MBP substrate), *Pf*CLK1F630C appeared to plateau before it reached the same maximum observed for *Pf*CLK1wt (**Figure 3.11**).

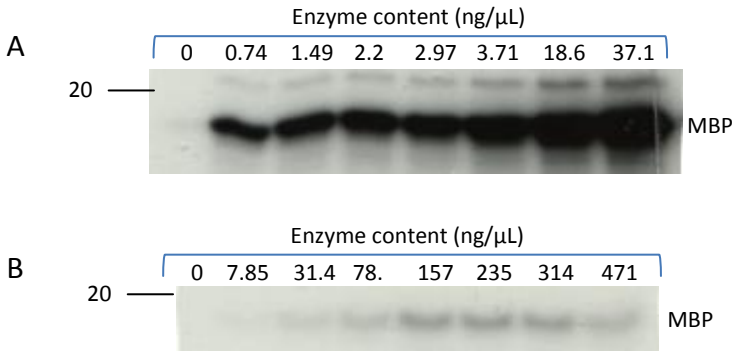

Figure 3.10: Autoradiographs depicting the phosphorylation of MBP (5.43 µM) using ATP (50 µM) with increasing concentrations of CLK1 from left to right. A: *Pf*CLK1wt; B: *Pf*CLK1F630C.

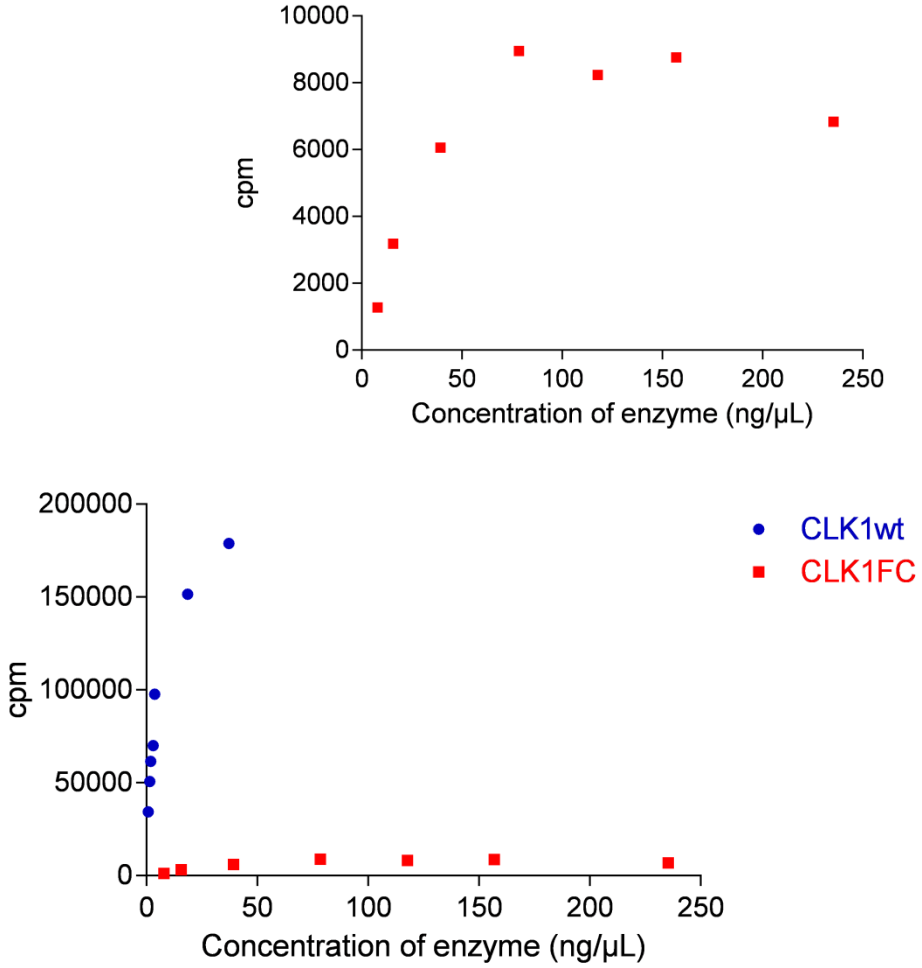

Figure 3.11: Scatter graphs showing increased cpm (i.e. increased phosphorylated MBP) with increasing enzyme concentration for both *Pf*CLK1wt and *Pf*CLK1F630C (bottom) and expanded to show data for *Pf*CLK1F630C more clearly (top).

Possible causes of the early observed plateau were thought to be:

- ADP acting as a competitive inhibitor
- Imidazole remaining after dialysis having an inhibitory effect
- Phosphorylated MBP not readily dissociating from the active site of *Pf*CLK1F630C

It was therefore decided that further investigation was required before kinetic parameters could be measured.

3.3.3.1 *Investigating ADP as competitive inhibitor*

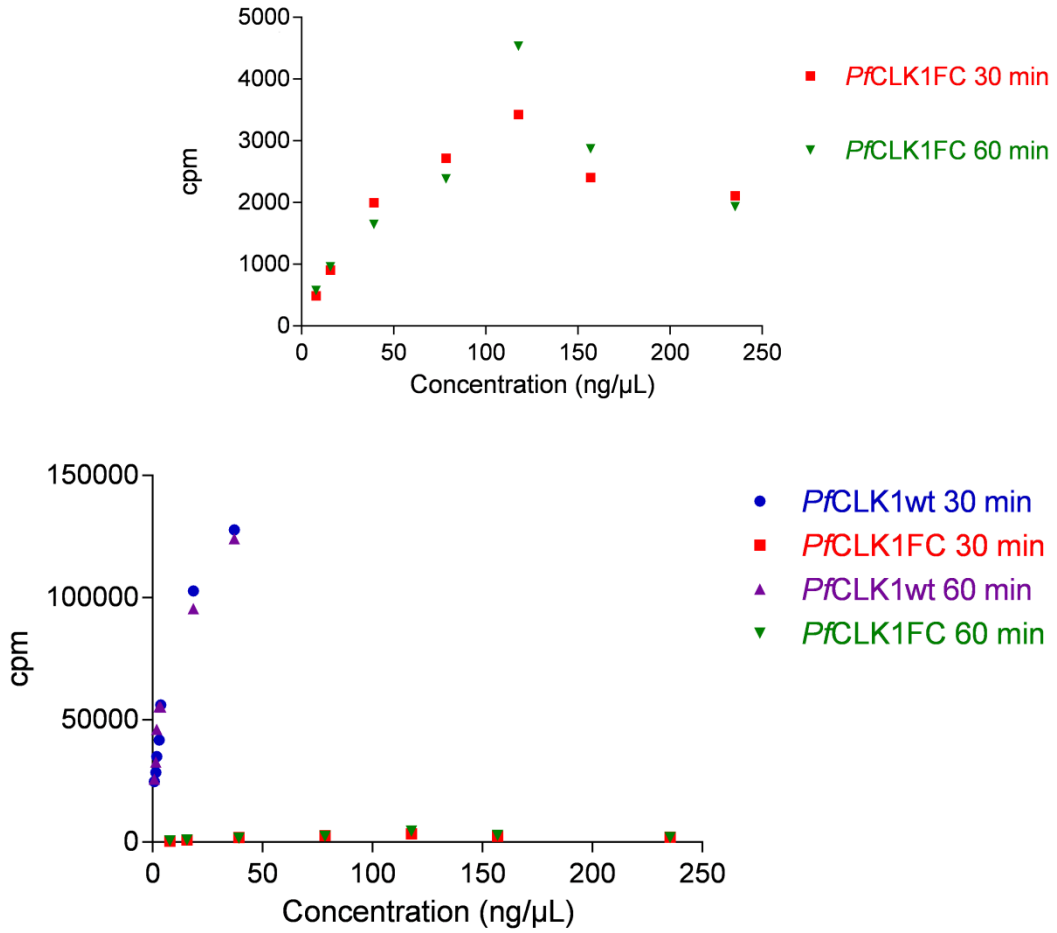

Figure 3.12: Scatter graphs showing increased cpm (i.e. increased phosphorylated MBP) with increasing enzyme concentration for both *Pf*CLK1wt and *Pf*CLK1F630C after 30 min incubation and after addition ATP and further incubation (bottom) and expanded to show data for *Pf*CLK1F630C more clearly (top).

To investigate whether the ADP produced during the phosphorylation could be acting as an inhibitor for the *Pf*CLK1F630C and not for *Pf*CLK1wt two experiments were devised. In the first instant the assays were repeated in a final volume of 40 µL and incubated for 30 min before a 20 µL aliquot was removed and the ATP concentration increased to 100 µM in the remaining sample. This was then incubated for a further 30 min and the phosphorylation of MBP under each set of conditions compared (**Figure 3.12**). Secondly, samples were pre-incubated with the ADP at either the concentration of ADP produced during the 30 min assays or at ten times that

concentration. The phosphorylation of MBP under these conditions was compared to the phosphorylation of MBP under the previous assay conditions (**Figure 3.13**). ADP was not found to have an inhibitory effect on the activity of either kinase.

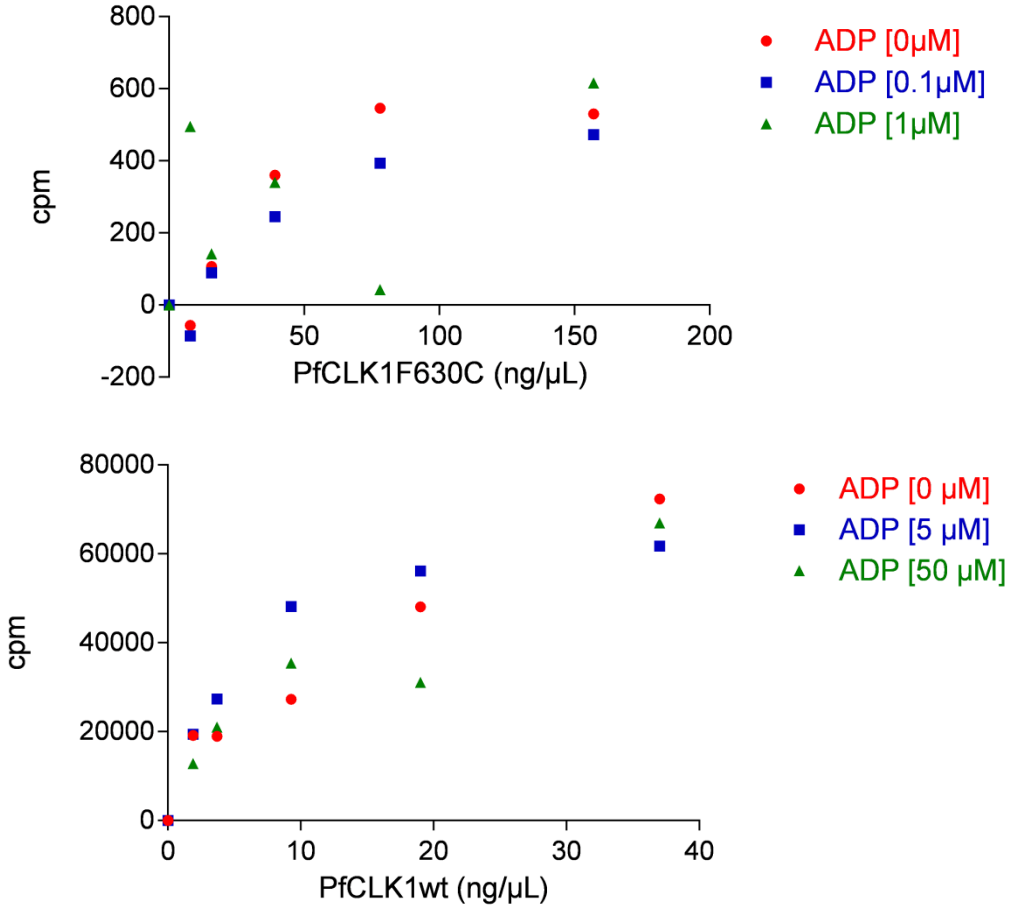

Figure 3.13: Scatter graphs showing increased cpm (i.e. increased phosphorylated MBP) with increasing enzyme concentration in the presence of ADP for *Pf*CLK1F630C (top) and *Pf*CLK1wt (bottom).

3.3.3.2 *Investigating imidazole acting as a competitive inhibitor*

Another possible factor affecting the behaviour of *Pf*CK1F630C was the presence of imidazole remaining after Ni-NTA-affinity purification and initial dialysis. An additional round of dialysis was performed on an aliquot of *Pf*CLK1F630C to further reduce the concentration of imidazole; however, this made no improvement to the activity pattern observed for *Pf*CLK1F630C.

3.3.3.3 *Investigating inhibition by phosphorylated MBP*

Finally it was postulated that phosphorylated MBP could be acting as an inhibitor towards *Pf*CLK1F630C (but not *Pf*CLK1wt) by having a higher binding affinity for the active site than MBP itself. The concentration of MBP was increased fivefold and the assay repeated. For *Pf*CLK1wt an increase in concentration of MBP from 5.43 µM to 27.15 µM caused no change in the phosphorylation pattern or initial rate of phosphorylation (**Figure 3.14**). The number of moles of phosphorylated MBP produced by the highest concentration of *Pf*CLK1wt used (37 ng/µL) at 27.15 µM MBP was 2-3 times greater than at 5.43 µM ATP. For *Pf*CLK1F630C an increase in concentration from 5.43 µM MBP to 27.15 µM MBP caused no improvement in the phosphorylation pattern/early plateau observed previously (**Figure 3.15**). The number of moles of phosphorylated MBP produced by the second highest concentration of *Pf*CLK1F630C used (157 ng/µL) at 27.15 µM was 1.5-4 times greater than at 5.43 µM MBP. Therefore, the concentrations used must be in the range of the K_m of MBP for both enzymes – at concentrations much lower than K_m, a fivefold increase in MBP concentration would result in a fivefold increase in rate; at concentrations above K_m, a fivefold increase in MBP concentration would result in no increase in rate.

In order to study the effect of phosphorylated MBP on the rate of the reaction, phosphorylated MBP would first need to be produced and isolated before activity checks were carried out in the presence of different concentrations of phosphorylated MBP. Due to a lack of isolated phosphorylated MBP this experiment was not carried out.

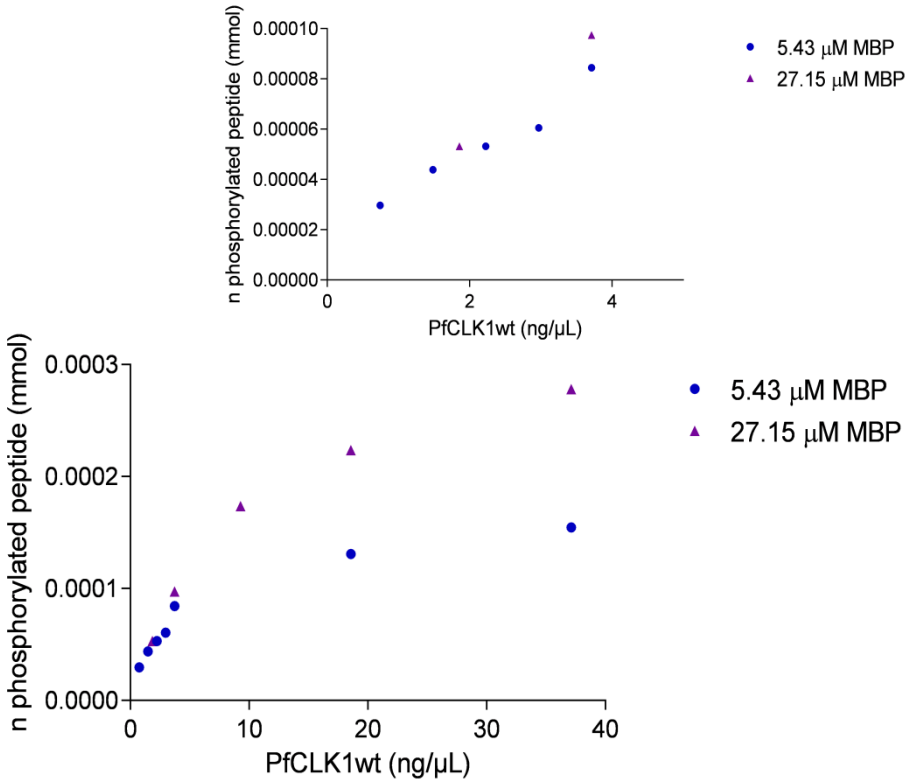

Figure 3.14: Scatter graphs showing increased cpm (i.e. increased phosphorylated MBP) with increasing enzyme concentration for *Pf*CLK1wt using 5.43 µM and 27.15 µM MBP (bottom) and expanded to show no difference in the initial rate at the two concentrations of MBP (top).

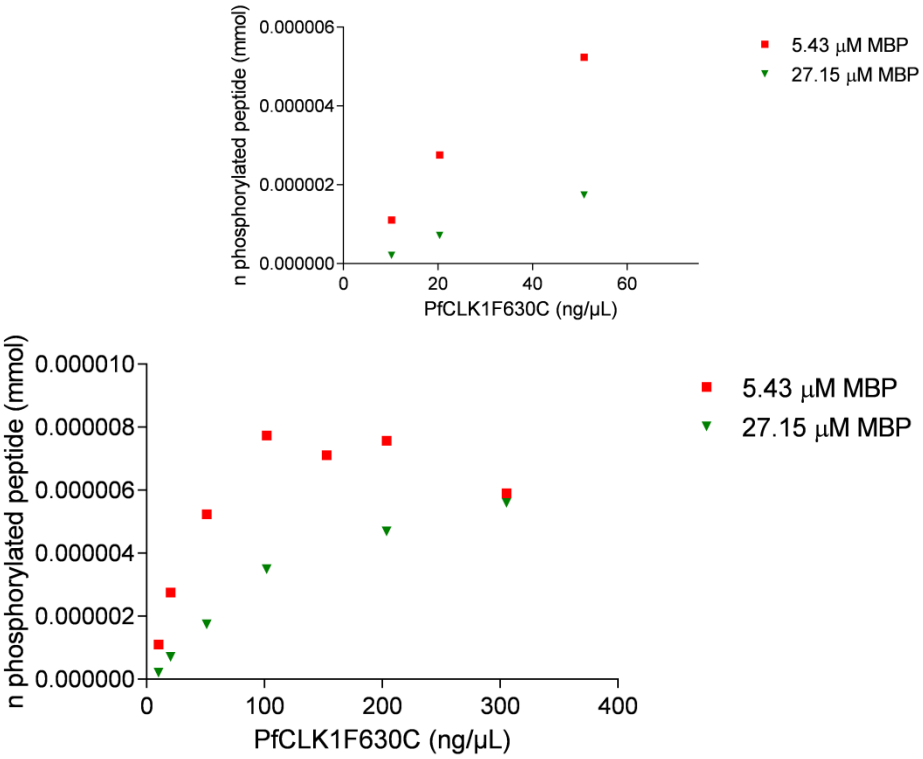

Figure 3.15: Scatter graphs showing increased cpm (i.e. increased phosphorylated MBP) with increasing enzyme concentration for *Pf*CLK1F630C using 5.43 µM and 27.15 µM MBP (bottom). When expanded (top) the phosphorylation seen using 27.15 µM ATP appears to be less than when using 5.43 µM; this indicates a possible systematic error.

3.3.3.4 *The kinetic parameters of PfCLK1wt and PfCLK1F630C*

Kinetic parameters were calculated for *Pf*CLK1wt and *Pf*CLK1F630C (**Table 3.2**); however, these are only apparent values. There may be large errors in the values for the wild-type kinase due to the extent of turn-over (~27% MBP was phosphorylated under the assay conditions) and due to the strange and so far unexplained behaviour of the mutant kinase (although only ~5% MBP was phosphorylated, which would usually be an ideal level for steady state assumptions to be made).

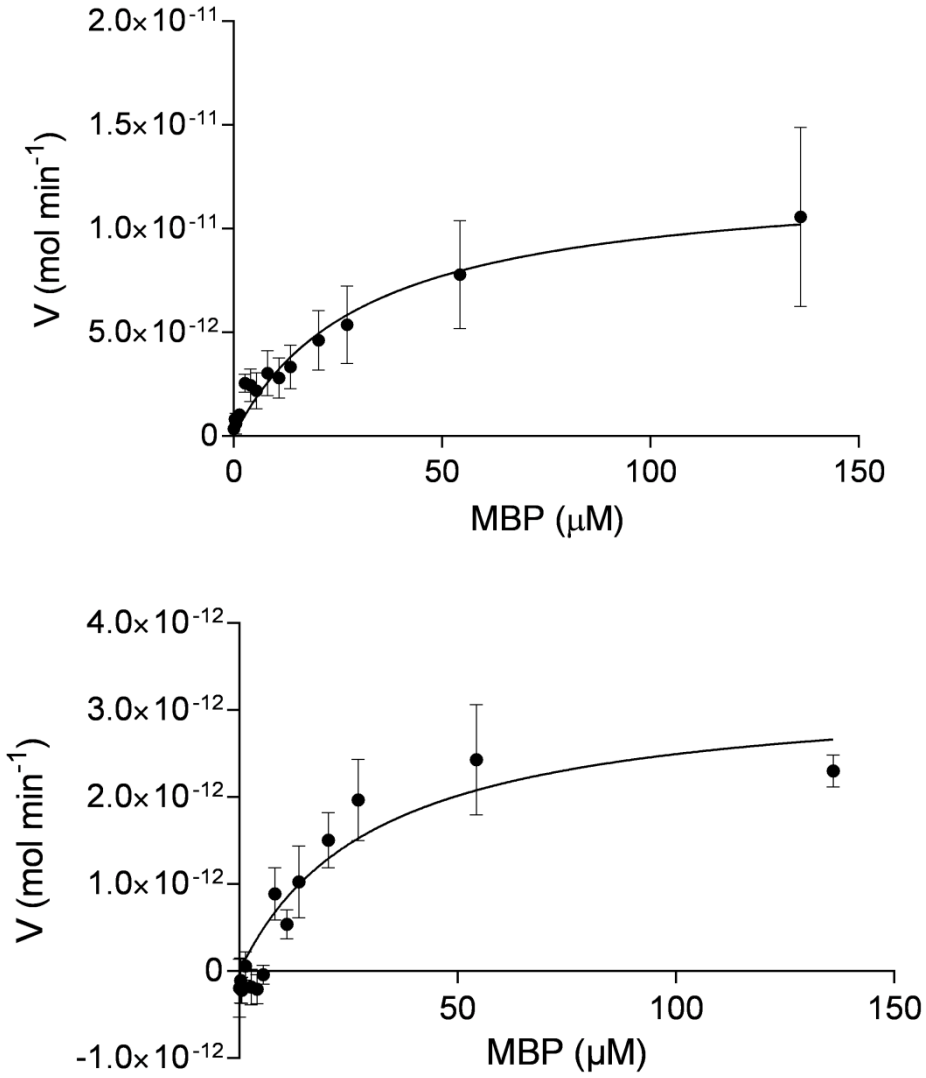

Figure 3.16: *Pf*CLK1wt & *Pf*CLK1F630C kinetic parameters. Non-linear regression of [MBP] against rate of phosphorylation of MBP, allowing the calculation of K_m, V_{max} & k_{cat} of MBP for *Pf*CLK1wt (top) and *Pf*CLK1F630C (bottom).

From the curve of the graphs it is deemed that a wide enough range of concentrations of MBP were studied to give accurate information on both V_{max} and $K_{m;}$[250] indeed, the approach to V_{max} can be observed (**Figure 3.16**). For *Pf*CLK1F630C some negative values were obtained for the rate at concentrations of MBP due to very low turn-over resulting in values being so close to the background level. Unfortunately, this is an unavoidable limitation of this experiment. For *Pf*CLK1wt it appears that a systematic error may have occurred as all of one data set slightly higher than the other.

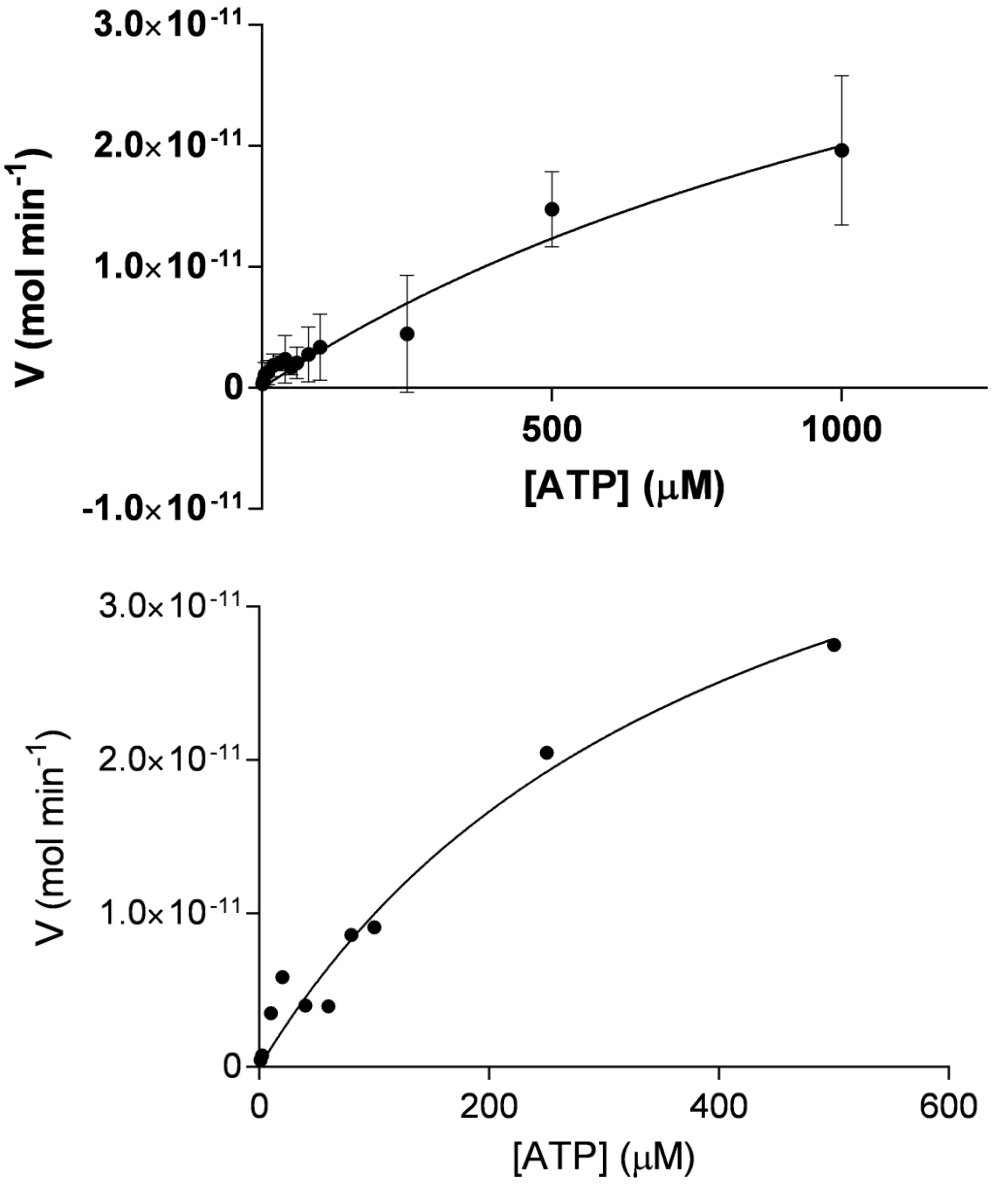

Figure 3.17: *Pf*CLK1wt & *Pf*CLK1F630C kinetic parameters. Non-linear regression of [ATP] against rate of phosphorylation of MBP, allowing the calculation of K_m, V_{max} & k_{cat} of ATP for *Pf*CLK1wt (top) and *Pf*CLK1F630C (bottom).

When measuring the apparent kinetic parameters of ATP for *Pf*CLK1wt and *Pf*CLK1F630C, negative values were recorded at the highest concentrations of ATP (5 mM for *Pf*CLK1wt and 1 mM and 5 mM for *Pf*CLK1F630C). This was due to the low [γ-^{32}P]-ATP:ATP ratio, resulting in radioactive decay counts approximately the same as the background level. A lack of rate values at higher concentrations of ATP could affect the shape of the curve, causing it to appear less steep than it should and falsely increasing K_m as well as potentially providing insufficient information about V_{max}.[250] Two duplicated data sets were collected for *Pf*CLK1wt but there was insufficient enzyme for the assay to be carried out in duplicate for *Pf*CLK1F630C, making the data less reliable.

Table 3.2: Apparent kinetic parameters measured for *Pf*CLK1wt & *Pf*CLK1F630C.

	***Pf*CLK1wt**		***Pf*CLK1F630C**	
	ATP	**MBP**	**ATP**	**MBP**
K_m (μM)	1632	31.22	4101	31.11
V_{max} (mol min^{-1})	5.27 x10^{-11}	1.26 x10^{-11}	5.08 x10^{-11}	3.27 x10^{-12}
k_{cat} (min^{-1})	2.19 x10^{-3}	5.23 x10^{-4}	3.24 x10^{-4}	2.09 x10^{-5}
k_{cat}/K_m (M^{-1}min^{-1})	1.34	16.74	0.08	0.67

3.3.3.5 *Attempted inhibition with electrophilic inhibitors*

Despite the much reduced activity and strange behaviour of *Pf*CLK1F630C, the panel of 23 electrophilic inhibitors were screened against both *Pf*CLK1F630C and *Pf*CLK1wt; no inhibitory effect was observed for either kinase (**Figure 3.18**). This was as hoped for *Pf*CLK1wt and removed concern that the inhibitors could bind non-covalently to the active site of the wild-type, resulting in reversible inhibition. Although, not observing inhibition of *Pf*CLK1F630C was disappointing, the peculiar behaviour of the mutant enzyme cannot be ruled out as the cause. Incorrect spatial orientation of the

gatekeeper residue and electrophilic inhibitor, i.e. the orbitals are not correctly aligned for bond formation, could also be the reason for lack of inhibition, particularly because these inhibitors were not designed specifically for these active sites but rather for gatekeeper cysteine mutations of other enzymes. It is also possible that the cysteine is not nucleophilic enough in the environment of the ATP-binding pocket to react with the electrophilic inhibitors.[286] However, it is unsurprising that under the conditions of these assays no inhibition was observed. Not only was *Pf*CLK1F630C not behaving as expected but in the work carried out by Shokat *et al.*[152] a much lower concentration of ATP (15 nM) was used than the K_m of ATP (22 µM) for T338C c-Src compared to this study (50 µM ATP, apparent K_m of ATP for *Pf*CLK1F630C 4 mM).

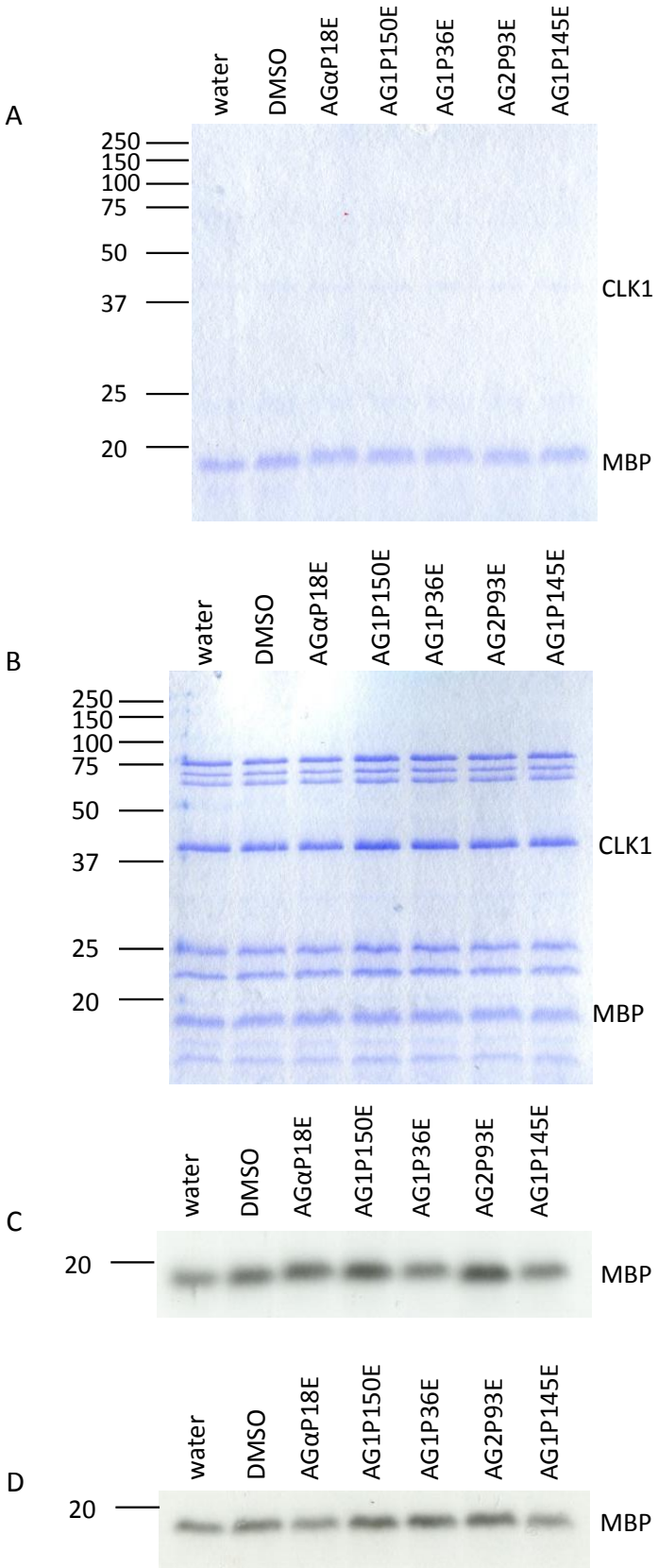

Figure 3.18: An example of inhibition assays performed with [γ-^{32}P]-ATP, MBP, *Pf*CLK1 & inhibitors (with water and DMSO as controls). A: Coomassie stain of *Pf*CLK1wt inhibition assay; B: Coomassie stain of *Pf*CLK1F630C inhibition assay; C: The corresponding autoradiograph for A; D: The corresponding autoradiograph for B.

3.4 Conclusion

Site-directed mutagenesis was successfully carried out to produce vectors containing the coding sequence for the bacterial expression of full length *Pf*CLK3F444C and kinase domain *Pf*CLK1F630C as protein as translational fusions with His_6. *Pf*CLK3wt, *Pf*CLK3F444C, *Pf*CLK1wt and *Pf*CLK1F630C were all expressed, purified and checked for kinase activity. Kinetic parameters were established for *Pf*CLK3wt but the mutant kinase *Pf*CLK3F444C was found to be inactive. *Pf*CLK1F630C was found to be active, albeit much less than its wild-type counterpart; however, as the concentration of *Pf*CLK1F630C increased, the rate of phosphorylation did not follow the expected pattern but instead plateaued far below the V_{max} of *Pf*CLK1wt. This indicated inhibition of *Pf*CLK1F630C. ADP, imidazole and phosphorylated MBP were implicated as possible causes and experiments were performed to investigate these suggestions but without success. Despite this behaviour, kinetic parameters were measured for both *Pf*CLK1wt and *Pf*CLK1F630C and electrophilic inhibitors were screened against *Pf*CLK1wt and *Pf*CLK1F630C. No inhibition of either kinase was observed. The lack of inhibition of the *Pf*CLK1F630C could be attributed to: its unconventional behaviour, indicating an underlying problem with the mutant; poor orbital overlap of the electrophilic inhibitor and the cysteine gatekeeper residue; cysteine not being nucleophilic enough to react with the inhibitor; the large quantity of ATP used in this study compared to that used by Shokat *et al*.[152]

3.5 Experimental

3.5.1 Recombinant DNA techniques

3.5.1.1 *Oligonucleotides*

Complementary oligonucleotide primers (56-57 bases in length) were designed. The complementary pairs of oligonucleotides, synthesised and desalted by Eurogentec, contained the appropriate mismatch bases. Sterile water (100 µL) was added to the oligonucleotides, which were then stored at -20 °C. The complementary pairs of oligonucleotides containing the appropriate mismatch bases (**Appendix A**) were used to prepare the mutants *Pf*CLK1F630C and *Pf*CLK3F444C studied in this chapter.

3.5.1.2 *Site-directed mutagenesis*

Site-directed mutagenesis was carried out using the Quikchange® II Site-Directed Mutagenesis Kit (Stratagene). The template vector (30 ng), forward and reverse primers (125 ng), dNTP (2 mM), *PfuUltra* HF DNA polymerase (2.5 U/µL), DMSO and water were mixed in thin-walled PCR tubes on ice to give a total volume of 50 µL (**Table 3.3**). The *PfuUltra* HF DNA polymerase and 10x reaction buffer were supplied in the kit. The mixture was incubated in a PCR machine with the programme as set out in (**Table 3.4**). 1µL *Dpn I* restriction enzyme (1 µL, 10 U/µL) was then added and the reaction mixture incubated at 37 °C for 1 hr to digest the parental DNA.

Table 3.3: Reaction volumes used in site-directed mutagenesis PCR (µL).

	*Pf*CLK1F630C	*Pf*CLK3F444C
Template Vector	0.9	0.8
Forward Primer	0.3	1.2
Reverse Primer	0.3	1.2
dNTP	5.0	5.0
10x Buffer	5.0	5.0
Water	37.5	33.3
DMSO	0.0	2.5
DNA Polymerase	1.0	1.0

Table 3.4: PCR cycling parameters.

Segment	Cycles	Temperature	Time
1	1	95 °C	1 min
2	18	95 °C	1 min
		55 °C	45 s
		68 °C	10 min

3.5.1.3 *DNA isolation and characterisation*

XL1-Blue supercompetent cells (50 µL) were thawed on ice and placed into a pre-chilled 14 mL BD Falcon polypropylene round-bottom tube. The *DpnI*-treated DNA (1 µL) was added; the tube gently swirled to mix the sample and then incubated on ice for 30 min. Heat shock was performed by incubating the mixture in a 42 °C water bath for 45 s, followed by incubation on ice for 2 min. SOC medium (500 µL, 42 °C) was added and the transformation reaction mixture incubated at 37 °C, 220-250 rpm for 1 hr. The cell culture (100 µL) was plated on LB agar petri dishes containing ampicillin (50 mg/L) and incubated at 37 °C overnight. A single colony was selected and grown in LB medium (5 mL) containing ampicillin (50 mg/L) overnight at 37 °C, 220-250 rpm. The plasmid was then extracted and purified using High Pure Plasmid Isolation Kit (Roche) and submitted to PNACL (University of Leicester) for sequence analysis.

3.5.2 Protein expression & purification

3.5.2.1 *Transformation & Expression*

BL21-CodonPlus (DE3)-RIPL competent cells (100 µL) were thawed on ice and placed into a pre-chilled 14 mL BD Falcon polypropylene round-bottom tube. The pLEICS-05 vector containing the coding sequence for the bacterial expression of the desired protein as a translational fusion with His_6 (~25 ng) was added; the tube gently swirled to mix the sample and then incubated on ice for 30 min. Heat shock was performed by incubating the mixture in a 42 °C water bath for 20 s, followed by incubation on ice for 2 min. SOC medium (900 µL, 42 °C) was added and the transformation reaction mixture incubated at 37 °C, 220-250 rpm for 30 min. The cell culture (100 µL) was plated on LB agar petri dishes containing ampicillin (50 mg/L) and chloramphenicol (50 mg/L) and incubated at 37 °C overnight. A single colony was selected and grown in LB medium (200 mL) containing ampicillin (50 mg/L) and chloramphenicol (50 mg/L) overnight at 37 °C, 220-250 rpm. The culture was then diluted 1:9 in LB medium containing ampicillin (50 mg/L) and chloramphenicol (50 mg/L) and allowed to recover at 37 °C, 220-225 rpm for 30 min, or until the optical density at 600 nm (OD_{600}) reached 0.6-0.8. Protein expression was induced by the addition of IPTG (100 µM final concentration) at 22 °C for CLK1 and 37 °C for *Pf*CLK3, 220-250 rpm for 4 hr. The cells were collected by centrifugation (10 min, 10 000 rpm, 4 °C) and the pellets stored at -80 °C until required.

3.5.2.2 *Ni-NTA-affinity chromatography*

Cell pellets were re-suspended in ice-cold Ni-NTA-lysis buffer (30 mL) containing triton X-100 (0.5%) and subjected to sonication (10 x 30 s with 30 s break at 4 °C). The cell free extracted was obtained by centrifugation (20 min, 20 000 rpm, 4 °C). The His_6-fusion protein was purified from the supernatant using a nickel-nitrilotracetic acid (Ni-NTA) agarose column. The resin (2 mL) was equilibrated with Ni-NTA-lysis buffer (5x column volumes) and the cell-free extract loaded on to the column. The column was then washed with Ni-NTA-lysis buffer (10x column volumes) and the His_6-fusion protein eluted in fractions of ~500 µL using elution buffer. Fractions containing the His_6-fusion protein, confirmed by SDS-PAGE, were pooled and dialysed for 4 hr, with stirring at 4 °C, against CLK-dialysis buffer (3 L) to remove imidazole. *Pf*CLK3F444C was concentrated (volume reduced from 2 mL to 0.5 mL).

3.5.2.3 *Total protein content and purity*

3.5.2.3.1 SDS-PAGE

In order to confirm the presence of the required protein and its purity, SDS-PAGE was performed on fractions from the Ni-NTA column and the combined fractions after dialysis (**Section 2.7.3.2**) using polyacrylamide gels (10%, 0.75 mm thickness). Protein samples were prepared for electrophoresis by adding an equal volume of 2x Laemmli buffer and heating at 60 °C for 3 min. The gels were run in SDS running buffer at 200 V for 45 min (or until the dye-front reached the end of the gel). The gels were stained by soaking in coomassie brilliant blue staining buffer and destained by soaking in destaining buffer. Precision plus unstained protein standards with protein markers of band sizes 250, 150, 100, 75, 50, 37, 25, 20, 15, & 10 kDa were used.

3.5.2.3.2 Bradford assay

The total protein content of the sample was measured using a Bradford assay. Protein sample (5 µL), water (995 µL) and Bradford reagent (1 mL) were mixed in a cuvette and allowed to react for 5 min. The absorbance of the sample at 595 nm was measured to give the concentration of the protein present. This was then used to calculate the amount of desired protein present from the densitometry of the SDS-PAGE (**Section 2.7.3.4.1**). For *Pf*CLK1wt and *Pf*CLK1F630C the desired His_6-fusion protein was deemed to be 10% of the total sample; i.e. 74 µg/mL and 314 µg/mL respectively and 30% of the total for *Pf*CLK3wt and *Pf*CLK3F444C; i.e. 246 µg/mL and 133 µg/mL respectively.

3.5.3 Establishing activity

3.5.3.1 *Qualitative analysis*

For *Pf*CLK1wt and *Pf*CLK1F630C kinase activity was tested in a final volume of 20 µL containing HEPES (17 mM), $MgCl_2$ (8.5 mM), DTT (0.85 mM), NaCl (150 mM), MBP (5.43 µM), ATP (50 µM, including [γ-32P]-ATP 500-1000 cpm/pmol) and enzyme (*Pf*CLK1wt 0 – 37.1 ng/µL; *Pf*CLK1F630C 0-471 ng/ µL). For *Pf*CLK3wt and *Pf*CLK3F444C kinase activity was tested in a final volume of 25 µL containing HEPES (12.8 mM), $MgCl_2$ (6.64 mM), DTT (0.88 mM), NaCl (72 mM), Tris (4.8 mM), MBP (4.34 µM), ATP (50 µM, including [γ-32P]-ATP 500-1000 cpm/pmol) and enzyme (*Pf*CLK3wt 0-48 ng/µL; *Pf*CLK3F444C and 0-116.1 ng/µL). In all four cases the samples were incubated for 30 min at 37 °C before 5 x Laemmli buffer (5 µL) was added to stop the reaction. Samples were heated at 60 °C for 3 min and run on a 15% SDS-PAGE gel at 200 V for

75 min. After staining with coomassie brilliant blue the gels were dried under vacuum at 80 °C for 45 min and exposed to autoradiographic film for 2-24 hr.

3.5.3.2 *Quantitative analysis*

For *Pf*CLK1wt and *Pf*CLK1F630C kinase activity was tested in a final volume of 20 µL containing HEPES (17 mM), $MgCl_2$ (8.5 mM), DTT (0.85 mM), NaCl (*Pf*CLK1wt 150 mM; *Pf*CLK1F630C 225 mM), MBP (5.43 µM), ATP (50 µM, including [γ-^{32}P]-ATP 500-1000 cpm/pmol) and enzyme (*Pf*CLK1wt 0-37.1 ng/µL; *Pf*CLK1F630C 0-471 ng/ µL). For *Pf*CLK3wt kinase activity was tested in a final volume of 25 µL containing HEPES (15.20-17.60 mM), Tris (0.4-2.4 mM), $MgCl_2$ (7.62-8.92 mM), DTT (0.76-0.88 mM), NaCl (6-13.2 mM), MBP (4.34 µM), ATP (50 µM, including [γ-32P]-ATP 500-1000 cpm/pmol) and enzyme (0-48 ng/µL). The samples were incubated for 30 min at 37 °C before being spotted on to squares of P81 phosphocellulose paper and allowed to dry for 20 min. The samples were washed with H_3PO_4 (0.5%, 3 x 10 min washes) before being placed into Ultimate Gold scintillation fluid (5 mL) and the radioactive decay measured using a scintillator.

3.5.4 Experiments to attempt to overcome low plateau

3.5.4.1 *Additional ATP*

Kinase activity was tested in a final volume of 40 µL containing HEPES (17 mM), $MgCl_2$ (8.5 mM), DTT (0.85 mM), NaCl (*Pf*CLK1wt 150 mM; *Pf*CLK1F630C 225 mM), MBP (5.43 µM), ATP (50 µM, including [γ-32P]-ATP 500-1000 cpm/pmol) and enzyme (0-471 ng/µL). The samples were incubated for 30 min at 37 °C before 20 µL samples were spotted on to squares of P81 phosphocellulose paper and allowed to dry for 20 min. ATP was added to bring the concentration to 100 µM and the samples were

incubated for a further 30 min, after which time the remaining 20 µL samples were spotted on to P81 phosphocellulose paper and allowed to dry for 20 min. The samples were washed with H_3PO_4 (0.5%, 3 x 10 min washes) before being placed into Ultimate Gold scintillation fluid (5 mL) and the radioactive decay measured using a scintillator.

3.5.4.2 *ADP as a potential inhibitor*

Assays were performed as described *vide supra* (**Section 3.5.3.2**) but with the following amendment: samples were pre-incubated with ADP (*Pf*CLK1F630C 0.1 and 1 µM; *Pf*CLK1wt 5 and 50 µM) for 10 min prior to the addition of ATP.

3.5.4.3 *Increased concentration of MBP*

Assays were performed as described in (**Section 3.5.3.2**) with an increased concentration of MBP (27.15 µM).

3.5.4.4 *Time course assay*

A time course assay was performed for *Pf*CLK3wt in a final volume of 25 µL containing HEPES (14.40-39.00 mM), $MgCl_2$ (7.36-7.96 mM), DTT (0.88-0.94 mM), NaCl (48 mM), Tris (3.2 mM), MBP (4.34 µM) ATP (50 µM, including [γ-32P]-ATP 500-1000 cpm/pmol) and enzyme (38.6 ng/µL). The samples were incubated for 15-90 min at 37 °C before being frozen on dry ice. Samples were then thawed, spotted on to squares of P81 phosphocellulose paper and allowed to dry for 20 min. The samples were washed with H_3PO_4 (0.5%, 3 x 10 min washes) before being placed into Ultimate Gold scintillation fluid (5 mL) and the radioactive decay measured using a scintillator.

3.5.5 Kinetic parameters for ATP and MBP

For *Pf*CLK1 kinetic parameters were determined in a final volume of 20 µL containing HEPES (17 mM), $MgCl_2$ (8.5 mM), DTT (0.85 mM), NaCl (15 mM *Pf*CLK1wt; 115 mM

*Pf*CLK1F630C), MBP (0-54 µM) ATP (0-1 mM, including [γ-32P]-ATP 500-1000 cpm/pmol) and enzyme (*Pf*CLK1wt 0.925 ng/µL; *Pf*CLK1F630C 120.89 ng/µL). For *Pf*CLK3wt kinetic parameters were determined in a final volume of 25 µL containing HEPES (14.40-39.00 mM), $MgCl_2$ (7.36-7.96 mM), DTT (0.88-0.94 mM), NaCl (48 mM), Tris (3.2 mM), MBP (0-4.34 µM) ATP (0-0.1 mM, including [γ-32P]-ATP 500-1000 cpm/pmol) and enzyme (39.43 ng/µL). The samples were incubated for 30 min at 37 °C before being spotted on to squares of P81 phosphocellulose paper and allowed to dry for 20 min. The samples were washed with H_3PO_4 (0.5%, 3 x 10 min washes) before being placed into Ultimate Gold scintillation fluid (5 mL) and the radioactive decay measured using a scintillator.

3.5.6 Inhibition Attempt

Inhibition assays for *Pf*CLK1wt were carried out in a final volume of 20 µL containing HEPES (11 mM), $MgCl_2$ (5.75 mM), DTT (0.80 mM), NaCl (75 mM), Tris (5 mM), DMSO (5%), MBP (5.43 µM), ATP (50 µM, including [γ-32P]-ATP 500-1000 cpm/pmol) and enzyme (17.5 ng/µL). Inhibition assays for PfCLK1F630C were carried out in a final volume of 20 µL containing HEPES (15 mM), $MgCl_2$ (7.55 mM), DTT (0.80 mM), NaCl (5 mM), Tris (1 mM), MBP (5.43 µM), ATP (50 µM, including [γ-32P]-ATP 500-1000 cpm/pmol) and enzyme (300 ng/µL). The samples were incubated for 30 min at 37 °C before 5x Laemmli buffer (5 µL) was added to stop the reaction. Samples were heated at 60 °C for 3 min and run on a 15% SDS-PAGE gel at 200 V for 75 min. The gels were dried under vacuum at 80 °C for 45 min and exposed to autoradiographic film for 12 hr.

4 Conclusion

A range of γ-modified nucleotide triphosphates were synthesised for the study of phosphorylation by *Pf*CK2α and mammalian CK2. Phosphoramidates were found to be unstable in the acidic conditions required for MALDI-TOF MS sample preparation; therefore, tag transfer to the peptide substrate could not be directly observed. Apparent IC_{50} values were measured for four ATP analogues (**58**, **59**, **60** & **48**). ATPγEt (**63**) was found not to be a substrate of mammalian CK2 or *Pf*CK2α but was found to act as an inhibitor of both kinases. No evidence was found to support the acceptance of GTP as a co-substrate by *Pf*CK2α. *Pf*CK2α was found to rapidly lose activity, even when stored at -80 °C, making kinetic studies challenging. The penultimate step in the synthesis of the CK2 inhibitor CX-4945 (**55**) was reached.

Gatekeeper mutants of *Pf*CLK1 and *Pf*CLK3 were successfully produced. *Pf*CLK1wt, *Pf*CLK1F630C, *Pf*CLK3wt and *Pf*CLK3F444C were expressed and purified for kinetic analysis. *Pf*CLK1F630C was found to have much reduced activity compared to its wildtype counterpart and *Pf*CLK3F444C was found to be completely inactive. Under the assay conditions used, *Pf*CLK1F630C was not sensitive to any of the 23 electrophilic inhibitors tested; therefore, the production of the corresponding mutant parasites was not pursued.

5 Future work

ATP phosphoramidate analogues, such as ATPγNH-PEG-N_3 (**60**), are limited in their use as agents for tagging kinase substrates due to the instability of the P-N bond under the acidic conditions of the de-salting step required prior to MALDI-TOF analysis. Due to inadequate resolution of phosphorylated peptide, tagged phosphorylated peptide and unphosphorylated peptide without the use of acidic buffer, LCMS is also unsuitable for the kinetic analysis for establishing the transfer of the tagged phosphate or for directly measuring the kinetic parameters of the ATP phosphoramidate compounds.[211] The synthesis of alternative ATP analogues that can withstand the acidic Zip Tip purification conditions are required for the confirmation of tag transfer by mass spectrometry or an alternative non-acidic method of analysis is required.

5.1 Synthesis of other ATP analogues

ATPγS (**48**) was shown to be a suitable substrate for mammalian *Pf*CK2α and ATPγSEt (**62**) was successfully synthesised, albeit in very low yield. Therefore, the optimisation of this reaction could provide enough material for enzyme assays with ATPγSEt (**62**), providing insight into the use of ATPγS analogues for tagging kinase substrates.

The synthesis of ATPγO-PEG-N_3 (**61**) was not achieved due to time constraints. Further investigation into methods for this synthesis is highly desirable due to their similarity to natural ATP. They have also been shown to be far more stable to acidic conditions than their phosphoramidate counterparts.[174]

ATPγEt (**63**) was not found to be a substrate for mammalian CK2 or *Pf*CK2α; however, it was shown to inhibit the activity of both kinases. Therefore, it is possible that introducing an electron withdrawing group such as CF_3 would enable tagged phosphorylation to occur with a phosphonate derivative of ATP. Hence, the synthesis of compounds such as ATPγCF_2CH_3 (**104**), ATPγCH_2CF_3 (**105**) or ATPγCF_2CF_3 (**106**) is of high interest.

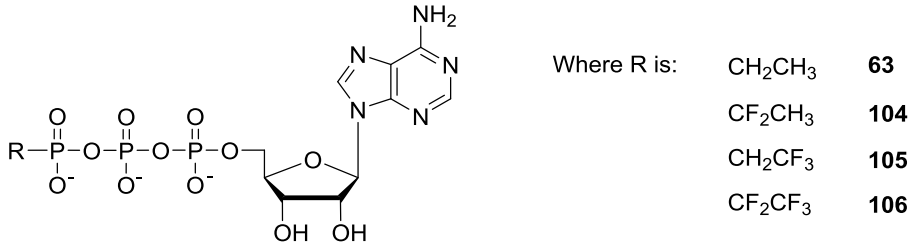

Figure 5.1: Structures of some fluorinated analogues of ATPγEt (63), which could be synthesised in an attempt to tag kinase substrates using ATP phosphonates.

5.2 The use of Caliper Capillary Electrophoresis for directly measuring the kinetic parameters of ATP analogues

Caliper Capillary electrophoresis offers a method of analysing enzymatic assays without the need for addition of a quenching agent or further purification. It uses the principles of capillary electrophoresis in a microfluidic environment to monitor the concentration of fluorescently labelled substrates and products. Phosphorylation of a peptide results in a change in electrophoretic mobility due to the peptide gaining two negative charges. By monitoring the ratio of the product:starting material peaks, the reaction process can be monitored at set time intervals and hence, kinetic analysis performed.[287] As this monitoring system can be used without acidic buffers,[288] the P-N bond of phosphoramidate ATP analogues would be stable to these analytical

conditions. The phophoramidate group transferred to the substrate from ATP phosphoramidate analogues would only increase the negative charge of the substrate by one, instead of the two observed in regular phosphorylation. It is hypothesised that this tagged phosphorylated peptide would, therefore, have an electrophoretic mobility in between that of the unphosphorylated peptide and the phosphorylated peptide (**Figure 5.2**). Thus, Caliper capillary electrophoresis has the potential to allow for the direct measurement of kinetic parameters of ATP phosphoramidate analogues. It can also provide significant support for the current rationalisation that the tag is transferred and then cleaved during the acidic Zip Tip purification procedure, rather than cleaved prior to phosphorylation. Consequently, the re-synthesis of ATP phosphoramidate analogues is highly desired for this work to commence.

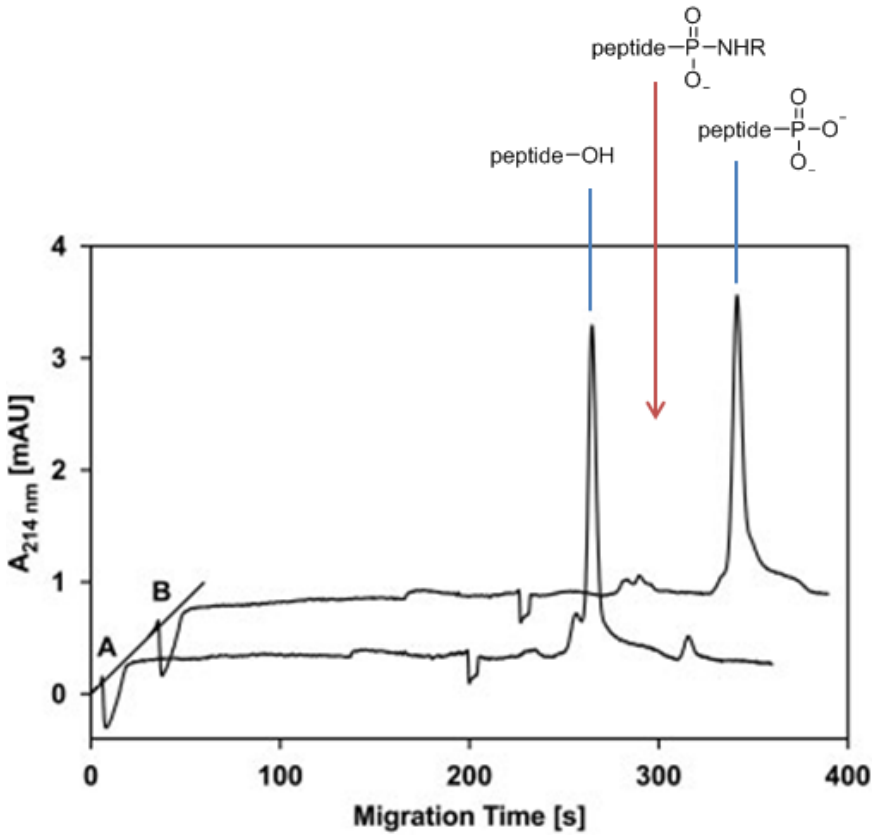

Figure 5.2: Overlay of two CE electropherograms showing the electrophoretic mobility shift observed after substrate phosphorylation. A: The peptide substrate starting material. B: The phosphorylated peptide substrate. The region the tagged-phosphorylated peptide is expected is indicated with a red arrow. Adapted from Gratz *et al*.[287]

5.3 Improving the nucleophilicity of cysteine gatekeeper mutants

It has been shown that further mutations to the active site can restore catalytic activity to gatekeeper mutants.[148] Therefore, this could be investigated as a way to restore activity to *Pf*CLK3F444C and to improve the activity of *Pf*CLK1F360C. The nucleophilicity of the cysteine gatekeeper mutant is a direct result of the pH of the microenvironment in which it sits.[286] Therefore, the nucleophilicity could be increased by altering the pH of the microenvironment through further mutations to other residues within the ATP binding pocket. This could enable the production of cysteine gatekeeper mutants which are sensitive to electrophilic inhibitors. These mutants could then be used to study the function of *Pf*CLK1 and *Pf*CLK3 within the *P. falciparum* parasite.

Appendix A

Primers used for the construction of cysteine gatekeeper mutants of *Pf*CLK1 and *Pf*CLK3:

CLK3F444C sense 5’ to 3’

AGT-AGT-ATA-AAA-TAT-AAA-AAT-CAT-TTA-TGT-TTA-GTA-TGT-GAG-TGG-ATG-TGG-GGT-AAC

CLKF444C anti sense 5’ to 3’

AGT-AGT-ATA-AAA-TAT-AAA-AAT-CAT-TTA-TGT-TTA-GTA-TGT-GAG-TGG-ATG-TGG-GGT-AAC

CLK1F630C sense 5’ to 3’

AGT-AGT-ATA-AAA-TAT-AAA-AAT-CAT-TTA-TGT-TTA-GTA-TGT-GAG-TGG-ATG-TGG-GGT-AAC

CLK1F630C antisense 5’ to 3’

TGA-TGG-ACC-TAA-TGG-TTC-ACA-TAT-TAA-ACA-CAT-ATG-GTC-ATA-ATA-CAT-AAA-TTT-CC

Appendix B

Buffers and solutions

LB media (1 L):

10 g NaCl

10 g tryptone

5 g yeast extract

In water (1 L), adjust to pH 7.

LB agar (1 L):

2 g agar

LB media (1 L) (*vide supra*)

SOB (1 L):

20 g tryptone

5 g yeast extract

0.5 g NaCl

10 mL KCl (250 mM)

5 mL $MgCl_2$ (2 M)

In water (1 L), adjusted to pH 7.

SOC (1 L):

20 mL glucose (1 M)

In SOB (1 L)

Coomassie stain:

50% MeOH

10% acetic acid

40% water

0.05% Brilliant Blue R-250

Destain:

50% MeOH

10% acetic acid

40% water

Laemmli buffer (2x):

4% SDS

20% glycerol

10% 2-mercaptoethanol

0.004% bromophenol blue

125 mM Tris, pH 6.8

PBS buffer (1 L):

8 g NaCl

0.2g KCl

1.44g Na_2HPO_4

0.24 KH_2PO_4

In water (1 L), adjusted to pH 7.4

SDS-PAGE loading buffer (1 L):

1 g Brillant Blue

25 mM Tris

192 mM glycine

0.1% SDS pH 8.3

SDS-PAGE running buffer (1 L):

25 mM Tris

192 mM glycine

0.1% SDS pH 8.3

Ni-NTA lysis buffer (100 mL):

20 mM Tris

150 mM NaCl

1 mM DTT

20 mM imidazole

1 tablet complete protease inhibitors (Roche)

1 tablet complete phosphatase inhibitors (Roche)

In water (100 mL), adjusted to pH 8

Ni-NTA Elution buffer (100 mL):

20 mM Tris

150 mM NaCl

1 mM DTT

350 mM imidazole

1 tablet protease inhibitor

1 tablet phosphatase inhibitor

In water (100 mL), adjusted to pH 7.4

Dialysis buffer:

1 mM DDT

20 mM Tris

300 mM NaCl

1 mM $MgCl_2$

In water adjusted to pH 7.4

MALDI-TOF MS matrix:

10 mg/ mL DHB

1:1 acetonitrile:water

0.1% H_3PO_4

References

(1) *World Malaria Report 2012*; World Health Organization: Geneva Switzerland.

(2) WHO *World Malaria Report 2008*; World Health Organization: Geneva Switzerland, 2008.

(3) Carter, E. D. *Enemy in the blood: malaria, environment and development in Argentina*; University of Alabama Press: Tuscaloosa. AL, USA, 2012.

(4) Cox, F. E. G. *Clin. Microbiol. Rev.* **2002**, *15*, 595–612.

(5) Cormier, L. A. *New frontiers in historical ecology: ten-thousand year fever: rethinking hunam and wild-primate malarias*; Left Coast Press: Walnut Creek, CA, USA, 2011.

(6) Greenwood, B. M.; Fidock, D. A.; Kyle, D. E.; Kappe, S. H. I.; Alonso, P. L.; Collins, F. H.; Duffy, P. E. *J. Clin. Invest.* **2008**, *118*, 1266–76.

(7) Roll Back Malaria *Economic costs of malaria*; Geneva Switzerland, 2002.

(8) Sherman.. I. W. *Twelve diseases that changed our world*; ASM Press: Washington, DC, USA, 2007.

(9) Singh, B.; Sung, L. K.; Matusop, A.; Radhakrishnan, A.; Shamsul, S. S.; Cox-Singh, J.; Thomas, A.; Conway, D. J. *Lancet* **2004**, *363*, 1017–1024.

(10) WHO Fact sheet N°94 April 2010.

(11) Organisation, W. H.; WHO *The Biology of Malaria Parasites*; 1987.

(12) Bray, R.; Garnham, P. *Br. Med. Bull.* **1982**, *38*, 117–122.

(13) Sherman, I. W. *Magic bullets to conqure malaria: from quinine to quinghaosu*; ASM Press: Washington, DC, USA, 2011.

(14) Cox-Singh, J.; Davis, T. M. E.; Lee, K.-S.; Shamsul, S. S. G.; Matusop, A.; Ratnam, S.; Rahman, H. A.; Conway, D. J.; Singh, B. *Clin. Infect. Dis.* **2008**, *46*, 165–71.

(15) Sinden, R. E. *Adv. Parasitol.* **1983**, *22*, 153–216.

(16) Doerig, C.; Billker, O.; Haystead, T.; Sharma, P.; Tobin, A. B.; Waters, N. C. *Trends Parasitol.* **2008**, *24*, 570–577.

(17) Simonetti, A. B. *Mem. Inst. Oswaldo Cruz* **1996**, *91*, 519–541.

(18) *Principles of Pharmacology*; Golan, D. E.; Tahjian, A. H.; Armstrong, E. J.; Armstrong, A. W., Eds.; 3rd ed.; Lippincott Williams & Wilkins: Philadelphia, USA, 2012.

(19) Miller, L. H.; Baruch, D. I.; Marsh, K.; Doumbo, O. K. *Nature* **2002**, *415*, 673–9.

(20) Trampuz, A.; Jereb, M.; Muzlovic, I.; Prabhu, R. M. *Crit. Care* **2003**, *7*, 315–23.

(21) Gardner, M. J.; Hall, N.; Fung, E.; White, O.; Berriman, M.; Hyman, R. W.; Carlton, J. M.; Pain, A.; Nelson, K. E.; Bowman, S.; Paulsen, I. T.; James, K.; Eisen, J. A.; Rutherford, K.; Salzberg, S. L.; Craig, A.; Kyes, S.; Chan, M.-S.; Nene, V.; Shallom, S. J.; Suh, B.; Peterson, J.; Angiuoli, S.; Pertea, M.; Allen, J.; Selengut, J.; Haft, D.; Mather, M. W.; Vaidya, A. B.; Martin, D. M. A.; Fairlamb, A. H.; Fraunholz, M. J.; Roos, D. S.; Ralph, S. A.; McFadden, G. I.; Cummings, L. M.; Subramanian, G. M.; Mungall, C.; Venter, J. C.; Carucci, D. J.; Hoffman, S. L.; Newbold, C.; Davis, R. W.; Fraser, C. M.; Barrell, B. *Nature* **2002**, *419*, 498–511.

(22) Rosenberg, R.; Wirtz, R. A.; Schneider, I.; Burge, R. *Trans. R. Soc. Trop. Med. Hyg.* **1990**, *84*, 209–212.

(23) Krugliak, M.; Zhang, J.; Ginsburg, H. *Mol. Biochem. Parasitol.* **2002**, *119*, 249–56.

(24) Egan, T. J. *J. Inorg. Biochem.* **2008**, *102*, 1288–99.

(25) Wiser, M. F. *Protozoa and human disease*; Garland Science: New York, NY, USA, 2011.

(26) Pang, H. P.; Dale, M. M.; Ritter, J. M.; Moore, P. K. *Pharmacology*; Hunter, L., Ed.; 5th ed.; Elsevier Churchill Livingstone: Philadelphia, USA, 2005.

(27) Fidock, D. A.; Nomura, T.; Talley, A. K.; Cooper, R. A.; Dzekunov, S. M.; Ferdig, M. T.; Ursos, L. M. B.; bir Singh Sidhu, A.; Naudé, B.; Deitsch, K. W.; Su, X.; Wootton, J. C.; Roepe, P. D.; Wellems, T. E. *Mol. Cell* **2000**, *6*, 861–871.

(28) Roepe, P. D. *Biochemistry* **2011**, *50*, 163–71.

(29) Mather, M. W.; Darrouzet, E.; Valkova-Valchanova, M.; Cooley, J. W.; McIntosh, M. T.; Daldal, F.; Vaidya, A. B. *J. Biol. Chem.* **2005**, *280*, 27458–65.

(30) Dunkle, J. A.; Xiong, L.; Mankin, A. S.; Cate, J. H. D. *Proc. Natl. Acad. Sci. U. S. A.* **2010**, *107*, 17152–7.

(31) Meshnick, S. R. *Int. J. Parasitol.* **2002**, *32*, 1655–60.

(32) Hong, Y.-L.; Yang, Y.-Z.; Meshnick, S. R. *Mol. Biochem. Parasitol.* **1994**, *63*, 121–128.

(33) Asawamahasakda, W.; Ittarat, I.; Pu, Y. M.; Ziffer, H.; Meshnick, S. R. *Antimicrob. Agents Chemother.* **1994**, *38*, 1854–1858.

(34) White, N. J. *Antrimicrobial agents Chemother.* **1997**, *41*, 1413–1422.

(35) Nilsen, A.; LaCrue, A. N.; White, K. L.; Forquer, I. P.; Cross, R. M.; Marfurt, J.; Mather, M. W.; Delves, M. J.; Shackleford, D. M.; Saenz, F. E.; Morrisey, J. M.; Steuten, J.; Mutka, T.; Li, Y.; Wirjanata, G.; Ryan, E.; Duffy, S.; Kelly, J. X.; Sebayang, B. F.; Zeeman, A.-M.; Noviyanti, R.; Sinden, R. E.; Kocken, C. H. M.; Price, R. N.; Avery, V. M.; Angulo-Barturen, I.; Jiménez-Díaz, M. B.; Ferrer, S.; Herreros, E.; Sanz, L. M.; Gamo, F.-J.; Bathurst, I.; Burrows, J. N.; Siegl, P.; Guy, R. K.; Winter, R. W.; Vaidya, A. B.; Charman, S. A.; Kyle, D. E.; Manetsch, R.; Riscoe, M. K. *Sci. Transl. Med.* **2013**, *5*, 177ra37.

(36) Rottmann, M.; McNamara, C.; Yeung, B. K. S.; Lee, M. C. S.; Zou, B.; Russell, B.; Seitz, P.; Plouffe, D. M.; Dharia, N. V; Tan, J.; Cohen, S. B.; Spencer, K. R.; González-Páez, G. E.; Lakshminarayana, S. B.; Goh, A.; Suwanarusk, R.; Jegla, T.; Schmitt, E. K.; Beck, H.-P.; Brun, R.; Nosten, F.; Renia, L.; Dartois, V.; Keller, T. H.; Fidock, D. A.; Winzeler, E. A.; Diagana, T. T. *Science* **2010**, *329*, 1175–80.

(37) Delves, M. J. *Future Med. Chem.* **2012**, *4*, 2251–63.

(38) *The World Health Report 1999 - Making a difference*; World Health Organization: Geneva Switzerland.

(39) Carter, R.; Mendis, K. N. *Clin. Microbiol. Rev.* **2002**, *15*, 564–94.

(40) Brito, I. *Heal. Policy Harvard* **2001**, *2*, 61–66.

(41) Dobson, M. J.; Malowany, M.; Snow, R. W. *Parassitologia* **2000**, *42*, 149–66.

(42) In *Disease control priorities in developing countries*; Jamison, D. T.; Breman, J. G.; Measham, A. R., Eds.; World Bank: Washington, DC, USA, 2006.

(43) White, N. J.; Nosten, F.; Looareesuwan, S.; Watkins, W. M.; Marsh, K.; Snow, R. W.; Kokwaro, G.; Ouma, J.; Hien, T. T.; Molyneux, M. E.; Taylor, T. E.; Newbold, C. I.; Ruebush, T. K.; Danis, M.; Greenwood, B. M.; Anderson, R. M.; Olliaro, P. *Lancet* **1999**, *353*, 1965–7.

(44) Chareonviriyaphap, T.; Bangs, M. J.; Ratanatham, S. *Southeast Asian J. Trop. Med. Public Health* **2000**, *31*, 225–237.

(45) Marsh, K. *Lancet* **1998**, *352*, 924.

(46) Gates, M. F. In *Gates Foundation Malaria Forum*; 2007.

(47) Roberts, L.; Enserink, M. *Science* **2007**, *318*, 1544–5.

(48) Tanner, M.; de Savigny, D. *Bull. World Heal. Organ.* **2008**, *86*, 82–86.

(49) WHO Q&A on artemisinin resistance http://www.who.int/malaria/media/artemisinin_resistance_qa/en/index.html.

(50) Malaria Consortium Artemisinin resistance in Southeast Asia http://www.malariaconsortium.org/pages/drug_resistance.htm.

(51) Chugh, M.; Sundararaman, V.; Kumar, S.; Reddy, V. S.; Siddiqui, W. A.; Stuart, K. D.; Malhotra, P. *Proc. Natl. Acad. Sci. U. S. A.* **2013**, *110*, 5392–7.

(52) Burnett, G.; Kennedy, E. P. *J. Biol. Chem.* **1954**, *211*, 969–980.

(53) Krebs, E. G. *Annu. Rev. Biochem.* **1998**, *67*, xii–xxxii.

(54) Taylor, S. S.; Kornev, A. P. *Trends Biochem. Sci.* **2011**, *36*, 65–77.

(55) Hunter, T. *Cell* **1995**, *80*, 225–236.

(56) Cohen, P. *Nat. Rev. Drug Discov.* **2002**, *1*, 309–315.

(57) Manning, G.; Whyte, D. B.; Martinez, R.; Hunter, T.; Sudarsanam, S. *Science.* **2002**, *298*, 1912–1934.

(58) Manning, G.; Plowman, G. D.; Hunter, T.; Sudarsanam, S. *Trends Biochem. Sci.* **2002**, *27*, 514–20.

(59) Shiu, S.-H.; Li, W.-H. *Mol. Biol. Evol.* **2004**, *21*, 828–40.

(60) Loftus, B.; Anderson, I.; Davies, R.; Alsmark, U. C. M.; Samuelson, J.; Amedeo, P.; Roncaglia, P.; Berriman, M.; Hirt, R. P.; Mann, B. J.; Nozaki, T.; Suh, B.; Pop, M.; Duchene, M.; Ackers, J.; Tannich, E.; Leippe, M.; Hofer, M.; Bruchhaus, I.; Willhoeft, U.; Bhattacharya, A.; Chillingworth, T.; Churcher, C.; Hance, Z.; Harris, B.; Harris, D.; Jagels, K.; Moule, S.; Mungall, K.; Ormond, D.; Squares, R.; Whitehead, S.; Quail, M. A.; Rabbinowitsch, E.; Norbertczak, H.; Price, C.; Wang, Z.; Guillén, N.; Gilchrist, C.; Stroup, S. E.; Bhattacharya, S.; Lohia, A.; Foster, P. G.; Sicheritz-Ponten, T.; Weber, C.; Singh, U.; Mukherjee, C.; El-Sayed, N. M.; Petri, W. A.; Clark, C. G.; Embley, T. M.; Barrell, B.; Fraser, C. M.; Hall, N. *Nature* **2005**, *433*, 865–8.

(61) Knighton, D. R.; Zheng, J. H.; Ten Eyck, L. F.; Xuong, N. H.; Taylor, S. S.; Sowadski, J. M. *Science* **1991**, *253*, 414–20.

(62) Knighton, D. R.; Zheng, J. H.; Ten Eyck, L. F.; Ashford, V. A.; Xuong, N. H.; Taylor, S. S.; Sowadski, J. M. *Science* **1991**, *253*, 407–14.

(63) Hanks, S. K.; Hunter, T. *Faseb J.* **1995**, *9*, 576–596.

(64) Rodnight, R.; Lavin, B. E. *Biochem. J.* **1964**, *93*, 84–91.

(65) Niefind, K.; Pütter, M.; Guerra, B.; Issinger, O. G.; Schomburg, D.; Putter, M. *Nat. Struct. Biol.* **1999**, *6*, 1100–1103.

(66) Nolen, B.; Taylor, S.; Ghosh, G. *Mol. Cell* **2004**, *15*, 661–675.

(67) Taylor, S. S.; Radzio-Andzelm, E. *Structure* **1994**, *2*, 345–355.

(68) Johnson, L. N.; Noble, M. E. .; Owen, D. J. *Cell* **1996**, *85*, 149–158.

(69) Steinberg, R. A.; Cauthron, R. D.; Symcox, M. M.; Shuntoh, H. *Mol. Cell. Biol.* **1993**, *13*, 2332–41.

(70) Kornev, A. P.; Taylor, S. S.; Ten Eyck, L. F. *Proc. Natl. Acad. Sci. U. S. A.* **2008**, *105*, 14377–82.

(71) Liu, Y.; Shah, K.; Yang, F.; Witucki, L.; Shokat, K. M. *Bioorg. Med. Chem.* **1998**, *6*, 1219–26.

(72) Azam, M.; Seeliger, M. A.; Gray, N. S.; Kuriyan, J.; Daley, G. Q. *Nat. Struct. Mol. Biol.* **2008**, *15*, 1109–18.

(73) Daub, H.; Specht, K.; Ullrich, A. *Nat. Rev. Drug Discov.* **2004**, *3*, 1001–10.

(74) Kannan, N.; Neuwald, A. F. *J. Mol. Biol.* **2005**, *351*, 956–972.

(75) Rubin, G. M. *Science* **2000**, *287*, 2204–2215.

(76) Pearce, L. R.; Komander, D.; Alessi, D. R. *Nat. Rev. Mol. Cell Biol.* **2010**, *11*, 9–22.

(77) Zhu, G. Z.; Fujii, K.; Liu, Y.; Codrea, V.; Herrero, J.; Shaw, S. *J. Biol. Chem.* **2005**, *280*, 36372–36379.

(78) Klimecka, M.; Muszyńska, G. *Acta Biochim. Pol.* **2007**, *54*, 219–233.

(79) Carmel, G.; Leichus, B.; Cheng, X.; Patterson, S.; Mirza, U.; Chait, B.; Kuret, J. *J. Biol. Chem.* **1994**, *269*, 7304–7309.

(80) Knippschild, U.; Gocht, A.; Wolff, S.; Huber, N.; Löhler, J.; Stöter, M. *Cell. Signal.* **2005**, *17*, 675–689.

(81) Gietzen, K. F. *J. Biol. Chem.* **1999**, *274*, 32063–32070.

(82) Neel, S. A. C. and B. G.; Malumbres, M.; Barbacid, M. *Curr. Opin. Genet. Dev.* **2007**, *17*, 60–65.

(83) Biondi, R. M.; Nebreda, A. R. *Biochem. J.* **2003**, *372*, 1–13.

(84) Aparicio, J. G.; Applebury, M. L. *J. Biol. Chem.* **1996**, *271*, 27083–9.

(85) Garbem, D. L.; Lowell, D. G. *J. Biol. Chem.* **1995**, *269*, 30741–30744.

(86) Mishra, N. S.; Tuteja, R.; Tuteja, N. *Arch. Biochem. Biophys.* **2006**, *452*, 55–68.

(87) Casaletto, J. B.; McClatchey, A. I. *Nat. Rev. Cancer* **2012**, *12*, 387–400.

(88) Robertson, S. C.; Tynan, J. A.; Donoghue, D. J. *Trends Genet.* **2000**, *16*, 265–271.

(89) Parkinson Study Group PRECEPT Investigators. *Neurology* **2007**, *69*, 1480–90.

(90) Ward, P.; Equinet, L.; Packer, J.; Doerig, C. *BMC Genomics* **2004**, *5*.

(91) Parsons, M.; Worthey, E. A.; Ward, P. N.; Mottram, J. C. *BMC Genomics* **2005**, *6*.

(92) Hoffman, S. L.; Bancroft, W. H.; Gottlieb, M.; James, S. L.; Burroughs, E. C.; Stephenson, J. R.; Morgan, M. J. *Nature* **1997**, *387*, 647.

(93) Kooij, T. W. A.; Janse, C. J.; Waters, A. P. *Nat. Rev. Microbiol.* **2006**, *4*, 344–57.

(94) Talevich, E.; Mirza, A.; Kannan, N. *BMC Evol. Biol.* **2011**, *11*, 321.

(95) Kappes, B.; Doerig, C. D.; Graeser, R. *Parasitol. Today* **1999**, *15*, 449–454.

(96) Anamika; Srinivasan, N.; Krupa, A. *Proteins Struct. Funct. Bioinforma.* **2005**, *58*, 180–189.

(97) Silva-Neto, M. A. C.; Atella, G. C.; Shahabuddin, M. *J. Biol. Chem.* **2002**, *277*, 14085–91.

(98) Billker, O.; Dechamps, S.; Tewari, R.; Wenig, G.; Franke-Fayard, B.; Brinkmann, V. *Cell* **2004**, *117*, 503–514.

(99) Barik, S. *J. Biol. Chem.* **1997**, *272*, 26132–26138.

(100) Doerig, C.; Endicott, J.; Chakrabarti, D. *Int. J. Parasitol.* **2002**, *32*, 1575–1585.

(101) Lin, D. T.; Goldman, N. D.; Syin, C. *Mol. Biochem. Parasitol.* **1996**, *78*, 67–77.

(102) Graeser, R.; Kury, P.; Franklin, R. M.; Kappes, B. *Mol. Microbiol.* **1997**, *23*, 151–159.

(103) Dorin, D. *J. Biol. Chem.* **1999**, *274*, 29912–29920.

(104) Droucheau, E.; Primot, A.; Thomas, V.; Mattei, D.; Knockaert, M.; Richardson, C.; Sallicandro, P.; Alano, P.; Jafarshad, A.; Baratte, B.; Kunick, C.; Parzy, D.; Pearl, L.; Doerig, C.; Meijer, L. *Biochim. Biophys. Acta - Proteins Proteomics* **2004**, *1697*, 181–196.

(105) Kappes, B.; Yang, J.; Suetterlin, B. W.; Rathgeb-Szabo, K.; Lindt, M. J.; Franklin, R. M. *Mol. Biochem. Parasitol.* **1995**, *72*, 163–178.

(106) Abdi, A.; Eschenlauer, S.; Reininger, L.; Doerig, C. *Cell. Mol. Life Sci.* **2010**, *67*, 3355–69.

(107) Dorin, D.; Le Roch, K.; Sallicandro, P.; Alano, P.; Parzy, D.; Poullet, P.; Meijer, L.; Doerig, C. *Eur. J. Biochem.* **2001**, *268*, 2600–2608.

(108) O'Connell, M. J.; Krien, M. J. E.; Hunter, T. *Trends Cell Biol.* **2003**, *13*, 221–228.

(109) Bracchi, V.; Langsley, G.; Thélu, J.; Eling, W.; Ambroise-Thomas, P. *PfKIN, an SNF1 type protein kinase of Plasmodium falciparum predominantly expressed in gametocytes*; 1996; Vol. 76, pp. 299–303.

(110) Moehrle, J.; Zhao, Y.; Wernli, B.; Kappes, B. *Biochem. J.* **1997**, *328*, 677–687.

(111) Dorin, D.; Semblat, J.-P.; Poullet, P.; Alano, P.; Goldring, J. P. D.; Whittle, C.; Patterson, S.; Chakrabarti, D.; Doerig, C. *Mol. Microbiol.* **2005**, *55*, 184–96.

(112) Nunes, M. C.; Goldring, J. P. D.; Doerig, C.; Scherf, A. *Mol. Microbiol.* **2007**, *63*, 391–403.

(113) Wells, T. N. C. *Science* **2010**, *329*, 1153–4.

(114) Cohen, P. *Trends Biochem. Sci.* **2000**, *25*, 596–601.

(115) Doerig, C.; Abdi, A.; Bland, N.; Eschenlauer, S.; Dorin-Semblat, D.; Fennell, C.; Halbert, J.; Holland, Z.; Nivez, M.-P.; Semblat, J.-P.; Sicard, A.; Reininger, L. *Biochim. Biophys. Acta* **2010**, *1804*, 604–12.

(116) Davies, T. G.; Bentley, J.; Arris, C. E.; Boyle, F. T.; Curtin, N. J.; Endicott, J. A.; Gibson, A. E.; Golding, B. T.; Griffin, R. J.; Hardcastle, I. R.; Jewsbury, P.; Johnson, L. N.; Mesguiche, V.; Newell, D. R.; Noble, M. E. M.; Tucker, J. A.; Wang, L.; Whitfield, H. J. *Nat. Struct. Biol.* **2002**, *9*, 745–9.

(117) Holton, S.; Merckx, A.; Burgess, D.; Doerig, C.; Noble, M.; Endicott, J. *Structure* **2003**, *11*, 1329–1337.

(118) Doerig, C. *Biochim. Biophys. Acta* **2004**, *1697*, 155–68.

(119) Pascual, J. *Nephrol. Dial. Transplant* **2006**, *21 Suppl 3*, iii18–23.

(120) *Kinase Inhibitors, Methods and Protocols*; Kuster, B., Ed.; Humana: New York, NY, USA, 2012.

(121) Davies, S. P.; Reddy, H.; Caivano, M.; Cohen, P. *Biochem. J.* **2000**, *351*, 95–105.

(122) Posy, S. L.; Hermsmeier, M. A.; Vaccaro, W.; Ott, K.-H.; Todderud, G.; Lippy, J. S.; Trainor, G. L.; Loughney, D. A.; Johnson, S. R. *J. Med. Chem.* **2011**, *54*, 54–66.

(123) Bamborough, P.; Drewry, D.; Harper, G.; Smith, G. K.; Schneider, K. *J. Med. Chem.* **2008**, *51*, 7898–914.

(124) Dar, A. C.; Shokat, K. M. *Annu. Rev. Biochem.* **2011**, *80*, 769–95.

(125) Zuccotto, F.; Ardini, E.; Casale, E.; Angiolini, M. *J. Med. Chem.* **2010**, *53*, 2681–94.

(126) Knight, Z. A.; Shokat, K. M. *Chem. Biol.* **2005**, *12*, 621–637.

(127) Zhang, J.; Yang, P. L.; Gray, N. S. *Nat. Rev. Cancer* **2009**, *9*, 28–39.

(128) Murphy, R. C.; Ojo, K. K.; Larson, E. T.; Castellanos-Gonzalez, A.; Perera, B. G. K.; Keyloun, K. R.; Kim, J. E.; Bhandari, J. G.; Muller, N. R.; Verlinde, C. L. M. J.; White, A. C.; Merritt, E. A.; Van Voorhis, W. C.; Maly, D. J. *ACS Med. Chem. Lett.* **2010**, *1*, 331–335.

(129) Murphy, R. C.; Ojo, K. K.; Billker, O. *J. Clin. Invest.* **2012**, *60*, 169–170.

(130) Liao, J. J.-L. *J. Med. Chem.* **2007**, *50*, 409–24.

(131) Cohen, M. S.; Zhang, C.; Shokat, K. M.; Taunton, J. *Science* **2005**, *308*, 1318–21.

(132) Ojo, K. K.; Pfander, C.; Mueller, N. R.; Burstroem, C.; Larson, E. T.; Bryan, C. M.; Fox, A. M. W.; Reid, M. C.; Johnson, S. M.; Murphy, R. C.; Kennedy, M.; Mann, H.; Leibly, D. J.; Hewitt, S. N.; Verlinde, C. L. M. J.; Kappe, S.; Merritt, E. A.; Maly, D. J.; Billker, O.; Van Voorhis, W. C. *J. Clin. Invest.* **2012**, *122*, 2301–5.

(133) Kato, K.; Sudo, A.; Kobayashi, K.; Sugi, T.; Tohya, Y.; Akashi, H. *Parasitol. Int.* **2009**, *58*, 394–400.

(134) Barf, T.; Kaptein, A. *J. Med. Chem.* **2012**, *55*, 6243–62.

(135) Kwarcinski, F. E.; Fox, C. C.; Steffey, M. E.; Soellner, M. B. *ACS Chem. Biol.* **2012**, *7*, 1910–7.

(136) Zhang, S.; Huang, W.-C.; Li, P.; Guo, H.; Poh, S.-B.; Brady, S. W.; Xiong, Y.; Tseng, L.-M.; Li, S.-H.; Ding, Z.; Sahin, A. A.; Esteva, F. J.; Hortobagyi, G. N.; Yu, D. *Nat. Med.* **2011**, *17*, 461–9.

(137) O'Connor, C. J.; Laraia, L.; Spring, D. R. *Chem. Soc. Rev.* **2011**, *40*, 4332–45.

(138) Stockwell, B. R. *Trends Biotechnol.* **2000**, *18*, 449–455.

(139) Walsh, D. P.; Chang, Y.-T. *Chem. Rev.* **2006**, *106*, 2476–530.

(140) Liu, Y.; Gray, N. S. *Nat. Chem. Biol.* **2006**, *2*, 358–64.

(141) Hanauer, A. *J. Med. Genet.* **2002**, *39*, 705–713.

(142) Shah, K.; Liu, Y.; Deirmengian, C.; Shokat, K. M. *Proc. Natl. Acad. Sci. U. S. A.* **1997**, *94*, 3565–3570.

(143) Elphick, L. M.; Lee, S. E.; Child, E. S.; Prasad, A.; Pignocchi, C.; Thibaudeau, S.; Anderson, A. A.; Bonnac, L.; Gouverneur, V.; Mann, D. J. *Chembiochem* **2009**, *10*, 1519–26.

(144) Niswender, C. M.; Ishihara, R. W.; Judge, L. M.; Zhang, C.; Shokat, K. M.; McKnight, G. S. *J. Biol. Chem.* **2002**, *277*, 28916–22.

(145) Blethrow, J. D.; Glavy, J. S.; Morgan, D. O.; Shokat, K. M. *Proc. Natl. Acad. Sci. U. S. A.* **2008**, *105*, 1442–7.

(146) Eblen, S. T.; Kumar, N. V.; Shah, K.; Henderson, M. J.; Watts, C. K. W.; Shokat, K. M.; Weber, M. J. *J. Biol. Chem.* **2003**, *278*, 14926–35.

(147) Witucki, L. A.; Huang, X.; Shah, K.; Liu, Y.; Kyin, S.; Eck, M. J.; Shokat, K. M. *Chem. Biol.* **2002**, *9*, 25–33.

(148) Zhang, C.; Kenski, D. M.; Paulson, J. L.; Bonshtien, A.; Sessa, G.; Cross, J. V; Templeton, D. J.; Shokat, K. M. *Nat. Methods* **2005**, *2*, 435–441.

(149) Bishop, A. C.; Ubersax, J. A.; Petsch, D. T.; Matheos, D. P.; Gray, N. S.; Blethrow, J.; Shimizu, E.; Tsien, J. Z.; Schultz, P. G.; Rose, M. D.; Wood, J. L.; Morgan, D. O.; Shokat, K. M. *Nature* **2000**, *407*, 395–401.

(150) Chakrabarti, P.; Pal, D. *Prog. Biophys. Mol. Biol.* **2001**, *76*, 1–102.

(151) Lozano-Núñez, A.; Ikeda, K. N.; Sauer, T.; de Graffenried, C. L. *Mol. Biol. Cell* **2013**, *24*, 1321–33.

(152) Garske, A. L.; Peters, U.; Cortesi, A. T.; Perez, J. L.; Shokat, K. M. *Proc. Natl. Acad. Sci. U. S. A.* **2011**, *108*, 15046–15052.

(153) Blair, J. A.; Rauh, D.; Kung, C.; Yun, C.-H.; Fan, Q.-W.; Rode, H.; Zhang, C.; Eck, M. J.; Weiss, W. A.; Shokat, K. M. *Nat. Chem. Biol.* **2007**, *3*, 229–38.

(154) Vulpetti, A.; Bosotti, R. *Farm.* **2004**, *59*, 759–765.

(155) Martić, S.; Kraatz, H.-B. *Chem. Sci.* **2013**, *4*, 42.

(156) Simard, J. R.; Getlik, M.; Grütter, C.; Pawar, V.; Wulfert, S.; Rabiller, M.; Rauh, D. *J. Am. Chem. Soc.* **2009**, *131*, 13286–96.

(157) Lacey, V. K.; Parrish, A. R.; Han, S.; Shen, Z.; Briggs, S. P.; Ma, Y.; Wang, L. *Angew. Chem. Int. Ed. Engl.* **2011**, *50*, 8692–6.

(158) Maly, D. J.; Allen, J. A.; Shokat, K. M. *J. Am. Chem. Soc.* **2004**, *126*, 9160–1.

(159) Liu, K.; Kalesh, K. a; Ong, L. B.; Yao, S. Q. *Chembiochem* **2008**, *9*, 1883–1888.

(160) Statsuk, A. V; Maly, D. J.; Seeliger, M. A.; Fabian, M. A.; Biggs, W. H.; Lockhart, D. J.; Zarrinkar, P. P.; Kuriyan, J.; Shokat, K. M. *J. Am. Chem. Soc.* **2008**, *130*, 17568–74.

(161) Suwal, S.; Pflum, M. K. H. *Angew. Chem. Int. Ed. Engl.* **2010**, *49*, 1627–30.

(162) Wang, Q.; Cahill, S. M.; Blumenstein, M.; Lawrence, D. S. *J. Am. Chem. Soc.* **2006**, *128*, 1808–9.

(163) Wang, Q.; Dai, Z.; Cahill, S. M.; Blumenstein, M.; Lawrence, D. S. *J. Am. Chem. Soc.* **2006**, *128*, 14016–7.

(164) Wang, Q.; Zimmerman, E. I.; Toutchkine, A.; Martin, T. D.; Graves, L. M.; Lawrence, D. S. *ACS Chem. Biol.* **2010**, *5*, 887–95.

(165) Brumbaugh, J.; Schleifenbaum, A.; Gasch, A.; Sattler, M.; Schultz, C. *J. Am. Chem. Soc.* **2006**, *128*, 24–5.

(166) Nyati, S.; Ranga, R.; Ross, B. D.; Rehemtulla, A.; Bhojani, M. S. *Anal. Biochem.* **2010**, *405*, 246–254.

(167) Lee, H.-M.; Larson, D. R.; Lawrence, D. S. *ACS Chem. Biol.* **2009**, *4*, 409–27.

(168) Rothman, D. M.; Vazquez, M. E.; Vogel, E. M.; Imperiali, B. *J. Org. Chem.* **2003**, *68*, 6795–8.

(169) Vaghefi, M. *Nucleoside triphosphates and their analogs*; Taylor and Francis: London, 2005.

(170) Boyle, S. N.; Koleske, A. J. *Biochemistry* **2007**, *46*, 11614–20.

(171) Elphick, L. M.; Lee, S. E.; Gouverneur, V.; Mann, D. J. *ACS Chem. Biol.* **2007**, *2*, 299–314.

(172) Green, K. D.; Pflum, M. K. H. *J. Am. Chem. Soc.* **2007**, *129*, 10–11.

(173) Green, K. D.; Kay, M.; Pflum, H.; Pflum H., M. K.; Green D., K.; Pflum, M. K. H. *Chembiochem* **2009**, *10*, 234–237.

(174) Hacker, S. M.; Mex, M.; Marx, A. *J. Org. Chem.* **2012**, *77*, 10450–4.

(175) Draganescu, A. *J. Biol. Chem.* **2000**, *275*, 4555–4560.

(176) Eckstein, F. *Annu. Rev. Biochem.* **1985**, *54*, 367–402.

(177) Facemyer, K. C.; Cremo, C. R. *Bioconjug. Chem.* **1992**, *3*, 408–413.

(178) Allen, J. J.; Lazerwith, S. E.; Shokat, K. M. *J. Am. Chem. Soc.* **2005**, *127*, 5288–5289.

(179) Allen, J. J.; Li, M.; Brinkworth, C. S.; Paulson, J. L.; Wang, D.; Hübner, A.; Chou, W.-H.; Davis, R. J.; Burlingame, A. L.; Messing, R. O.; Katayama, C. D.; Hedrick, S. M.; Shokat, K. M. *Nat. Methods* **2007**, *4*, 511–6.

(180) Lee, S. E.; Elphick, L. M.; Kramer, H. B.; Jones, A. M. E.; Child, E. S.; Anderson, A. A.; Bonnac, L.; Suwaki, N.; Kessler, B. M.; Gouverneur, V.; Mann, D. J. *Chembiochem* **2011**, *12*, 633–40.

(181) Wang, Z.; Lévy, R.; Fernig, D. G.; Brust, M. *J. Am. Chem. Soc.* **2006**, *128*, 2214–5.

(182) Patricelli, M. P.; Szardenings, A. K.; Liyanage, M.; Nomanbhoy, T. K.; Wu, M.; Weissig, H.; Aban, A.; Chun, D.; Tanner, S.; Kozarich, J. W. *Biochemistry* **2007**, *46*, 350–8.

(183) Song, H.; Kerman, K.; Kraatz, H.-B. *Chem. Commun. (Camb).* **2008**, *4*, 502–4.

(184) Martic, S.; Labib, M.; Freeman, D.; Kraatz, H. B. *Chem. Eur. J.* **2011**, *17*, 6744–6752.

(185) Martić, S.; Gabriel, M.; Turowec, J. P.; Litchfield, D. W.; Kraatz, H.-B. *J. Am. Chem. Soc.* **2012**, *134*, 17036–45.

(186) Ulrich, S. M.; Buzko, O.; Shah, K.; Shokat, K. M. *Tetrahedron* **2000**, *56*, 9495–9502.

(187) Ulrich, S. M.; Sallee, N. A.; Shokat, K. M. *Bioorg. Med. Chem. Lett.* **2002**, *12*, 3223–3227.

(188) Kraybill, B. C.; Elkin, L. L.; Blethrow, J. D.; Morgan, D. O.; Shokat, K. M. *J. Am. Chem. Soc.* **2002**, *124*, 12118–12128.

(189) Lasa, M.; Marin, O.; Pinna, L. A. *Eur. J. Biochem.* **1997**, *243*, 719–725.

(190) Meggio, F.; Pinna, L. A. *FASEB J.* **2003**, *17*, 349–68.

(191) Marin, O. *J. Biol. Chem.* **1999**, *274*, 29260–29265.

(192) Ghavidel, A.; Schultz, M. C. *Cell* **2001**, *106*, 575–584.

(193) Guo, C.; Yu, S.; Davis, A. T.; Wang, H.; Green, J. E.; Ahmed, K. *J. Biol. Chem.* **2001**, *276*, 5992–9.

(194) Ahmed, K.; Gerber, D. A.; Cochet, C. *Trends Cell Biol.* **2002**, *12*, 226–230.

(195) Rodriguez, F. A.; Contreras, C.; Bolanos-Garcia, V.; Allende, J. E. *Proc. Natl. Acad. Sci. U. S. A.* **2008**, *105*, 5693–8.

(196) Bibby, A. C.; Litchfield, D. W. *Int. J. Biol. Sci.* **2005**, *1*, 67–79.

(197) Niefind, K.; Guerra, B.; Ermakowa, I.; Issinger, O. G. *Embo J.* **2001**, *20*, 5320–5331.

(198) Domańska, K.; Zieliński, R.; Kubiński, K.; Sajnaga, E.; Masłyk, M.; Bretner, M.; Szyszka, R. *Acta Biochim. Pol.* **2005**, *52*, 947–951.

(199) Lozeman, F. J.; Litchfield, D. W.; Piening, C.; Takio, K.; Walsh, K. A.; Krebs, E. G. *Biochemistry* **1990**, *29*, 8436–8447.

(200) Gietz, R. D.; Graham, K. C.; Litchfield, D. W. *J. Biol. Chem.* **1995**, *270*, 13017–13021.

(201) Pinna, L. A.; Meggio, F. *Prog. Cell Cycle Res.* **1997**, *3*, 77–97.

(202) Graham, K. C. *J. Biol. Chem.* **2000**, *275*, 5003–5010.

(203) Pinna, L. A. *J. Cell Sci.* **2002**, *115*, 3873–3878.

(204) Marin, O.; Sarno, S.; Boschetti, M.; Pagano, M. A.; Meggio, F.; Ciminale, V.; D'Agostino, D. M.; Pinna, L. A. *FEBS Lett.* **2000**, *481*, 63–67.

(205) Bidwai, A. P.; Reed, J. C.; Glover, C. V *Arch. Biochem. Biophys.* **1993**, *300*, 265–70.

(206) Sarno, Stefania; Ghisellini, Paola;Cesaro, Lucs; Battistutta, Roberto; Pinna, L. A.; Sarno, S.; Ghisellini, P.; Cesaro, L.; Battistutta, R.; Pinna, L. A. *Mol. Cell. Biochem.* **2001**, *227*, 13–19.

(207) Schemarova, I. V *Curr. Issues Mol. Biol.* **2006**, *8*, 27–49.

(208) Wilkes, J. M.; Doerig, C. *BMC Genomics* **2008**, *9*, 412.

(209) Pendyala, P. R.; Ayong, L.; Eatrides, J.; Schreiber, M.; Pham, C.; Chakrabarti, R.; Fidock, D. A.; Allen, C. M.; Chakrabarti, D. *Mol. Biochem. Parasitol.* **2008**, *158*, 1–10.

(210) Solyakov, L.; Halbert, J.; Alam, M. M.; Semblat, J.-P.; Dorin-Semblat, D.; Reininger, L.; Bottrill, A. R.; Mistry, S.; Abdi, A.; Fennell, C.; Holland, Z.; Demarta, C.; Bouza, Y.; Sicard, A.; Nivez, M.-P.; Eschenlauer, S.; Lama, T.; Thomas, D. C.; Sharma, P.; Agarwal, S.; Kern, S.; Pradel, G.; Graciotti, M.; Tobin, A. B.; Doerig, C. *Nat. Commun.* **2011**, *2*, 565.

(211) Graciotti, M. An integrated approach to unravelling Malaria cell signalling pathways, University of Leicester, 2013.

(212) Wilson, L. K. *J. Biol. Chem.* **1997**, *272*, 12961–12967.

(213) Yurimoto, S.; Fujimoto, T.; Magari, M.; Kanayama, N.; Kobayashi, R.; Tokumitsu, H. *BMC Biochem.* **2012**, *13*, 27.

(214) Bostrom, S. L.; Dore, J.; Griffith, L. C. *Biochem. Biophys. Res. Commun.* **2009**, *390*, 1154–9.

(215) Stoehr, S.; Smolen, J. *Blood* **1990**, *75*, 479–487.

(216) Gschwendt, M.; Kittstein, W.; Kielbassa, K.; Marks, F. *Biochem. Biophys. Res. Commun.* **1995**, *206*, 614–620.

(217) Roig, J.; Mikhailov, A.; Belham, C.; Avruch, J. *Genes Dev.* **2002**, *16*, 1640–58.

(218) Schinkmann, K. *J. Biol. Chem.* **1997**, *272*, 28695–28703.

(219) Yde, C. W.; Ermakova, I.; Issinger, O. G.; Niefind, K. *J. Mol. Biol.* **2005**, *347*, 399–414.

(220) Pinna, L. A.; Baggio, B.; Moret, V.; Siliprandi, N. *Biochim. Biophys. Acta - Enzymol.* **1969**, *178*, 199–201.

(221) Pinna, L. A. *Cell. Mol. Biol. Res.* **1994**, *40*, 383–90.

(222) Hathaway, G. M.; Traugh, J. A. *J. Biol. Chem.* **1979**, *254*, 762–768.

(223) Jakobi, R.; Traugh, J. A. *J. Biol. Chem.* **1992**, *267*, 23894–23902.

(224) Srinivasan, N.; Antonelli, M.; Jacob, G.; Korn, I.; Romero, F.; Jedlicki, A.; Dhanaraj, V.; Sayed, M. F.-R.; Blundell, T. L.; Allende, C. C.; Allende, J. E. *Protein Eng. Des. Sel.* **1999**, *12*, 119–127.

(225) Gatica, M.; Hinrichs, M. V.; Jedlicki, A.; Allende, C. C.; Allende, J. E. *FEBS Lett.* **1993**, *315*, 173–177.

(226) Allende, J.; Allende, C. *FASEB J* **1995**, *9*, 313–323.

(227) Doerig, C.; Holland, Z.; Prudent, R.; Reiser, J. B.; Cochet, C. *Eukaryot. Cell* **2009**, *8*, 388–397.

(228) Dastidar, E. G.; Dayer, G.; Holland, Z. M.; Dorin-Semblat, D.; Claes, A.; Chêne, A.; Sharma, A.; Hamelin, R.; Moniatte, M.; Lopez-Rubio, J.-J.; Scherf, A.; Doerig, C. *BMC Biol.* **2012**, *10*, 5.

(229) Pagano, M. A.; Andrzejewska, M.; Ruzzene, M.; Sarno, S.; Cesaro, L.; Bain, J.; Elliott, M.; Meggio, F.; Kazimierczuk, Z.; Pinna, L. A. *J. Med. Chem.* **2004**, *47*, 6239–47.

(230) Nie, Z.; Perretta, C.; Erickson, P.; Margosiak, S.; Almassy, R.; Lu, J.; Averill, A.; Yager, K. M.; Chu, S. *Bioorg. Med. Chem. Lett.* **2007**, *17*, 4191–4195.

(231) Cozza, G.; Mazzorana, M.; Papinutto, E.; Bain, J.; Elliott, M.; di Maira, G.; Gianoncelli, A.; Pagano, M. A.; Sarno, S.; Ruzzene, M.; Battistutta, R.; Meggio, F.; Moro, S.; Zagotto, G.; Pinna, L. A. *Biochem. J.* **2009**, *421*, 387–95.

(232) Siddiqui-Jain, A.; Drygin, D.; Streiner, N.; Chua, P.; Pierre, F.; O'Brien, S. E.; Bliesath, J.; Omori, M.; Huser, N.; Ho, C.; Proffitt, C.; Schwaebe, M. K.; Ryckman, D. M.; Rice, W. G.; Anderes, K. *Cancer Res.* **2010**, *70*, 10288–10298.

(233) Ryu, B. J.; Baek, S.; Kim, J.; Bae, S. J.; Chang, S.-Y.; Heo, J.-N.; Lee, H.; Lee, S. Y.; Kim, S. H. *Bioorg. Med. Chem. Lett.* **2012**, *22*, 5470–5474.

(234) Ku, M. J.; Park, J. W.; Ryu, B. J.; Son, Y.-J.; Kim, S. H.; Lee, S. Y. *Bioorg. Med. Chem. Lett.* **2013**, *23*, 5609–5613.

(235) Sarno, S.; Pinna, L. A. *Mol. Biosyst.* **2008**, *4*, 889–94.

(236) Battistutta, R.; Mazzorana, M.; Cendron, L.; Bortolato, A.; Sarno, S.; Kazimierczuk, Z.; Zanotti, G.; Moro, S.; Pinna, L. A. *Chembiochem* **2007**, *8*, 1804–9.

(237) Sarno, S.; de Moliner, E.; Ruzzene, M.; Pagano, M. A.; Battistutta, R.; Bain, J.; Fabbro, D.; Schoepfer, J.; Elliott, M.; Furet, P.; Meggio, F.; Zanotti, G.; Pinna, L. A. *Biochem. J.* **2003**, *374*, 639–46.

(238) Pierre, F.; Chua, P. C.; O'Brien, S. E.; Siddiqui-Jain, A.; Bourbon, P.; Haddach, M.; Michaux, J.; Nagasawa, J.; Schwaebe, M. K.; Stefan, E.; Vialettes, A.; Whitten, J. P.; Chen, T. K.; Darjania, L.; Stansfield, R.; Anderes, K.; Bliesath, J.; Drygin, D.; Ho, C.; Omori, M.; Proffitt, C.; Streiner, N.; Trent, K.; Rice, W. G.; Ryckman, D. M. *J. Med. Chem.* **2011**, *54*, 635–54.

(239) Costas, C.; Yuriev, E.; Meyer, K. L.; Guion, T. S.; Hanna, M. M. *Nucleic Acids Res.* **2000**, *28*, 1849–1858.

(240) Susumu, K.; Uyeda, H. T.; Medintz, I. L.; Pons, T.; Delehanty, J. B.; Mattoussi, H. *J. Am. Chem. Soc.* **2007**, *129*, 13987–13996.

(241) Ratnakar, S. J.; Alexander, V. *Eur. J. Inorg. Chem.* **2005**, *2005*, 3918–3927.

(242) Huang, F.; Wu, H.; Wang, D.; Yang, W.; Cao, Y. *Chem. Mater.* **2004**, *16*, 708–716.

(243) Suwal, S.; Senevirathne, C.; Garre, S.; Pflum, M. K. H. *Bioconjug. Chem.* **2012**, *23*, 2386–91.

(244) Parang, K.; Till, J. H.; Ablooglu, A. J.; Kohanski, R. A.; Hubbard, S. R.; Cole, P. A. *Nat. Struct. Biol.* **2001**, *8*, 37–41.

(245) Parang, K.; Kohn, J. A.; Saldanha, S. A. A.; Cole, P. A. *FEBS Lett.* **2002**, *520*, 156–160.

(246) Semizarov, D. G. *J. Biol. Chem.* **1996**, *271*, 24389–24394.

(247) Alexandrova, L. *Nucleic Acids Res.* **1998**, *26*, 778–786.

(248) Shipitsin, A. V.; Victorova, L. S.; Shirokova, E. A.; Dyatkina, N. B.; Goryunova, L. E.; Beabealashvilli, R. S.; Hamilton, C. J.; Roberts, S. M.; Krayevsky, A. *J. Chem. Soc. Perkin Trans. 1* **1999**, 1039–1050.

(249) Chesnut, D. B. *J. Phys. Chem. A* **2003**, *107*, 4307–4313.

(250) Cornish-Bowden, A. *Fundamentals of Enzyme Kinetics*; 4th ed.; Wiley-Blackwell: Weinheim, 2012.

(251) Engelberg, K.; Paul, A. S.; Prinz, B.; Kono, M.; Ching, W.; Heincke, D.; Dobner, T.; Spielmann, T.; Duraisingh, M. T.; Gilberger, T.-W. *Biochem. J.* **2013**, *452*, 457–66.

(252) Burlingham, B. T.; Widlanski, T. S. *J. Chem. Educ.* **2003**, *80*, 214–null.

(253) Cheng, Y; Prusoff, W. *Biochem. Pharmacol.* **1973**, *22*, 3099–3108.

(254) Pierre, F.; Stefan, E.; Nédellec, A.-S.; Chevrel, M.-C.; Regan, C. F.; Siddiqui-Jain, A.; Macalino, D.; Streiner, N.; Drygin, D.; Haddach, M.; O'Brien, S. E.; Anderes, K.; Ryckman, D. M. *Bioorg. Med. Chem. Lett.* **2011**, *21*, 6687–92.

(255) Green, T W; Wuts, P. G. M. *Protective Groups in Organic Synthesis*; Third.; Wiley-Interscience: New York, 1999.

(256) Bräse, S.; Gil, C.; Knepper, K.; Zimmermann, V. *Angew. Chem. Int. Ed. Engl.* **2005**, *44*, 5188–240.

(257) Pastorin, G.; Wu, W.; Wieckowski, S.; Briand, J.-P.; Kostarelos, K.; Prato, M.; Bianco, A. *Chem. Commun. (Camb).* **2006**, 1182–4.

(258) Berchel, M.; Haelters, J.-P.; Couthon-Gourvès, H.; Deschamps, L.; Midoux, P.; Lehn, P.; Jaffrès, P.-A. *European J. Org. Chem.* **2011**, *2011*, 6294–6303.

(259) Lee, S. E.; Elphick, L. M.; Anderson, A. A.; Bonnac, L.; Child, E. S.; Mann, D. J.; Gouverneur, V. *Bioorg. Med. Chem. Lett.* **2009**, *19*, 3804–7.

(260) Rabouin, D.; Perron, V.; N'Zemba, B.; C.-Gaudreault, R.; Bérubé, G. *Bioorg. Med. Chem. Lett.* **2003**, *13*, 557–560.

(261) Brockmann, T. W.; Tour, J. M. *J. Am. Chem. Soc.* **1995**, *117*, 4437–4447.

(262) HUANG, F. *RNA* **2003**, *9*, 1562–1570.

(263) Sivakumar, K.; Xie, F.; Cash, B. M.; Long, S.; Barnhill, H. N.; Wang, Q. *Org. Lett.* **2004**, *6*, 4603–6.

(264) Knorre, D. G.; Kurbatov, V. A.; Samukov, V. V. *FEBS Lett.* **1976**, *70*, 105–108.

(265) Wehrli, W. E.; Verheyden, D. L.; Moffatt, J. G. *J Am Chem Soc* **1965**, *87*, 2265–2277.

(266) Tondi, D.; Calò, S.; Shoichet, B. K.; Costi, M. P. *Bioorg. Med. Chem. Lett.* **2010**, *20*, 3416–3419.

(267) Johnson, K. W.; Smith, K. A. *J. Biol. Chem.* **1991**, *266*, 3402–3407.

(268) Howell, B. W.; Afar, D. E.; Lew, J.; Douville, E. M.; Icely, P. L.; Gray, D. A.; Bell, J. C. *Mol. Cell. Biol.* **1991**, *11*, 568–572.

(269) Ben-David, Y.; Letwin, K.; Tannock, L.; Bernstein, A.; Pawson, T. *EMBO J.* **1991**, *10*, 317–25.

(270) Hanes, J.; von der Kammer, H.; Klaudiny, J.; Scheit, K. H. *J. Mol. Biol.* **1994**, *244*, 665–72.

(271) Yun, B.; Farkas, R.; Lee, K.; Rabinow, L. *Genes Dev.* **1994**, *8*, 1160–1173.

(272) Aubol, B. E.; Plocinik, R. M.; Hagopian, J. C.; Ma, C.-T.; McGlone, M. L.; Bandyopadhyay, R.; Fu, X.-D.; Adams, J. A. *J. Mol. Biol.* **2013**, *425*, 2894–2909.

(273) Colwill, K.; Pawson, T.; Andrews, B.; Prasad, J.; Manley, J. L.; Bell, J. C.; Duncan, P. I. *EMBO J.* **1996**, *15*, 265–75.

(274) Stamm, S. *J. Biol. Chem.* **2008**, *283*, 1223–7.

(275) Fedorov, O.; Huber, K.; Eisenreich, A.; Filippakopoulos, P.; King, O.; Bullock, A. N.; Szklarczyk, D.; Jensen, L. J.; Fabbro, D.; Trappe, J.; Rauch, U.; Bracher, F.; Knapp, S. *Chem. Biol.* **2011**, *18*, 67–76.

(276) Menegay, H.; Moeslein, F.; Landreth, G. *Exp. Cell Res.* **1999**, *253*, 463–473.

(277) Muraki, M.; Ohkawara, B.; Hosoya, T.; Onogi, H.; Koizumi, J.; Koizumi, T.; Sumi, K.; Yomoda, J.; Murray, M. V; Kimura, H.; Furuichi, K.; Shibuya, H.; Krainer, A. R.; Suzuki, M.; Hagiwara, M. *J. Biol. Chem.* **2004**, *279*, 24246–54.

(278) Mott, B. T.; Tanega, C.; Shen, M.; Maloney, D. J.; Shinn, P.; Leister, W.; Marugan, J. J.; Inglese, J.; Austin, C. P.; Misteli, T.; Auld, D. S.; Thomas, C. J. *Bioorg. Med. Chem. Lett.* **2009**, *19*, 6700–6705.

(279) Chan, G. W.; Mong, S.; Hemling, M. E.; Freyer, A. J.; Offen, P. H.; DeBrosse, C. W.; Sarau, H. M.; Westley, J. W. *J. Nat. Prod.* **1993**, *56*, 116–121.

(280) Watanabe, K.; Tsuda, Y.; Iwashima, M.; Iguchi, K. *J. Nat. Prod.* **2000**, *63*, 258–260.

(281) Debdab, M.; Carreaux, F.; Renault, S.; Soundararajan, M.; Fedorov, O.; Filippakopoulos, P.; Lozach, O.; Babault, L.; Tahtouh, T.; Baratte, B.; Ogawa, Y.; Hagiwara, M.; Eisenreich, A.; Rauch, U.; Knapp, S.; Meijer, L.; Bazureau, J.-P. *J. Med. Chem.* **2011**, *54*, 4172–86.

(282) Tahtouh, T.; Elkins, J. M.; Filippakopoulos, P.; Soundararajan, M.; Burgy, G.; Durieu, E.; Cochet, C.; Schmid, R. S.; Lo, D. C.; Delhommel, F.; Oberholzer, A. E.; Pearl, L. H.; Carreaux, F.; Bazureau, J.-P.; Knapp, S.; Meijer, L. *J. Med. Chem.* **2012**, *55*, 9312–30.

(283) Duncan, P. I.; Stojdl, D. F.; Marius, R. M.; Scheit, K. H.; Bell, J. C. *Exp. Cell Res.* **1998**, *241*, 300–308.

(284) Karlas, A.; Machuy, N.; Shin, Y.; Pleissner, K.-P.; Artarini, A.; Heuer, D.; Becker, D.; Khalil, H.; Ogilvie, L. A.; Hess, S.; Mäurer, A. P.; Müller, E.; Wolff, T.; Rudel, T.; Meyer, T. F. *Nature* **2010**, *463*, 818–22.

(285) Rodgers, J. T.; Haas, W.; Gygi, S. P.; Puigserver, P. *Cell Metab.* **2010**, *11*, 23–34.

(286) Harris, T. K.; Turner, G. J. *IUBMB Life* **2002**, *53*, 85–98.

(287) Gratz, A.; Gotz, C.; Jose, J. *Electrophoresis* **2010**, *31*, 634–640.

(288) Dodson, C. A.; Bayliss, R. *J. Biol. Chem.* **2012**, *287*, 1150–7.

(289) Eichner, M. The Lifecycle of the malaria parasite http://www.uni-tuebingen.de/modeling/images/malaria_LifeCycle.gif.

(290) Fidock, D. A.; Rosenthal, P. J.; Croft, S. L.; Brun, R.; Nwaka, S. *Nat. Rev. Drug Discov.* **2004**, *3*, 509–20.

(291) Hanks, S. K. *Genome Biol.* **2003**, *4*, 111.

(292) Gamo, F.-J. J.; Sanz, L. M.; Vidal, J.; de Cozar, C.; Alvarez, E.; Lavandera, J.-L. L.; Vanderwall, D. E.; Green, D. V. S.; Kumar, V.; Hasan, S.; Brown, J. R.; Peishoff, C. E.; Cardon, L. R.; Garcia-Bustos, J. F. *Nature* **2010**, *465*, 305–U56.

(293) Baldauf, S. L. *Science* **2003**, *300*, 1703–6.

(294) Simard, J. R.; Grütter, C.; Pawar, V.; Aust, B.; Wolf, A.; Rabiller, M.; Wulfert, S.; Robubi, A.; Klüter, S.; Ottmann, C.; Rauh, D. *J. Am. Chem. Soc.* **2009**, *131*, 18478–88.